# Elucidating the molecular mechanisms of p110δ activation in T cell antigen receptor signalling

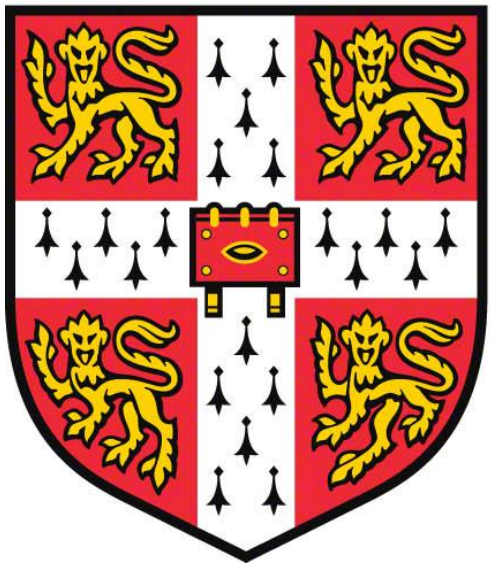


**Daisy Luff**

Fitzwilliam College

University of Cambridge


September 2018

This dissertation is submitted for the degree of Doctor of Philosophy

# Preface

This dissertation is the result of my own work and includes nothing which is the outcome of work done in collaboration except as declared in the Preface and specified in the text. I further state that no substantial part of my dissertation has already been submitted, or, is being concurrently submitted for any such degree, diploma or other qualification at the University of Cambridge or any other University or similar institution. This dissertation does not exceed the prescribed word limit for the Degree Committee of the Faculty of Biology.

*Declaration of data obtained in collaboration or from a technical service provider:*

LC-MS/MS analyses were undertaken at the Babraham Institute Mass Spectrometry Facility, Cambridge, by David Oxley, Katarzyna Wojdyla and Judith Webster.

RNA sequencing data was produced by Hicham Bouabe (Babraham Institute, Cambridge).

DNA Sanger sequencing was carried out by GATC (Eurofins Genomics, Germany).

# Table of Contents

# Abstract

Phosphoinositide 3-kinases (PI3Ks) are activated in immune cells downstream of the antigen recognition receptors, the signals from which are crucial for the development, differentiation and activation of lymphocytes. Engagement of the T cell antigen receptor (TCR) initiates a signalling cascade leading to the rapid induction of PI3K activity. The class IA catalytic isoform p110δ is known to be the dominant PI3K involved in signal transduction downstream of the TCR. However, the mechanism by which the TCR recruits and activates p110δ remains unresolved. This study has used a combination of proteomic, biochemical and gene editing approaches to identify proteins that are involved in the regulation of p110δ activity during TCR signalling.

This work has optimised the AviTag affinity purification system for the isolation of endogenous p110 isoforms from primary murine lymphocytes. A quantitative proteomics approach was subsequently used to identify endogenous proteins that interact with p110δ in primary activated $CD4^+$ T cells upon TCR stimulation. This analysis has identified multiple adaptor proteins and co-stimulatory receptors that may regulate p110δ activity at the TCR signalosome. Intriguingly, the B-cell adaptor for phosphoinositide 3-kinase (BCAP) was found to associate with p110δ in a TCR stimulation-dependent manner. Biochemical analyses revealed that BCAP is upregulated in activated T cells and rapidly tyrosine phosphorylated upon TCR stimulation. Collectively, this work suggests that BCAP is a key adaptor for PI3K downstream of the TCR.

This study has also developed a CRISPR/Cas9-mediated gene editing approach to disrupt targets of interest in primary murine activated T cells via ribonucleoprotein (RNP) nucleofection. This system was used to investigate the roles of the p110δ-associated proteins, BCAP and inducible T-cell costimulator (ICOS), in TCR-induced PI3K signalling and cytokine production in activated T cells. Collectively, this work has demonstrated the potential of proteomic analysis coupled with CRISPR/Cas9 gene editing for the identification and interrogation of signalling pathway components in primary T lymphocytes. Using this approach, this study has uncovered molecular details of p110δ recruitment and activation downstream of the TCR.

# Abbreviations

| | |
|---|---|
| ABD | Adaptor-binding domain |
| ANOVA | Analysis of variance |
| AP | Affinity purification |
| AP1 | Activator protein 1 |
| APC | Antigen-presenting cell |
| AP-MS | Affinity purification coupled with mass spectrometry |
| BCAP | B-cell adaptor for phosphoinositide 3-kinase |
| BCL10 | B-cell lymphoma 10 |
| BCR | B cell receptor |
| BH | Breakpoint cluster region homology domain |
| CAR | Coxsackievirus and adenovirus receptor |
| CBM | CARMA1-BCL10-MALT1 |
| CD2AP | CD2-associated protein |
| CRISPR | Clustered regularly interspaced short palindromic repeats |
| crRNA | CRISPR RNA |
| CSK | C-terminal Src kinase |
| CTL | Cytotoxic T lymphocytes |
| DAG | Diacylglycerol |
| EGF | Epidermal growth factor |
| EP | Electroporated |
| ERK | extracellular signal-related kinase |
| FB | FACs buffer |
| FDR | False discovery rate |
| FOXO | Forkhead box O |
| GAB | Grb2-associated binding |
| GADS | GRB2-related adaptor downstream of Shc |
| GAP | GTPase-activating protein |

| | |
|---|---|
| GEF | Guanine nucleotide exchange factors |
| GO | Gene Ontology |
| GPCR | G protein-coupled receptor |
| GPI | Glycosyl phosphatidylinositol |
| GRB2 | Growth factor receptor-bound protein 2 |
| GRK | GPCR kinase |
| gRNA | Single guide RNA |
| GSK3 | Glycogen synthase 3 |
| ICOS | Inducible T-cell costimulator |
| IKK | IκB kinase |
| Indel | Insertion/deletion |
| IP | Immunoprecipitation |
| $IP_3$ | Inositol triphosphate |
| IRS2 | Insulin receptor substrate 2 |
| ISG15 | Interferon stimulated gene 15 |
| ITAM | Immunoreceptor tyrosine-based activation motifs |
| ITK | Interleukin-2 Inducible T cell kinase |
| JAML | Junctional adhesion molecule-like |
| KO | Knock out |
| LAT | Linker for activation of T cells |
| LCK | Leukocyte C-terminal Src kinase |
| LC-MS/MS | Liquid chromatography-tandem mass spectrometry |
| MALT1 | Mucosa-associated lymphoid tissue lymphoma translocation gene 1 |
| MB | MACs buffer |
| MFI | Mean fluorescence intensity |
| MHC | Major histocompatibility complex |
| MS | Mass spectrometry |
| mTORC2 | Mammalian target of rapamycin complex 2 |
| NHEJ | Non-homologous end joining |
| NFAT | Nuclear factor of activated T cells |

| | |
|---|---|
| NFκB | Nuclear factor κB |
| PAM | Protospacer adjacent motif |
| PDK1 | 3-phosphoinositide-dependent kinase 1 |
| PH | Pleckstrin homology |
| PI | Phosphatidylinositol |
| PI3K | Phosphoinositide 3-kinase |
| PLCγ1 | Phosphoinositide phospholipase C-gamma-1 |
| RBD | Ras-binding domain |
| RNAi | RNA interference |
| RNP | Ribonucleoprotein |
| RTK | Receptor tyrosine kinase |
| S6K1 | Ribosomal protein S6 kinase beta-1 |
| SDS-PAGE | Sodium dodecyl sulphate polyacrylamide gel electrophoresis |
| SFK | Src-family kinase |
| SH2 | Src homology 2 |
| SH3 | Src homology 3 |
| SH3KBP1 | SH3-domain kinase binding protein 1 |
| SHP-2 | SH2 domain-containing tyrosine phosphatase |
| SLP-76 | SH2 domain containing leukocyte protein of 76 kDa |
| SOS1 | Son of sevenless homolog 1 |
| STS-2 | suppressor of TCR signalling 2 |
| TCR | T cell receptor |
| TF | Transcription factor |
| Th | T helper |
| TIDE | Tracking of Indels by Decomposition |
| TMT | Tandem mass tag |
| tracrRNA | trans-activating RNA |
| TRIM | TCR-interacting molecule |
| VPS34 | Vacuolar protein sorting-associated protein 34 |
| WASP | Wiskott-Aldrich syndrome protein |

| | |
|---|---|
| WT | Wild type |
| ZAP-70 | ζ-chain-associated protein kinase of 70 kDa |

# Chapter 1

# Introduction

## 1.1 The PI3K family

The phosphoinositide 3-kinases (PI3Ks) are a ubiquitous family of lipid kinases that play essential roles in cellular signal transduction. These enzymes phosphorylate the D-3 position of the inositol ring in phosphoinositides, generating second messengers vital to many signalling pathways involved in responses such as cell survival, proliferation, migration and adhesion (Rameh & Cantley, 1999). The PI3K family is divided into three classes based on their structure and substrate specificity.

### 1.1.1 Class I PI3Ks

Class I PI3Ks phosphorylate PI(4,5)$P_2$ ($PIP_2$) to produce the lipid second messenger PI(3,4,5)$P_3$ ($PIP_3$). In mammalian cells, four class I catalytic isoforms are expressed – p110α, β, γ and δ (Vanhaesebroeck *et al*, 2010). The p110 catalytic subunits form heterodimers with different regulatory subunits, which further separates this class in two. Class IA isoforms, p110α, p110β and p110δ, can associate equally with one of five 'p85' regulatory subunits: p85α, p55α, p50α (splice variants encoded by *Pik3r1*); p85β (*Pik3r2*); and p55γ (*Pik3r3*). The class IB catalytic subunit, p110γ, associates with either a p101 (*Pik3r5*) or p84/87 (*Pik3r6)* regulatory subunit (Stephens *et al*, 1997; Suire *et al*, 2005).

The catalytic and regulatory subunits of class IA PI3Ks are multidomain proteins (Figure 1.1). Structurally, the p110 catalytic subunits consist of an adaptor-binding domain (ABD), a Ras-binding domain (RBD), a C2 domain, a helical domain, and a C-terminal catalytic domain. The p85 regulatory subunits all contain a coiled-coil domain known as the inter-SH2 (iSH2), flanked by two Src homology 2 domains (SH2), nSH2 and cSH2. In addition, the p85α and p85β subunits contain an N-terminal SH3 domain and a breakpoint cluster region homology domain (BH) flanked by two proline-rich regions, which are absent in p55α, p50α and p55γ. The ABD of each p110 binds with high affinity to the p85 iSH2, which is essential for stabilisation of the catalytic subunit (Yu *et al*, 1998). In contrast, the ABD of the class IB isoform, p110γ, lacks a p85-binding

motif, but otherwise p110γ shares the same multidomain organisation as class IA p110 catalytic subunits (Amzel *et al*, 2008). The domain architectures of the p110γ regulatory subunits, p101 and p84/87, have not yet been defined (Burke & Williams, 2015).

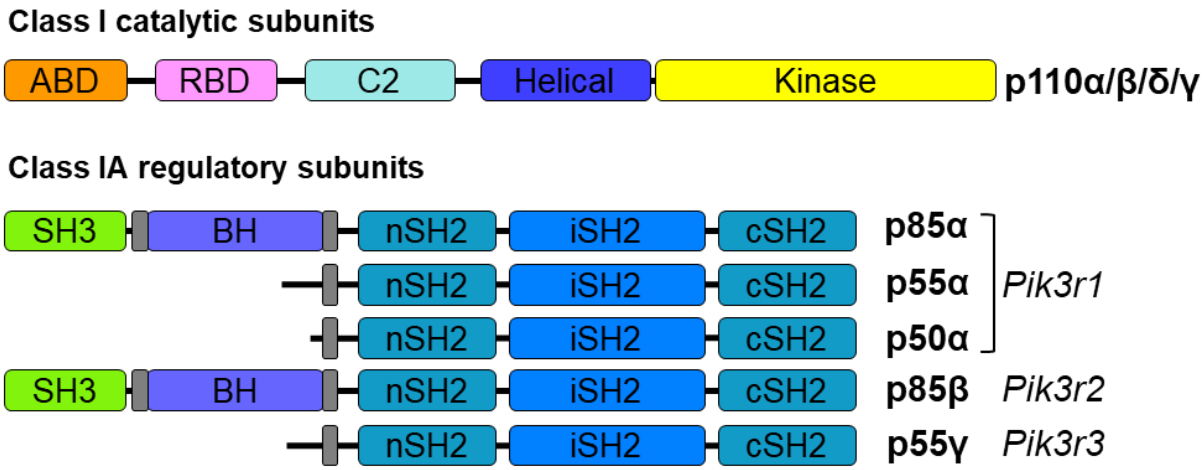


**Figure 1.1 Class I PI3Ks**
Domain organisations of the class I catalytic subunits, p110α, p110β, p110γ and p110δ, and the class IA p85 regulatory subunits: p85α, p55α, p50α (encoded by *Pik3r1);* p85β (*Pik3r2*); and p55γ (*Pik3r3*). ABD, adaptor-binding domain; RBD, Ras-binding domain; SH3, Src homology 3 domain; BH, breakpoint cluster region homology domain; nSH2, N-terminal Src homology 2 domain; iSH2, inter-SH2; cSH2, C-terminal SH2 domain; proline-rich regions are in grey. Domain architectures of the p110γ regulatory subunits, p101 and p84/87 (not shown), are incompletely defined.

A further distinction between the class I PI3Ks lies in their adaption to upstream regulation by different cell surface receptors. As cytosolic enzymes, PI3K activation necessitates recruitment to their substrate, $PIP_2$, located in lipid membranes. A broad range of receptors couple to specific PI3K isoforms, generally receptor tyrosine kinases (RTKs), tyrosine kinase-associated receptors and G protein-coupled receptors (GPCRs).

Class IA PI3Ks are activated downstream of RTKs and tyrosine kinase-associated receptors, including antigen, co-stimulatory and cytokine receptors. The p85 SH2 domains facilitate direct interaction with receptors or associated adaptor proteins that contain phosphorylated tyrosine residues. In contrast, the class IB PI3K, p110γ, is activated by GPCRs, a large family that includes the chemokine receptors. Both p110γ regulatory subunits, p101 and p84/87, mediate binding to Gβγ subunits of heterotrimeric G proteins. However, this distinction of the classes is not clear cut. The p110β heterodimer is unique in that it can be activated by both RTKs and GPCRs. A Gβγ-binding site located in the linker region between the C2 domain and helical domain of p110β enables this isoform to act as a coincidence detector, integrating signals from both RTKs and

GPCRs (Guillermet-Guibert *et al*, 2008; Dbouk *et al*, 2012; Kulkarni *et al*, 2011; Houslay *et al*, 2016). Similarly, in B lymphocytes and natural killer cells, p110δ can be activated by chemokine GPCRs, although the exact mechanism is still unknown (Reif *et al*, 2004; Saudemont *et al*, 2009). Furthermore, p110γ can be activated downstream of both RTKs and GPCRs in murine macrophages (Schmid *et al*, 2011). Thus, each class I PI3K isoform has a different capacity to integrate signals from upstream receptors, and isoform-specific roles of PI3Ks may depend on their ability to synergise signals from multiple inputs.

The class I PI3Ks also demonstrate distinct expression profiles. p110α and p110β are ubiquitously expressed, whereas p110γ and p110δ are predominantly expressed in immune cells (Vanhaesebroeck *et al*, 2010). This leukocyte-enriched expression of p110δ may be explained by the presence of a conserved transcription factor (TF)-binding cluster located upstream of *Pik3cd* exon 2 that contains at least four leukocyte-related TF-binding sites (Kok *et al*, 2009).

Common to the class I family is their enzymatic production of $PIP_3$. This lipid second messenger regulates the localisation and activity of a multitude of effector proteins that contain a sub-family of pleckstrin homology (PH) domains. Mammalian cells express over 200 PH-domain containing proteins, with an estimated ~40 demonstrating selectivity for binding to $PIP_3$ over $PI(4,5)P_2$ and $PI(3,4)P_2$ (Lemmon, 2008; Park *et al*, 2008). The most prominent of these effectors is protein kinase B (AKT), but others include Ras superfamily guanine nucleotide exchange factors (GEFs), GTPase-activating proteins (GAPs), protein kinases and adaptor proteins. Ultimately, class I PI3K effectors initiate a cascade of phosphorylation events and protein-protein interactions that regulate multiple cellular responses, including cell survival, growth, migration, metabolism and differentiation (Rameh & Cantley, 1999).

### 1.1.2 Class II and class III PI3Ks

The sole class III PI3K, vacuolar protein sorting-associated protein 34 (VPS34), is unique among the family in that it only phosphorylates phosphatidylinositol (PI), forming PI(3)P (Backer, 2008). VPS34 thus regulates PI(3)P-dependent processes, such as phagocytosis, autophagy and endocytosis (Kihara *et al*, 2001; Itakura *et al*, 2008; Jaber & Zong, 2013). VPS34 forms a constitutive complex with p150 (VPS15), which is thought to be required for its lipid kinase activity and membrane association (Rostislavleva *et al*, 2015). The class II PI3Ks, PI3KC2α, PI3KC2β and PI3KC2γ, produce PI(3)P as well as PI(3,4)P, although PI(3)P is thought to be the

main *in vivo* product, for PI3KC2α at least (Maffucci & Falasca, 2014). Class II PI3Ks are monomeric enzymes, distinguished by a C-terminal C2 domain not present in other PI3Ks. As the least investigated PI3K class, their mechanisms of action and activation are still unclear, but they exhibit disparate, isoform-specific functions in cell migration, intracellular trafficking and exocytosis (Falasca & Maffucci, 2012; Mavrommati *et al*; 2016).

This study is focused on the class I PI3Ks, specifically the class IA isoform p110δ.

## 1.2 Regulation of class IA PI3K kinase activity

Given that class I PI3Ks regulate diverse and essential cellular processes via production of $PIP_3$, tight regulation of their kinase activity is essential. PI3K activation requires a combination of recruitment to $PIP_2$ within lipid membranes and protein interactions with their regulatory subunits that induce conformational changes to the catalytic subunit. Inherently, both could be achieved through binding to a single interaction partner. However, class I PI3Ks also receive activatory input from Ras-family proteins in an isoform-specific manner (Burke & Williams, 2015).

### 1.2.1 The role of class IA regulatory subunits

Key to the control of class IA lipid kinase activity are the p85 regulatory subunits, which serve a dual function by both inhibiting basal p110 activity and facilitating its activation. All class IA p110 catalytic isoforms are inhibited by interactions with the iSH2 and nSH2 domains of the p85 regulatory subunit (Figure 1.2; Backer, 2010; Burke *et al* 2011; Zhang *et al*, 2011). These inhibitory contacts exist between the p85 iSH2 and p110 C2 domain (Wu *et al*, 2009), as well as between the p85 nSH2 and the helical, kinase and C2 domains (Miled *et al*, 2007; Mandelker *et al*, 2009). However, there are interesting differences in the p85-mediated inhibition of each p110 isoform. The iSH2 to C2 contact is partially disrupted in the p110β heterodimer, compared to p110α and p110δ (Dbouk *et al*, 2010). Furthermore, p110β and p110δ make an additional inhibitory contact with the cSH2 of p85 via the C-terminal lobe of their kinase domains (Burke & Williams, 2013; Burke *et al*, 2011; Zhang *et al*, 2011). Thus, it appears that p110β and p110δ may be under more strict control via the p85 regulatory subunit than p110α.

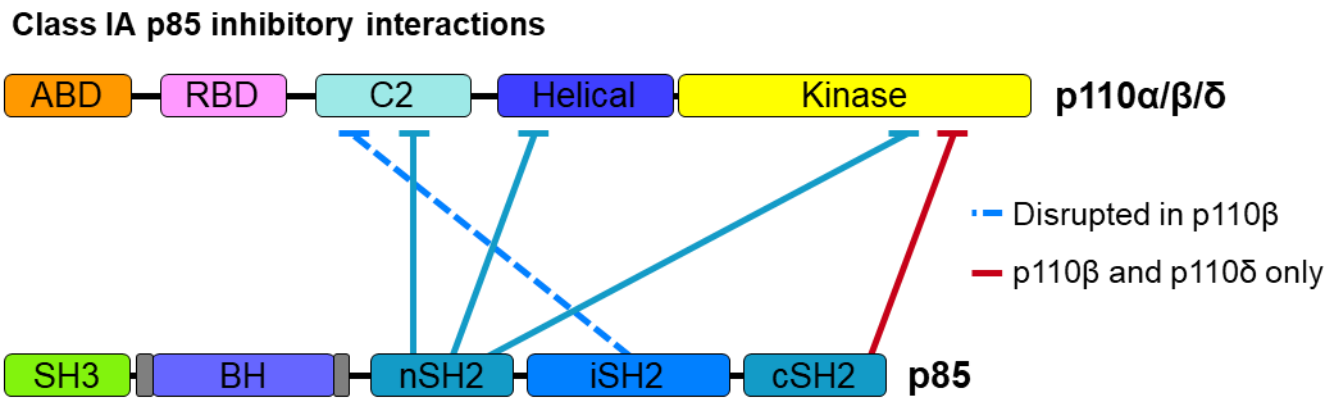


**Figure 1.2 Class IA PI3K inhibitory contacts between the p85 and p110 subunits**
All class IA p110 catalytic subunit isoforms are inhibited by interactions between the p85 iSH2 domain and the p110 C2 domain, as well as between the p85 nSH2 domain and the p110 C2, helical and kinase domains. p110β and p110δ heterodimers contain an additional inhibitory contact between the p85 cSH2 domain and the C-terminal lobe of the p110 kinase domain. The iSH2:C2 domain contact is partially disrupted in p110β heterodimers.

The critical mode of activation of the class IA PI3Ks involves release of these p85:p110 inhibitory contacts upon binding of the p85 SH2 domains to other proteins. SH2 domains are well-characterised phosphotyrosine-binding modules with distinct specificities for particular peptide motifs (Huang *et al*, 2008). The p85 SH2 domains specifically recognise phosphorylated tyrosines located within YxxM motifs (Songyang *et al*, 1993). Importantly, these interactions compete with the p110 subunit for binding to the p85 SH2 domains. In all class IA enzymes, binding to phosphotyrosyl YxxM peptides releases the nSH2 to helical domain inhibitory contact. The additional cSH2:kinase domain contact present in p110β and p110δ heterodimers is also disrupted by phosphotyrosine-peptide binding, with concomitant exposure of the C-lobe of their kinase domains (Burke & Williams, 2013). The iSH2:C2 interaction in the p110β heterodimer is released in the presence of phosphorylated YxxM peptide, whereas for p110α and p110δ heterodimers, subsequent membrane binding is required to achieve the same disruption (Burke & Williams, 2013). Thus, there are stereotypical conformational changes upon activation of the class IA PI3Ks, but also isoform-specific modes of p85 regulation.

The importance of p85 inhibitory function is demonstrated by the activating E542K, E545K and Q546K helical domain mutants of p110α commonly found in human cancer. These mutations mimic the disruption of the nSH2:p110α inhibitory interface that is normally induced by phosphotyrosine protein binding to the p85α nSH2 domain (Miled *et al*, 2007; Burke *et al*, 2012). The analogous E525K mutation in p110δ leads to hyperactive enzyme activity and is

associated with the human immunodeficiency disease, activated PI3K-delta syndrome (APDS) (Dornan *et al*, 2017).

Protein-protein interactions involving the p85 regulatory subunit of class IA PI3Ks directly lead to activation of their lipid kinase activity. Furthermore, p85α binding to phosphotyrosine peptides increases the affinity of the p110δ heterodimer for $PIP_2$-containing membranes, possibly by inducing conformational changes that expose regions necessary for lipid interactions (Burke *et al*, 2011). Thus, receptor tyrosine kinases (RTKs) and tyrosine-phosphorylated adaptor proteins that bind to the p85 SH2 domains are key regulators of class IA PI3Ks.

### 1.2.2 The role of Ras-family proteins

Class IA kinase activity is not only regulated via the p85 regulatory subunit; each p110 subunit contains a Ras-binding domain that allows for an additional level of regulation via interaction with Ras-family small GTPases. The crystal structure of p110γ in complex with RAS demonstrated conformational change in the catalytic domain upon RAS binding, which led to the hypothesis that RAS can drive allosteric regulation of PI3K lipid kinase activity (Pacold *et al*, 2000). RAS may also act to tether PI3K to the plasma membrane, although the C2 domain may be more important for the membrane association of p110δ (Denley *et al*, 2008). Moreover, the binding of membrane-resident HRAS to p110α and p110δ appears to strengthen their membrane interactions (Siempelkamp *et al*, 2017). Interestingly, the oncogenic p110α H1047R mutation enhances interaction of the kinase domain with lipid membranes, and this mutant is active in the absence of RAS binding (Zhao & Vogt, 2008; Burke *et al*, 2012).

The p110 subunits show a high level of sequence divergence within the RBD (Fritsch *et al*, 2013), and so, unsurprisingly, they each interact with different members of the Ras superfamily. The RBD of p110α, p110γ, and p110δ can bind to Ras or R-Ras subfamily members (Fritsch *et al*, 2013). RAS binding acts synergistically with tyrosine-phosphorylated proteins and Gβγ subunits to optimally activate the lipid kinase activity of p110α/p110δ and p110γ, respectively (Rodriguez-Viciana *et al*, 1994, 1996; Pacold *et al*, 2000; Siempelkamp *et al*, 2017). In contrast, p110β is not activated by the Ras subfamily, but instead by the Rho subfamily GTPases, CDC42 and RAC1, via its RBD (Fritsch *et al*, 2013). Interestingly, only RRAS1, RRAS2 (TC21) and HRAS have been demonstrated to activate p110δ lipid kinase activity, although p110δ is able to bind to NRAS and KRAS (Rodriguez-Viciana *et al*, 2004; Siempelkamp *et al*, 2017). It is clear that

interaction with Ras superfamily members represents another mode of isoform-specific regulation of the PI3Ks.

The activation of class IA PI3Ks, and subsequent phosphorylation of their substrate $PIP_{2,}$ is therefore regulated at two levels; via binding of the regulatory subunit to tyrosine-phosphorylated proteins and through interaction of the RBD with Ras small GTPases. The former also directly influences the localisation of PI3K, ultimately regulating its recruitment to the plasma membrane and its substrate $PIP_2$. Due to the role of class IA PI3Ks in fundamental cellular signalling processes, decades of work have focused on the molecular mechanisms underlying their regulation and dysregulation in many cell types, including those of the immune system.

In lymphocytes, class I PI3Ks are activated downstream of the antigen, cytokine and chemokine receptors, the signals from which control the development, differentiation and activation of lymphocytes (Okkenhaug & Vanhaesebroeck, 2003). Key studies using gene-targeted mice and isoform-selective PI3K inhibitors have demonstrated that the class IA catalytic isoform p110δ is the dominant PI3K involved in signal transduction initiated by the T cell antigen receptor (TCR) upon antigen recognition (Okkenhaug *et al*, 2002, 2006; Garçon *et al*, 2008). However, the mechanism by which the TCR recruits and activates p110δ remains unresolved. This body of work is focused on the molecular basis of p110δ regulation in T lymphocytes; specifically, downstream of the TCR.

## 1.3 Class IA PI3Ks in T lymphocytes

T lymphocytes play a central role in adaptive immunity, serving as the effectors of cellular immune responses. The protection afforded by the adaptive immune system is dependent on its ability to recognise and respond to virtually any foreign antigen. This is mediated by the diversity and specificity of the T cell antigen receptor (TCR) and the signalling events it induces upon antigen engagement. Given the fundamental role that PI3K signalling plays in cell signal transduction, it is no surprise that PI3K is required for the development and activation of T lymphocytes.

T cells differentiate in the thymus from bone marrow-derived precursors and emerge as naïve T cells to populate the peripheral lymph nodes and spleen. This tightly controlled process ensures development of the TCR repertoire while eliminating cells with high self-reactive potential (Starr

*et al*, 2003). Double negative ($CD4^-CD8^-$) thymic precursors undergo rearrangement of the TCRβ and TCRα chains by sequential VDJ or VJ recombination, respectively. Productive rearrangement of the TCRβ chain allows cells to progress through the 'β-checkpoint' to become $CD4^+CD8^+$ double positive thymocytes, followed by rearrangement of the TCRα chain. Thymocytes expressing a recombined TCRβ and TCRα chain are positively selected for low-affinity binding to self-antigen presented by major histocompatibility complex (MHC) molecules. However, those that bind with high affinity and are likely to be self-reactive are eliminated by clonal deletion during negative selection (Hogquist & Jameson, 2014). Two distinct mature T cell lineages migrate out of the thymus: MHC class II-restricted $CD4^+$ and MHC class I-restricted $CD8^+$. Mature T cells develop in mice that lack both the class IA isoforms p110α and p110δ (Ramadani *et al*, 2010). However, the combined loss of p110δ and p110γ causes a near complete block in development at the β-checkpoint (Swat *et al*, 2006; Webb *et al*, 2005). This was revealed to be due to a requirement for signalling through the chemokine receptor CXCR4, a GPCR that preferentially activates p110γ, at the β-checkpoint, while the pre-TCR engages p110δ (Janas *et al*, 2010).

The final stage of T cell differentiation occurs in peripheral lymphoid tissues, where naïve $CD4^+$ and $CD8^+$ T cells may encounter antigen on antigen-presenting cells (APCs) and become activated via the TCR and co-stimulatory receptors. Upon antigen encounter, naïve $CD8^+$ T cells differentiate into effector cytotoxic T lymphocytes (CTLs), which play a fundamental role in anti-viral and anti-tumour responses. Antigen recognition by naïve $CD4^+$ cells leads to clonal expansion and differentiation into effector cells, usually termed T helper (Th) cells due to their role in aiding other immune cells, such as B lymphocytes, macrophages and $CD8^+$ T cells, to orchestrate a context-dependent immune response (So & Fruman, 2012). PI3K has been shown to play a key role in $CD4^+$ T cell antigen-induced clonal expansion, differentiation and cytokine production (Okkenhaug *et al*, 2006; Soond *et al*, 2010). This can be attributed to the rapid activation of PI3K following initiation of the TCR signalling cascade upon peptide-MHC engagement (Costello *et al*, 2002; Harriague & Bismuth, 2002; Garçon *et al*, 2008).

### 1.3.1 The TCR signalling pathway

Engagement of the TCR by an antigenic peptide, bound in the cleft of an MHC class I or II molecule, is the critical binding event that ultimately leads to T cell activation, proliferation and acquisition of effector functions. Recognition of antigen induces the TCR signalling cascade,

dependent first on the activation of several protein tyrosine kinases and subsequently on the assembly of scaffolding hubs, which allow the activation of key downstream signalling pathways. The molecules and sequence of events that link proximal and distal segments of the TCR signalling pathway have been intensely studied, yet the mechanism of PI3K recruitment remains unresolved.

The clonotypic TCR confers antigen binding specificity via the ectodomain of the α and β chain heterodimer, TCRαβ, which is non-covalently associated with a multi-subunit CD3 complex, comprising invariant CD3γ, δ, ε and ζ chains that form γε, δε and ζζ dimers (Wang & Reinherz, 2012). None of the proteins within the TCR-CD3 complex contain intrinsic enzymatic activity, therefore signal transduction relies on the recruitment of kinases. This is mediated via phosphorylated immunoreceptor tyrosine-based activation motifs (ITAMs) present within the CD3 cytoplasmic tails. Each CD3γ, δ, and ε chain contains one ITAM, of the sequence (D/E)xxYxx(L/I)$x_{6-8}$Yxx(L/I), whereas the ζ chain contains three; thus, the TCR harbours twenty potential tyrosine phosphorylation sites (Love & Hayes, 2010). The two tyrosines located within ITAM motifs are phosphorylated by the Src-family kinase (SFK) LCK, which is critical for the early propagation of TCR signalling.

LCK is associated with the plasma membrane via N-terminal myristoylated and palmitoylated residues, but also interacts with the cytoplasmic tail of CD4 and CD8 co-receptors (Turner *et al*, 1990). CD4 and CD8 interact with MHC class II or class I molecules, respectively, on the surface of APCs during antigen presentation (König *et al*, 1992). Consequently, LCK is brought into proximity of the TCR complex, where it can phosphorylate the CD3 and ζ chain ITAMs (Holdorf *et al*, 2002). LCK activity is regulated by phosphorylation and dephosphorylation of two conserved tyrosine resides, a mechanism common to SFKs. Phosphorylation of Y505 by C-terminal Src kinase (CSK) leads to an intramolecular interaction with the LCK SH2 domain, locking the kinase in an inactive conformation (Bergman *et al*, 1992; Xu *et al*, 1997). In contrast, autophosphorylation of Y394 in the enzyme activation loop is thought to stabilise an active confirmation (Hardwick & Sefton, 1997). Both residues are dephosphorylated by CD45, a highly abundant transmembrane tyrosine phosphatase (D'Oro *et al*, 1996). Thus, LCK activity can be regulated via its recruitment to TCR microclusters and localisation with CD45 and CSK.

A proportion of LCK is constitutively active at the plasma membrane of resting T cells (Nika *et al*, 2010; Stirnweiss *et al*, 2013). Therefore, an additional level of regulation is required to prevent inappropriate phosphorylation of the CD3 ITAMs and to set the threshold of T cell activation

(Brownlie & Zamoyska, 2013). It is still unclear precisely how recognition of peptide-MHC allows LCK phosphorylation of the CD3 chains. One model proposed for this TCR 'triggering' suggests that peptide-MHC binding to the TCR induces a conformational change in the CD3ε and ζ subunits, exposing ITAMs that are usually buried in the lipid bilayer via lipid-interacting basic-rich stretch (BRS) motifs in the CD3 cytoplasmic domains (Xu *et al*, 2008; Guo *et al*, 2017). Exposed BRS motifs in the CD3ε chain may also directly mediate the recruitment of LCK (Li *et al*, 2017). However, triggering upon antigen recognition may also occur via segregation of the TCR from the tyrosine phosphatase CD45, which dephosphorylates CD3 ITAMs in resting cells (Varma *et al*, 2006; James & Vale, 2012; Carbone *et al*, 2017). In this respect, LCK, CSK and CD45 form a minimal network that controls the phosphorylation state of the TCR (Hui & Vale, 2014).

Tyrosine phosphorylated CD3 ITAMs are subsequently able to recruit SH2 domain-containing proteins, the most crucial being the Syk-family tyrosine kinase, ζ-chain-associated protein kinase of 70 kDa (ZAP-70). Tandem SH2 domains in ZAP-70 bind to doubly phosphorylated ITAMs in the CD3 and ζ chains, which is thought to perturb an autoinhibitory conformation and allow access to two regulatory tyrosines, Y315 and Y319 (Yan *et al*, 2013). These residues, as well as Y493 in the enzyme activation loop, are phosphorylated by LCK, leading to complete destabilisation of the autoinhibited conformation and full activation of ZAP-70 (Au-Yeung *et al*, 2018). Upon recruitment and activation at the TCR, ZAP-70 phosphorylates multiple tyrosine residues in two key scaffold proteins: the transmembrane linker for activation of T cells (LAT) and the cytoplasmic SH2 domain–containing leukocyte protein of 76 kDa (SLP-76) (Bubeck Wardenburg *et al*, 1996; Zhang *et al*, 1998). LAT and SLP-76 provide an essential link between the proximal tyrosine phosphorylation events of TCR signalling and the activation of distal signalling pathways.

Once phosphorylated, LAT acts as a molecular hub by nucleating multiprotein signalling complexes. Phosphotyrosines in LAT are bound by the SH2 domains of PLCγ1, GRB2, and GADS (Zhang *et al*, 2000). SH3 domains in the adaptor protein GRB2 (growth factor receptor–bound protein 2) bind to proline-rich regions in the Ras guanine nucleotide exchange factor (GEF) son of sevenless (SOS1), recruiting it into the vicinity of its membrane-associated substrate RAS, which in turn leads to the activation of extracellular signal-related kinase (ERK) (Quilliam, 2007). PLCγ1 (phospholipase Cγ1) catalyses the hydrolysis of $PIP_2$ to the second messengers $I(1,4,5)P_3$ ($IP_3$) and diacylglycerol (DAG). $IP_3$ causes the release of $Ca^{2+}$ from intracellular stores and promotes $Ca^{2+}$ influx from the extracellular space, thus elevating intracellular $Ca^{2+}$ levels,

whereas DAG recruits RASGRP and PKCθ to the plasma membrane, initiating the RAS-ERK and nuclear factor-κB (NF-κB) pathways, respectively (Spitaler & Cantrell, 2004). As well as binding to LAT, GADS (GRB2-related adaptor downstream of Shc) recruits SLP-76, which itself directly recruits the Rho-family GEF VAV, the adaptor NCK, and the Tec-family kinase ITK (Koretzky *et al*, 2006). Collectively, the protein complexes recruited by tyrosine phosphorylated LAT and SLP-76 activate the key signalling effectors ERK, PKCθ and calcineurin, which ultimately activate several transcription factors, including nuclear factor of activated T cells (NFAT), activator protein 1 (AP-1) and NF-κB (Gaud *et al*, 2018; Figure 1.3). Together, these orchestrate antigen-induced T cell proliferation, survival, cytokine production and effector functions during T cell activation (Foletta *et al*, 1998; Gerondakis & Siebenlist, 2010; Hermann-Kleiter & Baier, 2010).

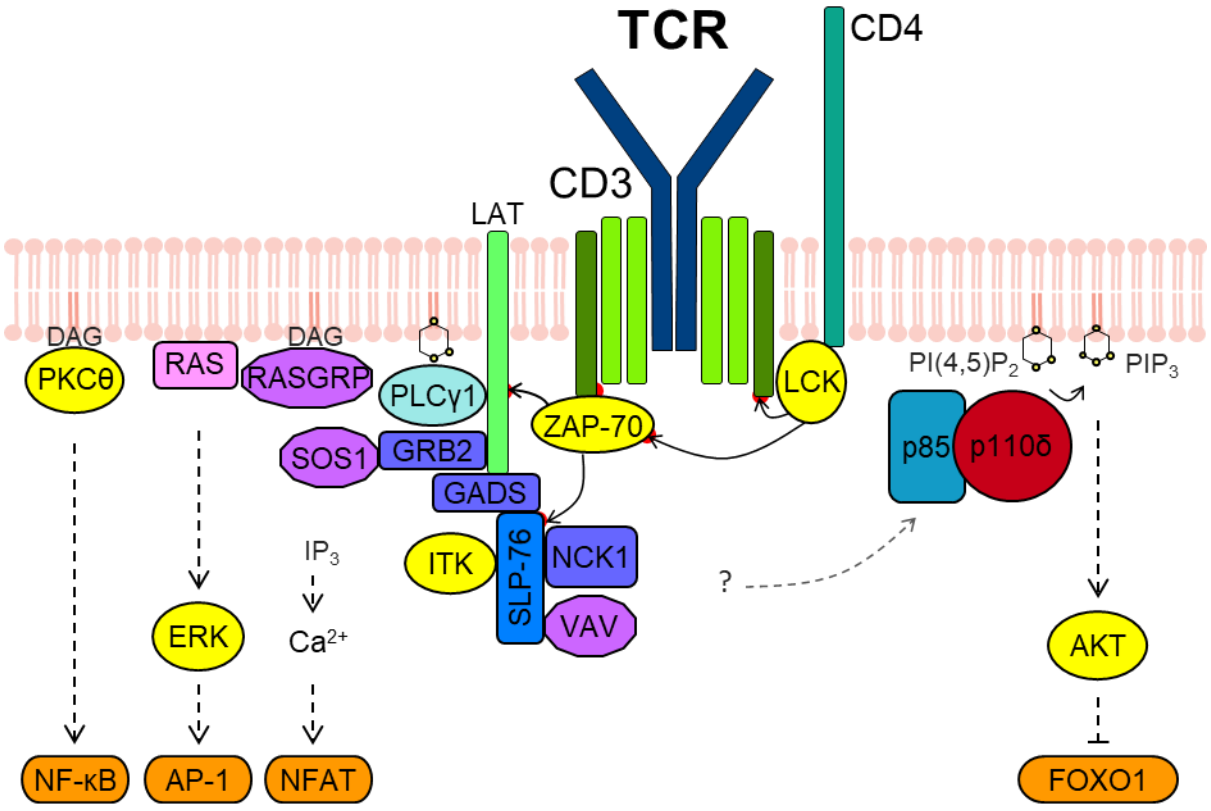


**Figure 1.3 The TCR signalosome**
Following TCR engagement, tyrosine phosphorylation of the CD3 and ζ chain ITAMs and ZAP-70 by LCK, and of the adaptor proteins LAT and SLP-76 by ZAP-70, leads to the recruitment of multiprotein signalling complexes. PLCγ1 catalyses production of the second messengers $IP_3$ and DAG, leading to increased calcium flux and PKCθ localisation to the plasma membrane, while RAS is activated via recruitment of the GEFs, SOS1 and RASGRP. The mechanisms of PI3K recruitment and activation at the TCR signalosome are unclear. Collectively, TCR-induced tyrosine phosphorylation events and protein-protein interactions activate the RAS-ERK, NF-κB, PI3K and calcium signalling pathways, leading to changes in gene regulation orchestrated by the transcription factors NF-κB, AP-1, FOXO1 and NFAT.

### 1.3.2 PI3K-AKT signalling downstream of the TCR

Activation of PI3K is one of the earliest signalling events to occur upon conjugate formation between T cells and APCs. The accumulation of $PIP_3$ can be observed rapidly at the plasma membrane following formation of the immune synapse (Costello *et al*, 2002; Harriague & Bismuth, 2002). Furthermore, p85α heterodimers are recruited to the immune synapse from the cytosol within a few seconds of antigen recognition (Fabre *et al*, 2005). PI3K is thus activated proximal to the TCR and plays a role in early TCR signal transduction via the production of the second messenger $PIP_3$.

$PIP_3$ at the inner leaflet of the plasma membrane serves as a docking site for proteins that contain pleckstrin homology (PH) domains, providing a means of targeting cytosolic proteins to the membrane (Fruman *et al*, 1999). Such proteins include the key TCR signalling effectors PLCγ1, SOS, RAS-GAP, VAV, ITK, and TEC (Balagopalan *et al*, 2010), and the archetypical PI3K effector, AKT. $PIP_3$ activates the serine/threonine kinases AKT and 3-phosphoinositide-dependent kinase 1 (PDK1) via their PH domain-mediated recruitment to the membrane and consequent co-localisation. AKT is autoinhibited in the absence of $PIP_3$ by an interaction between its PH domain and kinase domain (Lučić *et al*, 2018). Binding of the PH domain with $PIP_3$ results in a conformational change that allows phosphorylation of residue T308, located in the catalytic domain activation loop, by PDK1 (Alessi *et al*, 1997). PI3K thus regulates AKT by producing the $PIP_3$ required for co-localisation with PDK1 and subsequent activation (Stokoe *et al*, 1997). Indeed, mutation of the PDK1 PH domain attenuates AKT T308 phosphorylation in T cells (Waugh *et al*, 2009). AKT is additionally phosphorylated at S473 by mammalian target of rapamycin complex 2 (mTORC2) to achieve maximal activation (Sarbassov *et al*, 2005).

AKT modulates a number of key signalling pathways via phosphorylation of its substrates (Figure 1.4). AKT phosphorylates and inhibits TSC1/2, a negative regulator of mTORC1, and thus promotes mTORC1 mediated cell growth, protein synthesis and metabolism through activation of ribosomal protein S6 kinase beta-1 (S6K1) and inhibition of 4E-BP (Laplante & Sabatini, 2012). AKT also inhibits glycogen synthase kinase 3 (GSK3), which leads to increased glycogen synthesis and promotes cell cycle progression by preventing GSK3-mediated degradation of BCL1 (Cyclin D1), c-JUN and c-MYC (Hers *et al*, 2011). In addition to these targets, AKT also translocates to the nucleus and phosphorylates forkhead box O (FOXO) family transcription factors. This promotes the nuclear exclusion and cytosolic sequestration of FOXO, thereby reducing the expression of FOXO target genes that are involved in apoptosis and cell cycle arrest, such as *Bim*

and *FasL* (Hedrick *et al*, 2012). Indeed, FOXO1, the predominant paralogue expressed in T cells, translocates completely from the nucleus in T cells that encounter antigen upon APCs (Fabre *et al*, 2005). Thus, PI3K-AKT signalling induced by antigen recognition promotes cell growth, metabolism and survival during T cell activation.

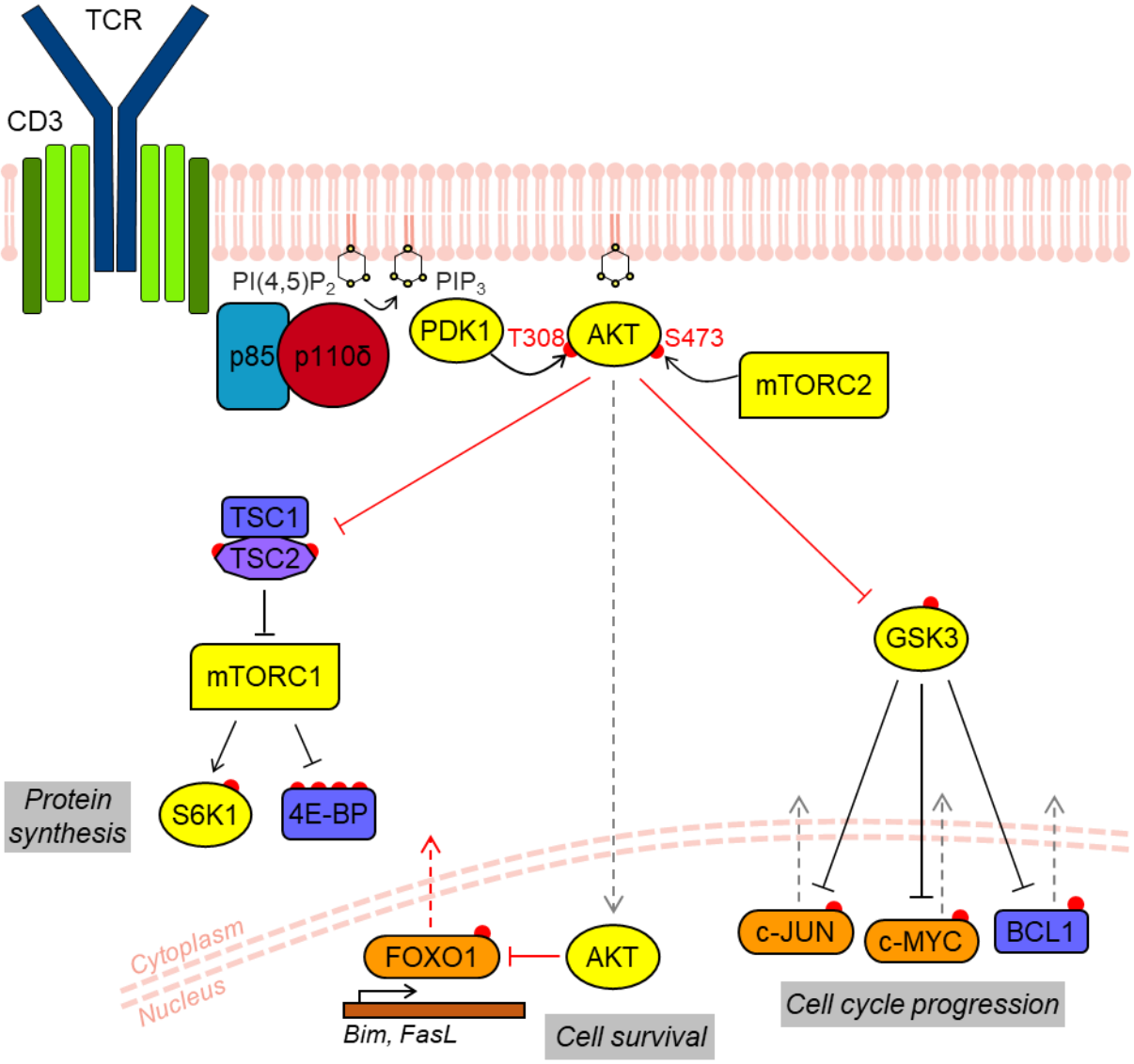


**Figure 1.4 PI3K-AKT signalling downstream of the TCR**
Following TCR engagement, $PIP_3$ produced by PI3K acts as a docking site for PDK1 and AKT at the plasma membrane. AKT is subsequently activated via phosphorylation at T308 and S473 by PDK1 and mTORC2, respectively. AKT phosphorylates the effector proteins TSC2, GSK3 and FOXO1, resulting in their inhibition and ultimately leading to increased protein synthesis, cell survival and cell cycle progression.

### 1.3.3 PI3K recruitment to the TCR signalosome

While the molecular details of PI3K-AKT signalling are well understood, it is unclear precisely how the mature T cell receptor activates this pathway. Recruitment of PI3K to the TCR signalosome and subsequent activation would likely require interaction with proteins containing phosphorylated YxxM motifs, which are specifically recognised by the SH2 domains of the p85 regulatory subunit (Songyang *et al*, 1993).

The CD3 cytoplasmic chains and the adaptors LAT and SLP-76 lack such motifs. Nevertheless, the adaptor protein SLP-76 has been shown to interact with the nSH2 of p85 using a yeast-2-hybrid approach (Shim *et al*, 2004). SLP-76 contains three non-canonical YE(S/P)P tyrosine phosphorylation motifs in its N-terminal region. The SLP-76 association with p85 appears to require either p-Y113 or p-Y128, located within YESP motifs (Shim *et al*, 2004). SLP-76-deficient Jurkat T cells reconstituted with Y113F or Y128F SLP-76 mutants also exhibit impaired AKT activation upon TCR-stimulation (Shim *et al*, 2011). However, these residues are also required for the recruitment of VAV and NCK to the TCR signalosome (Raab *et al*, 1997; Wunderlich *et al*, 1999). Therefore, it is not clear which of these molecules could be involved in PI3K activation, or whether p85 associates with SLP-76 in primary T cells. It has also been suggested that the p85 SH2 domains interact with non-canonical phosphotyrosine motifs in LAT and ZAP-70. An association between p85 and LAT occurs in Jurkat T cells (Zhang *et al*, 1998) and p85 demonstrates direct binding to LAT residues Y171 and Y191 *in vitro*, both of which are located within YVNV motifs (Paz *et al*, 2001). Similarly, ZAP-70 has been shown to interact with the cSH2 of p85 *in vitro* (Moon *et al*, 2005). Whether these interactions occur in a physiological context upon TCR antigen engagement is yet to be shown.

The transmembrane adaptor TCR-interacting molecule (TRIM) has been proposed to act as a PI3K docking site in activated T cells, due to the presence of a YxxM motif in its cytoplasmic domain that is phosphorylated by ZAP-70 (Bruyns *et al*, 1998). However, TRIM-deficient primary $CD4^+$ T cells do not exhibit impaired TCR-dependent activation of AKT, suggesting that this adaptor is not required for PI3K signalling in this context (Kölsch *et al*, 2006).

Aside from phosphotyrosine-mediated recruitment mechanisms, p85 could also form interactions with TCR-associated proteins via its SH3 domain, proline-rich regions and Ras-binding domain. Indeed, Src-family kinases LYN and FYN can interact via their SH3 domains with p85 *in vitro* (Prasad *et al*, 1993; Pleiman *et al*, 1994). Ras-family proteins are thought to activate PI3K lipid kinase activity, synergistically with tyrosine-phosphorylated proteins, through binding

to the catalytic subunit RBD, and may tether the enzyme to the membrane. Additionally, they could recruit PI3K to receptor signalosomes, a role that is illustrated by the Ras GTPase TC21. TC21 can bind to the RBD of p110δ and activate its lipid kinase activity (Rodriguez-Viciana *et al*, 2004). Interestingly, TC21 is constitutively associated with non-phosphorylated ITAMs of the CD3 chains (Delgado *et al*, 2009). TC21-deficient T cells exhibit reduced levels of basal AKT phosphorylation and reduced p85α association with the TCR (Delgado *et al*, 2009). TC21 is therefore hypothesised to be involved in 'tonic' TCR signalling via the PI3K-AKT pathway for T cell homeostasis. However, TC21-deficient T cells also exhibit reduced AKT phosphorylation upon TCR stimulation *in vitro* (Delgado *et al*, 2009). Whether TC21 is involved in p110δ recruitment to the TCR upon antigen engagement, or solely serves to activate p110δ kinase activity in co-operation with a phosphotyrosine-mediated mechanism, is currently unresolved.

Another protein proposed to recruit and activate PI3K upon TCR stimulation is the co-stimulatory receptor, CD28. Its role in this context, however, has been much debated.

### 1.3.4 The role of the CD28 co-stimulatory receptor in TCR-PI3K signalling

Recognition of antigenic peptides presented by MHC molecules induces the TCR signalling pathway, but the outcome on T cell function and fate is also determined by co-stimulatory and co-inhibitory receptors, which are engaged upon the interaction with APCs (Chen & Flies, 2013). This two-signal model of T cell activation, in which both TCR and co-stimulatory signalling are required for full T cell activation, is illustrated by the CD28 co-receptor (June *et al*, 1987). CD28 is constitutively expressed on naïve T cells and provides signals for cell growth and survival upon ligation by its ligand B7-1 (CD80) or B7-2 (CD86), present on the surface of antigen-presenting cells (Esensten *et al*, 2016). CD28 ligation alone fails to activate T cells, but without CD28 co-ligation the TCR can induce an anergic state or cell death (Jenkins *et al*, 1988; Mueller *et al*, 1989).

Clustering of the TCR and CD28 is induced in the early stages of peptide-MHC recognition and is dependent on CD28 ligation by its ligand on the surface of APCs (Yokosuka *et al*, 2008). The cytoplasmic tail of CD28 contains a YMNM motif, which upon tyrosine phosphorylation can bind to p85 (Prasad *et al*, 1994). The importance of this CD28-PI3K interaction in the context of TCR signalling has been a subject of much debate (Rudd & Schneider, 2003). CD28 engagement by its ligand CD80 transiently enhances PI3K recruitment to TCR-CD28 microclusters during initial TCR activation (Yokosuka *et al*, 2008). In addition, $PIP_3$ accumulation at the immune synapse is

reduced in antigen-specific $CD28^{-/-}$ T cells activated by peptide-MHC on APCs, although AKT activation is unimpaired in $CD28^{-/-}$ T cells upon TCR stimulation (Garçon *et al*, 2008). Thus, CD28 contributes to sustaining $PIP_3$ production at the immune synapse. However, studies using T cells expressing the $CD28^{Y170F}$ YMNM mutant demonstrated that direct interaction between PI3K and CD28 via the YMNM motif is not required for $PIP_3$ production at the immune synapse (Garçon *et al*, 2008). Thus, it is thought that CD28 maintains PI3K activity via other means. Indeed, CD28 co-stimulation has been shown to sustain LCK activity at the immune synapse, via an interaction involving the C-terminal PYAP motif in the cytoplasmic domain of CD28 (Holdorf *et al*, 2002; Dobbins *et al*, 2016). LCK binds first to clusters of basic residues in CD28 and then phosphorylates Y207 of the PYAP motif, such that this motif becomes a binding site for the LCK SH2 domain. The ability of CD28 to sustain LCK activity is a plausible mechanism for how CD28 maintains PI3K signalling, given that LCK may phosphorylate other docking sites for p85 at the immune synapse. Thus, there may be a more general role for CD28 in enhancing TCR signalling rather than specifically regulating PI3K activation. Furthermore, CD28 forms a stable complex with PKCθ at the immunological synapse, which is hypothesised to be the specific mediator of CD28 co-stimulatory signalling (Coudronniere *et al*, 2000; Yokosuka *et al*, 2008). Indeed, CD28 associates with RLTPR, a scaffolding protein that is required for CD28 co-stimulation and the localisation of PKCθ and CARMA1 to the immune synapse (Liang *et al*, 2013; Roncagalli *et al*, 2016). Consequently, a crucial function of CD28 co-stimulation during T cell activation is induction of the NF-κB signalling pathway via RLTPR, PKCθ and CARMA1 (Liang *et al*, 2013).

The mechanism of PI3K recruitment to the TCR signalosome clearly remains unresolved. However, it has become clear over the past two decades that the class IA isoform p110δ appears to be preferentially recruited or activated upon TCR signalling

### 1.3.5 p110δ is the dominant PI3K isoform in mature T cells

T lymphocytes express all class I catalytic subunits, albeit p110δ and p110γ are highly enriched compared to p110α and p110β (Okkenhaug *et al*, 2002). The generation of knock-in mice that express PI3K isoforms with loss-of-function point mutations has allowed the precise study of the unique and redundant roles of class I catalytic isoforms in T lymphocytes, while avoiding the compensatory effects associated with deletion of individual isoforms (So & Fruman, 2012). Furthermore, crystal structures of their catalytic ATP-binding pockets led to the development of compounds with selectivity for specific class I isoforms (Vadas *et al*, 2011). Using gene-targeted

mice with an inactivating D910A mutation in the p110δ catalytic domain, p110δ has been shown to play a dominant role in TCR signalling (Okkenhaug *et al*, 2002).

T cells from mice expressing kinase-inactive $p110\delta^{D910A}$ fail to activate AKT phosphorylation upon TCR and CD28 co-stimulation, and do not produce $PIP_3$ above basal levels (Okkenhaug *et al*, 2002; Stark *et al*, 2018). Equally, wild type T cells treated with a p110δ-selective inhibitor demonstrate the same impairment in TCR-induced $PIP_3$ production and AKT activation. (Stark *et al*, 2018). Furthermore, antigen-specific $p110\delta^{D910A/D910A}$ T cells exhibit greatly reduced $PIP_3$ accumulation at the immune synapse formed with antigen-presenting cells, equivalent to T cells treated with a p110δ-selective inhibitor (Garçon *et al*, 2008). These studies have clearly demonstrated that p110δ is the dominant PI3K isoform activated by the TCR in mature T cells, responsible for the majority of the $PIP_3$ produced and essential for subsequent AKT activation.

Additional studies have revealed that mature $CD4^+$ T cell differentiation and effector cytokine production is under the control of p110δ (Okkenhaug *et al*, 2006; Soond *et al*, 2010). $p110\delta^{D910A/D910A}$ $CD4^+$ T cells exhibit reduced proliferation and production of effector cytokines, IFNγ and IL-4, in response to antigen presentation and co-stimulation both *in vitro* and *in vivo* (Okkenhaug *et al*, 2006). Differentiation along the Th1 and Th2 lineages is also impaired in $p110\delta^{D910A/D910A}$ T cells. Similar defects are evident in both naïve and effector/memory $CD4^+$ T cells treated with a p110δ-selective inhibitor, which exhibit supressed proliferation and strongly reduced production of IFNγ and TNFα *in vitro* following TCR stimulation (Soond *et al*, 2010). These studies indicate that p110δ plays an important role in the TCR-induced effector functions of both naïve and previously activated $CD4^+$ T cells (Okkenhaug & Fruman, 2010).

Given the importance and dominance of p110δ activity in T cell activation and function, there is a clear rationale to understand its regulation downstream of TCR engagement. This is only emphasised by the potential of p110δ as a therapeutic target in autoimmune and inflammatory diseases and cancer (So & Fruman, 2012). Despite this interest, the mechanisms that regulate p110δ activity in T cells, and determine isoform-specificity, are still unclear. Therefore, using a combination of proteomic, biochemical and gene editing approaches, this body of work has investigated the molecular basis of p110δ regulation in T lymphocytes. Specifically, with the aim to identify and characterise proteins involved in the recruitment and activation of p110δ downstream of the TCR.

# Chapter 2

# Optimisation of AviTag affinity purification for the study of p110δ interaction partners in primary lymphocytes

## 2.1 Introduction

A key aim of this study was to identify proteins involved in the recruitment and activation of p110δ at the TCR signalosome. The motivation for this was two-fold. First, despite extensive study of the major components involved in TCR-mediated signalling, the precise mechanisms of PI3K recruitment to the TCR are still unclear. Second, while previous genetic and biochemical studies have demonstrated that p110δ is the dominant class IA PI3K isoform in TCR signalling, the reason for this is unknown. One hypothesis is that isoform specificity may be mediated via preferential recruitment or activation of p110δ over p110α. Thus, in both respects, the current understanding of PI3K regulation in T lymphocytes would be advanced by the identification of proteins that specifically interact with the p110δ heterodimer downstream of TCR engagement. To identify physiologically relevant p110δ interactors, this work aimed to study endogenously expressed proteins in primary lymphocytes. Therefore, a system was required for the isolation of specific PI3K p110 isoforms from primary T cells, and the subsequent analysis of associated proteins.

Affinity purification coupled with mass spectrometry (AP-MS) was chosen for this purpose, as it enables unbiased identification of protein-protein interactions under physiological conditions (Gingras *et al*, 2007). AP-MS relies on a method to efficiently isolate protein complexes from cells. A widely used approach involves the introduction of an epitope tag at an endogenous gene locus, leading to expression of a tagged bait protein that can be purified using an affinity matrix specific for the epitope (Dunham *et al*, 2012). In this manner, mice have recently been generated that express the class IA PI3K isoforms fused to the AviTag biotinylation consensus sequence (T. Chessa, unpublished work). The AviTag sequence is inserted at the C-terminus of the mouse *Pik3cd* or *Pik3ca* gene, such that p110δ or p110α are expressed under the control of their endogenous promoters with a 15-amino acid AviTag (Figure 2.1A). This tag is specifically

recognised and biotinylated by the *E. coli* biotin ligase BirA, which can be expressed in transgenic mice (Beckett *et al*, 1999; de Boer *et al*, 2003; Figure 2.1B). Therefore, in parallel with p110-AviTag mice, transgenic mice have also been generated that constitutively express BirA under the control of the endogenous ROSA26 promoter (T. Chessa, unpublished work). Thus, AviTagged p110 isoforms can be biotinylated *in vivo* following co-expression of BirA. The obvious advantage of this system is that AviTagged p110 subunits, and their binding partners, can be purified in a single step from cell lysates using streptavidin-conjugated magnetic beads. Furthermore, the high affinity of the biotin-streptavidin interaction allows for high stringency during purification, without the risk of eluting the tagged protein. Importantly, this system allows for the specific purification of either p110δ or p110α. Naturally biotinylated or biotin-associated proteins, such as biotin-dependent carboxylases (Tong, 2013), would also be captured by streptavidin-conjugated beads. However, by comparison with control purifications from cells expressing BirA alone, it should be possible to exclude these irrelevant proteins from downstream analysis.

Thus, the PI3K-AviTag system was chosen for the study of endogenous p110δ protein-protein interactions in primary T lymphocytes. In this approach, primary T cells would be isolated from mice expressing AviTagged-p110δ and BirA ($p110\delta^{Avi/Avi}BirA^{+/-}$) or mice expressing BirA alone ($BirA^{+/-}$) and stimulated *in vitro* via the TCR (Figure 2.1C). Cells would then be lysed and their lysates subjected to affinity purification using streptavidin-conjugated magnetic beads. The proteins isolated using this technique could then be analysed by immunoblotting and identified by mass spectrometry. This work therefore aimed to validate and optimise the AviTag system for the study of p110δ-specific interaction partners in primary T lymphocytes.

A

```
775  IIFKNGDDLRQDMLTLQMIQLMDVLWKQEGLDLRMTPYGCLPTGDRTGLI  824
825  EVVLHSDTIANIQLNKSNMAATAAFNKDALLNWLKSKNPGEALDRAIEEF  874
875  TLSCAGYCVATYVLGIGDRHSDNIMIRESGQLFHIDFGHFLGNFKTKFGI  924
925  NRERVPFILTYDFVHVIQQGKTNNSEKFERFRGYCERAYTILRRHGLLFL  974
975  HLFALMRAAGLPELSCSKDIQYLKDSLALGKTEEEALKHFRVKFNEALRE  1024
1025 SWKTKVNWLAHNVSKDNRQSGGLNDIFEAQKIEWHE               1060
```

B

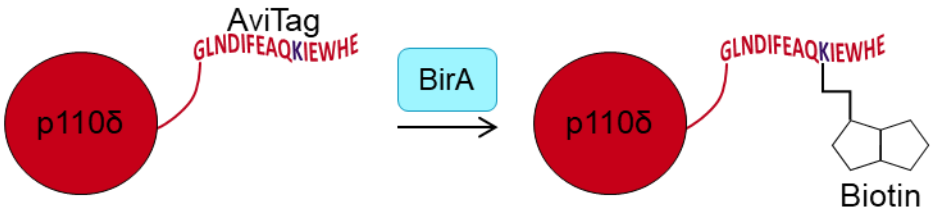


C

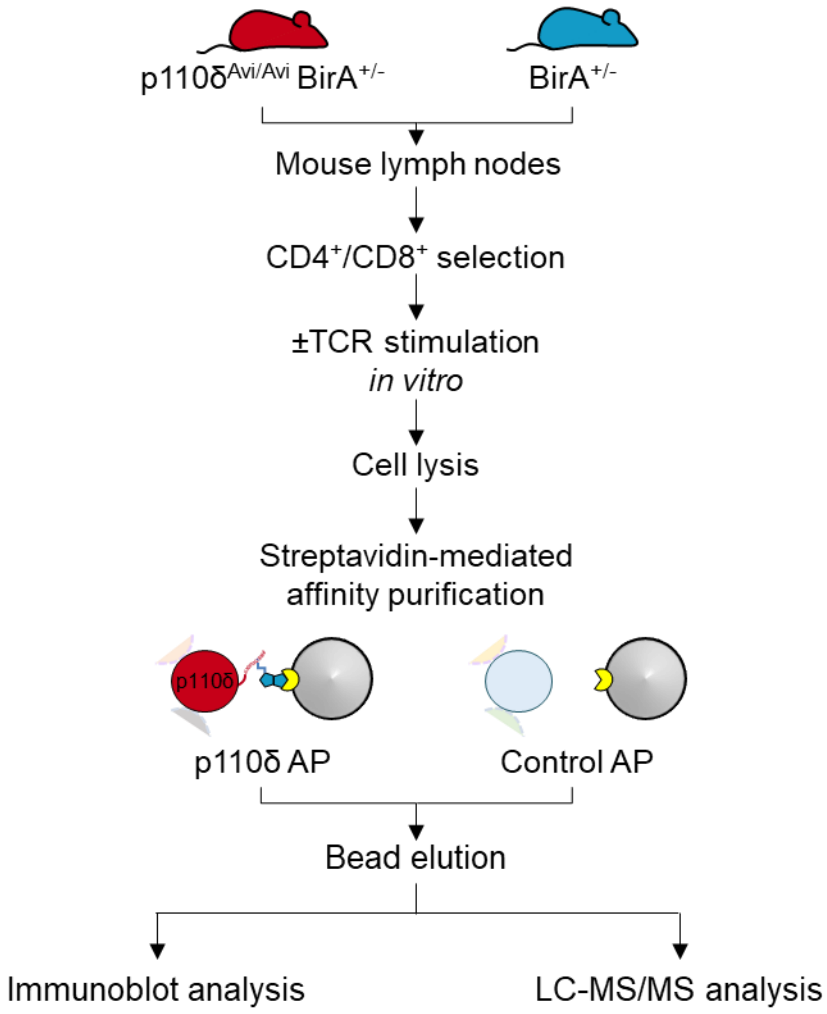

**Figure 2.1 The AviTag affinity purification system for the study of p110δ in primary lymphocytes.**

**A.** The C-terminal amino acid sequence of murine AviTagged-p110δ, comprising the kinase domain (775-1028, yellow), C-terminal tail (1029-1043), 2-amino acid linker (grey) and AviTag sequence (red).

**B.** AviTagged-p110δ (or p110α) is expressed under the control of its endogenous promoter with a C-terminal 15-amino acid AviTag (GLNDIFEAQKIEWHE). This tag acts as a substrate mimic for the *E. coli* biotin ligase, BirA, which specifically recognises and biotinylates the AviTag sequence.

**C.** Strategy for the purification of p110δ from primary T lymphocytes. Lymphocytes are isolated from the lymph nodes of mice expressing AviTagged-p110δ and BirA ($p110\delta^{Avi/Avi}BirA^{+/-}$) or control mice expressing BirA alone ($BirA^{+/-}$) and stimulated *in vitro*. Cells are lysed and p110δ is purified from lysates by incubation with streptavidin-conjugated magnetic beads. Protein complexes are eluted from the beads and subjected to immunoblotting or LC-MS/MS analysis. Non-specific interactors are distinguished from p110δ-specific interactors by comparison of p110δ affinity purifications (APs) with proteins identified in control APs.

## 2.2 Results

### 2.2.1 Validation of the AviTag system for the study of specific PI3K p110 isoforms in primary lymphocytes

It was first determined whether AviTagged p110δ protein was successfully expressed at endogenous levels in primary lymphocytes. To this end, naïve T and B lymphocytes were isolated from the lymph nodes and spleens, respectively, of p110δ$^{Avi/Avi}$ mice homozygous for AviTagged-p110δ. Immunoblotting of cell lysates with antibodies specific for p110δ or the AviTag peptide sequence confirmed that AviTagged-p110δ was expressed in both T and B lymphocytes at an equivalent level to wild type p110δ (Figure 2.2).

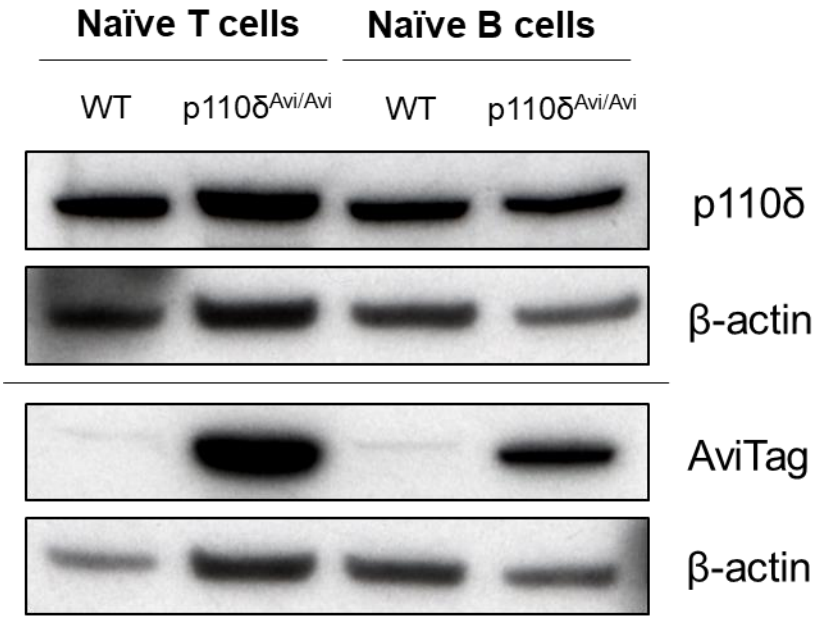


**Figure 2.2 AviTagged p110δ is expressed at endogenous levels in primary naïve T and B lymphocytes from p110δ$^{Avi/Avi}$ mice.**
Immunoblot analysis of cell lysates from wild type and p110δ$^{Avi/Avi}$ naïve T and B lymphocytes. Naïve T and B cells were isolated from the lymph nodes and spleens, respectively, of wild type (WT) and p110δ$^{Avi/Avi}$ mice and 2 million cells of each genotype were lysed. Whole cell lysates were then separated by SDS-PAGE in duplicate. Each half of the immunoblot was probed with anti-p110δ or anti-AviTag and then anti-β-actin.

p110δ$^{Avi/Avi}$ mice were then crossed with BirA$^{+/+}$ mice expressing the biotin ligase BirA to generate p110δ$^{Avi/Avi}$BirA$^{+/-}$ animals. Previous studies have demonstrated that heterozygous expression of BirA is sufficient to biotinylate AviTagged PI3K isoforms *in vivo* (T. Chessa, unpublished work). Experiments were performed to assess whether p110δ was biotinylated in p110δ$^{Avi/Avi}$BirA$^{+/-}$ primary naïve T cells and could thus be purified from cell lysates using

streptavidin-conjugated magnetic beads. Cells were stimulated by crosslinking of CD3 and CD28 and their lysates were incubated with 50 µl streptavidin-conjugated magnetic beads for one hour. Affinity-purified proteins were eluted from the beads by boiling in denaturing LDS gel loading buffer and then analysed by immunoblotting (Figure 2.3). Strikingly, p110δ was completely depleted from cell lysates, and was detected at high abundance in the bead eluate. Furthermore, the p85 regulatory subunit was co-purified with p110δ, as detected using a pan-p85 antibody that recognises all p85 isoforms (Deane *et al*, 2004), indicating successful isolation of the PI3K heterodimer. The presence of the TCR-associated adaptor proteins GRB2 and NCK1 was also investigated but neither could be detected in p110δ affinity purifications by immunoblotting.

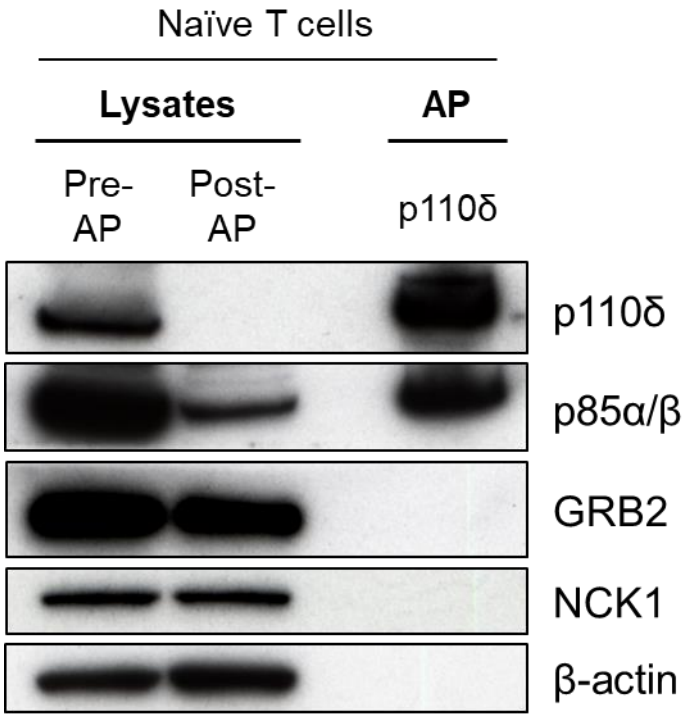


**Figure 2.3 Efficient affinity purification of p110δ and co-purification of p85 from naïve T cells.**
Immunoblot analysis of cell lysates and affinity purifications from $p110\delta^{Avi/Avi}BirA^{+/-}$ naïve T cells. Fifty-two million naïve T cells were isolated from the lymph nodes of 3 mice and stimulated with 1 µg/ml anti-CD3 and 5 µg/ml anti-CD28 for 3 minutes. Cells were lysed and lysates containing 0.318 mg total protein were subjected to affinity purification with 50 µl streptavidin-conjugated magnetic beads for 1 hour at 4 °C. Equal proportions of lysates from before (Pre-AP) and after (Post-AP) bead purification, equivalent to 1.5 million cells, were separated by SDS-PAGE alongside $\frac{2}{7}$ of the bead eluate (AP). Immunoblots were probed with anti-p110δ, anti-pan-p85 (which detects all p85 isoforms; Deane *et al*, 2004), anti-GRB2, anti-NCK1 and anti-β-actin. The immunoblot shown is representative of two independent experiments.

It was clear from this analysis that not all cellular p85 was depleted from lysates upon p110δ affinity purification. This observation was replicated in further experiments, which demonstrated near complete purification of p110δ from naïve $CD4^+$ T cell lysates but not of the p85 isoforms p85α/β, p55α and p50α (Figure 2.4). Lysates from control $BirA^{+/-}$ naïve $CD4^+$ T cells were also subjected to affinity purification. As expected, no depletion of p110δ, p85α/β, p55α or p50α was observed in these lysates, confirming the specificity of the streptavidin-mediated bead purification. Quantification and normalisation of the p85 detected in cell lysates before and after p110δ affinity purification, in two independent experiments, revealed that an average of 17 %, 13 % and 14 % of p85α/β, p55α and p50α, respectively, remained following p110δ purification. To investigate this further, naïve $CD4^+$ T cells were isolated from the lymph nodes of $p110\alpha^{Avi/WT}BirA^{+/-}$ mice, which heterozygously express AviTagged-p110α and BirA. Cell lysates were subjected to affinity purification with streptavidin-conjugated magnetic beads and bead eluates were analysed by immunoblotting for p110α and p85 isoforms (Figure 2.5). AviTagged-p110α, accounting for half of the total p110α expressed, was efficiently purified from lysates. The p85α/β and p50α regulatory subunits were also co-purified with p110α, but p55α could not be detected in bead eluates by immunoblotting. Taken together, this demonstrated that p110α:p85 heterodimers were present in naïve $CD4^+$ T cells and that they likely accounted for a proportion of the residual p85 that remained following affinity purification of p110δ from naïve $CD4^+$ T cell lysates. These experiments also indicated that p110δ forms heterodimers with all p85 isoforms in naïve T cells, while p110α forms heterodimers with p85α/β and p50α, at least. It was also noteworthy that the p50α isoform was more highly expressed than p55α in naïve $CD4^+$ T cells.

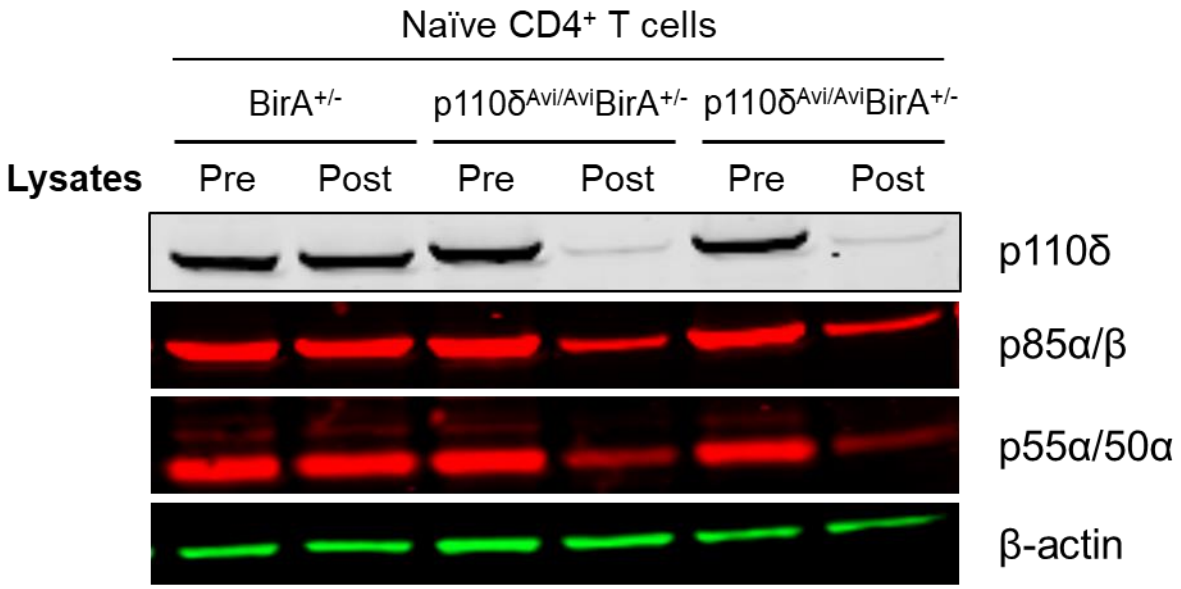


**Figure 2.4 Efficient affinity purification of p110δ from naïve CD4⁺ T cells.**
Immunoblot analysis of cell lysates from BirA$^{+/-}$ and p110δ$^{Avi/Avi}$BirA$^{+/-}$ naive CD4$^{+}$ T cells before and after streptavidin-mediated affinity purification. Naïve CD4$^{+}$ T cells were isolated from the lymph nodes of 3 to 5 mice of each genotype. Lysates from 34, 38 and 25 million cells of each genotype (containing 0.202, 0.143, and 0.133 mg total protein, respectively) were then subjected to affinity purification by incubation with 50 µl streptavidin-conjugated magnetic beads for 1 hr at 4 °C. Equal proportions of lysates from before (Pre) and after (Post) each bead purification were separated by SDS-PAGE and immunoblots were probed for p110δ, p85 (pan-p85) and β-actin. The signal detected for p85α/β, p55α and p50α in post-AP lysates was quantified using Image Studio and normalised to the signal for β-actin in the same lane, and then calculated as a percentage of that in Pre-AP lysates. The three affinity purifications were performed in three independent experiments.

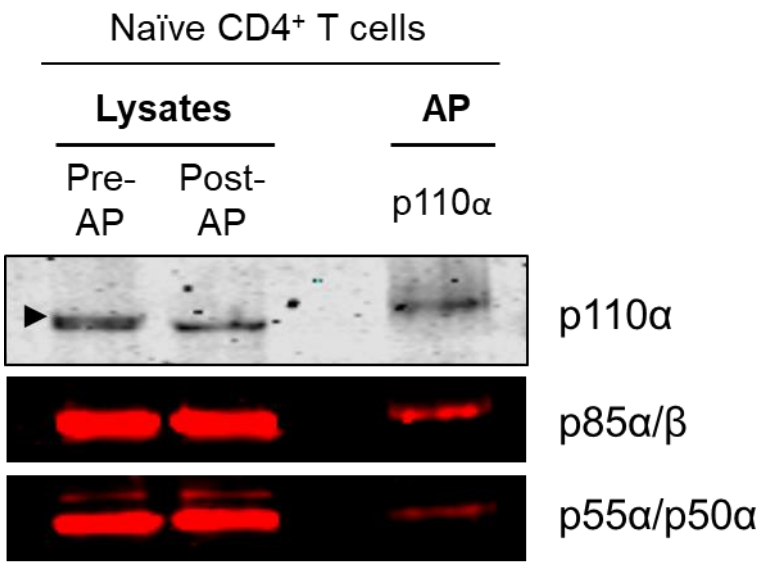


**Figure 2.5 Co-purification of p85 with p110α from naïve CD4⁺ T cells.**
Immunoblot analysis of cell lysates and affinity purifications from p110α$^{Avi/WT}$BirA$^{+/-}$ naïve CD4⁺ T cells. Twenty-five million cells isolated from the lymph nodes of 2 mice were stimulated with 1 µg/ml anti-CD3 and 2 µg/ml anti-CD28 for 2 minutes, lysed and cell lysates were subjected to affinity purification with 50 µl streptavidin-conjugated magnetic beads for 1 hour at 4 °C. Equal proportions of lysates from before (Pre-AP) and after (Post-AP) bead purification were separated by SDS-PAGE alongside $\frac{2}{7}$ of the p110α affinity purification (AP). Immunoblots were probed for p110α and p85 (pan-p85). AviTagged-p110α appears as a higher molecular weight species to wild type p110α in heterozygous Pre-AP lysates, indicated with a black arrow. The blot shown is representative of two independent experiments.

These initial experiments demonstrated that the AviTag affinity purification system was an efficient method for isolating endogenous p110δ from primary naïve lymphocytes. The aim of this study was to use this approach to purify p110δ-associated proteins from primary T cells for subsequent MS identification. This technique, affinity purification coupled with mass spectrometry (AP-MS), requires a high amount of starting material (total cellular protein) to enable detection of low abundance interactors and transient protein-protein interactions (Morris *et al*, 2014). Accordingly, recent studies using AP-MS to study TCR-associated proteins in primary T cells have used $1 \times 10^8$ activated and expanded CD4⁺ T cells for each affinity purification (Roncagalli *at al*, 2014; Voisinne *et al*, 2016). In the experiments presented here thus far, only 0.133 – 0.318 mg of total protein was obtained for each purification from 25 – 52 million naïve T cells, which were isolated from up to five mice. Indeed, preliminary qualitative LC-MS/MS analyses of these p110δ purifications did not identify any proteins at a level of abundance that would enable their designation as specific p110δ interactors with any confidence. In addition, the majority of the proteins identified were present in purifications

from both $BirA^{+/-}$ and $p110\delta^{Avi/Avi}BirA^{+/-}$ cells. These outcomes were likely due to the low amount of starting material and a high abundance of non-specific background interactors.

Consequently, the AviTag-AP approach was modified in two respects. First, the technique was adapted to purify p110δ from *in vitro* activated and expanded primary T cell blasts. Second, the affinity purification protocol was optimised in an effort to reduce non-specifically interacting proteins while maintaining interactions with low affinity or transient binding partners.

### 2.2.2 Validation and optimisation of p110δ AviTag-mediated affinity purification from primary T blasts

To increase the amount of protein subjected to affinity purification, subsequent experiments aimed to purify p110δ from primary T blasts, as blasted lymphocytes are larger in size than naïve T cells and can be expanded to high numbers *in vitro*. For this purpose, cells were isolated from the lymph nodes of $p110\delta^{Avi/Avi}BirA^{+/-}$ mice and activated for 48 hours with soluble anti-CD3, followed by expansion for 5 days in the presence of IL-2 to generate T blasts. Total T blasts were then purified, rested without IL-2 for 75 minutes, and stimulated by crosslinking of CD3 and CD28 for 2 minutes. The efficiency of the AviTag-AP approach for the isolation of AviTagged-p110δ from more than $1 \times 10^8$ T blasts was then investigated.

To this end, lysates from $1.42 \times 10^8$ stimulated T blasts were subjected to affinity purification using streptavidin-conjugated magnetic beads. Two durations of bead incubation were tested in parallel: 1 hour, as used previously, and 30 minutes. This shorter time was chosen with the intention to minimise both the loss of transient interactions with p110δ and the extent of non-specific binding to the magnetic beads. In addition, following bead incubation, three stringent, timed wash steps were performed at 4°C. Cell lysates from before and after bead purification were then analysed by immunoblotting (Figure 2.6). This revealed that a 30-minute bead incubation was sufficient to isolate 97 % of p110δ from cell lysates.

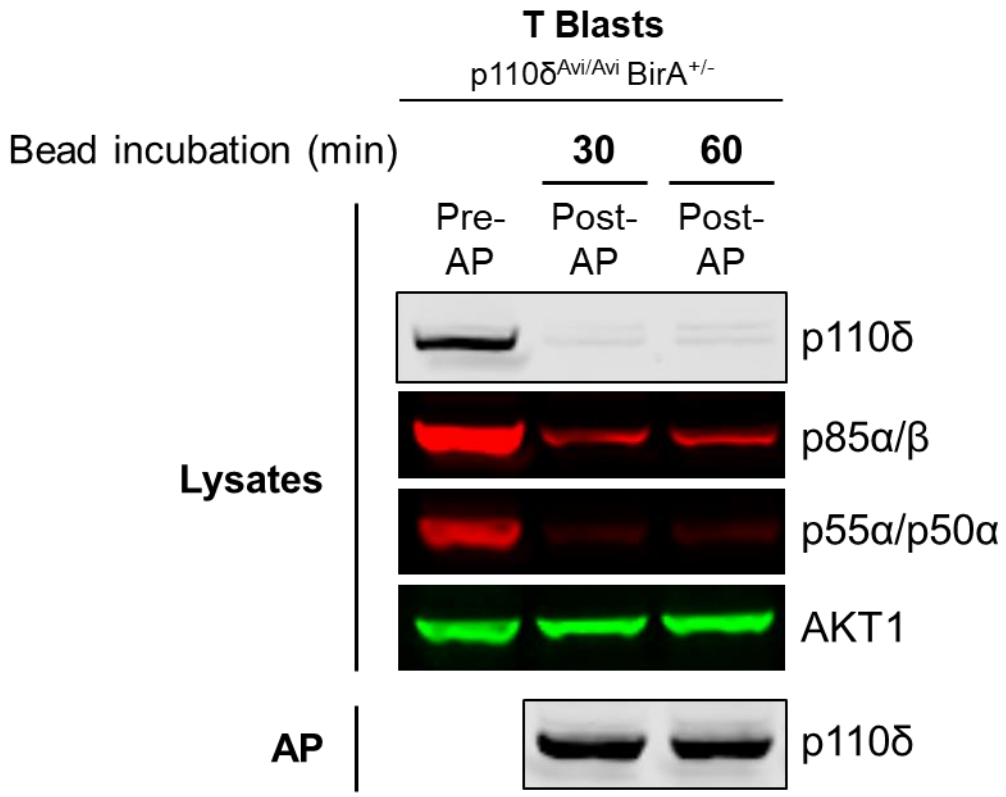


**Figure 2.6 Thirty-minutes bead incubation is sufficient to efficiently isolate p110δ from T blasts.**
Immunoblot analysis of cell lysates and affinity purifications from p110δ$^{Avi/Avi}$BirA$^{+/-}$ T blasts. Lysates from 142 million total T blasts that had been stimulated with 1 µg/ml anti-CD3 and 2 µg/ml anti-CD28 were subjected to affinity purification by incubation with 80 µl streptavidin-conjugated magnetic beads for either 30 minutes or 60 minutes at 4°C. Lysates equivalent to 4 million cells from before (Pre-AP) and after (Post-AP) bead purification were separated by SDS-PAGE alongside $\frac{1}{5}$ of each p110δ affinity purification (AP). Immunoblots were probed for p110δ, p85 (pan-p85) and AKT1. The signal detected for p110δ in Post-AP lysates was quantified using Image Studio and normalised to the signal for β-actin in the same lane, and then calculated as a percentage of p110δ in Pre-AP lysate.

Affinity purifications using this protocol were then performed on lysates from 1 × $10^8$ BirA$^{+/-}$, p110δ$^{Avi/Avi}$BirA$^{+/-}$ and p110α$^{Avi/WT}$BirA$^{+/-}$ CD4$^+$ T blasts, each containing ~1.7 mg total protein (Figure 2.7). Thus, the amount of protein subjected to affinity purification was approximately 3-fold that which could be obtained from an equal number of naïve T cells. Immunoblotting of the bead eluates demonstrated successful isolation of p110δ and all p85 regulatory subunits from p110δ$^{Avi/Avi}$BirA$^{+/-}$ T blasts, following 30 minutes incubation with 60 µl streptavidin-conjugated magnetic beads and strict wash steps (Figure 2.7). Importantly, the purification of p110δ was specific; neither p110δ nor p85α could be detected by immunoblotting in bead eluates from BirA$^{+/-}$ control purifications. Equally, p110δ could not be detected in p110α$^{Avi/WT}$BirA$^{+/-}$

purifications. Immunoblotting of lysates from the same experiment also confirmed that p110δ was expressed at equivalent levels in $BirA^{+/-}$, $p110\delta^{Avi/Avi}BirA^{+/-}$ and $p110\alpha^{Avi/WT}BirA^{+/-}$ $CD4^+$ T blasts.

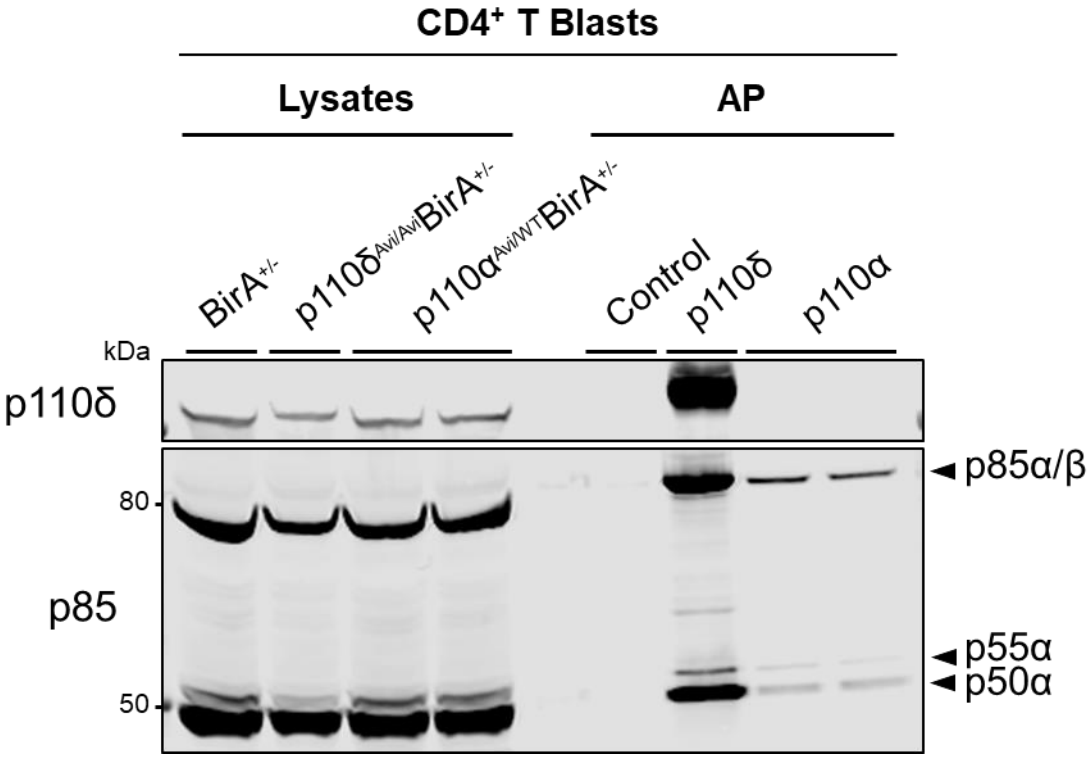


**Figure 2.7 Co-purification of p85 with p110δ and p110α from $CD4^+$ T blasts.**
Immunoblot analysis of cell lysates and affinity purifications from $p110\delta^{Avi/Avi}BirA^{+/-}$, $p110\alpha^{Avi/WT}BirA^{+/-}$ and $BirA^{+/-}$ (Control) $CD4^+$ T blasts. Lysates from $1 \times 10^8$ cells of each genotype, containing 1.685 ± 0.144 mg (mean ± SD, n=4) total protein were subjected to affinity purification by incubation with 60 µl streptavidin-conjugated magnetic beads for 30 min at 4 °C. Lysates equivalent to 2 million cells from before bead purification were separated by SDS-PAGE alongside $\frac{2}{7}$ of each control, p110δ and p110α affinity purification (AP). Immunoblots were probed for p110δ and p85 (pan-p85).

Collectively, this work demonstrated that AviTagged-p110δ could be purified efficiently and specifically from primary $CD4^+$ T blasts following a 30-minute one-step incubation with streptavidin-conjugated magnetic beads.

### 2.2.3 Optimisation of *in vitro* TCR stimulation of $CD4^+$ T blasts

This study intended to use the AviTag-AP approach to isolate proteins that associate with p110δ upon TCR stimulation. Engagement of the TCR induces extensive tyrosine phosphorylation of multiple proteins at the TCR signalosome (Guy & Vignali, 2009), and these phosphorylation

events are likely to be important for transient p85-SH2 domain-mediated interactions that lead to the recruitment and activation of p110δ. Earlier optimisation of the AviTag-AP protocol shortened the bead incubation time and performed all wash steps at 0 - 4°C in an effort to maintain transient interactions with p110δ. Nevertheless, it was also important to preserve TCR-induced phosphorylation events during bead purification by inhibiting protein phosphatases released upon cell membrane disruption. Therefore, the lysis buffer composition was examined.

The standard lymphocyte lysis buffer used in previous experiments contained sodium fluoride, which acts as an inhibitor of serine/threonine phosphatases. This recipe was improved further by the addition of the serine/threonine phosphatase inhibitors β-glycerophosphate and sodium pyrophosphate. Most importantly, the tyrosine phosphatase inhibitor sodium orthovanadate was also supplemented. The efficacy of the two lysis buffers was then compared by investigating the level of total cellular protein tyrosine phosphorylation in lysates from CD3+CD28 stimulated T cells (Figure 2.8). Immunoblotting of cell lysates showed that the modified lysis buffer preserved a greater number of stimulation-induced protein tyrosine phosphorylation events. However, this experiment also revealed that the extent of protein tyrosine phosphorylation induced by CD3 and CD28 crosslinking was noticeably low. This prompted work to optimise the conditions for TCR stimulation of $CD4^+$ T blasts. For this, the magnitude of cellular protein tyrosine phosphorylation upon TCR crosslinking was taken as a proxy for the extent of successful TCR signalosome activation. It was theorised that maximising TCR activation would induce the greatest number of interactions at TCR signalosomes, including those involved in the recruitment and activation of PI3K. Thus, it would be more likely that TCR stimulation-dependent p110δ protein interactions would be captured by affinity purification.

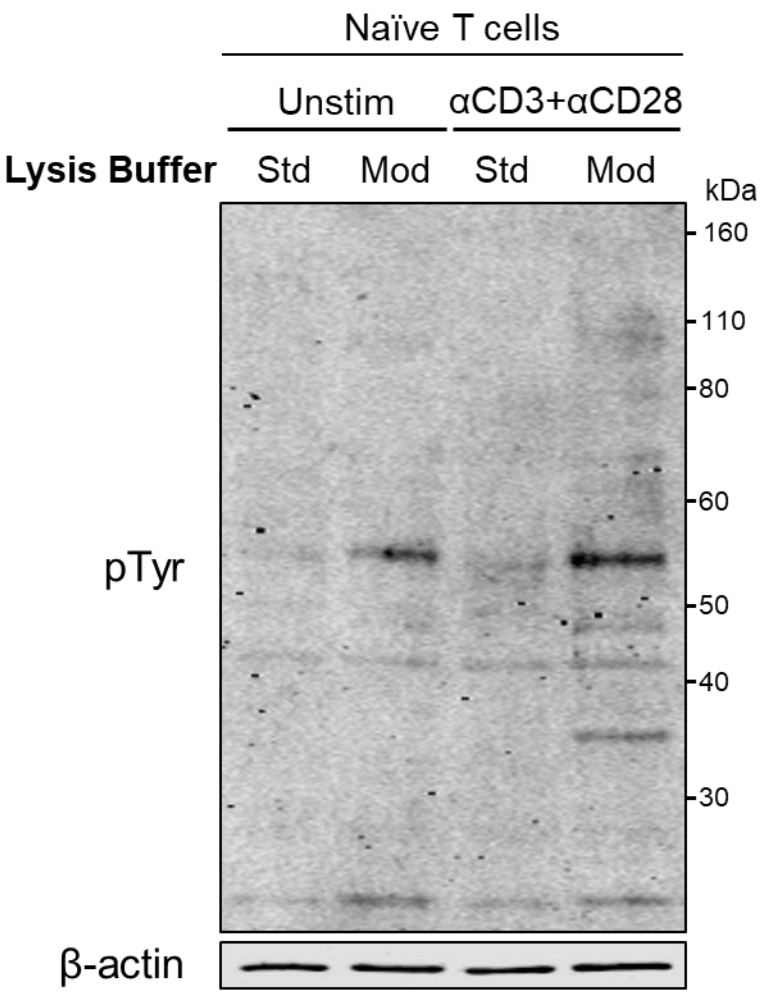


**Figure 2.8 Improved lysis buffer composition preserves total cellular protein tyrosine phosphorylation.**
Immunoblot analysis of cell lysates from p110δ$^{Avi/Avi}$BirA$^{+/-}$ primary naïve total T cells. Ten million cells per condition were incubated on ice for 30 minutes with 1 µg/ml anti-CD3 plus 2 µg/ml anti-CD28 (αCD3+αCD28) followed by crosslinking with anti-hamster IgG for 2 minutes at 37°C, or left unstimulated (Unstim) for 2 minutes at 37°C. Cells were lysed for 10 minutes on ice with either standard (Std) lysis buffer (1 % IGEPAL CA-630, 50 mM HEPES, 150 mM NaCl, 5 mM EDTA, 10 mM NaF, 10 mM Iodoacetamide, 5 mM protease inhibitor cocktail) or a modified (Mod) lysis buffer (1 % IGEPAL CA-630, 50 mM HEPES, 150 mM NaCl, 1 mM EDTA, 1 mM EGTA, 25 mM NaF, 10 mM Iodoacetamide, 2.5 mM sodium pyrophosphate, 5 mM β-glycerophosphate, 5 mM sodium orthovandate, 5 mM protease inhibitor cocktail). Lysates equivalent to 0.3 × $10^6$ cells were separated by SDS-PAGE and immunoblots were probed for phosphorylated tyrosine residues (pTyr) and β-actin.

The experiments presented thus far stimulated T cells by crosslinking antibodies targeted to CD3 and CD28 on the cell surface. This aimed to mimic the clustering of the TCR and CD28 co-stimulatory receptor that is induced in the early stages of MHC-presented peptide recognition by the TCR, which is dependent on CD28 ligation by its ligand B7-1 or B7-2 on antigen-

presenting cells (Yokosuka *et al*, 2008). Nevertheless, the co-receptor CD4 also interacts with antigen-presenting MHC class II (König *et al*, 1992). This proximity to the TCR complex allows LCK associated with the CD4 cytoplasmic tail to phosphorylate CD3 ITAMs, leading to the initiation and amplification of the TCR signalling cascade (Barber *et al*, 1989; Holdorf *et al*, 2002; Wang *et al*, 2010).

Therefore, combinations of CD3, CD28 and CD4 crosslinking were investigated for their ability to induce protein tyrosine phosphorylation (pTyr) in p110$\delta^{Avi/Avi}$BirA$^{+/-}$ CD4$^{+}$ T blasts (Figure 2.9). Doubling of the anti-CD3 and anti-CD28 antibody concentrations used in previous experiments had little effect on induced pTyr. In contrast, addition of anti-CD4 greatly increased the level of pTyr induced upon crosslinking. Furthermore, absence of anti-CD28 did not reduce this level of pTyr. Therefore, crosslinking of CD3 and CD4 appeared to induce the greatest extent of protein tyrosine phosphorylation, while successfully activating AKT, and was thus used in subsequent experiments for TCR stimulation.

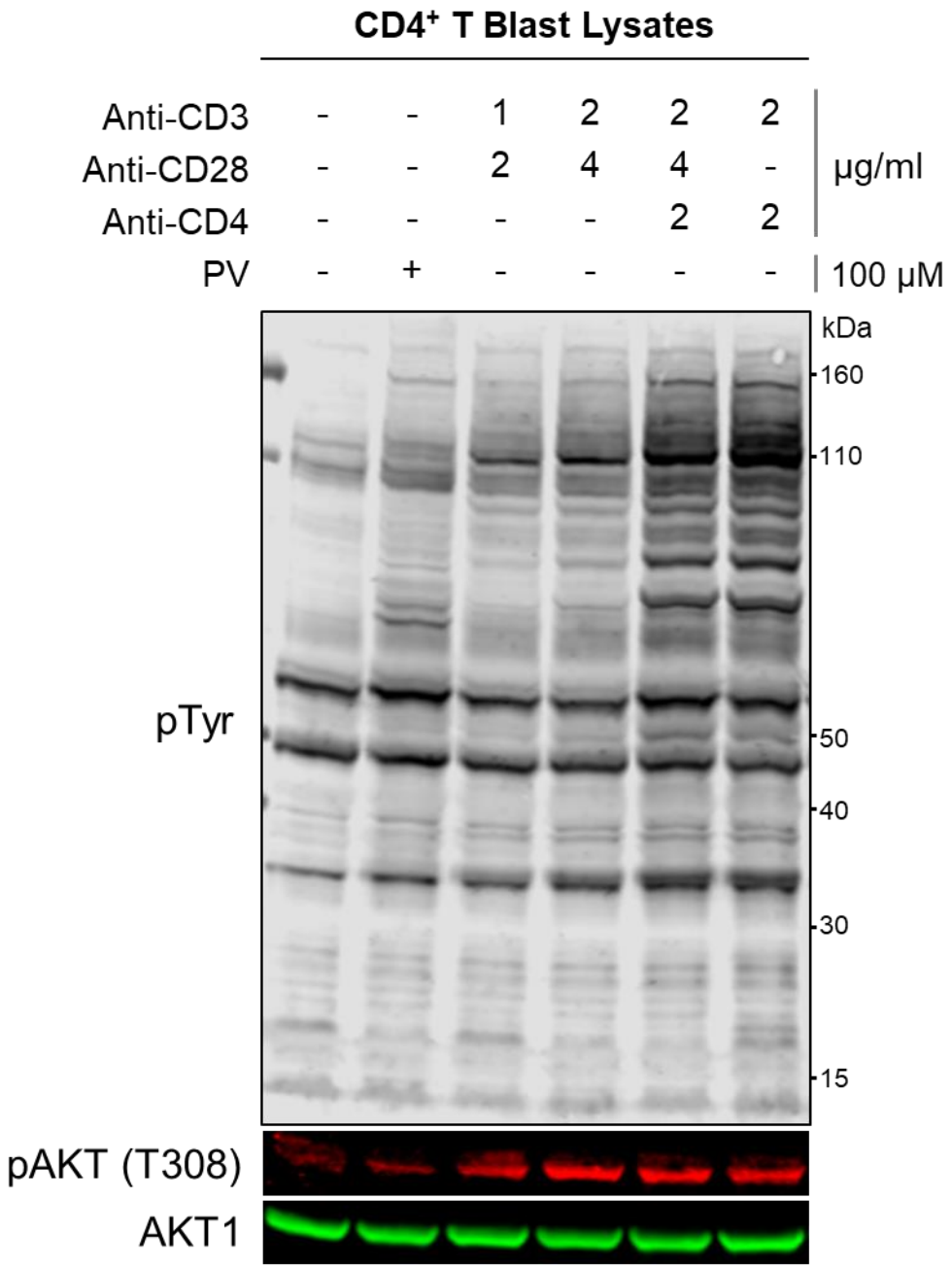


**Figure 2.9 Greatest cellular protein tyrosine phosphorylation in CD4⁺ T blasts is achieved by CD3 and CD4 crosslinking.**

Immunoblot analysis of cell lysates from p110δ$^{Avi/Avi}$BirA$^{+/-}$ CD4⁺ T blasts. Thirty-million CD4⁺ T blasts per condition were incubated on ice for 30 minutes with anti-CD3 plus anti-CD28 or anti-CD4 in the combinations and concentrations indicated, followed by crosslinking with 13 µg/ml anti-hamster IgG for 2 minutes at 37°C, or were left unstimulated or stimulated with 100 µM pervanadate (PV) for 2 minutes at 37°C. Lysates equivalent to 1.5 million cells were separated by SDS-PAGE and immunoblots were probed for phosphorylated tyrosine residues (pTyr), phosphorylated AKT (pAKT T308) and total AKT1.

The optimal time point for TCR stimulation-induced protein tyrosine phosphorylation was also investigated. p110δ$^{Avi/Avi}$BirA$^{+/-}$ CD4$^{+}$ T blasts were stimulated by crosslinking of anti-CD3 and anti-CD4 for between 30 seconds and 3 minutes and lysates were analysed by immunoblotting (Figure 2.10). This revealed that the greatest levels of total cellular pTyr were induced between 1 – 2 minutes of crosslinking. Cell lysates were also subjected to affinity purification with streptavidin-magnetic beads to isolate p110δ, and the bead eluates were then analysed by immunoblotting for pTyr and p110δ. Intriguingly, multiple tyrosine-phosphorylated proteins were co-purified with p110δ from stimulated cells (Figure 2.10). These associations appeared to peak at 1 minute of crosslinking. Based on these observations, TCR stimulation via anti-CD3 and anti-CD4 crosslinking for 1 minute was used in subsequent experiments. It was also apparent from these experiments that p110δ was constitutively tyrosine phosphorylated in CD4$^{+}$ T blasts. Moreover, a prominently tyrosine-phosphorylated protein of ~115 kDa appeared to associate with p110δ upon TCR stimulation.

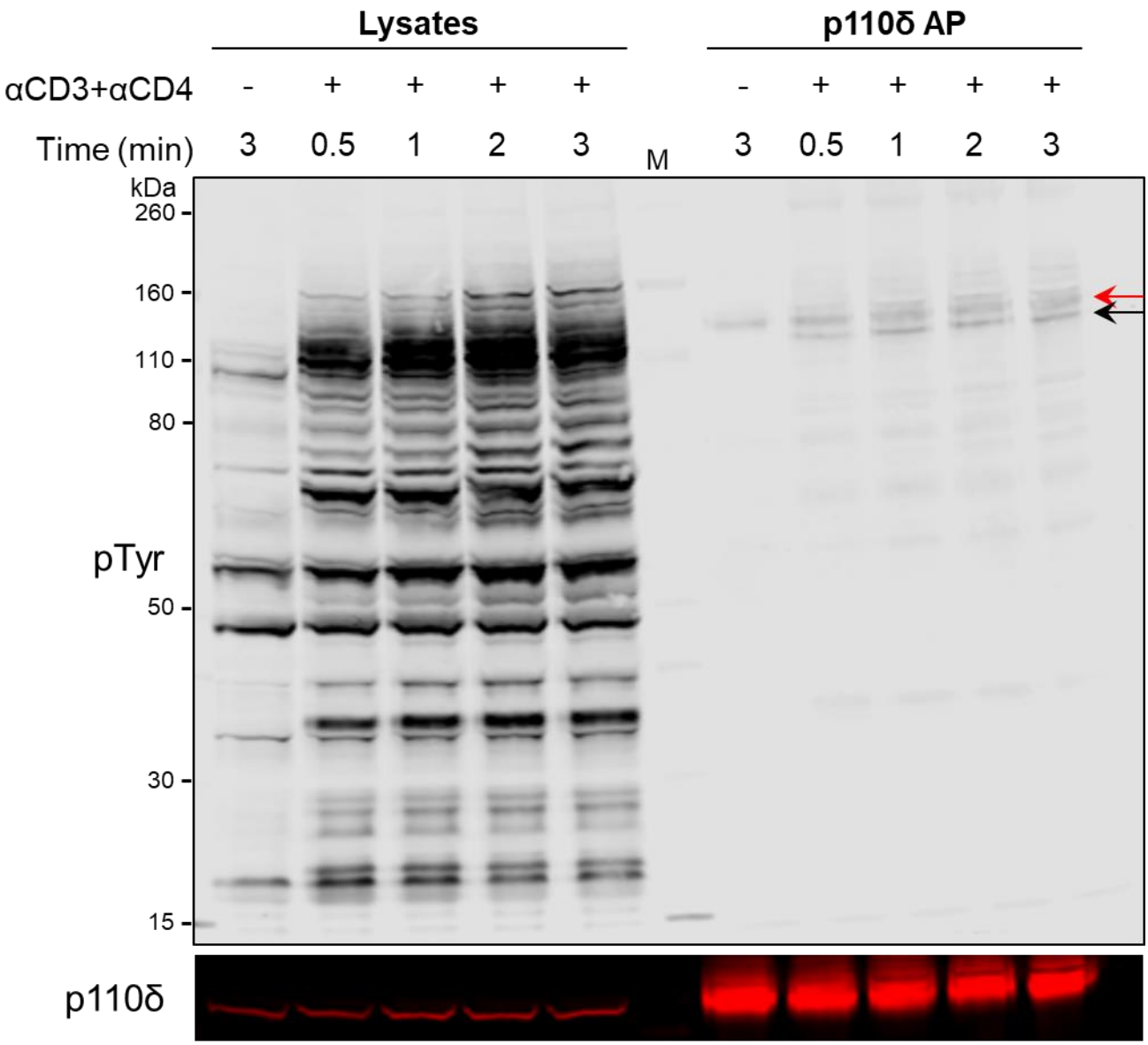


**Figure 2.10 Investigating the optimal timepoint for TCR stimulation to induce maximal cellular protein tyrosine phosphorylation in CD4⁺ T blasts.**
Immunoblot analysis of cell lysates and affinity purifications from p110δ$^{Avi/Avi}$BirA$^{+/-}$ CD4⁺ T blasts. Fifty-three million CD4⁺ T blasts per condition were incubated on ice for 30 minutes with 2 µg/ml anti-CD3 plus anti-CD4 followed by crosslinking at 37°C with 13 µg/ml anti-hamster IgG for the times indicated, or left unstimulated (-) for 3 minutes at 37°C. Cell lysates were then subjected to affinity purification using 60 µl streptavidin-conjugated magnetic beads. Lysates equivalent to 1.3 million cells from before bead purification were separated by SDS-PAGE alongside $\frac{2}{7}$ of each p110δ affinity purification (AP). Immunoblots were probed for phosphorylated tyrosine residues (pTyr) and p110δ. The immunoblot shown is representative of two independent experiments. The red arrow indicates the position of p110δ. The black arrow highlights a prominently tyrosine-phosphorylated protein of ~115 kDa that co-purified with p110δ. M indicates the marker lane.

It was next investigated whether doubling the anti-CD3 and anti-CD4 concentrations used for TCR stimulation would further increase total cellular pTyr or the number of pTyr proteins associated with p110δ. There was a noticeable increase in the tyrosine phosphorylation of higher molecular weight proteins in whole cell lysates from cells stimulated with the higher anti-CD3 and anti-CD4 antibody concentration (Figure 2.11). The tyrosine phosphorylation status of LAT (linker for activation of T cells) was also examined. LAT is phosphorylated by the tyrosine kinase ZAP-70 upon TCR activation and acts as an adaptor for multiple SH2 domain-containing proteins involved in the amplification of TCR signalling (Zhang *et al*, 1998). Tyrosine phosphorylation of a protein that migrated by SDS-PAGE according to the position of LAT was enhanced using the higher concentration of anti-CD3 and anti-CD4 (Figure 2.11). $p110\delta^{Avi/Avi}BirA^{+/-}$ cell lysates from this experiment were also subjected to affinity purification with streptavidin-magnetic beads to isolate p110δ, and the bead eluates were analysed by immunoblotting. There were slightly more pTyr proteins co-purified with p110δ following stimulation with the doubled concentration of anti-CD3 and anti-CD4. These pTyr bands were also more pronounced, suggesting that the phosphorylated proteins were purified at higher abundance. Strikingly, tyrosine-phosphorylated proteins were not detected by immunoblotting in control purifications from $BirA^{+/-}$ cells. This indicated that the tyrosine-phosphorylated proteins isolated by affinity purification were specifically associated with p110δ.

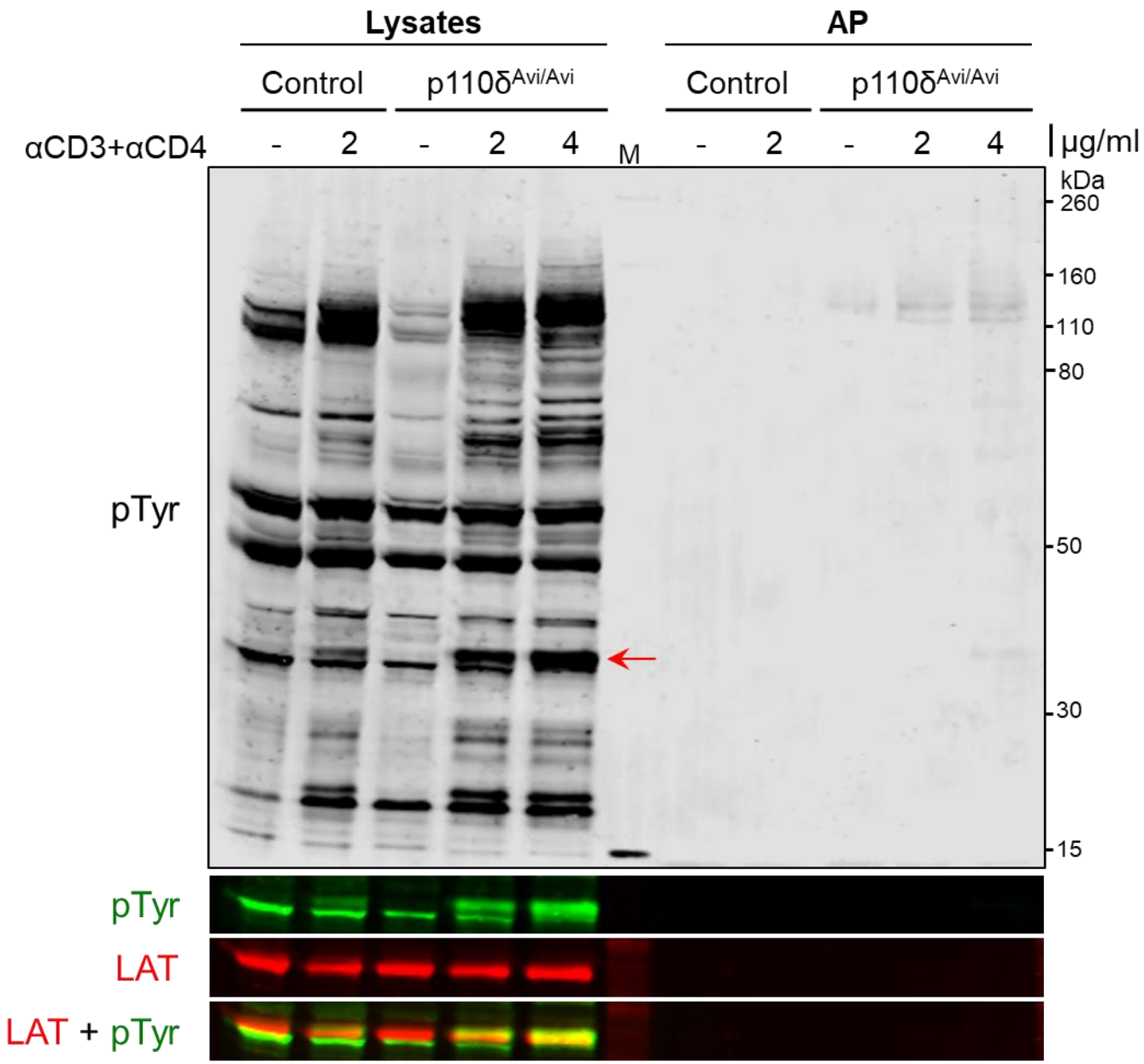


**Figure 2.11 Increased antibody concentrations for TCR crosslinking induce maximal cellular protein tyrosine phosphorylation and tyrosine phosphorylation of LAT in CD4⁺ T blasts.**
Immunoblot analysis of cell lysates and affinity purifications from p110δ$^{Avi/Avi}$BirA$^{+/-}$ (p110δ$^{Avi/Avi}$) and BirA$^{+/-}$ (Control) CD4⁺ T blasts. Fifty million CD4⁺ T blasts per condition were incubated on ice for 30 minutes with 2 µg/ml or 4 µg/ml anti-CD3 and anti-CD4 (αCD3+αCD4), followed by crosslinking at 37°C with 13 µg/ml anti-hamster IgG for 1 minute, or left unstimulated (-) at 37°C for 1 minute. Cell lysates were subjected to affinity purification by incubation with 30 µl streptavidin-conjugated magnetic beads for 30 min at 4 °C. Lysates equivalent to 1.2 million cells from before bead purification were separated by SDS-PAGE alongside half of each control and p110δ affinity purification (AP). Immunoblots were probed for phosphorylated tyrosine residues (pTyr) and LAT. The signals detected for pTyr and LAT are overlaid in the fourth panel in green and red, respectively. The red arrow represents the position of LAT on the pTyr blot. M indicates the marker lane.

Collectively, these experiments led to an optimised protocol for the efficient and specific purification of p110δ and associated proteins from $CD4^+$ T blasts (Figure 2.12). TCR stimulation of $CD4^+$ T blasts with 4 μg/ml anti-CD3 and anti-CD4 for 1 minute induced robust cellular tyrosine phosphorylation. p110δ protein could be efficiently purified from the lysates of $1 \times 10^8$ $CD4^+$ T blasts by incubation for only 30 minutes with 60 μl streptavidin-conjugated magnetic beads, followed by strict wash steps. Intriguingly, tyrosine-phosphorylated proteins could be co-purified specifically with p110δ in a TCR-stimulation dependent manner, including a prominently tyrosine-phosphorylated protein of ~115 kDa.

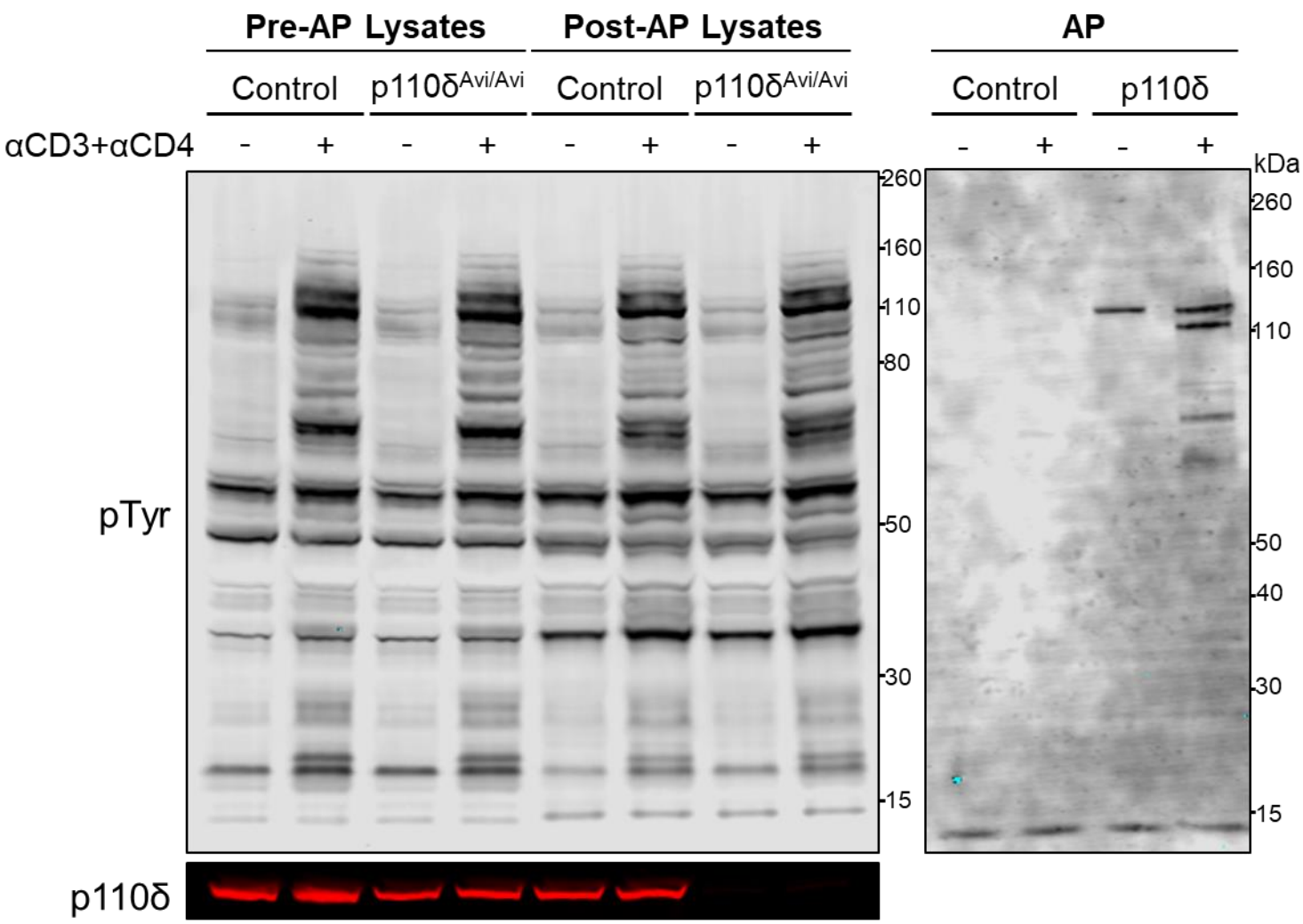


**Figure 2.12 An optimised protocol for efficient and specific AviTag-mediated affinity purification of p110δ from CD4⁺ T blasts.**

Immunoblot analysis of cell lysates and affinity purifications from p110δ$^{Avi/Avi}$BirA$^{+/-}$ (p110δ$^{Avi/Avi}$) and BirA$^{+/-}$ (Control) CD4$^{+}$ T blasts. One-hundred million CD4$^{+}$ T blasts per condition were stimulated by crosslinking 4 µg/ml αCD3+αCD4 for 1 minute (+), or were left unstimulated (-), and cell lysates were subjected to affinity purification with 60 µl streptavidin-conjugated magnetic beads for 30 min at 4°C. Lysates equivalent to 2.5 million cells from before (Pre-AP) and after (Post-AP) bead purification and $\frac{1}{5}$ of each control and p110δ affinity purification (AP) were separated by SDS-PAGE in parallel. Immunoblots were probed for phosphorylated tyrosine residues (pTyr) and p110δ.

## 2.3 Discussion

This work has demonstrated that the AviTag system is a valuable tool for the study of endogenous PI3K in primary lymphocytes. The isoforms p110δ and p110α could be purified efficiently and specifically from both naïve and blasted primary T cells that expressed AviTagged proteins and the biotin ligase BirA. The advantages of this approach for the investigation of PI3K protein-protein interaction are numerous. Firstly, the tagged isoforms were shown to be expressed at endogenous levels. Alternative systems that stably or transiently express tagged proteins often result in overexpression at non-physiological levels. This would likely lead to artefacts in interatomic studies, as the tagged proteins may associate with proteins that they do not normally bind (Aebersold & Mann, 2003). Conversely, lower than physiological expression levels may have the opposite effect. Secondly, AviTagged p110δ and p110α are expressed in primary cells, thus allowing their study in a physiological environment where protein localisation, post-translational modification and signalling-induced interactions should closely reflect those in the *in vivo* situation. This would not be possible using cell lines expressing tagged p110δ. For example, immortalised Jurkat T cells, which are commonly used in proteomics studies to investigate TCR signalling (Nguyen *et al*, 2009; Cao *et al*, 2012; Salek *et al*, 2013; Helou & Salomon, 2015), lack expression of the lipid phosphatases PTEN and SHIP1 that regulate PI3K signalling by dephosphorylating $PIP_3$ (Gioia *et al*, 2018). The use of primary T lymphocytes to study PI3K is therefore a better model of the physiological situation, as all endogenously expressed proteins should be present.

Consequently, the AviTag system offers a unique approach to isolate and identify physiologically relevant, TCR-induced protein-protein interactions involving PI3K. However, the potential of this system can only be realised if such interactions are captured and preserved, in sufficient abundance, upon purification of p110δ. Activated and expanded T blasts were therefore used to increase the quantity of protein subjected to affinity purification, as in previous studies (Roncagalli *at al*, 2014; Voisinne *et al*, 2016). This had two purposes; to compensate for the loss of protein during washing, and to increase the probability that low abundance interactors would be detected in downstream MS analyses.

It was of equal importance to maintain transient phosphorylation-dependent associations with p110δ during purification. Thus, further optimisation of the technique implemented short bead incubations with extensive inhibition of protein phosphatases. The conditions for TCR stimulation itself were also optimised to induce robust tyrosine phosphorylation in $CD4^+$ T

blasts. This process revealed that CD3 plus CD4 crosslinking induced high levels of protein tyrosine phosphorylation in $CD4^+$ T blasts, independently of CD28 crosslinking. This was not surprising, considering that CD4 has been shown to facilitate the rapid recruitment of the protein tyrosine kinase LCK to the TCR signalosome and subsequent LCK autophosphorylation, whereas CD28 is only thought to sustain LCK autophosphorylation (Holdorf *et al*, 2002; Dobbins *et al*, 2016). LCK is then able to phosphorylate immunoreceptor tyrosine-based activation motifs (ITAMs) within the TCR-CD3 complex, which subsequently recruit the cytosolic protein tyrosine kinase ZAP-70 (Wang *et al*, 2010). ZAP-70 in turn phosphorylates proteins including LAT and SLP-76. Thus, CD4 recruitment of LCK amplifies the TCR-induced protein tyrosine phosphorylation-mediated signalling cascade. This was evident in immunoblotting experiments of $CD4^+$ T blast lysates following CD3 plus CD4 crosslinking. The T cell stimulation strategy used in this study was therefore an appropriate *in vitro* model of peptide-bound MHC class II engagement of both the TCR and CD4 co-receptor. Inducing robust protein tyrosine phosphorylation in this manner would be expected to increase the number of signalling events at activated TCR signalosomes, and thus lead to robust recruitment and activation of PI3K. The interaction partners involved in PI3K regulation could then be captured by p110δ affinity purification.

When optimising the AviTag-AP protocol for downstream MS analysis, a balance had to be found between maintaining p110δ interactions with low affinity or transient binding partners and reducing non-specifically interacting proteins. It is widely accepted that affinity purifications of protein complexes also contain a vast number of non-relevant background proteins (Yang *et al*, 2008). Thus, modifications were made in an effort to reduce this. For example, implementing strict wash steps and a shorter bead incubation. Nevertheless, the one-step nature of the AviTag-AP technique, and the fact that proteins were crudely eluted from magnetic beads by boiling, meant that a high background was inevitable. However, given that the aim of this study was to discover p110δ interaction partners, it was preferable to retain a high background than to lose relevant interactions by using excessively stringent purification techniques. This view was supported by the increased tolerance for background contaminants afforded by modern MS analyses of affinity purifications; considerable advances in quantitative MS approaches, combined with improved statistical analyses, have allowed biologically relevant interactors to be distinguished from irrelevant background contaminants, and have thus reduced the number of false positives (Ong *et al*, 2005; Dunham *et al*, 2012; Li *et al*, 2012; Morris *et al*, 2014).

The AviTag system is highly suited for this differential MS approach, as two affinity purifications can be performed: one from p110δ$^{Avi/Avi}$BirA$^{+/-}$ lysates containing the tagged bait protein p110δ, and one using lysates from cells expressing BirA. It is expected that non-specific proteins interacting with the magnetic beads, or endogenously biotinylated proteins captured by streptavidin, would appear at a 1:1 ratio in each AP, whereas specific interactors would be enriched in bait purifications (Blagoev *et al*, 2003). This would then enable the differentiation of p110δ-associated proteins. Indeed, in the experiments presented herein, tyrosine-phosphorylated proteins were specifically co-purified with p110δ but were not detected in control affinity purifications from BirA$^{+/-}$ cells. Given that these proteins were detectable by immunoblotting, it was expected that they could be identified by LC-MS/MS analysis. Thus, subsequent experiments planned to analyse affinity purifications from p110δ$^{Avi/Avi}$BirA$^{+/-}$ and BirA$^{+/-}$ CD4$^{+}$ T blasts by LC-MS/MS analysis, with the aim to identify p110δ interaction partners following TCR engagement.

# Chapter 3

# Proteomic analysis of p110δ interactors downstream of TCR engagement in primary murine CD4$^+$ T lymphocytes

## 3.1 Introduction

Earlier work extensively optimised the AviTag-affinity purification technique for the isolation of endogenous p110δ complexes from primary activated CD4$^+$ T lymphocytes. This presented a unique approach to study proteins that specifically associate with p110δ in a physiological context. Moreover, it could be used to compare purified p110δ signalling complexes prior to and following TCR stimulation, thus allowing the identification of proteins that may regulate PI3K localisation and activity upon receptor engagement. The composition of such protein complexes can be determined though the coupling of affinity purification with mass spectrometry (Gingras *et al*, 2007; Yang *et al*, 2008).

Modern MS platforms are increasingly sensitive in characterising complex protein mixtures, such as those isolated by affinity purification (Morris *et al*, 2014). They therefore represent a powerful tool for identifying proteins that may be present in low abundance, either due to their expression level or due to the transient nature of their interaction with the bait. These types of interaction, possibly dependent on tyrosine phosphorylation events, are likely to be present in p110δ complexes. However, the high sensitivity of MS analysis means that non-specifically interacting proteins within p110δ purifications will also be detected. These irrelevant, background contaminants could obscure the identification of true interactions. One way to reduce this risk is to use stringent purification protocols. For example, the strict wash steps and short bead incubation times implemented in the current study. Unfortunately, increasing wash steps may exclude interactions that are transient, low affinity, or that occur with low abundance proteins. The AviTag-AP system is advantageous in this respect, as the single-step purification with magnetic beads minimises the amount of protein lost, and also increases the speed of purification so that transient interactions are more likely to be captured (Kean *et al*, 2012). Nevertheless, this increases the recovery of both specific and non-specific proteins (Chen &

Gingras, 2007). Therefore, even with a highly optimised AviTag affinity purification protocol, the sensitivity of downstream MS analysis necessitated a method to differentiate true p110δ protein interactions from non-specific background. This validation required two components: a reliable method to quantitate proteins, and a statistical analysis.

The current study therefore used a quantitative proteomics approach to analyse affinity-purified p110δ signalling complexes. The most widely used quantitative MS technologies are label-based (Ong & Mann, 2005). Isobaric labelling of peptide samples with tandem mass tags (TMTs) is one such technique, allowing multiple protein samples to be chemically labelled in parallel and then combined for LC-MS/MS analysis (Thompson *et al*, 2003). Isobaric TMTs are isotopic variants that generate reporter ions of different masses only upon fragmentation during tandem MS. The detected intensity of these distinct reporter ions allows accurate quantification of the relative abundance of any identified peptide in each original sample (Rauniyar & Yates, 2014). The advantage of TMT-based labelling is that up to ten samples can be analysed simultaneously using ten isobaric tag variants. This facilitates the analysis of biological replicates in one MS analysis, therefore providing greater statistical validation by removing inter-run variability. Furthermore, by combining identical peptides from multiple samples, the sensitivity of detection is improved for low abundance proteins (Li *et al*, 2012).

For its recognised advantages, the TMT isobaric labelling strategy was chosen for the quantitative MS analysis of p110δ affinity purification samples. Following TMT-based quantification, the relative abundance of identified proteins could be compared in bait-specific and control purifications and their enrichment determined using statistical analyses. As described previously, the AviTag system enables purifications from $BirA^{+/-}$ cell lysates to be used as background controls to exclude irrelevant proteins that are biotinylated or bind non-specifically to the magnetic beads. Following this approach, AviTag-AP coupled with quantitative TMT-based MS analysis was used to identify p110δ interaction partners in TCR-stimulated and unstimulated primary mouse $CD4^{+}$ T blasts.

## 3.2 Results

### 3.2.1 MS identification of a tyrosine-phosphorylated protein associated with p110δ in a TCR stimulation-dependent manner

Earlier experiments detected a prominently tyrosine-phosphorylated protein of ~115 kDa that appeared to associate with p110δ upon TCR-stimulation. Before conducting a high-throughput

quantitative MS analysis of p110δ affinity purifications, a small-scale mass spectrometry approach was used to investigate the identity of this protein.

Using the optimised AviTag affinity purification (AP) protocol, p110δ was isolated from the cell lysates of unstimulated and TCR-stimulated p110δ$^{Avi/Avi}$BirA$^{+/-}$ CD4$^{+}$ T blasts. A control purification was also performed on lysates from TCR-stimulated BirA$^{+/-}$ CD4$^{+}$ T blasts. For each purification, the same number of cells were lysed and thus the same amount of total protein was subjected to streptavidin-mediated purification, as confirmed by measuring the protein concentration of the lysates. A proportion of the bead eluates from each AP was first analysed by immunoblotting, alongside the corresponding cell lysates, to confirm both successful TCR-stimulation and co-purification of tyrosine-phosphorylated proteins (Figure 3.1). As observed previously, a tyrosine-phosphorylated protein of ~115 kDa was detected only in the TCR-stimulated p110δ AP. Subsequently, the remaining bead eluates were separated by SDS-PAGE. The region corresponding to 110 - 120 kDa was isolated from the polyacrylamide gel for each p110δ and control AP, and proteins that migrated within this molecular weight range were then extracted and analysed by LC-MS/MS.

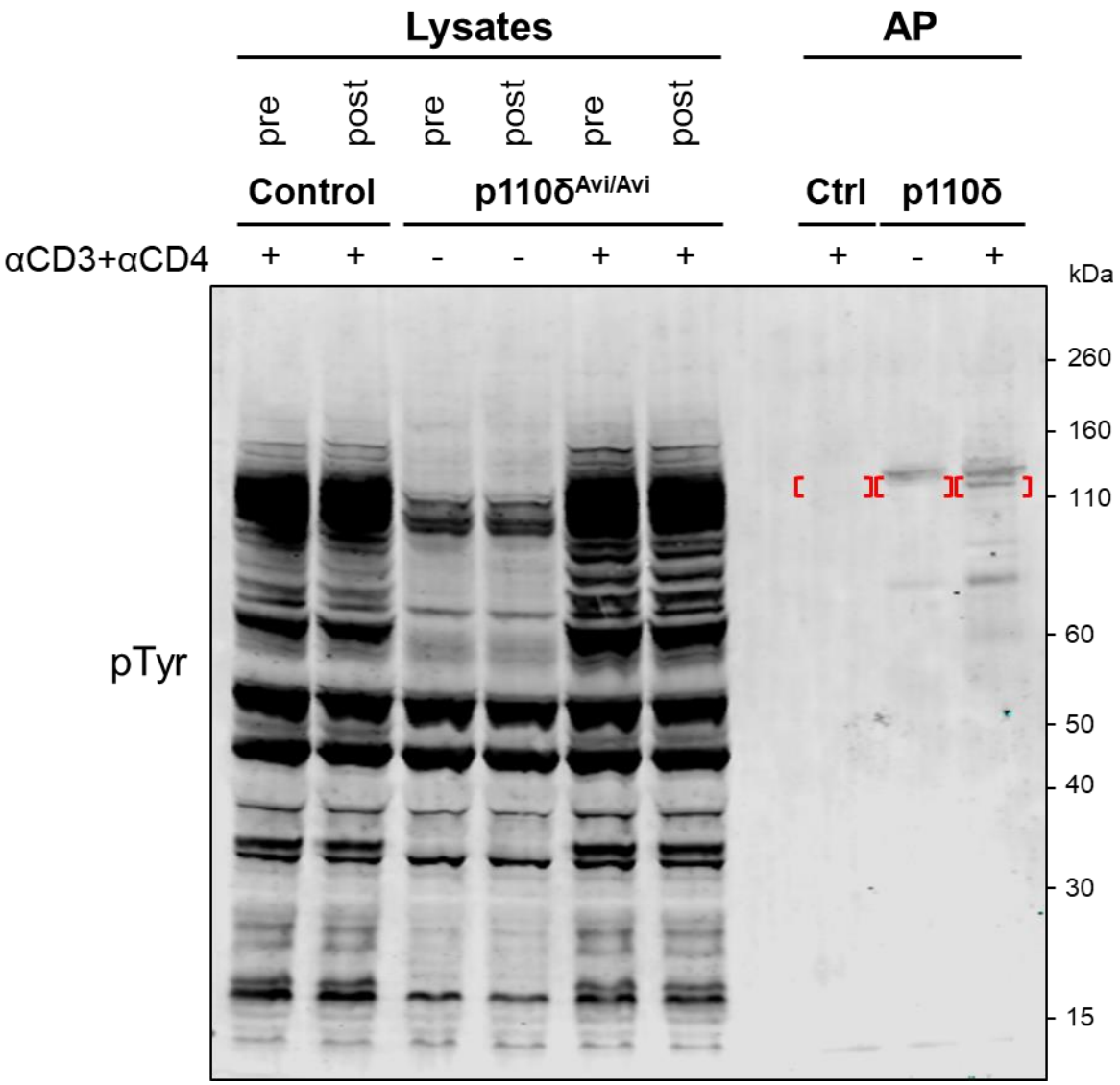


**Figure 3.1 Identifying a tyrosine-phosphorylated p110δ-associated protein of ~115 kDa.** Immunoblot analysis of cell lysates and affinity purifications from p110δ$^{Avi/Avi}$BirA$^{+/-}$ (p110δ$^{Avi/Avi}$) and BirA$^{+/-}$ (control) CD4$^{+}$ T blasts. One-hundred million CD4$^{+}$ T blasts per condition were stimulated with 4 µg/ml αCD3+αCD4 for 1 minute (+), or left unstimulated (-), and cell lysates were subjected to affinity purification using streptavidin-conjugated magnetic beads. Lysates equivalent to 2.16 million cells from before (pre) and after (post) bead purification were separated by SDS-PAGE, alongside $\frac{2}{7}$ of each control (Ctrl) and p110δ affinity purification (AP). Immunoblots were probed for phosphorylated tyrosine residues (pTyr). In parallel, the remainder of the same AP samples were separated by SDS-PAGE, and the region 110 - 120 kDa for each AP lane (indicated with red brackets on the immunoblot) was excised from the polyacrylamide gel and subjected to LC-MS/MS analysis.

A total of 241 high-confidence proteins were identified across all three samples. The fold enrichment for each protein was calculated as the ratio of its abundance in the stimulated p110δ AP to the stimulated control AP. The proteins were then ranked by their fold enrichment

in the stimulated p110δ purification. Only 26 proteins exhibited a 1.5-fold or greater enrichment in the p110δ purification or were absent in the control purification (Table 3.1). p110δ was the most abundant of these proteins and was not detected in the control purification. The PI3K regulatory subunit p85α was also identified in the stimulated and unstimulated p110δ purifications, at a higher abundance than in the control purification. It was noted that both PI3K subunits were detected with a higher abundance in the unstimulated p110δ purification than in the stimulated sample. Given that the total amount of protein subjected to streptavidin-mediated purification was the same for both, this could reflect a difference in the amount of PI3K protein that was recovered by the SDS-PAGE 'gel slice' strategy. Indeed, the small region analysed was cut along the 120 kDa band of p110δ protein, which was visible following Coomassie staining, and thus a difference in the slice area would affect the amount of p110δ recovered. Nevertheless, this analysis was most interested in proteins identified in the stimulated p110δ purification and not in the stimulated control purification. Thus, it was intriguing that one such protein had functional relevance to PI3K signalling: B-cell adaptor for phosphoinositide 3-kinase, BCAP. BCAP was identified from two unique peptides that were detected only in the TCR-stimulated p110δ affinity purification. The failure to detect BCAP in the unstimulated and control purification did not necessarily indicate that it was absent, as it may have been below the threshold of detection. Nevertheless, this qualitative MS analysis suggested that BCAP associated with p110δ in a TCR stimulation-dependent manner. The remaining p110δ-enriched proteins were determined to be non-relevant contaminants, based on their Gene Ontology (GO) annotation for molecular function and cellular component, as well as their low abundance or identification based on only one unique peptide.

| Protein Name | Protein abundance ($\times 10^6$) AP **Control** Stim | AP **p110δ** Unstim | AP **p110δ** Stim | **Fold Enrichment** (p110δ stim/ control stim) |
|---|---|---|---|---|
| p110δ | 0.0 | 1301.2 | 591.6 | - |
| Trypsinogen 7 | 0.0 | 0.0 | 6.1 | - |
| Nucleolar and coiled-body phosphoprotein 1 | 0.0 | 6.6 | 2.2 | - |
| 2-oxoglutarate dehydrogenase | 0.0 | 0.0 | 1.5 | - |
| BCAP | 0.0 | 0.0 | 1.0 | - |
| Exosome component 10 | 0.0 | 1.0 | 1.0 | - |
| Coronin-7 | 0.0 | 1.7 | 0.9 | - |
| Unconventional myosin-Ig | 0.0 | 0.0 | 0.9 | - |
| CREB/ATF bZIP transcription factor | 0.0 | 0.0 | 0.8 | - |
| Bromodomain-containing protein 2 | 0.0 | 0.0 | 0.8 | - |
| Spermatid-specific heat shock protein 70 | 0.0 | 1.2 | 0.7 | - |
| Exoc2 protein | 0.0 | 0.0 | 0.6 | - |
| 40S ribosomal protein S24 | 0.0 | 0.0 | 0.6 | - |
| Kif23 protein | 0.0 | 0.0 | 0.5 | - |
| Dhx36 protein | 0.0 | 0.0 | 0.5 | - |
| Endoplasmic reticulum chaperone BiP | 0.0 | 1.3 | 0.5 | - |
| Isocitrate dehydrogenase 1 | 0.0 | 0.0 | 0.4 | - |
| Heat shock protein HSP 90-beta | 0.0 | 2.7 | 0.4 | - |
| HIV Tat-specific factor 1 homolog | 0.0 | 0.0 | 0.4 | - |
| Integrator complex subunit 4 | 0.0 | 0.0 | 0.2 | - |
| p85α | 1.7 | 24.7 | 11.6 | 7.0 |
| Protein PML | 1.0 | 0.0 | 2.1 | 2.0 |
| Trifunctional purine biosynthetic protein adenosine-3 | 2.6 | 3.2 | 5.2 | 2.0 |
| C-1-tetrahydrofolate synthase | 2.8 | 2.3 | 5.4 | 1.9 |
| Neutral alpha-glucosidase AB | 3.7 | 2.4 | 6.6 | 1.8 |
| Endoplasmic reticulum aminopeptidase 1 | 2.4 | 3.0 | 3.6 | 1.5 |

**Table 3.1 Proteins identified by LC-MS/MS as enriched by p110δ affinity purification from CD4$^+$ T cells.**

Affinity purifications (AP) as described in Figure 3.1 were separated by SDS-PAGE and proteins that migrated in the region 110 - 120 kDa were extracted from the polyacrylamide gel and analysed by LC-MS/MS. For proteins identified with high-confidence, quantified protein abundance values were calculated within Proteome Discoverer 1.4 using the average of the peak areas for the three most abundant peptides per protein. The fold enrichment for each protein was calculated as the ratio of its abundance in the stimulated p110δ AP to the stimulated control AP. Identified proteins with a 1.5-fold or greater enrichment in stimulated p110δ purifications compared with control purifications, or those that were absent in the control purification but present in the stimulated p110δ AP, are shown.

BCAP is an adaptor protein expressed as two isoforms with observed molecular weights of 70 – 100 kDa (Okada *et al*, 2000). BCAP has been shown to associate with PI3K in mouse splenic B cells upon BCR crosslinking. Moreover, BCAP is tyrosine phosphorylated in B cells upon BCR activation, and associates with p85 in a BCR stimulation-dependent manner (Okada *et al*, 2000). It was therefore possible that BCAP was the tyrosine-phosphorylated protein of ~115 kDa that associated with p110δ in a TCR stimulation-dependent manner.

### 3.2.2 A quantitative AP-MS approach to identify p110δ-specific interactors in $CD4^+$ T blasts

The main aim of the present study was to identify proteins that interact with p110δ upon TCR engagement in primary $CD4^+$ T cells using AviTag-affinity purification in combination with quantitative mass spectrometry (AP-MS). To this end, using the earlier optimised protocol, $p110\delta^{Avi/Avi}BirA^{+/-}$ $CD4^+$ T blasts were stimulated by CD3 and CD4 crosslinking for 1 minute and lysed. Endogenous p110δ protein was then purified from cell lysates using streptavidin-conjugated magnetic beads. To be able to distinguish p110δ-specific interactors from non-specific background contaminants in downstream analysis, control purifications were also performed on lysates of stimulated $BirA^{+/-}$ $CD4^+$ T blasts. For each purification, the same number of cells were used, resulting in the same amount of total protein subjected to streptavidin-mediated purification, as confirmed by measuring the protein concentration of the lysates. Three biologically independent experiments were carried out, and the quality and reproducibility of TCR stimulation across all three was assessed by immunoblotting (Figure 3.2). As seen previously, TCR-stimulation via CD3 and CD4 crosslinking induced strong and consistent tyrosine phosphorylation in all experiments. Furthermore, multiple tyrosine-phosphorylated proteins were isolated with p110δ from stimulated cells, with few visible in corresponding unstimulated samples. In contrast, tyrosine-phosphorylated proteins could not be detected by immunoblotting in control purifications from $BirA^{+/-}$ cells.

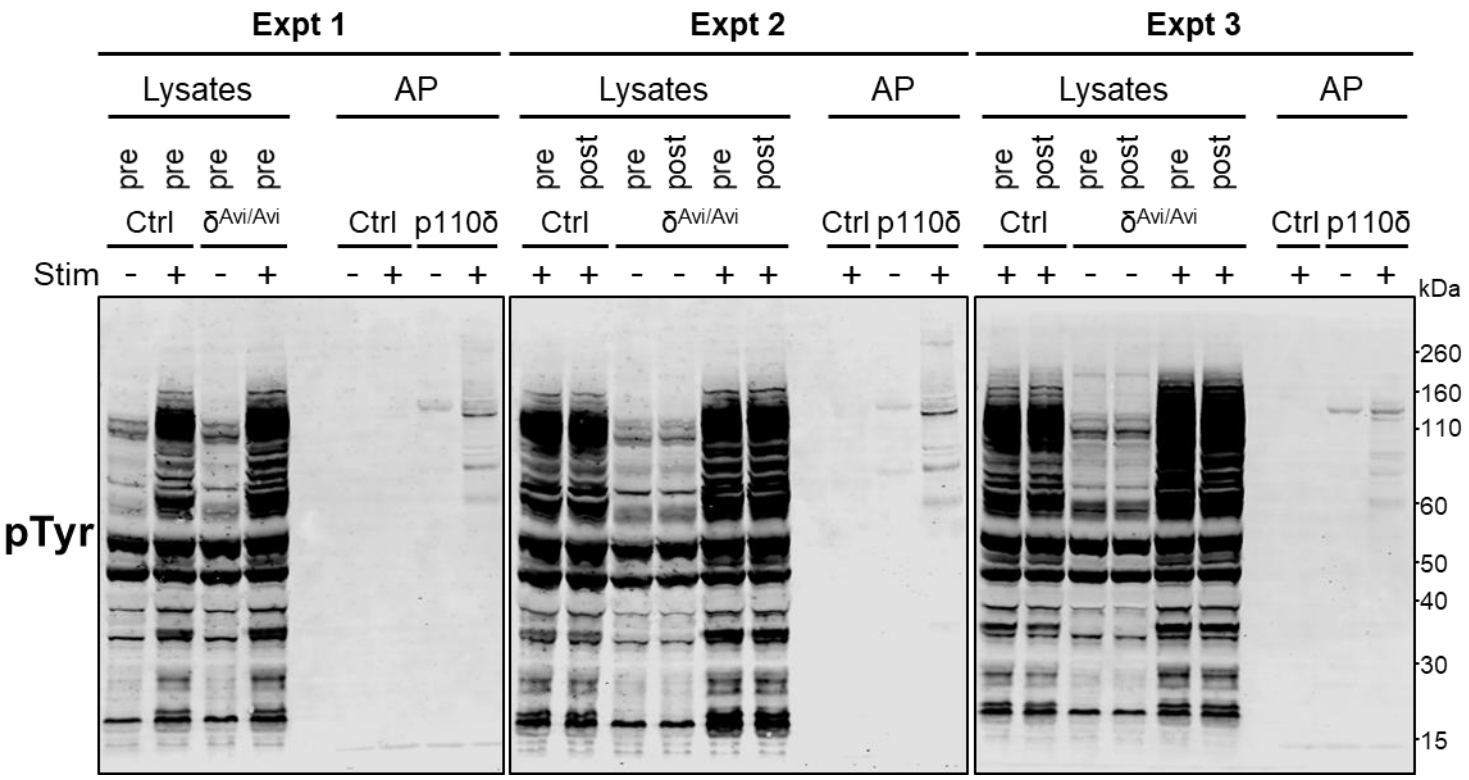


**Figure 3.2 p110δ and control affinity purifications from CD4⁺ T blasts for TMT labelling-based MS analysis.**

Immunoblot analysis of cell lysates and affinity purifications (AP) from CD4⁺ T blasts. One-hundred million p110δ$^{Avi/Avi}$BirA$^{+/-}$ (δ$^{Avi/Avi}$) or BirA$^{+/-}$ (Ctrl) CD4⁺ T blasts were stimulated for each AP with 4 μg/ml αCD3+αCD4 for 1 minute (+), or left unstimulated (-), and their cell lysates were subjected to affinity purification using streptavidin-conjugated magnetic beads. Lysates (equivalent to 2.16 million cells) from before (pre) and after (post) bead purification were separated by SDS-PAGE alongside $\frac{2}{7}$ of each affinity purification and immunoblotted for phosphorylated tyrosine residues (pTyr). Blots shown are from three independent experiments (labelled Expt 1, 2 and 3).

Ten affinity purification samples from the three independent experiments, representing unstimulated and stimulated control and p110δ purifications, were then digested and the peptide samples were labelled in parallel with one of ten isobaric Tandem Mass Tags (TMT) (Figure 3.3). Unfortunately, one unstimulated p110δ AP sample from experiment 1 was voided due to a faulty TMT reagent. The remaining nine labelled peptide samples were combined and analysed by LC-MS/MS.

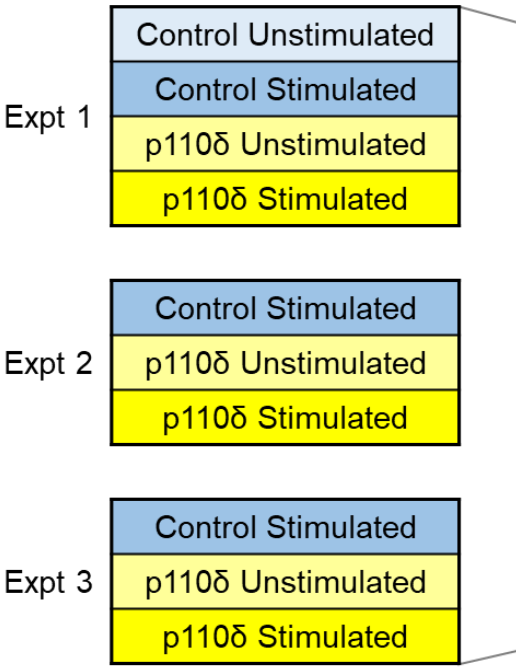


| Sample | AP | Repeat # |
|---|---|---|
| 1 | Control Unstimulated | 1 |
| 2 | Control Stimulated | 1 |
| 3 | Control Stimulated | 2 |
| 4 | Control Stimulated | 3 |
| 5* | p110δ Unstimulated | 1 |
| 6 | p110δ Unstimulated | 2 |
| 7 | p110δ Unstimulated | 3 |
| 8 | p110δ Stimulated | 1 |
| 9 | p110δ Stimulated | 2 |
| 10 | p110δ Stimulated | 3 |

**Figure 3.3 p110δ and control affinity purification samples analysed by TMT-labelling based LC-MS/MS.**
Ten streptavidin-mediated affinity purifications (AP) from unstimulated and stimulated $p110\delta^{Avi/Avi}BirA^{+/-}$ (p110δ) or $BirA^{+/-}$ (control) $CD4^+$ T blasts were denatured, reduced, alkylated and digested to generate peptide samples. The ten peptide samples were then labelled in parallel with one of ten isobaric tandem mass tags (10plex TMTs) and combined for LC-MS/MS analysis. *One sample (number 5) was not analysed due to a faulty TMT label.

### 3.2.3 Proteins specifically associated with p110δ in $CD4^+$ T blasts

LC-MS/MS analysis identified 3,473 proteins with high confidence in the nine affinity purification samples, which were quantified and normalised in each sample based on their associated reporter ion intensities. To determine whether an identified protein was specifically associated with p110δ, or whether it was a background contaminant, the $\log_2$-transformed abundance for each protein was compared in stimulated p110δ purifications and stimulated control purifications, using the Perseus computational platform (Tyanova *et al*, 2016; Tyanova & Cox, 2018). The mean $\log_2$-fold change calculated for each protein was used to select those with a mean 1.5-fold or greater enrichment in stimulated p110δ purifications (Table 3.2). A statistical analysis was also performed for all proteins to determine those that were significantly differentially abundant in p110δ and control purifications, using a two-tailed Student's t-test that was corrected for multiple hypothesis testing using a permutation-based false discovery rate (FDR) threshold. The FDR threshold chosen defines the maximum acceptable proportion of

expected false positives among the set of proteins that are determined to be significantly differentially abundant (Burger, 2018). With a stringent FDR threshold of 0.05, 53 of 3,473 tested proteins were deemed to be significantly differentially abundant, whereas 175 proteins were significantly differentially abundant with an FDR of ≤0.20. The conservative FDR threshold was therefore chosen to consider a higher number of potential true interactors, with the acknowledged risk of selecting potential false positives (Giai Gianetto *et al*, 2014). Combining this differential analysis with a fold change threshold of 1.5 revealed 30 proteins that were significantly enriched in p110δ purifications as compared to controls (FDR≤0.20; Table 3.2). Seven proteins were enriched more than 1.5-fold but did not reach significance with an FDR less than or equal to 0.20.

A bioinformatic analysis was subsequently performed using Gene Ontology (GO) annotation to determine the main molecular and biological functions of the identified p110δ-associated proteins (Table 3.2). Based on this analysis, five additional MS identified proteins with an enrichment of between 1.25- and 1.44-fold were selected for further consideration. These were the TCR co-receptors CD4 and CD28, the TCR complex CD3γ chain, and two signalling adaptor proteins, CRK and NCK1. CRK and NCK1 were selected as proteins of interest as they are both recruited to the TCR signalosome upon TCR stimulation (Gil *et al*, 2002; Dong *et al*, 2017). Nevertheless, of these five proteins, only NCK1 was significantly enriched (FDR≤0.20).

| Protein Name | Mean Fold Enrich-ment | p value | Student's t-test Significance (FDR≤0.05) | Student's t-test Significance (FDR≤0.20) | Molecular Function | Biological Function |
|---|---|---|---|---|---|---|
| **p85α** | 8.16 | <0.001 | + | + | PI3K regulatory subunit | PI3K signalling |
| **p110δ** | 6.81 | <0.001 | + | + | PI3K catalytic subunit | PI3K signalling |
| **p85β** | 5.69 | <0.001 | + | + | PI3K regulatory subunit | PI3K signalling |
| **GAB2** | 5.11 | <0.001 | + | + | Adaptor protein | Signal transduction |
| **ISG15** | 5.07 | <0.001 | + | + | Ub-like modifier | Ubl conjugation pathway |
| **GAB3** | 4.31 | <0.001 | + | + | Adapter protein | Signal transduction |
| **IRS2** | 3.43 | 0.001 | + | + | Adaptor protein | Insulin receptor signalling |
| **ICOS** | 3.24 | 0.002 | + | + | Cell surface receptor | T cell costimulation |
| **BICRA** | 3.14 | <0.001 | + | + | BRD4-binding | Chromatin remodelling |
| **SHP-2** | 3.12 | <0.001 | + | + | Protein tryosine phosphatase | Signal transduction |
| **IQGAP3** | 2.92 | 0.006 | | + | GTPase activating protein | Ras-ERK signal transduction |
| **STS-2** | 2.54 | 0.001 | + | + | Protein tyrosine phosphatase | TCR signalling regulation |
| **CBL** | 2.47 | 0.001 | + | + | E3 ubiquitin-protein ligase | TCR signalling regulation |
| **JAML** | 2.20 | <0.001 | + | + | Junctional adhesion molecule-like | Cell adhesion |
| **BCAP** | 2.19 | 0.040 | | | Adaptor protein | PI3K signalling |
| **TOMM20** | 2.17 | 0.001 | + | + | Preprotein receptor | Mitochondrial protein translocation |
| **AKT2** | 2.12 | <0.001 | + | + | Protein serine/threonine kinase | PI3K signalling |
| **GRB2** | 2.09 | 0.001 | + | + | Adaptor protein | Signal transduction |
| **NUDCD2** | 2.09 | 0.021 | | | Co-chaperone protein | Protein folding |
| **TMEM199** | 1.97 | 0.049 | | | V-ATPase assembly factor | Endo-lysosomal acidification |
| **TFAP4** | 1.97 | 0.007 | | + | DNA binding | Transcription factor |
| **CD5** | 1.93 | 0.008 | | + | Cell surface receptor | TCR signalling regulation |
| **CRKL** | 1.91 | 0.003 | | + | Adaptor protein | Signal transduction |
| **WASHC1** | 1.89 | 0.011 | | + | Actin binding | Endosomal transport |
| **FSD1L** | 1.88 | 0.001 | + | + | Microtubule association | Microtubule organisation |
| **STAT1** | 1.81 | 0.027 | | | DNA binding | Transcription factor |
| **SH3KBP1** | 1.73 | 0.005 | | + | Adaptor protein | Signal transduction |
| **SOD2** | 1.68 | 0.023 | | | Oxidoreductase | Oxidative stress response |
| **LARS2** | 1.64 | 0.005 | | + | tRNA synthetase | Protein synthesis |
| **MALT1** | 1.62 | <0.001 | + | + | Cysteine protease | NF-κB signalling |
| **PLP2** | 1.56 | 0.132 | | | Integral membrane protein | Membrane integrity |
| **SSBP4** | 1.55 | 0.002 | | + | DNA binding | Transcription regulation |
| **MRPL44** | 1.54 | <0.001 | + | + | Mitochondrial ribosomal protein | Mitochondrial translation |
| **CD2AP** | 1.51 | 0.005 | | + | Adaptor protein | TCR signalling regulation |
| **TTF2** | 1.51 | 0.001 | + | + | DNA-dependent ATPase | Transcription regulation |
| **GRK2** | 1.51 | 0.019 | | | Protein serine/threonine kinase | GPCR signaling |
| **RUNX1** | 1.51 | 0.005 | | + | DNA binding | Transcription factor |
| **CD4** | 1.44 | 0.080 | | | Cell surface receptor | TCR co-receptor |
| **CD3γ** | 1.41 | 0.028 | | | Cell surface glycoprotein | TCR signal transduction |
| **CRK** | 1.31 | 0.021 | | | Adaptor protein | Signal transduction |
| **NCK1** | 1.28 | 0.002 | | + | Adaptor protein | Signal transduction |
| **CD28** | 1.25 | 0.048 | | | Cell surface receptor | TCR co-receptor |

**Table 3.2 Proteins identified by LC-MS/MS as specifically associated with p110δ in $CD4^+$ T blasts.**

Proteins identified by LC-MS/MS as enriched in p110δ affinity purifications. Quantified and normalised protein abundance values were analysed using Perseus. Values were $log_2$-transformed and the mean abundance in stimulated p110δ purifications was compared with the mean abundance in stimulated control purifications from 3 independent experiments. Statistical significance for the difference of the means for all identified proteins was determined using a two-tailed Student's t-test and corrected for multiple testing using a permutation-based false discovery rate (FDR) with a threshold of 0.05 in the first instance, and 0.20 in a second test. Proteins with a mean fold enrichment of 1.5 or greater in p110δ purifications were selected. Five proteins enriched less than 1.5-fold with a known role in TCR signal transduction were also selected, as shown below the broken line in the table.

Significantly differentially abundant proteins are indicated with a black + (FDR≤0.05) or red + (FDR≤0.20). Molecular and biological functions for each protein were determined based on their Gene Ontology (GO) annotations.

All 3,473 identified proteins were then plotted as a volcano scatter plot to allow visualisation of their differential abundance and associated statistical significance. The 31 significantly enriched p110δ-associated proteins appeared as clear outliers in the upper right quadrant of the plot (Figure 3.4; red scatter points). The validity of the analysis performed, and the specificity of the affinity purifications, was confirmed by the significant enrichment of p110δ, p85α and p85β in p110δ purifications. These PI3K subunits exhibited a high mean fold enrichment of 6.80, 8.16 and 5.69 in p110δ purifications, respectively.

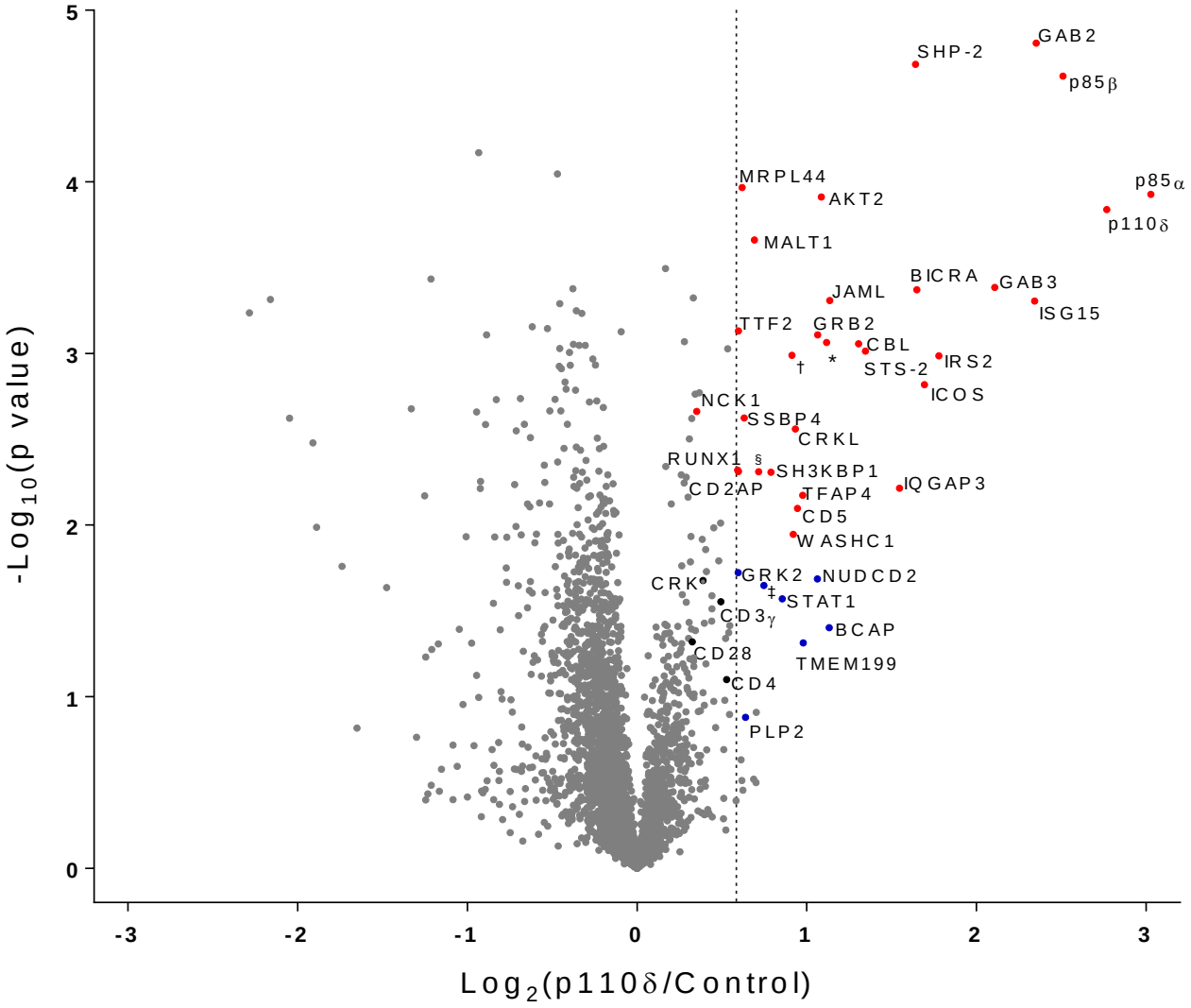


**Figure 3.4 Proteins specifically associated with p110δ in CD4⁺ T blasts.**
Volcano plot of proteins identified by LC-MS/MS in p110δ and control affinity purifications. Quantified and normalised protein abundance values were analysed using Perseus. Values were $log_2$-transformed and the mean abundance in stimulated p110δ purifications was compared with the mean abundance in stimulated control purifications from 3 independent experiments. Statistical significance for the difference of the means for each protein was determined using a two-tailed Student's t-test and corrected for multiple testing using a permutation-based false discovery rate (FDR) with a threshold of 0.20. The $-log_{10}$ p value for each protein was plotted against its mean $log_2$(fold change) in p110δ purifications compared with control purifications ($Log_2$ (p110δ/Control)). Significantly differentially abundant proteins are labelled and highlighted in red (FDR≤0.20) on the scatter plot. Proteins enriched greater than 1.5-fold but not reaching significance with an FDR≤0.20 are labelled and highlighted in blue. Proteins of interest with an enrichment of 1.25-1.44-fold are labelled in black. The vertical dotted line indicates a mean 1.5-fold enrichment in the stimulated p110δ purifications. Proteins TOMM20, FSD1L, SOD2 and LARS2 are labeled with an asterisk (*), dagger (†), double dagger (‡) and section (§), respectively, for clarity.

Combining the results of these analyses, it was remarkable that the majority of proteins significantly enriched with p110δ were involved in signal transduction, and specifically TCR signalling. Ten adaptor proteins were enriched (GAB2, GAB3, IRS2, BCAP, GRB2, CRKL, SH3KBP1, CD2AP, CRK, NCK1) along with five TCR co-receptor or co-stimulator membrane proteins (ICOS, CD5, CD4, CD3γ, CD28). In addition, two protein tyrosine phosphatases (SHP-2, STS-2) and an E3 ubiquitin-protein ligase (CBL) were significantly enriched, representing proteins that downregulate the propagation of TCR-induced signals. Interestingly, many of these proteins have been shown to have the capacity to bind to p85, and could therefore be involved in the recruitment, localisation or activation of PI3K at the TCR signalosome.

At this stage, removed from further analyses were proteins localised to the nucleus or mitochondria (BICRA, TOMM20, TFAP4, STAT1, SOD2, LARS2, SSBP4, MRPL44, TTF2, RUNX1) and those not known to be involved in signal transduction (NUDCD2, TMEM199, WASHC1, FSD1L, PLP2). Of the remaining 27 enriched proteins of interest, 21 were significantly differentially abundant with an expected FDR of 0.20 or less. The minimum expected FDR that could be attained when calling the other proteins significantly differentially abundant was 0.32 (BCAP), 0.22 (GRK2), 0.43 (CD4), 0.27 (CD3γ), 0.24 (CRK), and 0.34 (CD28). These FDRs were close to the imposed FDR threshold of 0.20; while these proteins were therefore not classed as significant, their biological relevance justified their inclusion as proteins of interest. The abundance of all 27 proteins of interest (including p110δ) was then compared in all nine unstimulated and stimulated affinity purifications to investigate the context of their association with p110δ upon TCR stimulation.

### 3.2.4 Proteins specifically associated with p110δ in a TCR-stimulation dependent manner in $CD4^+$ T blasts

The relative abundance levels of p110δ-associated proteins of interest were subsequently analysed across all nine affinity purification samples. This was to determine if their association with p110δ was dependent on TCR stimulation, and to examine the variation between biological replicates. To this end, the quantified abundance of each protein in all nine affinity purifications was normalised using Z-score transformation. Hierarchical clustering was then performed to group proteins with similar patterns of abundance across the samples, and this analysis was visualised by heat mapping (Figure 3.5).

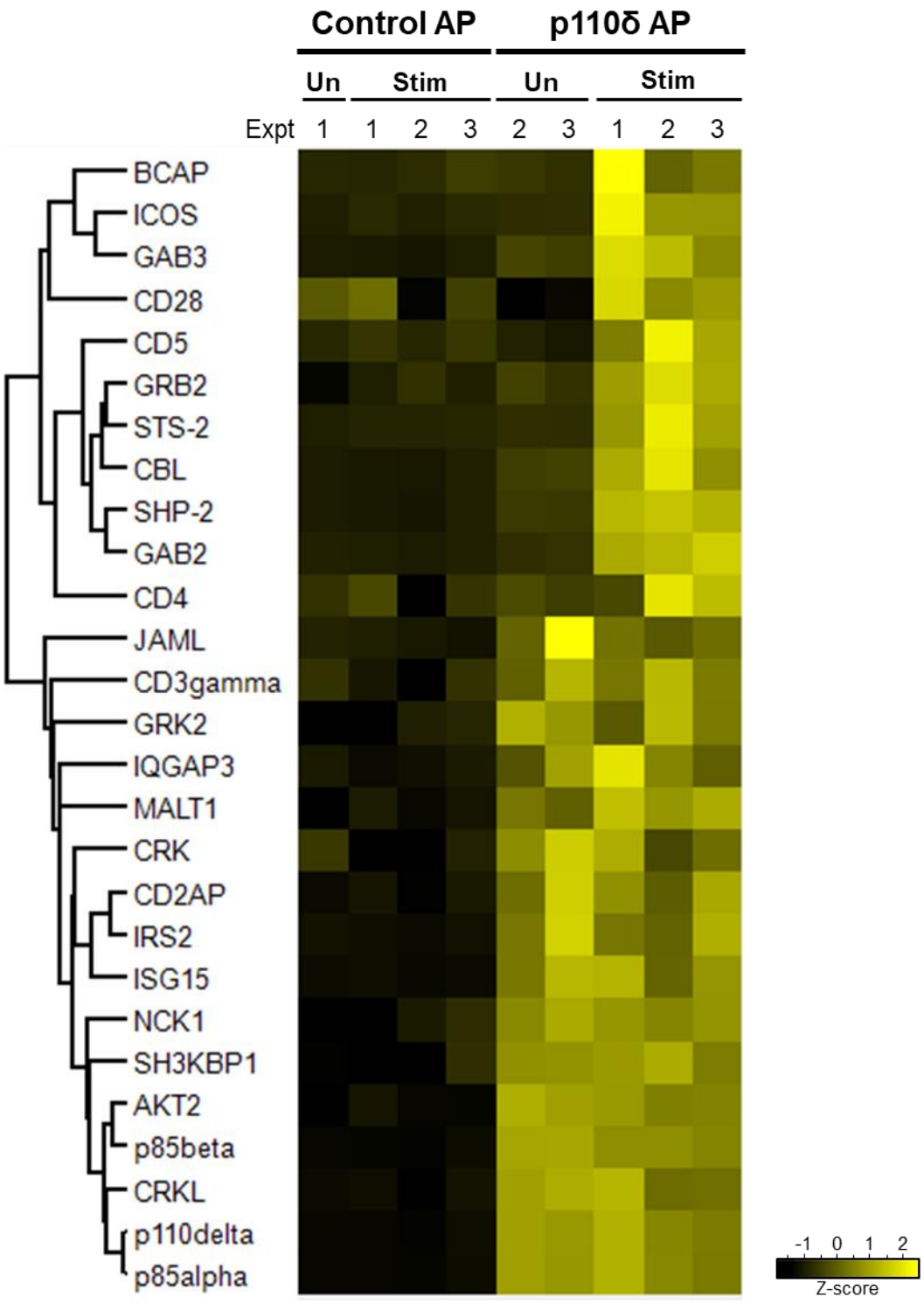


**Figure 3.5 Proteins specifically associated with p110δ in a TCR stimulation-dependent or stimulation-independent manner in CD4⁺ T blasts.**

Heat map with hierarchical clustering, visualising the relative abundance of p110δ-associated proteins in affinity purifications (APs) from unstimulated (Un) and TCR-stimulated (Stim) $p110\delta^{Avi/Avi}BirA^{+/-}$ (p110δ) and $BirA^{+/-}$ (control) $CD4^+$ T blasts. Quantified abundance values for each protein were $log_2$-transformed and normalised across all nine affinity purifications using Z-score transformation in Perseus. Hierarchical clustering was then performed using Euclidean distance and average linkage. Clustering is represented as a dendrogram. Z-scores are represented by a colour scale from black (low) to yellow (high).

Strikingly, hierarchical clustering revealed that there were two main groups of p110δ-enriched proteins - those that were associated with p110δ in a TCR stimulation-dependent manner, and those that appeared to be associated independently of stimulation. The p85α and p85β regulatory subunits were constitutively associated with p110δ, as expected. The proteins CRKL, AKT2, SH3KBP1 and NCK1 demonstrated a similar stimulation-independent pattern of abundance, indicating that they may also constitutively associate with p110δ. Nine enriched proteins (ISG15, IRS2, CD2AP, CRK, MALT1, IQGAP3, GRK2, CD3γ and JAML) exhibited noticeable variation in their relative abundance across both unstimulated and stimulated biological replicates of p110δ purifications. Nevertheless, among these proteins, MALT1 exhibited increased p110δ-association upon stimulation, whereas JAML, CRK, CD2AP, IRS2 and ISG15 were slightly more enriched in all unstimulated p110δ purifications compared to the corresponding stimulated p110δ purifications.

In contrast, eleven proteins (BCAP, ICOS, GAB3, CD28, CD5, GRB2, STS-2, CBL, SHP-2, GAB2 and CD4) demonstrated distinct TCR-stimulation dependent association with p110δ. This was clear for SHP-2 and GAB2, which both showed a consistent level of abundance and enrichment in stimulated purifications. The relative abundance of the other eight stimulation-dependent interactors was more variable across the three stimulated p110δ purifications. BCAP, ICOS, GAB3 and CD28 were detected with highest abundance in experiment 1, whereas CD5, GRB2, STS-2 and CBL were more abundant in experiment 2. Nevertheless, this analysis revealed that these proteins interacted specifically with p110δ upon TCR-stimulation, with low relative abundance in unstimulated p110δ purifications equivalent to that detected in control samples.

CD4, CD28, CRK and CD3γ were selected as proteins of interest based on their known functions, even though their enrichment in p110δ purifications was less than 1.5-fold, and this was not statistically significant. Their low enrichment in each p110δ purification, compared to its corresponding control, was evident by heatmap visualisation, as was the inconsistency of their enrichment. In experiment 1, CD4 was identified at a higher abundance in the control purification than its corresponding stimulated p110δ sample. Therefore, there was lower confidence associated with identifying these proteins as true interactors based on this MS data alone. However, their low enrichment may represent transient or low affinity binding to p110δ, or tertiary interaction via intermediate proteins. In contrast, the adaptor protein NCK1 was enriched by only 1.28-fold, yet the heatmap visualisation and statistical analysis revealed that

this enrichment was consistent and significant across all purifications. This justified the use of less stringent fold change and FDR thresholds to avoid excluding potential true interactors.

## 3.3 Discussion

This study aimed to identify p110δ interaction partners in $CD4^+$ T blasts downstream of TCR engagement. Use of a quantitative AP-MS approach led to the identification of 24 proteins that specifically associated with endogenous p110δ and had biologically relevant functions. Moreover, eleven of the proteins associated with p110δ in a TCR stimulation-dependent manner, highlighting their involvement in TCR-PI3K signalling.

Over 3,000 proteins were identified in total by LC-MS/MS in the affinity purifications that were analysed. This raises two important points. First, the use of TMT labelling and the consequent pooling of nine AP samples into one MS experiment enabled a much deeper analysis than that afforded by earlier label-free analyses. Secondly, the inclusion of control purifications and subsequent comparison of accurately quantified protein abundance between samples was clearly crucial to enable true interactors to be distinguished from the vast number of non-specific background interactors. TMT labelling also provided a high level of confidence in the relative quantification of the identified proteins in each sample, since run-to-run variation was eliminated. It was clear in the heatmap analysis of relative protein abundance that, instead, biological variability was the main source of variation. Therefore, it proved advantageous that it had been possible to analyse three independent biological replicates using the 10-plex TMT approach.

Differential abundance analysis was used to distinguish proteins that were significantly enriched in p110δ purifications. Firstly, proteins of interest were selected based on their fold enrichment. Secondly, the false discovery rate (FDR) threshold for determining significance was intentionally optimised to reduce the number of potentially true interactors rejected, while estimating the proportion of false positives that may be included, as recommended in the field of discovery proteomics (Giai Gianetto *et al*, 2016; Burger, 2018). This approach was justified in the current analysis, for example, by inclusion of the biologically relevant protein NCK1, which was not highly enriched, but was consistently found at a higher abundance in p110δ purifications and was therefore statistically significant. Using heatmapping to visualise relative abundance across the samples also proved valuable for examining potential interactors. For example, the

inconsistency in the enrichment of CD4 in p110δ purifications was clear by inspecting the heatmap. Furthermore, comparing the relative abundance of each protein across unstimulated and stimulated affinity purifications revealed the context of their association with p110δ. It is worth noting that, had an unstimulated p110δ AP sample not been voided during sample preparation, a statistical analysis could have been performed comparing stimulated p110δ purifications with unstimulated p110δ purifications. Nevertheless, meaningful insight was gained using heatmapping and hierarchical clustering. It was striking that 11 proteins were distinctly enriched in p110δ purifications from TCR-stimulated cells, compared with unstimulated cells. These proteins are of great interest, as they are most likely to be involved in the regulation of PI3K activity upon TCR engagement in $CD4^+$ T blasts. Alternatively, they may be involved in the effector functions of PI3K following TCR activation.

### 3.3.1 TCR stimulation-dependent p110δ-associated proteins

BCAP was identified as a p110δ-specific interactor in $CD4^+$ T blasts via two different MS approaches. First, using a small-scale MS analysis of proteins purified with p110δ that migrated by SDS-PAGE with an estimated molecular weight of ~115 kDa. This qualitative MS analysis suggested that BCAP associated with p110δ in a TCR stimulation-dependent manner. Based on a previous study demonstrating that BCAP is tyrosine phosphorylated upon antigen receptor crosslinking in B cells (Okada *et al*, 2000), it seemed likely that BCAP may have been the prominent pTyr-staining protein of ~115 kDa detected by immunoblotting in earlier AP experiments. This protein also associated specifically with p110δ only in TCR-stimulated $CD4^+$ T blasts. Subsequently, BCAP was identified as a p110δ interactor using a quantitative MS analysis of three biologically independent AP experiments. BCAP was enriched greater than 2-fold in p110δ affinity purifications compared to control purifications. Strikingly, BCAP associated with p110δ in a TCR stimulation-dependent manner, with consistently low relative abundance in control and unstimulated p110δ purifications. Nevertheless, statistical analysis only deemed BCAP to be significantly differentially abundant with an FDR of 0.32. This could be explained by the fact that BCAP was highly enriched with p110δ in one experiment, but to a lesser extent in the other two replicates. Thus, taking into account its mean fold enrichment, stimulation-dependent association, and identification by two different approaches, BCAP was considered likely to be a true p110δ interactor with biological relevance. This was supported by its known capacity to bind p85 (Okada *et al*, 2000). The variability in the detection of BCAP suggests that it

may interact with PI3K with low affinity or transiently. The most intriguing aspect of the identification of BCAP was that BCAP is believed to be predominantly expressed in B cells and macrophages, and not in T cells (Okada *et al*, 2000; Yamazaki *et al*, 2002). The expression and function of BCAP in activated T cells had not been studied. Therefore, BCAP was selected for subsequent biochemical analysis in $CD4^+$ T blasts.

Inducible T-cell costimulator (ICOS) demonstrated the same stimulation-dependent pattern of interaction with p110δ as BCAP, with a higher and statistically significant enrichment of 3.24-fold in p110δ purifications. ICOS is a co-receptor that plays an important role in the positive regulation of $CD4^+$ T cell activation and proliferation (Wikenheiser & Stumhofer, 2016). ICOS is not expressed on resting T cells but is rapidly induced following TCR crosslinking (Hutloff *et al*, 1999). ICOS ligation alone or in combination with CD3 crosslinking potently stimulates PI3K-AKT signalling in activated $CD4^+$ T cells (Arimura *et al*, 2002; Fos *et al*, 2008; Gigoux *et al*, 2009). This has been shown to be mediated by ICOS recruitment of the p85α regulatory subunits, via a YMFM motif in the ICOS cytoplasmic tail (Fos *et al*, 2008; Gigoux *et al*, 2009). Interestingly, ICOS appears to be responsible for the recruitment of the p50α regulatory subunit to the immune synapse in activated T cells, an isoform that is not recruited to the immune synapse in resting cells (Fos *et al*, 2008). In the present study, ICOS was identified as a p110δ-associated protein in $CD4^+$ T blasts upon CD3+CD4 crosslinking alone, in the absence of professional antigen-presenting cells that express its natural ligand ICOS-L. This is similar to a recently reported observation that p85α associates with ICOS in primary mouse $CD4^+$ T cells upon CD3 crosslinking alone (Pedros *et al*, 2016). This raises the possibility that ICOS may act as an adaptor for PI3K recruitment to the TCR independently of ICOS engagement. This could be investigated by examining the induction of phosphorylated AKT in ICOS-deficient $CD4^+$ T blasts upon CD3+CD4 crosslinking. Therefore, subsequent experiments aimed to study PI3K-AKT signalling in ICOS-deficient $CD4^+$ T blasts.

In addition to BCAP and ICOS, the proteins GRB2, GAB2, GAB3 and SHP-2 were identified as TCR stimulation-dependent p110δ-associated proteins, with a mean fold enrichment of 2.09, 5.11, 4.31 and 3.12, respectively. GRB2 is a ubiquitously expressed adaptor protein, comprising an SH2 domain and two SH3 domains, that plays a central role in regulating signal transduction downstream of the TCR (Samelson, 2002). The GRB2 SH2 domain binds to phosphorylated YxNx motifs in the scaffolding protein LAT (Zhang *et al*, 2000), while the GRB2 SH3 domains recruit the RAS GEF SOS1 to the membrane (Houtman *et al*, 2006). Together, this is thought to facilitate

the formation of LAT microclusters upon TCR stimulation, which is required for subsequent PLCγ1 phosphorylation and cytokine production (Bilal & Houtman, 2015). Moreover, the GRB2 SH3 domains have the capacity to bind to proline-rich regions in p85 (Wang *et al*, 1995; Weinger *et al*, 2008).

GRB2 also recruits members of the Grb2-associated binding (Gab) family to the TCR signalosome (Yamasaki *et al*, 2003). Interestingly, two Gab-family proteins were identified in the current study as stimulation-dependent p110δ associated proteins; GAB2 and GAB3. These proteins act as scaffolds, containing multiple binding motifs and domains for the assembly of signalling complexes, including a PH domain that localises them to $PIP_3$ in the membrane, and a proline-rich domain that allows binding to GRB2 (Adams *et al*, 2012). GRB2 is thought to recruit GAB2 to LAT upon TCR ligation (Yamasaki *et al*, 2003). GAB2 is tyrosine phosphorylated by ZAP-70 and has been shown to associate with p85 and the SH2 domain-containing tyrosine phosphatase (SHP-2) in a TCR stimulation dependent manner in Jurkat T cells (Nishida *et al*, 1999). The interaction with p85 is most likely mediated via three YxxM motifs, which are present in both GAB2 and GAB3 (Sármay *et al*, 2006). Similarly, phosphorylated YxxL and YxxV motifs in GAB2 and GAB3 engage tandem SH2 domains in SHP-2 (Gu *et al*, 1998), which activates the enzyme via conformational change (Barford & Neel, 1998). It is possible that SHP-2 dephosphorylates the p85 binding motif within GAB2 and GAB3; this mechanism has been observed in the case of GAB1 in epidermal growth factor (EGF)-stimulated mouse embryonic fibroblasts (Zhang *et al*, 2002) and BCR-FcγRIIb co-stimulated B cells (Koncz *et al,* 2001). Thus, GAB2 and GAB3 could participate in both positive and negative feedback loops in T cells with respect to PI3K regulation: the former via recruitment of PI3K to the TCR signalosome, which could be sustained by further GAB accumulation at the membrane through binding to $PIP_3$ via its PH domain; the latter by binding to SHP-2, which may induce release of PI3K from the complex to terminate PI3K signalling or prevent hyperactivation of the PI3K pathway. Interestingly, mature T cells from $Gab2^{-/-}$ mice exhibit slightly enhanced proliferation in response to TCR stimulation (Yamasaki *et al*, 2003), suggesting that an inhibitory role for GAB2 dominates in T cells, perhaps through recruitment of SHP-2 to the TCR signalosome. Taken as a whole, it is intriguing that GRB2, GAB2, GAB3 and SHP-2 were all identified in the present study as TCR stimulation-dependent p110δ interactors. It is therefore possible that these proteins were isolated as a single complex with p110δ. Indeed, GAB2 and SHP-2 demonstrated a highly similar pattern of abundance across p110δ affinity purifications.

It was interesting that several proteins identified as p110δ stimulation-dependent interactors have known roles in the negative regulation of TCR signalling. Specifically, CBL, STS-2 and CD5. These proteins were identified in p110δ purifications with a mean enrichment of 2.47, 2.54 and 1.93-fold, respectively.

The E3 ubiquitin-protein ligase CBL (c-CBL) is an important negative regulator of TCR signalling in thymocytes, involved in downmodulation of the TCR upon receptor engagement (Naramura *et al*, 1998, 2002). This is thought to be mediated via CBL-promoted ubiquitination of the CD3ζ chain, with ZAP-70 acting as an adaptor in this process to form a CD3ζ:ZAP-70:CBL complex (Wang *et al*, 2001). In addition, CBL has been shown to associate with LCK and target its ubiquitination and degradation upon CD3+CD4 stimulation in a human $CD4^+$ T cell line (Rao *et al*, 2002). However, CBL-deficient mature $CD4^+$ T cells exhibit reduced proliferation and ERK activation in response to anti-CD3 stimulation (Naramura *et al*, 2002). Interestingly, CBL is able to bind to the PI3K p85 SH2 domain via a YxxM motif that is phosphorylated by Src-family kinases (Hunter *et al*, 1999). This interaction leads to the ubiquitination of p85 in some cell types (Dufour *et al*, 2008; Bulut *et al*, 2013), but the mechanism of CBL-mediated PI3K regulation in primary mature T cells is unclear. It has been suggested that, aside from its E3 ubiquitin-protein ligase activity, CBL may act as a multivalent adaptor, given that it also comprises a proline-rich region, an SH2-containing tyrosine kinase binding (TKB) domain, and several phosphorylated tyrosine residues (Lee & Tsygankov, 2013). Thus, CBL could bind to several proteins at the plasma membrane, including PI3K via its phosphorylated YxxM motif.

CBL demonstrated the same pattern of interaction with p110δ across stimulated affinity purifications as the proteins STS-2, CD5 and GRB2. This is particularly interesting as all three proteins can bind directly to CBL; GRB2 can interact via its SH3 and SH2 domains with CBL upon TCR crosslinking, and this is thought to form a distinct complex to the GRB2:SOS1 complex (Meisner *et al*, 1995). STS-2 (suppressor of TCR signalling 2; UBASH3A) contains a ubiquitin binding UBA domain and an SH3 domain, which facilitates binding to the proline-rich region of CBL (Feshchenko *et al*, 2004). STS-2 is a protein tyrosine phosphatase involved in the downregulation of TCR signalling, which is thought to be mediated via its dephosphorylation of ZAP-70 (Carpino *et al*, 2004; San Luis *et al*, 2011). Interestingly, STS-2 has been shown to form a complex with ZAP-70 and the E3 ubiquitin ligase NRDP1 in primary $CD8^+$ T cells (Yang *et al*, 2015). It is thought that polyubiquitination of ZAP-70 by NRDP1 leads to its interaction with and dephosphorylation by STS-2, or the related protein STS-1. This is an interesting example of dual

E3 ubiquitin ligase-phosphatase-mediated termination of TCR signalling. The identification of STS-2 and CBL in the present AP-MS study suggests that p110δ may interact with an STS-2:CBL complex at the early stages of TCR stimulation.

The transmembrane co-receptor CD5 also plays a role in attenuating antigen-induced TCR signalling (Lozano *et al*, 2000). The CD5 cytoplasmic domain is rapidly tyrosine phosphorylated upon TCR stimulation and this leads to the recruitment of proteins that exert a negative regulatory function, including the tyrosine phosphatase SHP-1, which dephosphorylates ZAP-70 (Plas *et al*, 1996). LCK also binds to CD5 upon CD5 ligation in Jurkat T cells and phosphorylates the Src-family kinase FYN at an inhibitory tyrosine, which decreases FYN activity and consequently leads to a reduction in ZAP-70 phosphorylation (Bamberger *et al*, 2011). However, none of the phosphotyrosines in CD5 are located within YxxM motifs. Nevertheless, p85α has been shown to associate with CD5 via non-canonical motifs *in vitro*, although this has only been confirmed by immunoprecipitation in pervanadate-stimulated thymocytes (Dennehy *et al*, 1997). Interestingly, CD5 interacts directly with CBL (Dennehy *et al* 1998; Demydenko, 2010). Moreover, a recent study found that CBL associates with CD5 upon CD3+CD4 crosslinking in primary murine activated $CD4^+$ T cells (Voisinne *et al*, 2016). Additionally, in $CD5^{-/-}$ T cells, drastically fewer ubiquitinated proteins were found to be associated with CBL upon TCR stimulation. Thus, it has been suggested that CD5 recruits CBL to the plasma membrane upon TCR stimulation, where it mediates ubiquitination of substrates. Given that the present study identified both CD5 and CBL as p110δ interactors under similar physiological conditions as those used by Voisinne *et al*, it is not unreasonable to speculate that p110δ associates indirectly with CD5 via CBL.

The aforementioned study used an AP-MS approach to investigate the CBL signalosome after TCR stimulation of primary murine activated $CD4^+$ T cells (Voisinne *et al*, 2016). Intriguingly, among the proteins selected as specific CBL-interactors were p110δ, p85α, p85β, STS-2, CD5, GRB2, CRK, CRKL, CD2AP and SH3KBP1. These proteins were also identified in the current study as p110δ interactors. This shared interactome suggests that p110δ and CBL form a stable complex upon TCR stimulation. It also indicates that these proteins could associate directly or indirectly with either p110δ or CBL. In the current study, CRK, CRKL, CD2AP and SH3KBP1 associated constitutively with p110δ, whereas CBL was clearly associated with p110δ in a TCR-stimulation dependent manner. Thus, is it likely that CRK, CRKL, CD2AP and SH3KBP1 interact directly with p110δ. In contrast, STS-2 and CD5, which lack obvious p85-binding motifs,

associated with p110δ in a TCR stimulation-dependent manner and with a similar fold enrichment and pattern of abundance to CBL. Therefore, it is possible that STS-2 and CD5 were isolated via CBL. Ultimately, it appears that p110δ forms a complex with CBL, STS-2 and CD5 upon TCR stimulation in activated $CD4^+$ T cells.

The co-receptors CD4 and CD28 were also isolated with p110δ in a TCR-stimulation dependent manner. It was observed, however, that their enrichment in p110δ purifications compared with control purifications was low and inconsistent. One explanation for this is that they may interact with p110δ transiently, with low affinity, or indirectly. In support of the latter, a direct interaction between CD4 and PI3K has not been reported, and the CD4 cytoplasmic tail lacks p85-specific YxxM motifs (Wittlich *et al*, 2007). In contrast, CD28 is a well-characterised p85 interactor, with a YxxM motif that is tyrosine phosphorylated by Src-family kinases upon TCR engagement (Rudd & Schneider, 2003). However, it is interesting that an association of p110δ with CD28 occurred upon CD3+CD4 crosslinking alone, in the absence of CD28 co-stimulation or APCs expressing the CD28 ligands B7-1/B7-2. Only low levels of p85 association with CD28 are induced upon CD3 crosslinking alone (Alcázar *et al*, 2009). It is possible that crosslinking of both CD3 and CD4 at the cell surface brings CD28 into proximity with the TCR signalosome, facilitating CD28 tyrosine phosphorylation by LCK and subsequent p85:p110δ recruitment. Surprisingly, and in contrast to the co-receptors CD4 and CD28, the CD3γ chain was enriched in p110δ purifications independently of TCR stimulation. Albeit, as observed for CD4 and CD28, this enrichment was inconsistent across samples. Since CD3γ does not possess p85-binding motifs, it could be that CD3γ was isolated indirectly with another p110δ associated protein. Nevertheless, a proportion of p110δ may reside in proximity to the CD3 complex in resting $CD4^+$ T blasts.

### 3.3.2 TCR stimulation-independent p110δ-associated proteins

As previously mentioned, CRK, CRKL, CD2AP and SH3KBP1 were found to be associated with p110δ independently of TCR stimulation and can also interact with CBL. Intriguingly, the Crk-family members CRK and CRKL are thought to stabilise the binding of p85 to CBL (Gelkop *et al,* 2001). Upon TCR stimulation, the CRK SH2 domain recognises phosphorylated YxxP motifs in CBL (Reedquist *et al*, 1996). In addition, the N-terminal SH3 domain of CRK is able to interact with proline-rich regions of p85, which has been proposed to stabilise the interaction of p85 with the same CBL molecule (Gelkop *et al,* 2001). It has also been demonstrated in Jurkat T cells that CRK and CRKL rapidly associate with the phosphorylated CD3ζ chain upon TCR crosslinking (Dong *et*

*al*, 2017). Interestingly, the adaptor GAB2, which was also identified in the present study by AP-MS, contains multiple YxxP motifs that can bind to CRK, although GAB3 lacks such motifs (Sármay *et al*, 2006). Thus, the CRK SH2 domain can mediate interactions with CBL, CD3ζ and GAB2 upon their tyrosine phosphorylation. CRK and CRKL were found to be constitutively associated with p110δ. Therefore, the binding of CRK/CRKL to CBL, CD3ζ or GAB2 upon TCR stimulation may facilitate the recruitment of p110δ to the TCR signalosome.

CD2-associated protein (CD2AP) and SH3-domain kinase binding protein 1 (SH3KBP1) are members of the CMS/CIN85 family of adaptor proteins, which interact with CBL via their SH3 domains and are involved in the degradation of receptor tyrosine kinases via clathrin-mediated endocytosis (Dikic, 2002). CD2AP is required for the termination of TCR signalling and TCR downregulation (Lee *et al*, 2003). T cells from $CD2AP^{-/-}$ mice do not form an immune synapse upon peptide-MHC presentation by APCs and exhibit prolonged tyrosine-phosphorylation of ZAP-70 and CD3ζ. The CD2AP SH3 domains have been shown to interact with p85, but this association has not been demonstrated in T cells (Huber *et al*, 2003). In contrast, a proline-rich region in the rat homologue of SH3KBP1 has been shown to interact with the SH3 domain of p85 (Gout *et al*, 2000). Interestingly, human SH3KBP1 can form complexes with CRK, CBL and p85 in resting and EGF-stimulated HEK293 cells (Watanabe *et al*, 2000). The MS identification of CD2AP, SH3KBP1, CRK and CRKL as constitutive p110δ interactors in the present study suggests that p110δ may be part of a pre-formed complex with these proteins in resting $CD4^+$ T blasts. In support of this, CRKL and SH3KBP1 exhibited a highly similar pattern of abundance as p110δ across all p110δ affinity purifications that were analysed. This proposed pre-formed complex could be recruited to the plasma membrane via CBL upon TCR stimulation.

Several other proteins were constitutively associated with p110δ in $CD4^+$ T blasts. Of these proteins, NCK1 was considered of particular interest as it has been shown to interact with BCAP in B lymphocytes (Castello *et al*, 2013). NCK1 is one of two members in the Nck family of adaptor proteins, comprising one SH2 domain and three SH3 domains (Lettau *et al*, 2009). In T cells, NCK proteins are thought to be recruited to the TCR signalosome via two mechanisms. The first SH3 domain of NCK binds to a proline-rich region in the CD3ε chain that is exposed rapidly upon TCR antigen recognition, before tyrosine phosphorylation of the CD3ζ ITAMs (Gil *et al*, 2002). NCK is also recruited through binding of its SH2 domain to phosphorylated tyrosines in the scaffolding protein SLP-76 (Koretzky *et al*, 2006). SLP-76-associated NCK is thought to regulate actin remodelling upon TCR stimulation though recruitment of Wiskott-Aldrich

syndrome protein (WASP) to the immune synapse (Zeng *et al*, 2003). However, NCK-deficient primary T cells exhibit normal TCR aggregation and internalization, which are dependent on actin remodelling. Interestingly, NCK-deficient T cells demonstrate greatly reduced TCR-induced proliferation (Roy *et al*, 2010). An association between NCK proteins and PI3K has not yet been demonstrated in T cells; NCK1 lacks YxxM motifs but could mediate interactions with the p85 proline-rich regions via its SH3 domains.

Nevertheless, in B cells, NCK is thought to facilitate the recruitment of PI3K to the BCR signalosome via BCAP (Castello *et al*, 2013). NCK interacts with the second proline-rich region of BCAP via its three SH3 domains and is required for BCAP localisation to the BCR signalosome. This is mediated via the interaction of NCK with the immunoglobulin-α tail (Castello *et al*, 2013). Given that BCAP interacts with PI3K in B cells (Okada *et al*, 2000), NCK may recruit PI3K to the BCR. In support of this, AKT and FOXO1 phosphorylation are reduced in NCK1-deficient B cells (Castello *et al*, 2013). In the proteomics study herein, NCK was found to be constitutively associated with p110δ in $CD4^+$ T blasts, whereas the interaction of p110δ with BCAP was clearly TCR stimulation-dependent. It is possible that NCK facilitates the interaction between PI3K and BCAP upon TCR stimulation. Subsequently, NCK could recruit this complex to the TCR via binding to the CD3ε chain or SLP-76. This hypothesis requires biochemical examination of BCAP and NCK in $CD4^+$ T blasts.

Another protein of particular interest was insulin receptor substrate 2 (IRS2). IRS2 is a member of the IRS family of cytosolic scaffolding proteins and contains eight YxxM motifs (Sun *et al*, 1995). In the canonical IRS activation pathway, IRS proteins undergo insulin-dependent tyrosine phosphorylation by the insulin receptor kinase (IRK) and subsequently associate with p85 via their YxxM motifs (Balbis *et al*, 2000). Nevertheless, IRS proteins also signal downstream of integrin, cytokine and growth hormone receptors (Waters & Pessin, 1996). In mature T cells, IRS2 has been shown to associate with p85 downstream of IL-4 receptor activation (Wurster *et al*, 2002). Identification of IRS2 in the present study suggests that the TCR signalosome recruits IRS2 as an adaptor molecule for PI3K. Interestingly, tyrosine phosphorylation sites in the IRS2 homologue IRS1 can bind to GRB2, SHP2, NCK and CRK (Lee *et al*, 1993; Skolnik *et al*, 1993; Beitner-Johnson *et al*, 1996; Myers *et al*, 1998). It is therefore possible that IRS2 could act as a docking site for multiple p110δ-associated proteins that were identified in this study. Interestingly, IRS2 did not demonstrate TCR stimulation-dependent association with p110δ, suggesting that they could be constitutively associated in activated T cells. Further biochemical

analyses would be required to examine the tyrosine phosphorylation status of IRS2 in unstimulated T blasts, and to determine whether IRS2 forms TCR stimulation-dependent interactions with GRB2, SHP2, NCK or CRK.

The transmembrane receptor JAML (junctional adhesion molecule-like) was also identified as a stimulation-independent p110δ interactor. JAML promotes the adhesion of leukocytes to endothelial cells via binding to the coxsackievirus and adenovirus receptor (CAR) (Luissint *et al*, 2008). Intriguingly, JAML is upregulated on activated $CD8^+$ T cells and has also been shown to act as a co-stimulatory receptor specifically in a subset of epithelial γδ T cells (Witherden *et al*, 2010). In these cells, co-ligation of the TCR and JAML potentiates the proliferation and cytokine production induced by TCR stimulation alone (Witherden *et al*, 2010). Ligation of JAML alone also leads to the phosphorylation of AKT in this subset of T cells. This has been attributed to the interaction of p85 with JAML; CAR-mediated clustering of JAML on γδ T cells rapidly recruits PI3K to a YxxM motif in the JAML cytoplasmic tail (Verdino *et al*, 2010). PI3K was also found to be associated with JAML in resting cells, albeit at lower levels. In the present study, JAML was identified as a p110δ-associated protein in unstimulated and stimulated $CD4^+$ T blasts. This raises the possibility that PI3K may be constitutively associated with JAML in activated $CD4^+$ T cells, independently of TCR or JAML engagement. Thus, JAML may act as an adaptor for PI3K localisation at the plasma membrane in activated T cells. Furthermore, if an interaction with p85 occurs via the YxxM motif of JAML, this would require basal tyrosine phosphorylation of JAML in resting cells. The phosphorylation status of JAML and interaction with PI3K in $CD4^+$ T blasts warrants further biochemical analyses.

Surprisingly, the PI3K effector AKT2 was also identified as associated with p110δ in both unstimulated and stimulated $CD4^+$ T blasts. There are three mammalian AKT isoforms, AKT1, AKT2 and AKT3, which are highly homologous, and their functional redundancy appears to be tissue and context dependent (Vanhaesebroeck & Alessi, 2000; Manning & Toker, 2017). Nevertheless, all three isoforms are expressed in murine T cells (Juntilla *et al*, 2007). PI3K regulates AKT by producing the $PIP_3$ required for its co-localisation with PDK1 and subsequent activation at the plasma membrane (Stokoe *et al*, 1997). Interestingly, AKT2 is also activated by $PI(3,4)P_2$ located both in the plasma membrane and early endosomes (Liu *et al*, 2018). However, direct interaction between AKT and PI3K has not been reported. The TCR stimulation-independent association of AKT2 and p110δ in $CD4^+$ T blasts suggests that PI3K and AKT2 are co-localised in activated T cells before and after TCR engagement.

Another serine/threonine kinase, GRK2, was associated with p110δ in unstimulated and stimulated $CD4^+$ T blasts. GRK2 (β-adrenergic receptor kinase 1) is a ubiquitous member of the GPCR kinase (GRK) family, which, despite its name, phosphorylates a vast variety of receptors and cytosolic proteins (Penela *et al*, 2010). GRK2 contains a PH domain and binding to $PIP_2$ activates the enzyme, in combination with protein-protein interactions (DebBurman *et al* 1996). GRK2 has recently been shown to be involved in the transactivation of the chemokine receptor CXCR4 following TCR stimulation, which involves TCR-induced tyrosine phosphorylation of GRK2 by a Src-family kinase or ZAP-70 (Dinkel *et al*, 2018). While this suggests that GRK2 is localised to the TCR signalosome, it is unclear whether GRK2 interacts directly with PI3K. Interestingly, GRK2 has been reported to interact directly with AKT and to inhibit AKT kinase activity (Liu *et al*, 2005). Both GRK2 and AKT2 were identified by AP-MS as constitutively associated with p110δ. Thus, it is possible that this complex forms in activated $CD4^+$ T cells.

It is also unclear how IQGAP3 may be associated with p110δ in activated $CD4^+$ T cells. The IQGAP family of proteins are multimodular scaffolds that have been linked to the regulation of both microtubule and actin cytoskeletal reorganisation (Hedman *et al*, 2015). Indeed, IQGAP1 has been shown to negatively regulate TCR stimulation, partly via modulating F-actin dynamics (Gorman *et al*, 2012). However, the role of IQGAP3 in lymphocytes has not yet been studied. IQGAP3 is able to interact with the GTP-bound active form of RAS, as well as CDC42 and RAC1, and is thought to activate RAS by inhibiting its intrinsic GTPase activity (Nojima *et al*, 2008). It is unclear whether IQGAP3 could play a role in the activation or localisation of PI3K. Interestingly, inspection of the IQGAP3 amino acid sequence reveals the presence of two YxxM motifs. However, IQGAP3 was found to associate with p110δ independently of TCR stimulation in this study. The tyrosine phosphorylation status of IQGAP3 has not yet been studied; biochemical analyses of IQGAP3 in primary T cells would be required to investigate both its post-translational regulation and putative association with p85.

Similarly, an association of MALT1 with PI3K has not been previously reported, although its role in T cells is well-studied. Mucosa-associated lymphoid tissue lymphoma translocation gene 1 (MALT1) is a cysteine protease that forms a complex with CARMA1 and B-cell lymphoma 10 (BCL10) upon TCR stimulation, triggered by PKCθ phosphorylation of CARMA1. This CARMA1-BCL10-MALT1 (CBM) complex connects TCR signalling to the canonical NF-κB signalling pathway via activation of the IκB kinase (IKK) complex, which subsequently phosphorylates inhibitors of NF-κB and leads to nuclear translocation of NF-κB (Schulze-Luehrmann & Ghosh, 2006). MALT1

serves as both an adaptor and a protease, required for optimal NF-κB activation via proteolytic cleavage of several substrates, including A20, a deubiquitinase that negatively regulates NF-κB activation (Coornaert *et al*, 2008; Rebeaud *et al*, 2008). In addition to this role, the CARMA1-MALT1 complex, independently of IKK, is required for the optimal activation of mTORC1 in TCR-CD28 co-stimulated $CD4^+$ T cells (Hamilton *et al*, 2014). A direct association between the CBM complex and PI3K has not been demonstrated, thus it is unclear how p110δ may be associated with MALT1. It is possible that they share interaction partners or are co-localised at the TCR signalosome. Nevertheless, this putative link between the PI3K and NF-κB pathways warrants further investigation.

Lastly, the ubiquitin-like modifier ISG15 (interferon stimulated gene 15) was identified as a TCR stimulation-independent p110δ associated protein. ISG15 conjugation (ISGylation) of proteins may promote their degradation through the lysosome (Villarroya-Beltri *et al*, 2016). The physiological relevance of ISGylation in T cells remains to be elucidated (Friend *et al*, 2014). It is possible that p110δ-associated proteins identified in this study could be regulated by ISGylation.

### 3.3.3 Previously proposed p110δ interactors downstream of TCR engagement

It was noteworthy that proteins previously proposed to bind and recruit PI3K during TCR signalling were not identified by MS as p110δ interactors; for example, SLP-76, LAT, ZAP-70 and TC21. There are two possible interpretations of this observation: either these proteins do not interact with PI3K at the TCR signalosome in activated T cells, or, they do interact but were not detected by AP-MS. Previous studies demonstrated the capacity for SLP-76, LAT and ZAP-70 to bind to p85 *in vitro* (Paz *et al*, 2001; Shim *et al*, 2004; Moon *et al*, 2005). However, these interactions may not occur in the physiological environment of the cell. Associations with PI3K have also been reported in the immortalised Jurkat T cell line, in the case of LAT and SLP-76 (Zhang *et al*, 1998; Shim *et al*, 2004), and in naïve lymph node cells, in the case of TC21 (Delgado *et al*, 2009). However, the same interactions may not occur in activated $CD4^+$ T cells; the recruitment of PI3K to the TCR may rely on different adaptors in immortalised and naïve T cells compared to activated T cells.

Alternatively, interactions with these proteins may be of low affinity or occur with fast kinetics, and therefore could have been lost during the affinity purification procedure. Indeed, the interaction of p110γ with NRAS via its RBD is both low affinity and transient (Pacold *et al*, 2000), and thus it is likely that interactions of p110δ with Ras GTPases, such as TC21, may not be

preserved during affinity purification. Furthermore, p85 has been predicted to bind to SLP-76 and LAT via the non-canonical phosphotyrosine motifs YESP and YVNV, respectively (Paz *et al*, 2001; Shim *et al*, 2004). These interactions may be of low affinity, given that the p85 SH2 domains preferentially bind to phosphotyrosine motifs containing methionine at the +3 position and bind optimally to bidentate YxxM motifs that can engage both SH2 domains simultaneously (Songyang *et al*, 1993; Burke *et al*, 2011).

A further explanation is that p85 may interact only indirectly with LAT and SLP-76 in activated T cells, and consequently their association may not have been detected by affinity purification. In the present study, the adaptors GRB2 and NCK1 were identified by MS as p110δ-associated proteins, and these proteins are known to interact with phosphotyrosines in LAT and SLP-76, respectively (Zhang *et al*, 2000; Koretzky *et al*, 2006). Therefore, a multiprotein complex may form at the TCR signalosome whereby PI3K is recruited to LAT and SLP-76 via GRB2 and NCK1. This could explain the observations of previous studies that isolated p85 with LAT and SLP-76 by co-immunoprecipitation (Zhang *et al*, 1998; Shim *et al*, 2004).

Collectively, the quantitative AP-MS approach identified proteins that specifically associate with endogenous p110δ in $CD4^+$ T blasts. It was remarkable that the majority of proteins identified were known to be involved in TCR signal transduction, and, moreover, that most are able to interact directly with p85. Thus, it is possible to speculate on the molecular organisation of the p110δ interactome that was identified herein, based on previously reported protein-protein interactions (Figure 3.6). From the 24 selected proteins of interest, the first protein chosen for biochemical validation and analysis was BCAP. This was for two intriguing reasons. First, BCAP is proposed to act as an adaptor for PI3K recruitment to the B cell antigen receptor, and thus may play an analogous role in T cells. Secondly, BCAP was not thought to be expressed in T lymphocytes. Therefore, subsequent experiments aimed to investigate the expression and regulation of BCAP in primary $CD4^+$ T blasts.

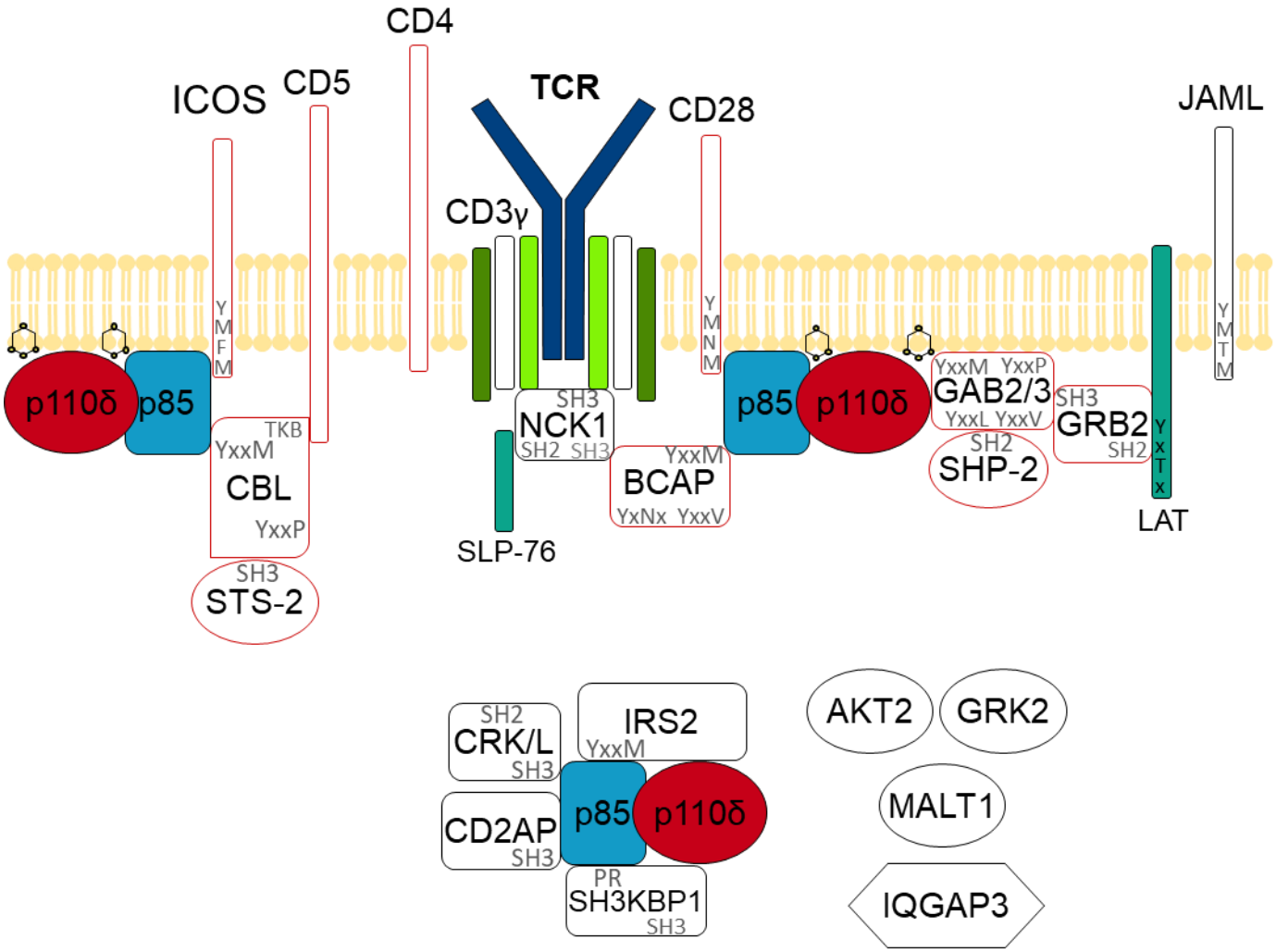


**Figure 3.6 The p110δ interactome in CD4⁺ T blasts.**
A model for the protein-protein interactions involved in p110δ recruitment and activation at the TCR signalosome, based on proteins identified by a quantitative proteomic analysis of p110δ affinity purifications from primary CD4⁺ T blasts. Proteins that associated with p110δ in a TCR stimulation-dependent manner are drawn in red (unfilled). TCR stimulation-independent interactors are in black (unfilled). SLP-76, LAT, and the TCR-CD3 complex are included but were not identified by AP-MS. Amino acid motifs and protein domains involved in previously reported interactions between proteins are annotated in grey. See section 3.3 text for detailed descriptions of the proteins shown.

# Chapter 4

# A new role for BCAP in TCR-PI3K signalling in activated T cells

## 4.1 Introduction

BCAP was first identified in chicken DT40 B cells by affinity purification using the N-terminal SH2 domain of p85 (Okada *et al*, 2000). It was concluded that BCAP is expressed predominantly in B cells and macrophages, based on the absence of BCAP mRNA in the T cell lines EL-4 and BW5147 (Okada *et al*, 2000) and the lack of BCAP protein detected in naïve mouse splenic $CD3^+$ T cells (Yamazaki *et al*, 2002). Two BCAP transcripts are generated by alternative initiation or splicing of the *Pik3ap1* gene and encode two isoforms in mouse B cells, with observed molecular weights of 70 and 72 kDa (short isoform) and 98 and 100 kDa (long isoform) (Okada *et al*, 2000).

BCAP is tyrosine phosphorylated in mouse B cells upon BCR crosslinking and associates with PI3K p85 in a BCR stimulation-dependent manner, which correlates with BCAP phosphorylation (Okada *et al*, 2000). Tyrosine phosphorylation of BCAP and its association with p85 is also induced by CD19 crosslinking alone (Inabe & Kurosaki, 2002). Furthermore, BCR-dependent tyrosine phosphorylation of long-isoform BCAP is reduced in DT40 cells in the absence of NCK, an adaptor protein that binds to immunoglobulin-α of the BCR complex (Castello *et al*, 2013). BCAP recruitment to the BCR signalosome is also impaired in these NCK-deficient cells. Collectively, these studies have elucidated the role of BCAP as an adaptor for PI3K recruitment to the BCR upon receptor engagement.

The identification of BCAP as a p110δ-associated protein in the present study suggests a new role for BCAP in $CD4^+$ activated T cells. The fact that this association was TCR stimulation-dependent indicates that BCAP may be involved in the recruitment and activation of PI3K upon TCR engagement. Experiments were therefore undertaken to investigate the expression and regulation of BCAP in $CD4^+$ activated T cells.

## 4.2 Results

### 4.2.1 BCAP is expressed in primary CD4$^+$ T blasts

Lysates from activated CD4$^+$ T cells (T blasts) were analysed by immunoblotting for BCAP protein expression (Figure 4.1A). In the absence of BCAP$^{-/-}$ cells as a negative control, T blast lysates were compared with those from naïve splenic B cells and previous reports probing murine B cells using the same anti-BCAP antibody (Okada *et al*, 2000; Yamazaki *et al*, 2002; Inabe & Kurosaki, 2002). Several protein species were detected within the expected molecular weight ranges for long and short BCAP isoforms in both cell types. In naïve B cells, the relative abundances of these species differed in unstimulated and BCR-stimulated cells, possibly reflecting an increase in phosphorylated BCAP upon stimulation that migrates more slowly by SDS-PAGE. This was not as pronounced in CD4$^+$ T blasts, and BCAP protein levels appeared lower than in naïve B cells. Analysis of BCAP in whole cell lysates was complicated somewhat by the high number of potentially non-specific proteins detected by immunoblotting using the anti-BCAP antibody.

To more clearly study the BCAP isoforms present in CD4$^+$ T blasts, immunoprecipitation was performed to specifically enrich BCAP protein for immunoblot analysis. This revealed the expression of distinct long and short BCAP isoforms in CD4$^+$ T blasts (Figure 4.1B).

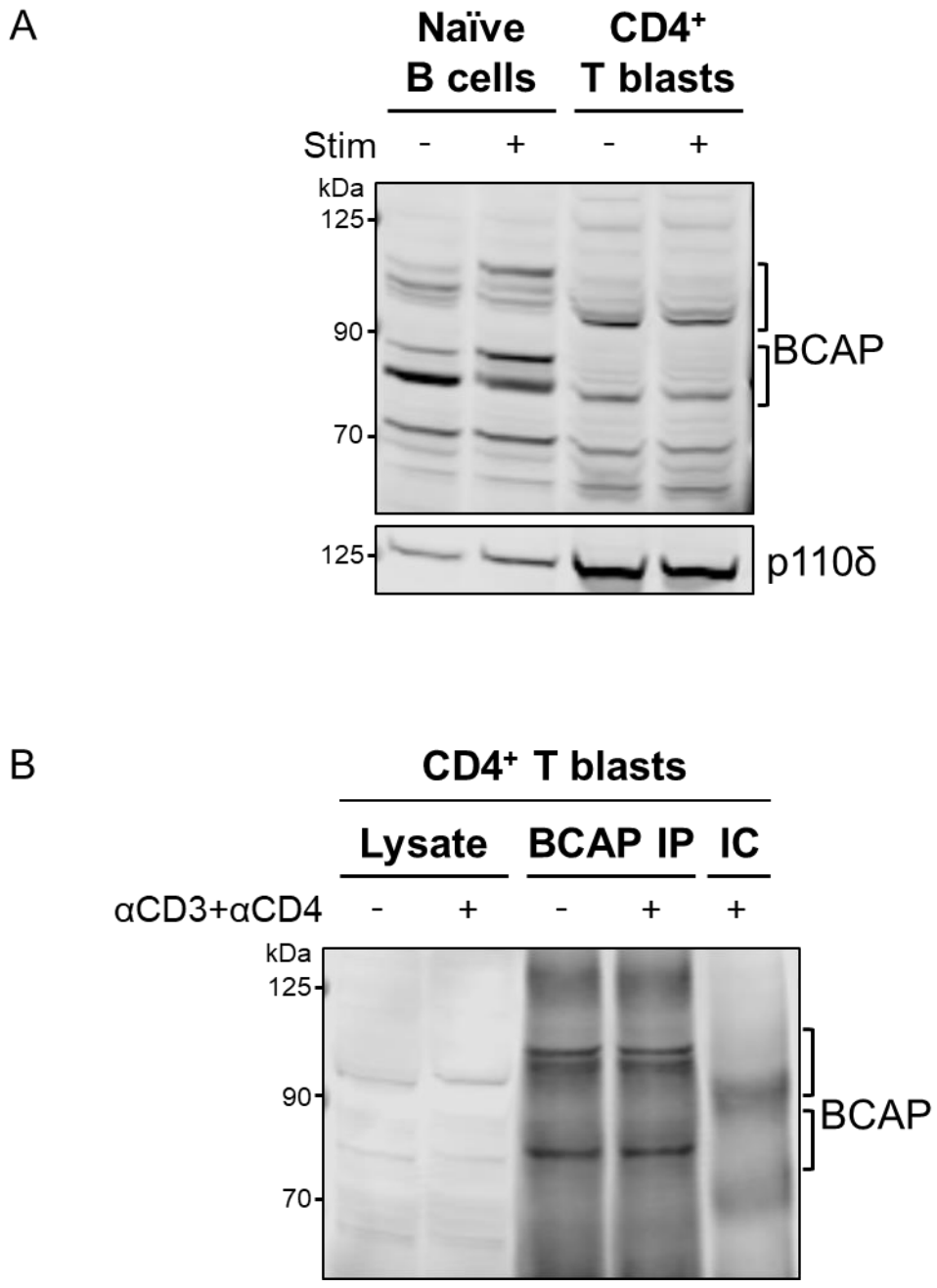


**Figure 4.1 BCAP is expressed in CD4⁺ T blasts.**

**A.** Immunoblot analysis of BCAP protein in naïve splenic B cells and CD4⁺ T blasts. Naïve B cells were stimulated with 50 µg/ml anti-mouse IgM $(Fab')_2$ for 2.5 minutes and CD4⁺ T blasts were stimulated with 4 µg/ml αCD3+αCD4 for 1 minute. Cell lysates equivalent to 1.33 million unstimulated (-) or stimulated (+) cells were separated by SDS-PAGE and immunoblotted for BCAP and p110δ. Brackets indicate the expected BCAP protein species.

**B.** Immunoprecipitation of BCAP protein from CD4⁺ T blasts. Twenty-million CD4⁺ T blasts were stimulated with 4 µg/ml αCD3+αCD4, or left unstimulated, for 1 minute and cell lysates were immunoprecipitated with anti-mouse BCAP antibody or IgG isotype control (IC). Cell lysates equivalent to 1.33 million cells were separated by SDS-PAGE alongside $\frac{3}{10}$ of each immunoprecipitation (IP) and immunoblotted for BCAP.

To compare the BCAP isoforms detected in $CD4^+$ T blasts with those expressed in B cells, BCAP was also immunoprecipitated from naïve splenic B cells. B cells were stimulated by BCR crosslinking for various times and purified BCAP was analysed by immunoblotting (Figure 4.2). Similar to previous reports, B cells expressed five BCAP species, four of which were tyrosine phosphorylated upon BCR activation. Notably, there was an increase in the abundance of species 5, and a concomitant decrease in species 4, upon BCR stimulation, with both species inducibly tyrosine phosphorylated. This suggests that species 5 could be a highly phosphorylated form of species 4. A similar pattern was observed for species 1 and 2. Interestingly, this shift in BCAP species was not seen in $CD4^+$ T blasts upon TCR stimulation (Figure 4.1B).

Tyrosine phosphorylation of BCAP in B cells peaked at 2.5 minutes and returned to basal levels at 10 minutes, although the abundances of species 2 and 5 were still elevated at this time point compared with unstimulated levels (Figure 4.2). The PI3K regulatory subunit p85 co-immunoprecipitated at low abundance with BCAP from both unstimulated and stimulated cells. This could reflect the basal tyrosine phosphorylation of BCAP seen in these experiments, and not in previous reports (Okada *et al*, 2000). A slight increase in p85 association with BCAP was observed at 2.5 minutes following BCR-stimulation, correlating with the peak of phosphorylation. Unfortunately, an isotype control IP could not be included in this experiment, due to low cell numbers, to confirm the specificity of the p85 co-immunoprecipitation.

Overall, these experiments indicate that long and short isoforms of BCAP are expressed in both naïve B cells and $CD4^+$ T blasts, but their post-translational regulation downstream of the BCR and TCR, respectively, may differ.

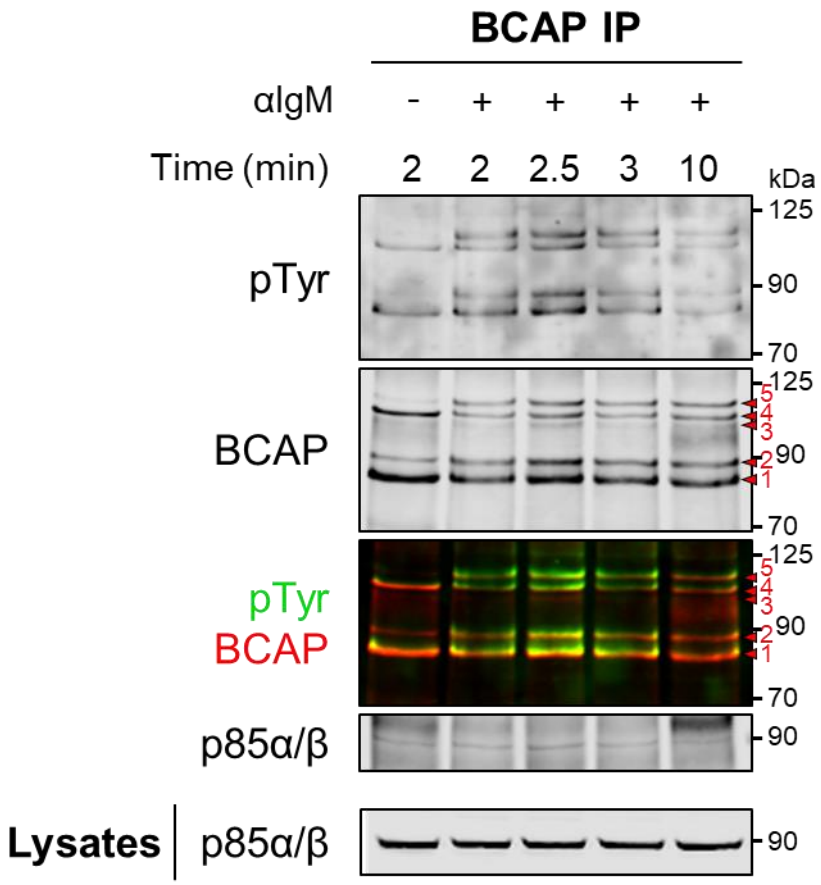


**Figure 4.2 Tyrosine phosphorylation of BCAP upon BCR stimulation in naïve B cells.**
Immunoprecipitation of BCAP protein from naïve splenic B cells. Ten-million cells per condition were stimulated with 50 µg/ml anti-mouse IgM $(Fab')_2$ (αIgM), or left unstimulated, for the times indicated and cell lysates were immunoprecipitated with anti-mouse BCAP antibody. Two-fifths of each IP and lysates equivalent to 1 million cells were separated by SDS-PAGE and immunoblotted for phosphotyrosine (pTyr), BCAP and p85 (pan-p85). The signals detected for pTyr and BCAP are overlaid in the third panel in green and red, respectively. Red arrows indicate BCAP species 1, 2, 3, 4 and 5.

### 4.2.2 BCAP is phosphorylated upon TCR stimulation and associates with PI3K in primary CD4$^+$ T blasts

To investigate whether BCAP is post-translationally modified upon TCR engagement, BCAP was immunoprecipitated from CD4$^+$ T blasts that had been stimulated by CD3 and CD4 crosslinking for various times (Figure 4.3). As in B cells, CD4$^+$ T blasts expressed five BCAP species, but there was no increase in the abundance of species 2 or 5 upon stimulation. Strikingly, there was a rapid induction of BCAP tyrosine phosphorylation upon TCR stimulation, and this was greatest for the long-isoform species, 4 and 5. Species 5 had the lowest abundance of the five, yet exhibited strong tyrosine phosphorylation, suggesting that it may contain multiple phosphorylated tyrosine residues. This phosphorylation dissipated completely within 2 minutes of TCR crosslinking. In contrast, the strong tyrosine phosphorylation of species 4 decreased over 5 minutes but did not return to basal levels in the time studied. Tyrosine phosphorylation of short-isoform species 1 and 2 was considerably lower than that observed for the long isoforms but demonstrated the same pattern of dephosphorylation as species 4 and 5, respectively.

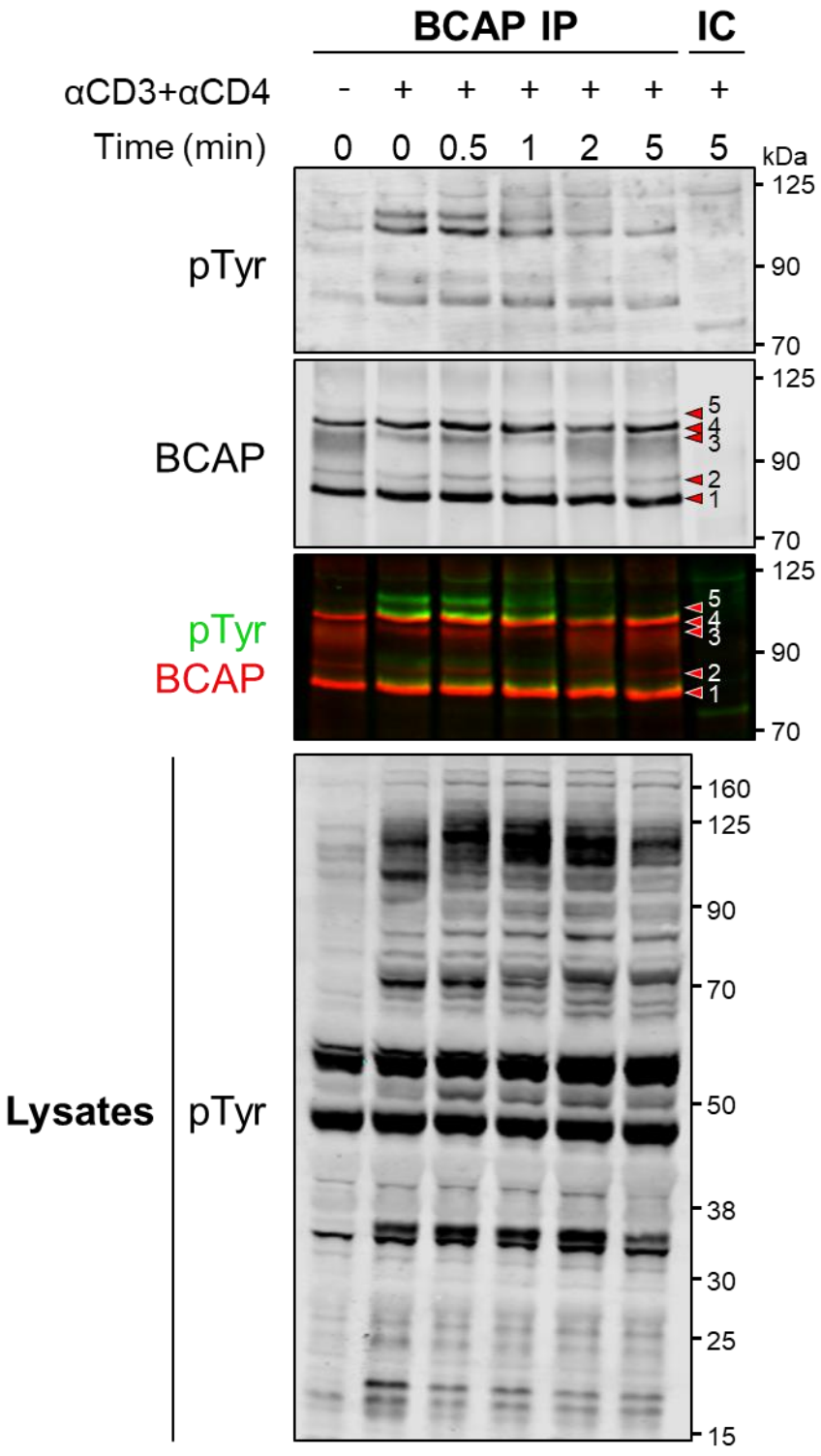


**Figure 4.3 BCAP is tyrosine phosphorylated upon TCR stimulation in CD4⁺ T blasts.**
Immunoprecipitation of BCAP protein from CD4⁺ T blasts. Twenty-million CD4⁺ T blasts per condition were stimulated with 4 µg/ml αCD3+αCD4 for the indicated times and cell lysates were immunoprecipitated with anti-mouse BCAP antibody or IgG isotype control (IC). One-third of each IP and lysates equivalent to 1 million cells were separated by SDS-PAGE and immunoblotted for phosphotyrosine (pTyr) and BCAP. The signals detected for pTyr and BCAP are overlaid in the third panel in green and red, respectively. Arrows indicate BCAP species 1, 2, 3, 4 and 5. Blots shown are representative of 3 independent experiments.

It was next examined whether BCAP associates with PI3K in CD4$^+$ T blasts. Immunoblot analysis revealed that low levels of p85 co-immunoprecipitated with BCAP and this appeared to be from TCR-stimulated cells only (Figure 4.4). p85 association with BCAP appeared to be almost absent after 5 minutes stimulation. The low abundance of p85 associated with BCAP could reflect that their interaction is transient or of low affinity.

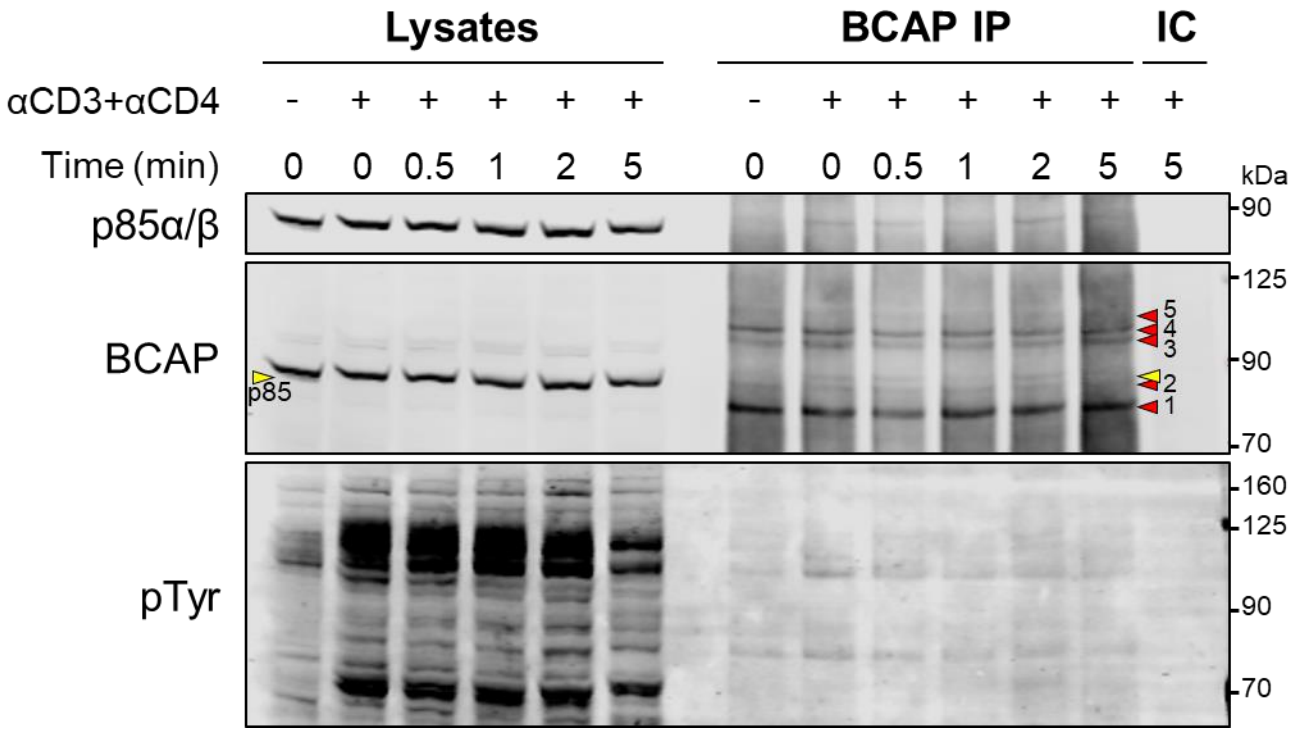


**Figure 4.4 BCAP associates with p85 at low levels in CD4$^+$ T blasts.**
Immunoprecipitation of BCAP and co-immunoprecipitation of p85 from CD4$^+$ T blasts. Twenty-million CD4$^+$ T blasts per condition were stimulated with 4 μg/ml αCD3+αCD4 for the indicated times and cell lysates were immunoprecipitated with anti-mouse BCAP antibody or IgG isotype control (IC). One-third of each IP and lysates equivalent to 1 million cells were separated by SDS-PAGE and immunoblotted for p85 (pan-p85), phosphotyrosine (pTyr) and BCAP. Red arrows indicate BCAP species 1, 2, 3, 4 and 5. Yellow arrows represent p85α/β detected in the previous immunoblot. Blots shown are representative of 3 independent experiments.

Collectively, these results demonstrate that BCAP is rapidly phosphorylated upon TCR engagement in activated CD4$^+$ T cells and suggest that BCAP associates with PI3K in a TCR stimulation-dependent manner. Based on the previously identified role of BCAP in BCR-PI3K signalling, this suggests that BCAP may act as an adaptor for PI3K recruitment downstream of the TCR.

### 4.2.3 BCAP is upregulated in activated T cells

BCAP was identified in the present study as a p110δ-associated protein in activated $CD4^+$ T cells and was found to be tyrosine phosphorylated in these cells upon TCR stimulation. It remained unanswered whether BCAP was also expressed in naïve $CD4^+$ T cells, and if it was similarly regulated in naïve cells. Therefore, immunoprecipitations using anti-BCAP antibody were performed on lysates from primary mouse naïve $CD4^+$ T cells (Figure 4.5). The BCAP protein species 1, 2, 4 and 5 were not detected in naïve T cells. The low-abundance non-tyrosine phosphorylated BCAP species 3, found in $CD4^+$ T blasts and naïve B cells, was detected by immunoblotting in naïve $CD4^+$ T cells. However, the identity of this species cannot be confirmed as BCAP protein without further experiments using $BCAP^{-/-}$ cells. Nevertheless, these results indicate that BCAP protein is expressed in activated $CD4^+$ T cells at markedly higher levels than in naïve T cells.

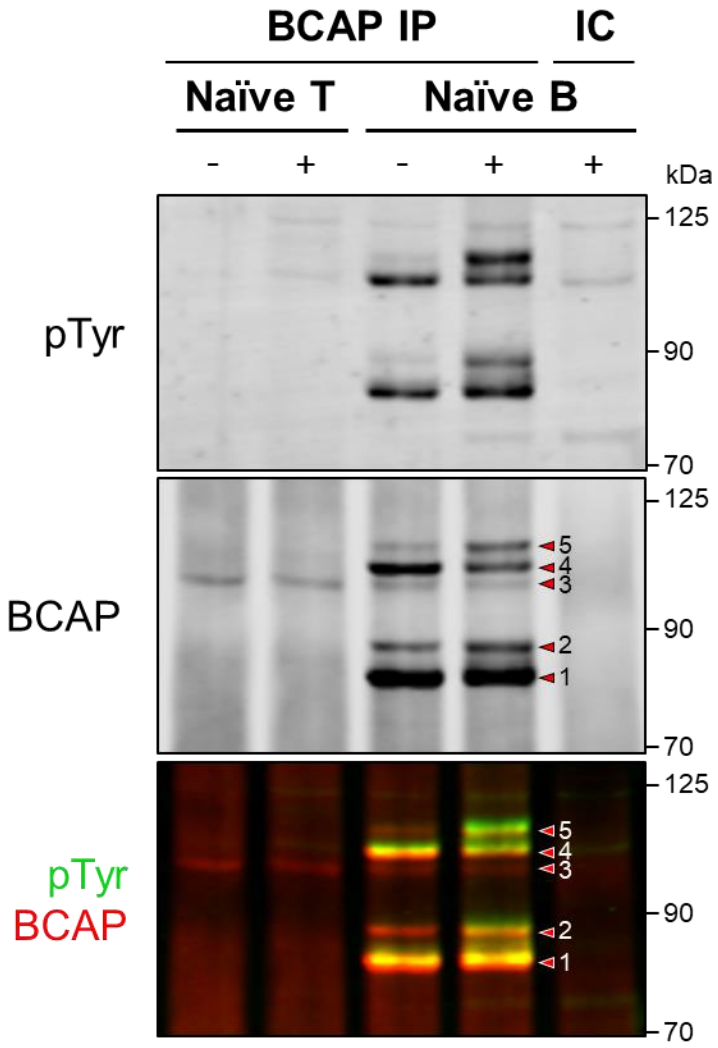


**Figure 4.5 BCAP is not expressed in naïve CD4⁺ T cells.**
Immunoprecipitation of BCAP protein from naïve CD4⁺ T cells and naïve splenic B cells. Naïve CD4⁺ T cells were stimulated with 4 µg/ml αCD3+αCD4 for 30 seconds and naïve B cells were stimulated with 50 µg/ml anti-mouse IgM $(Fab')_2$ for 2.5 minutes. Cell lysates from 10-million unstimulated (-) or stimulated (+) cells were immunoprecipitated with anti-mouse BCAP antibody or IgG isotype control (IC). One-half of each IP was separated by SDS-PAGE and immunoblotted for phosphotyrosine (pTyr) and BCAP. The signals detected for pTyr and BCAP are overlaid in the third panel in green and red, respectively. Red arrows indicate BCAP species 1, 2, 3, 4 and 5.

The observations made in CD4⁺ T cells raised the question of whether naïve and activated CD8⁺ T cells also exhibited distinct differences in BCAP expression. To this end, *in vivo* RNA sequencing data from naïve and antigen-specific effector murine CD8⁺ T cells were analysed for expression of *Pik3ap1*, which encodes BCAP (Figure 4.6). The normalised transcript abundance detected for the gene *Lyn* was used as a threshold for expression, as LYN is not expressed in primary T lymphocytes (Yamanashi *et al*, 1989; Beavitt *et al*, 2005; Tsantikos *et al*, 2009). Strikingly, *Pik3ap1* was not expressed in naïve CD8⁺ T cells, but it was expressed in effector CD8⁺ T cells.

For comparison, the expression of four genes associated with the differentiation of naïve $CD8^+$ cells into effector $CD8^+$ cells, *Cd44*, *Sell*, *Foxo1* and *Bach2*, were also examined. The cell adhesion molecule CD44 is an early indicator for T cell activation that is upregulated upon TCR stimulation and is likely to be important for effector T cell migration (DeGrendele *et al*, 1997). In contrast, L-selectin (CD62L; encoded by *Sell*) is downregulated upon T cell activation, which is thought to allow homing of effector cells to sites of infection (Andersson *et al*, 1994). The transcription factor *Foxo1* is also downregulated by TCR signals upon T cell activation (Stittrich *et al*, 2010; Bothur *et al*, 2015; Ban *et al*, 2017), as is *Bach2*, a transcriptional repressor that maintains the naïve T cell state (Tsukumo *et al*, 2013). In line with previous studies, RNA sequencing analysis from this study showed an upregulation of *Cd44* and downregulation of *Sell*, *Foxo1* and *Bach2* in effector $CD8^+$ T cells compared with naïve $CD8^+$ T cells (Figure 4.6). The fact that BCAP-encoding *Pik3ap1* was distinctly upregulated in parallel with these transcriptional changes strengthens the conclusions from earlier experiments that BCAP plays a role in activated T cells.

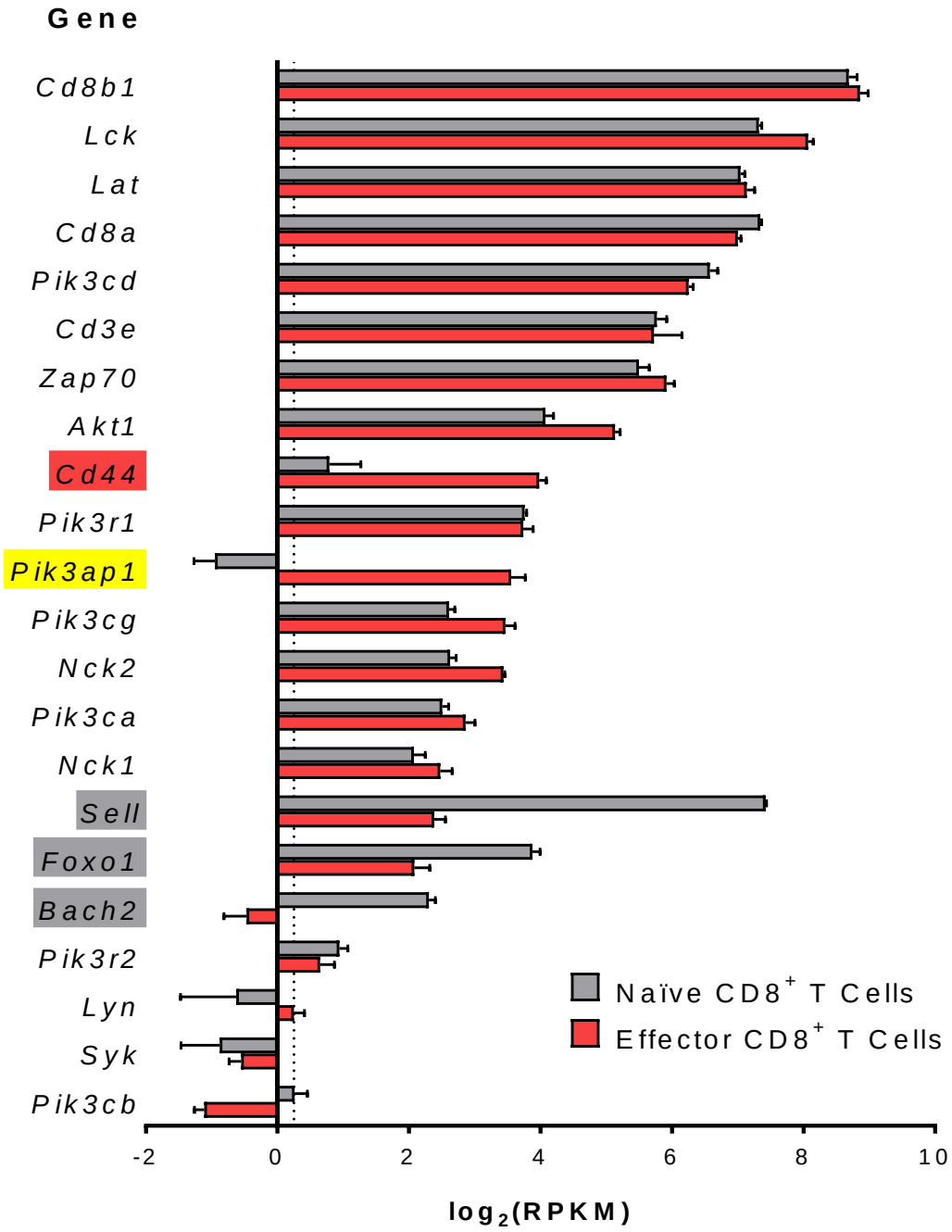


**Figure 4.6 BCAP is upregulated in effector CD8⁺ T cells.**
Expression levels of selected genes in naïve and effector CD8⁺ T cells as determined by RNA sequencing. Naïve ($CD44^{-}CD62L^{hi}$) $CD8^{+}$ T cells were purified by flow cytometric sorting from splenic cells of wild type mice. Effector ($CD44^{+}CD62L^{lo}$H-$2K^{b}$-SIINFEKL$^{+}$ antigen-specific) $CD8^{+}$ T cells were purified by flow cytometric sorting from splenic cells of wild type mice on day 7 post-infection with ΔActA-Lm-Ova. Normalised transcript abundances for each gene are reported as Reads Per Kilobase of transcript per Million mapped reads (RPKM). Bars represent the mean of 3 (naïve) or 4 (effector) biological replicates, each from one mouse. Error bars show SEM. The dotted line drawn at $\log_2$(RPKM)=0.25 indicates the threshold used for expression. Genes downregulated in effector cells are highlighted in grey; genes upregulated in effector cells are highlighted in red. *Pik3ap1*, encoding BCAP, is highlighted in yellow.
*This experiment was performed by Hicham Bouabe and the data were re-analysed for the current study.*

## 4.3 Discussion

Earlier AP-MS analyses identified BCAP as a TCR stimulation-dependent p110δ-associated protein in activated $CD4^+$ T cells. Subsequent experiments have shown that BCAP is rapidly tyrosine phosphorylated upon TCR engagement (Figure 4.3) and concurrently associates with p85 (Figure 4.4). Together, these results suggest that BCAP may serve as an adaptor protein in activated T cells, involved in PI3K recruitment to the TCR and plasma membrane.

Tyrosine phosphorylation of BCAP upon TCR stimulation could provide binding sites to the p85 PI3K regulatory subunit. Murine BCAP contains three YxxM motifs (Okada *et al*, 2000). The p85 subunit contains two SH2 domains that bind with high affinity to phosphorylated tyrosines located within YxxM motifs (Songyang *et al*, 1993). The p85 SH2:pYxxM interaction is important not only for recruitment of PI3K to the plasma membrane, through interaction with YxxM-containing proteins, but also for increasing PI3K activity via release of SH2 domain inhibitory contacts with p110 upon binding (Burke & Williams, 2013). Indeed, BCAP was first isolated from chicken DT40 B cells using the N-terminal SH2 domain of p85 (Okada *et al*, 2000). Furthermore, a mutant long-isoform chicken BCAP protein in which four YxxM motifs are mutated to FxxM does not associate with p85 in DT40 B cells upon BCR stimulation or CD19-crosslinking (Okada *et al*, 2000; Inabe & Kurosaki, 2002). In addition, this FxxM mutant does not restore the decreased activation of AKT observed in BCAP-deficient DT40 cells, as measured by *in vitro* kinase assays. Immunoprecipitation studies have also shown that BCAP-deficient DT40 cells expressing the FxxM BCAP mutant do not exhibit the highest molecular weight tyrosine phosphorylated BCAP species that are seen in wild type cells (Okada *et al*, 2000). However, tyrosine phosphorylation of BCAP is still observed in these cells. This suggests that high-molecular weight BCAP species (species 5 in this study) represent the long isoform phosphorylated at one or more YxxM motifs, but that additional tyrosine phosphorylation sites are also present. Indeed, long-isoform murine BCAP contains 23 potential phosphotyrosine residues. Collectively, these studies demonstrate that in B cells, BCAP is likely to bind to the SH2 domains of p85 via its YxxM motifs.

In the present study, long-isoform BCAP species 5 was strongly tyrosine phosphorylated upon TCR-stimulation, despite having lower abundance than the other species present (Figure 4.3). Therefore, this species may contain multiple phosphorylated tyrosine residues, which could be located within YxxM motifs. Interestingly, p85 still co-immunoprecipitated with BCAP at time points following BCR stimulation when phosphorylation of species 5 could no longer be detected, while species 1 and 4 remained tyrosine phosphorylated (Figure 4.4). Taken together,

these results suggest that p85 could associate with phosphorylated tyrosines in either the long or short isoform or BCAP, or it may bind via other protein domains. BCAP also contains three proline-rich regions, and it is not known if these interact with the SH3 domain of p85. Both isoforms of BCAP contain three YxxM motifs (at Y420, Y445 and Y460) and differ only by the absence of residues 1-179, which form a Toll/interleukin-1 receptor (TIR) domain (Halabi *et al*, 2017).

Unlike in BCR-stimulated naïve B cells, where all BCAP species were tyrosine phosphorylated similarly, the TCR-induced tyrosine phosphorylation of BCAP was predominantly of the long-isoform species 4 and 5 (Figure 4.3). This could indicate a dominant role for the long isoform in activated T cells. It may also reflect the difference in available tyrosine kinases with specificity for BCAP in T blasts, compared with those in naïve B cells. Studies using LYN-, SYK- and BTK-deficient DT40 B cells have suggested that SYK and BTK initiate and sustain BCR-mediated BCAP tyrosine phosphorylation, respectively, whereas LYN negatively regulates this phosphorylation (Okada *et al*, 2000). In the absence of LYN, higher molecular weight forms of BCAP appear more phosphorylated (Okada *et al*, 2000). In contrast, CD19-mediated BCAP tyrosine phosphorylation appears to require LYN in DT40 B cells that express exogenous CD19 (Inabe & Kurosaki, 2002). Interestingly, recruitment of NCK, an adaptor for BCAP, to BCR signalosomes is impaired in LYN-deficient DT40 cells (Castello *et al*, 2013). Furthermore, long-isoform BCAP can be phosphorylated by LYN *in vitro*, and can associate with both SYK and LYN (Halabi *et al*, 2017). Whether LYN directly phosphorylates BCAP, or regulates SYK activity in this role, is unclear. The interpretation of these studies must also consider that chicken DT40 cells do not express CD19; in mouse B cells, where CD19 is expressed, BCAP recruitment and phosphorylation may differ.

In $CD4^+$ T blasts, the rapid tyrosine phosphorylation of BCAP upon TCR crosslinking suggests that BCAP is regulated by kinases in close proximity to the TCR signalosome. The main Src-family tyrosine kinases involved in the early stages of TCR activation are LCK and FYN (Palacios & Weiss, 2004). LCK is associated with the CD4 and CD8 coreceptors (Turner *et al*, 1990), while FYN interacts with the TCR-CD3 complex (Timson Gauen *et al*, 1992), and both LCK and FYN contain SH2 and SH3 domains. LCK phosphorylates immunoreceptor tyrosine-based activation motifs (ITAMs) located within the CD3ζ chain, which then recruit the SYK-family tyrosine kinase ZAP-70 via its tandem SH2 domains (Wang *et al*, 2010). LCK, FYN and ZAP-70 are potential candidates that could be responsible for the tyrosine phosphorylation of BCAP in activated T cells, which would require further investigation using specific kinase-deficient T cells.

While BCAP is thought to recruit PI3K to the BCR, BCAP itself is not a membrane-associated protein. In B cells, BCAP is found mainly in the cytoplasmic fraction (Okada *et al*, 2000). The adaptor protein NCK has been shown to recruit BCAP to the BCR signalosome (Castello *et al*, 2013). NCK associates with the BCR via a region of the immunoglobulin-α tail containing the non-ITAM phosphorylated residue Y204, which is dependent on the expression of LYN. NCK interacts with the second proline-rich region of BCAP via its three SH3 domains. The NCK family proteins NCK1 and NCK2 are both expressed in activated mouse $CD4^+$ T cells (Figure 4.6). Moreover, NCK, via its first SH3 domain, binds to a proline-rich region in the CD3ε chain, which is exposed upon TCR antigen recognition and occurs before tyrosine phosphorylation of the CD3ζ ITAMs (Gil *et al*, 2002). It is therefore possible that NCK could recruit BCAP to the TCR signalosome in activated T cells. Interestingly, NCK1 was identified by AP-MS in the present study as a TCR stimulation-independent p110δ-associated protein. This suggests that NCK1 is constitutively associated with PI3K; upon TCR stimulation, NCK could stabilise an interaction between BCAP and PI3K and facilitate PI3K recruitment to the TCR signalosome. This hypothesis warrants further study.

Aside from 3 YxxM motifs and 3 proline-rich regions, murine BCAP also contains a YxNx (Y375-PNT) and a YxxV (Y513-HIV) motif. These tyrosine phosphorylated sequences are well characterised as consensus binding motifs for the SH2 domains of GRB2 and SHP-2, respectively (Songyang *et al*, 1993, 1994). Intriguingly, GRB2 and SHP-2 were both identified by AP-MS as TCR-stimulation dependent p110δ-associated proteins in the present study. While interaction between BCAP and these proteins has not yet been demonstrated, it is possible that they may associate in a TCR-proximal complex involving PI3K. It has been shown that BCAP is able to form dimers, mediated by its N terminal Dof/BANK/BCAP (DBB) domain (Halabi *et al*, 2017). This raises the possibility that dimerised BCAP could bind to multiple proteins simultaneously at the TCR signalosome.

It remains unanswered how BCAP affects PI3K activation and subsequent signalling downstream of the TCR. In BCAP-deficient DT40 B cells, $PIP_3$ production upon BCR-stimulation is decreased by 50%, while AKT activation, measured by *in vitro* kinase assay, is also reduced (Okada *et al*, 2000). As previously discussed, DT40 cells do not express CD19, thus BCAP may play a more essential role in these cells. Indeed, activation of PI3K and AKT, measured by their kinase activity *in vitro*, appears to be unaffected in $BCAP^{-/-}$ mouse splenic B cells, in which CD19 may substitute as the main PI3K adaptor (Yamazaki *et al*, 2002). Nevertheless, the residual $PIP_3$ production observed

in DT40 cells indicates that there are BCAP-independent mechanisms of PI3K activation in these B cells. If BCAP is assumed to perform an analogous role in T cells, it may serve to activate the PI3K-AKT pathway upon TCR engagement. Due to the observations that BCAP is expressed predominantly in B cells and macrophages, and not in naïve T cells, previous studies using $BCAP^{-/-}$ mice have not examined the functional impact on PI3K signalling in effector T cells. These studies revealed that $BCAP^{-/-}$ mice exhibit normal thymic development, with only marginally decreased numbers of $CD3^+$ T cells in the spleen (Yamazaki *et al*, 2002). To uncover the role of BCAP in PI3K signalling downstream of the TCR, BCAP-deficient activated T cells would be required.

The current study revealed that BCAP is not expressed in naïve $CD4^+$ T cells but is upregulated in activated $CD4^+$ and $CD8^+$ T cells. This intriguing observation raises the question of whether BCAP becomes a critical adaptor for PI3K upon expression in activated T cells, or if it plays a redundant role with other constitutively expressed proteins. It also suggests that there could be a rewiring of TCR-induced signalling upon differentiation of effector T cells, which may alter the regulation of PI3K activity.

The biochemical study of BCAP in activated $CD4^+$ T cells demonstrated that tyrosine phosphorylation of BCAP and its association with PI3K are induced by TCR crosslinking. Subsequent experiments aimed to investigate the role of BCAP in TCR-PI3K signalling by interrogating BCAP-deficient $CD4^+$ T blasts.

# Chapter 5

# Interrogating TCR-PI3K signalling using CRISPR/Cas9 gene editing in primary murine T cells

## 5.1 Introduction

The identification of p110δ-associated proteins in activated T cells prompted work to investigate their functions as potential regulators of PI3K signalling downstream of TCR engagement. This called for a system of intervention to disrupt candidate proteins and analyse downstream perturbations in the pathway. In order to interrogate their function in the same physiological scenario in which they were identified by mass spectrometry, this assay required application to primary murine T blasts expanded by *in vitro* culture. This necessity was reinforced by the observation that two proteins of interest, BCAP and ICOS, are expressed only in activated, and not naïve, T cells. In the absence of specific small-molecule inhibitors against the candidate proteins, their study necessitated genetic knock out, or knock in loss-of-function. Due to the number of proteins that could be investigated, and the availability of such models, transgenic mice were not a suitable option for this purpose. Therefore an *in vitro* gene editing approach was required.

Commonly used strategies for gene knock down in primary T cells involve RNA interference via viral-based transduction of vectors encoding siRNA/shRNA or direct transfection of siRNA (Freeley & Long, 2013). These methods are often time consuming, labour intensive and low-efficiency. Following the emergence of CRISPR/Cas9 technology as a powerful tool for genome engineering across many cell types (Doudna & Charpentier, 2014), considerable efforts have been made to advance Cas9-mediated gene editing techniques in primary T cells for therapeutic and research applications. This has driven the development of various approaches to express or directly deliver Cas9 nuclease and short guide RNA (gRNA) in human T cells, with variable editing efficiencies (Mandal *et al*, 2014; Wang *et al*, 2014; Li *et al*, 2015; Su *et al*, 2016). The delivery of *in vitro*-assembled Cas9:gRNA ribonucleoproteins (Cas9 RNPs) has been demonstrated as a rapid and efficient method for gene editing in primary activated human $CD4^+$ T cells (Hendel *et al*,

2015; Schumann *et al*, 2015). Electroporation of Cas9 RNP complexes targeting *CXCR4* led to efficient knock out of the cell surface receptor CXCR4 in activated human $CD4^+$ T cells (Schumann *et al*, 2015). Following this pioneering work, RNP nucleofection has been successfully used for the CRISPR/Cas9-mediated knock out of CCR5 (Hendel *et al*, 2015), CD7 (Gomes-Silva *et al*, 2017), CD3 (Ren *et al*, 2017) and PD-1 (Rupp *et al*, 2017) in primary activated human T cells.

The RNP-based delivery method is advantageous for CRISPR/Cas9 editing of primary murine cells *in vitro* as it does not require mice expressing transgenic Cas9. Given that RNPs also exhibit rapid turnover in cells within 24 hours (Kim *et al*, 2014), the RNP-based method therefore avoids the increased frequency off-target cleavage that may be associated with Cas9 expressed by a constitutive transgene, or even a long-persisting plasmid (Schumann *et al*, 2015; Kornete *et al*, 2018). Furthermore, RNP delivery has been shown to be less toxic to human T cells than the nucleofection of plasmid DNA (Hendel *et al*, 2015).

Recently, in the first reported use of RNP delivery for CRISPR/Cas9 editing in mouse primary T cells, Seki & Rutz (2018) have demonstrated high efficiency knock out of CD90, CTLA-4 and PD1 in purified murine $CD8^+$ T cells. These cells had been activated with anti-CD3, anti-CD28 and IL-2 for 3 days prior to nucleofection using a Lonza 4D nucleofection system. In parallel, Kornete *et al* (2018) have achieved high efficiency knock out of CD90 in purified murine $CD4^+$ T cells following 24-hour activation with anti-CD3, anti-CD28 and IL-2, using the Neon transfection system.

The current study set out to adapt the RNP nucleofection method to enable CRISPR/Cas9-mediated gene editing in primary murine total T cells that had been activated with anti-CD3 for two days in the same manner as previous experiments (Figure 5.1A). This was with the aim to knock out MS-identified p110δ-associated proteins to interrogate their potential functions as regulators of TCR-PI3K signalling in activated T cells.

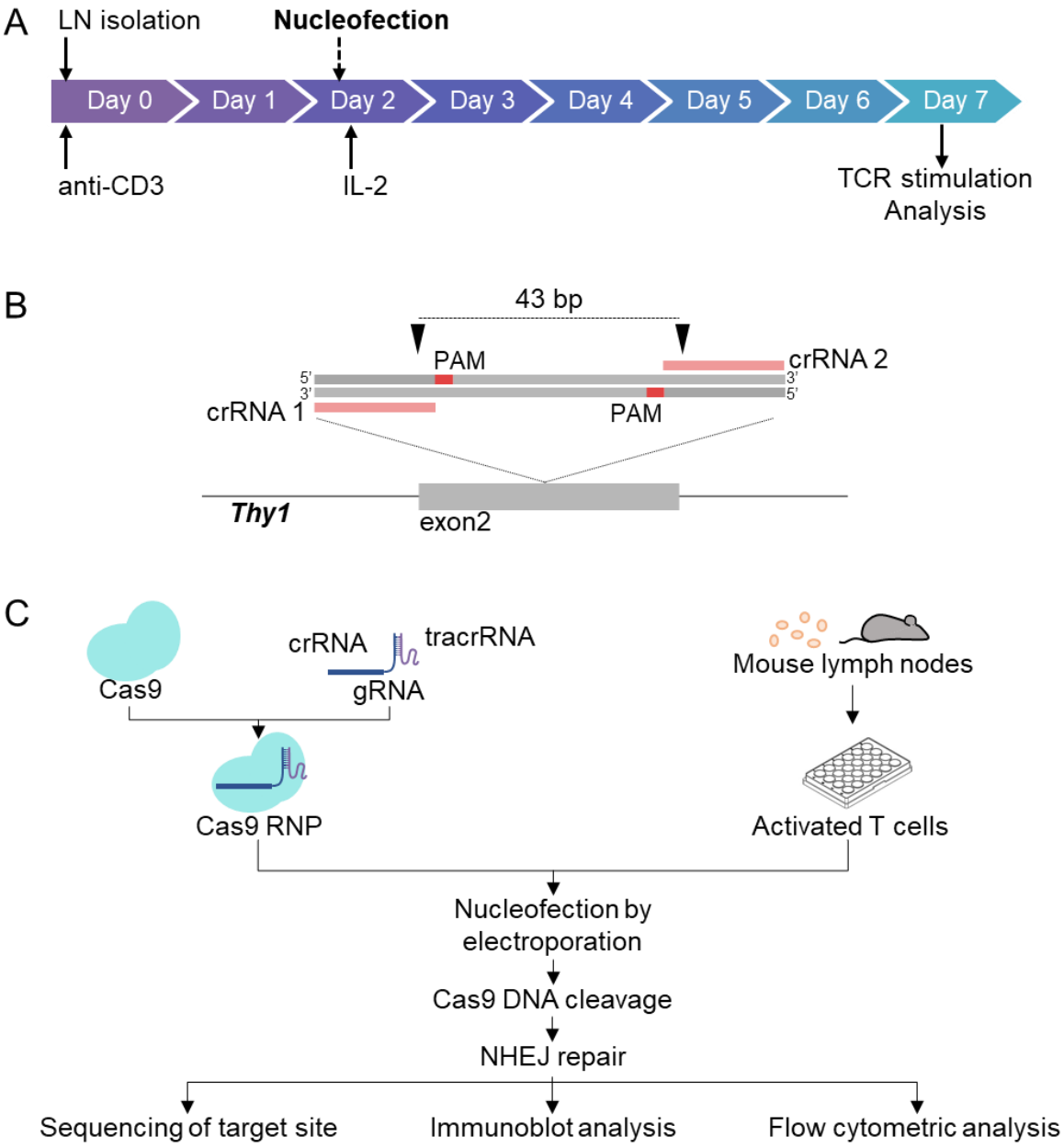


**Figure 5.1 Experimental workflow for CRISPR/Cas9 gene editing via RNP nucleofection in primary activated murine T cells.**

**A.** *in vitro* culture of primary activated murine T cells. Cells are isolated from mouse lymph nodes and activated for 48 hours with 1 µg/ml soluble anti-CD3. Activated cells are then cultured for a further 5 days in 20 ng/ml rhIL-2. Cells are re-stimulated on day 7 for biochemical and flow cytometric analysis.

**B.** Schematic representation of CRISPR guide crRNA sequences (pink) designed to edit exon 2 of the mouse *Thy1* gene. The protospacer adjacent motif (PAM) is recognised by Cas9 nuclease. Arrows indicate the predicted Cas9 cleavage sites, separated by 43 bp.

**C.** Strategy for RNP nucleofection. Recombinant Cas9 protein is complexed with tracrRNA:crRNA duplex to form the Cas9 RNP, which is then delivered by electroporation into primary mouse total T cells that have been activated for 48 h with anti-CD3. Insertions/deletions (indels) generated via Cas9 cleavage-induced non-homologous end joining (NHEJ) are analysed by Sanger sequencing of PCR amplicons spanning the target locus. Protein loss and functional impact is determined by flow cytometric analysis of cells and immunoblotting of cell lysates.

## 5.2 Results

### 5.2.1 Generation of knock out primary activated murine T cells via Cas9:gRNA RNP nucleofection

To test the feasibility and efficacy of RNP delivery for CRISPR/Cas9 gene editing in activated mouse T cells, the highly expressed, glycosyl phosphatidylinositol (GPI)-anchored T cell surface glycoprotein CD90, encoded by the gene *Thy1*, was chosen as a target for knock out. CD90 expression can be easily assessed by flow cytometry, and *Thy1* has been successfully edited by CRISPR/Cas9 in primary mouse T cells in previous reports (Kornete *et al*, 2018; Seki & Rutz, 2018).

Two CRISPR RNA (crRNA) guide sequences were designed to recognise *Thy1* exon 2, with their Cas9 cleavage sites separated by 43 bp (Figure 5.1B). Both guides had no predicted off-target sites in coding regions. The synthetic *Thy1*-specific crRNAs were then annealed with trans-activating crRNA (tracrRNA), which possesses complementarity to the Cas9 nuclease, to form a single guide RNA (gRNA) (Figure 5.1C). Recombinant Cas9 protein was complexed with either *Thy1* gRNA 1, *Thy1* gRNA 2, or equimolar amounts of both gRNAs, at a molar ratio shown to be effective for gene editing in human $CD8^+$ T cells (unpublished work). Total T cells that had been activated for 48 hours with anti-CD3 were nucleofected with *Thy1* Cas9 ribonucleoproteins (RNPs) by electroporation, then cultured for 48 hours with IL-2 before analysis by flow cytometry.

Nucleofection of *Thy1* Cas9 RNPs resulted in the loss of CD90 surface protein in both $CD8^+$ and $CD4^+$ T cells (Figure 5.2A). Up to 31.2 % and 18.6 % of *Thy1* RNP-nucleofected $CD8^+$ and $CD4^+$ T cells, respectively, did not express CD90 at 48 h post-nucleofection, indicating homozygous knockout due to biallelic disruption of the *Thy1* gene. Flow cytometry also revealed an increase in the proportion of cells expressing low levels of CD90 after *Thy1* RNP nucleofection (Figure 5.2B), which may reflect heterozygous knock out due to monoallelic gene disruption, or incomplete CD90 protein turnover from the cell surface.

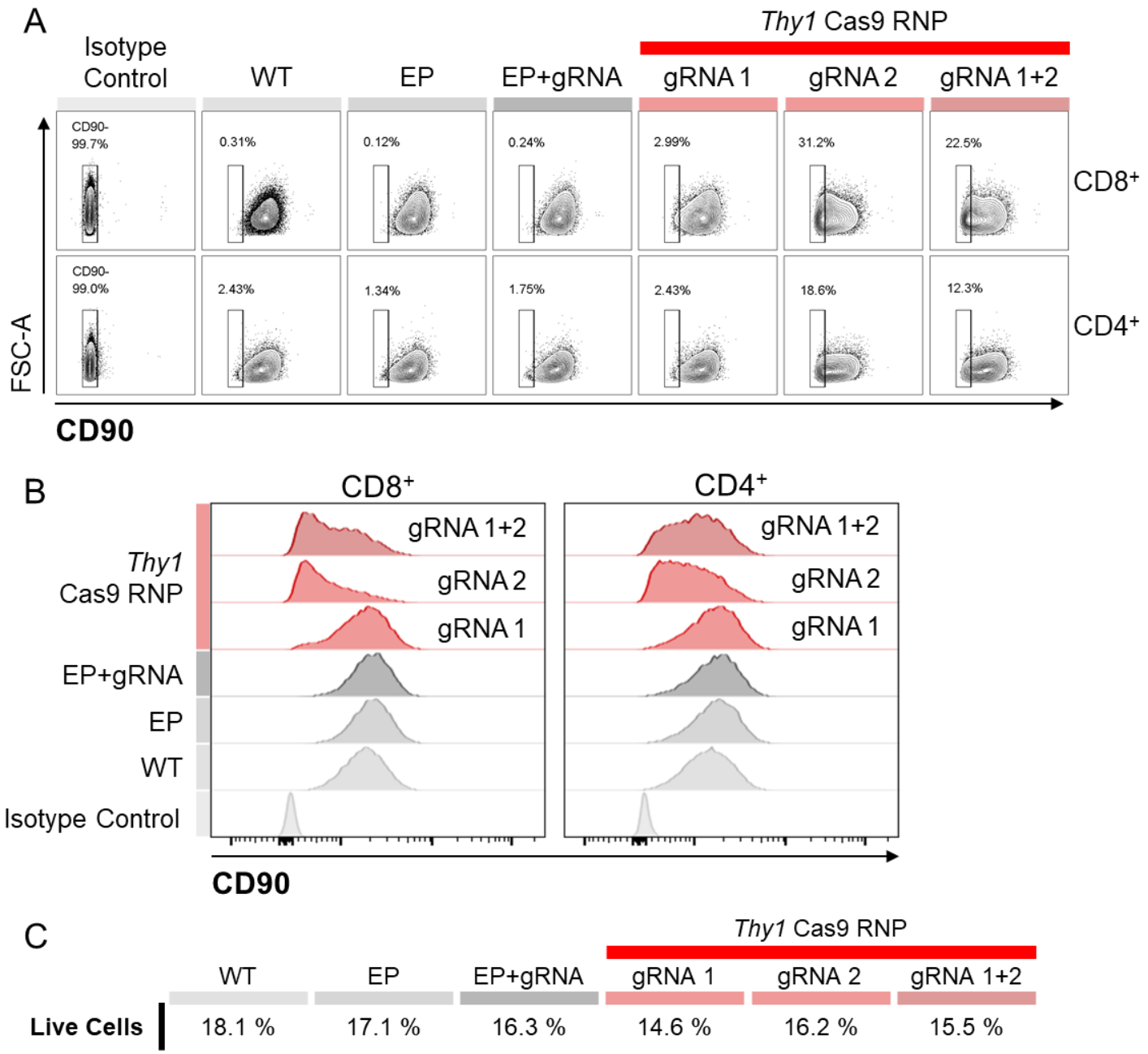


**Figure 5.2 Successful knock out of CD90 in primary activated murine CD8⁺ and CD4⁺ T cells via Cas9 RNP nucleofection.**

**A.** CD90 cell-surface expression assessed by flow cytometry in control (non-electroporated (WT), electroporated (EP), and electroporated with gRNA only (EP+gRNA)) and *Thy1* Cas9 RNP-nucleofected CD8⁺ and CD4⁺ activated T cells 48 h post-nucleofection. Cas9 was complexed with one of two gRNAs targeting *Thy1* (gRNA 1 or gRNA 2) or equimolar amounts of both guides (gRNA 1+2), in the ratio 36.6:27 pmol Cas9:gRNA. $0.5 \times 10^6$ cells were electroporated for each condition, or rested in nucleofection buffer for WT. Flow plots indicate the percentage of live CD8⁺ and CD4⁺ cells falling within the CD90⁻ gate, drawn according to isotype control-stained cells.

**B.** Histograms of CD90 cell-surface staining assessed by flow cytometry, with cell counts normalised to the mode, corresponding to the same samples shown in A.

**C.** Cell viability assessed by flow cytometry, expressed as the percentage of live single cells at 48 h post-nucleofection, corresponding to the same samples shown in A and B. Data are from one experiment performed in duplicate with one technical replicate shown.

Cas9 RNPs complexed with *Thy1* gRNA 2 achieved greater CD90 knock out efficiency than those complexed with *Thy1* gRNA 1. The simultaneous use of both *Thy1* gRNAs was also tested, as this approach has been shown to increase the efficiency of gene disruption due to deletion of the exonic sequence between the two Cas9 cleavage sites (Mandal *et al*, 2014; Hendel *et al,* 2015). In this experiment, use of both *Thy1* gRNAs in combination generated lower CD90 knock out frequency compared to *Thy1* gRNA 2 alone, suggesting low efficiency sequence disruption at the *Thy1* gRNA 1 target site.

The viability of cells at 48 hours post-electroporation was also assessed by flow cytometry (Figure 5.2C). The proportion of live cells following RNP-nucleofection was, on average, only ~3 % lower than for non-electroporated cells (WT), and similar to cells that had been electroporated with or without gRNA alone. This indicates that neither RNP delivery nor gene editing were considerably cytotoxic to activated T cells.

The successful ablation of CD90 expression demonstrated that CRISPR/Cas9 gene editing via RNP nucleofection was a viable method to generate knock out $CD8^+$ and $CD4^+$ cells from primary activated murine total T cells *in vitro*.

### 5.2.2 Optimisation of CRISPR/Cas9 gene editing via RNP nucleofection in primary activated murine T cells

While successful knock out of CD90 was achieved using RNP delivery, the proportion of $CD90^-$ cells generated was low, at ~20 - 30 %. Therefore, the RNP nucleofection protocol was optimised to increase the efficiency of gene knock out.

The efficiency of DNA cleavage at target sites is limited by the amount of Cas9:gRNA complex present in the nucleus (Osakabe *et al*, 2016). While increasing the amount of Cas9 protein nucleofected may increase cutting frequency, introducing excessive amounts of exogenous protein into lymphocytes would likely increase cytotoxicity and thus reduce cell viability. Furthermore, Cas9 quantity cannot be varied independently of gRNA amount. Cas9 is expected to form a 1:1 molar complex with gRNA within the RNP complex, yet the ratio used to assemble RNPs *in vitro* is usually higher, with gRNA in excess (Hendel *et al*, 2015; Seki & Rutz, 2018, Kornete *et al*, 2018). The optimal ratio has not been empirically determined, and may vary depending on experimental conditions. Use of chemically synthesised gRNAs, as in this study, does not trigger an innate immune response and associated cytotoxicity in human $CD4^+$ T cells,

unlike *in vitro* transcribed sgRNA (Kim *et al*, 2018). Nevertheless, introducing excessive synthetic RNA could reduce cell viability. The optimal amount of Cas9 and gRNA used for each RNP nucleofection was thus investigated, to increased gene editing efficiency while maintaining cell viability. A third factor to be considered was the number of cells subjected to nucleofection; an optimal concentration of cells within the electroporation mixture would allow a maximum number of cells to receive RNP complexes while remaining viable under the applied voltage.

The most appropriate way to optimise these three interdependent factors was to model their combined contributions to knock out efficiency and cell viability. This was achieved by performing a set of 17 *Thy1* RNP nucleofections that were designed to use specific combinations of Cas9 amount, gRNA amount and cell number, within defined practical limits (Table 5.1). The outcomes would allow efficiency and viability to be modelled as functions of the three variables, using response surface methodology, and thus optimal values could be determined. The 17 nucleofections were performed and analysed in parallel. Knock out efficiency at 48 hours-post nucleofection was measured as the frequency of insertions and deletions (indels) generated at the Cas9:gRNA target site within *Thy1*. This was determined using TIDE (Tracking of Indels by Decomposition) analysis (Brinkman *et al*, 2014), by deconvolution of Sanger sequencing traces of PCR amplicons spanning the *Thy1* gRNA target site, with comparison to control sequences of the same region from wild type cells (Figure 5.3A). The cutting efficiency reported by TIDE indicates the percentage of indels present within the total cell population at the Cas9 cleavage sites. In parallel, cell viability and CD90 surface expression were analysed by flow cytometry at 48 hours post-nucleofection. It was clear simply by examining the variation in knock out efficiency across each of the 17 populations that the amount of Cas9 and gRNA nucleofected, along with the number of cells electroporated, had a considerable impact on efficiency and viability (Table 5.1). Cutting efficiency and CD90 expression measured in cells from nucleofections 17 and 15 are shown in Figure 5.3 as representative examples of low and high knock out efficiency, respectively.

| | *Factor 1* | *Factor 2* | *Factor 3* | *Response 1* | *Response 2* | *Response 3* |
|---|---|---|---|---|---|---|
| Nucleofection # | **Cell Number** $\times 10^6$ | **Cas9** µg | **gRNA*** pmol | **Cutting Efficiency** % | **Protein KO** % | **Viability** % |
| 1 | **1.5** | **5.5** | **75** | 21.8 | 24.25 | 25.05 |
| 2 | **2.5** | **5.5** | **125** | 47.9 | 15.2 | 17.2 |
| 3 | **1.5** | **10** | **25** | 24.8 | 22.95 | 22.55 |
| 4 | **0.5** | **1** | **75** | † | 2.64 | 7.5 |
| 5 | **2.5** | **5.5** | **25** | 22.9 | 19.7 | 23.55 |
| 6 | **1.5** | **5.5** | **75** | 24.3 | 29.8 | 26.4 |
| 7 | **1.5** | **5.5** | **75** | 29.7 | 30.85 | 22.05 |
| 8 | **0.5** | **10** | **75** | 40.9 | 26.6 | 12 |
| 9 | **1.5** | **5.5** | **75** | 19.2 | 25.5 | 21.1 |
| 10 | **1.5** | **1** | **125** | 4.4 | 5.775 | 24.2 |
| 11 | **1.5** | **10** | **125** | 38.8 | 33.75 | 18.55 |
| 12 | **1.5** | **1** | **25** | 11.4 | 7.45 | 19.45 |
| 13 | **1.5** | **5.5** | **75** | 31.6 | 25.2 | 16.7 |
| 14 | **0.5** | **5.5** | **125** | 36.6 | 18 | 12.3 |
| 15 | **2.5** | **10** | **75** | 51.1 | 37.9 | 18.25 |
| 16 | **0.5** | **5.5** | **25** | 38.8 | 25.2 | 14 |
| 17 | **2.5** | **1** | **75** | 6.1 | 9.895 | 22.25 |

**Table 5.1 Experimental design for optimisation of CRISPR/Cas9 gene editing via RNP nucleofection.**

Design-Expert software was used to design 17 nucleofection conditions to enable optimisation of RNP-mediated gene editing by response surface methodology. Three factors (cell number, Cas9 amount, and gRNA amount) were varied between defined limits ($0.5 – 2.5 \times 10^6$, 1 – 10 µg and 25 – 125 pmol, respectively) according to Box-Behnken design. The 17 nucleofections were performed in parallel and responses were measured at 48 h post-nucleofection. Cutting Efficiency indicates the percentage of indels present within the total cell population at the Cas9 cleavage sites in *Thy1* exon 2, as determined by TIDE analysis of Sanger sequencing traces of PCR amplicons spanning this region. Protein KO (% $CD8^+CD90^-$ live cells) and Viability (% live cells) were determined by flow cytometry and represent the average of duplicate samples. *gRNA was an equimolar mixture of *Thy1* gRNA 1 and gRNA 2. †Could not obtain quality Sanger sequence reads for TIDE analysis of NF 4.

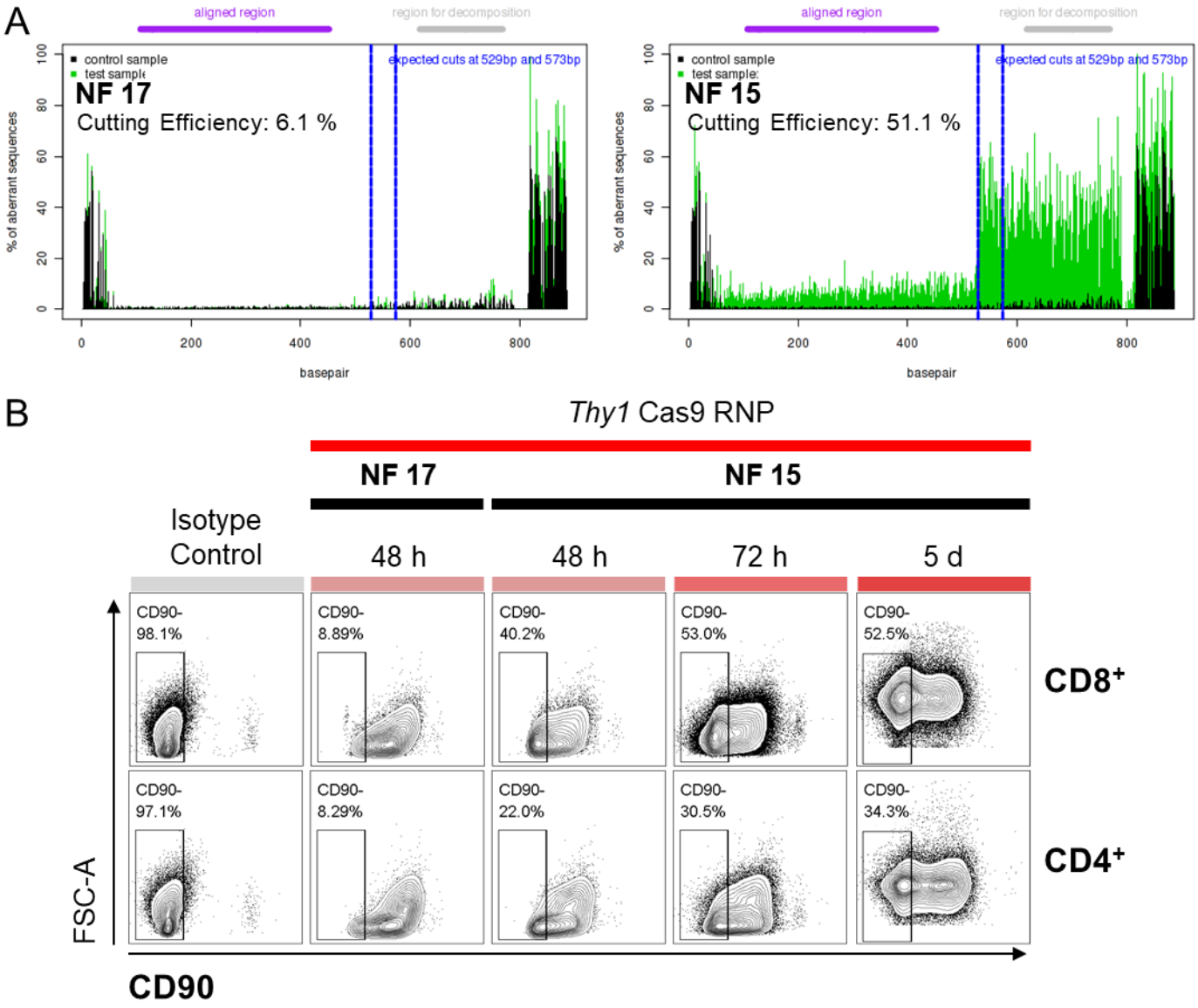


**Figure 5.3 Optimisation of CRISPR/Cas9 gene editing via RNP nucleofection in primary activated murine T cells.**

**A and B.** Representative examples of low efficiency (NF 17) and high efficiency (NF 15) *Thy1* disruption from the 17 nucleofections detailed in Table 5.1. Cas9 was complexed with equimolar amounts of *Thy1* gRNA 1 and gRNA 2, in the ratio 1 µg:75 pmol (NF 17) or 10 µg:75 pmol (NF 15) Cas9:gRNA. $2.5 \times 10^6$ cells were electroporated for each condition.

**A.** TIDE graphs showing the aberrant sequence signal at the *Thy1* target site at 48 h post-nucleofection in *Thy1* RNP-nucleofected total T cells (NF 17, left, and NF 15, right; 'test', in green), compared to wild type total T cells ('control'; in black). Plots show the expected Cas9 cleavage sites (blue lines), the region used for decomposition (grey line) and the region used for sequence alignment with control (purple line). Decomposition of the sequence by TIDE determines the percentage of indels present in the total population, as indicated on the graphs.

**B.** CD90 cell-surface expression, assessed by flow cytometry in $CD8^+$ and $CD4^+$ T blasts nucleofected with *Thy1* Cas9 RNP, at 48 h, 72 h and 5 days (5 d) post-nucleofection. Flow plots indicate the percentage of live $CD8^+$ or $CD4^+$ cells falling within the $CD90^-$ gate, drawn according to isotype control-stained cells. Data are from one flow cytometry experiment performed in duplicate, with one technical replicate shown.

In addition to these analyses performed at 48 hours, *Thy1*-edited cells were expanded further and found to be viable at 5 days post-nucleofection (Figure 5.3B). It was also observed that the proportion of $CD90^-$ cells within the population increased from 48 to 72 hours for both $CD8^+$ and $CD4^+$ cells, indicating that CD90 protein turnover from the cell surface required longer than 48 hours following *Thy1* gene disruption. This may also explain the discrepancy between the estimated gene cutting efficiency and protein knock out efficiency observed at 48 hours in some cases (Table 5.1). Although, the frequency of editing was not expected to equal the proportion of CD90-knock out cells, as indel frequency does not distinguish between heterozygous and homozygous knock out. Nevertheless, in the majority of nucleofections, these percentages were similar, suggesting that there was a high proportion of biallelic gene editing in these samples. Regardless, these results indicated that protein loss should be analysed from 72 hours post-nucleofection. The proportion of $CD90^-$ cells within the $CD8^+$ and $CD4^+$ populations did not change considerably from 72 to 5 days, indicating that there was no survival or proliferative defect, or advantage, in *Thy1*-edited cells. The $CD8^+$ population exhibited a consistently higher proportion of $CD90^-$ knock out cells compared with the $CD4^+$ population at 48 h, 72 h and 5 days post-nucleofection, suggesting that this was due to a difference in *Thy1* editing frequency rather than protein turnover.

The generation of ~50 % *Thy1*-edited cells from several of the tested nucleofection conditions indicated that the RNP nucleofection protocol could be improved. To this end, response surface methodology was used to model cutting efficiency, protein knock out and cell viability as quadratic functions of the three variable factors (Cas9 amount, gRNA amount and cell number). Optimal values for each factor that were within the experimental space tested were determined using the Design-Expert software package, with the aim to maximise cutting efficiency and protein knock out while targeting high viability. These values ($2.16 \times 10^6$ cells; 10 µg Cas9; 94 pmol gRNA) were used in subsequent RNP nucleofections. Notably, the fact that the maximum quantity of Cas9 tested (10 µg) was calculated as an optimum suggests that the 'true' optimum for Cas9 amount may lie outside of the experimental space tested. Thus, it was predicted that the maximum *Thy1* editing efficiency that could be achieved with these values would be similar to the highest observed in these experiments; approximately 50 %.

This optimised protocol for RNP nucleofection in primary murine T blasts, and strategy for the analysis of knock out efficiency, was subsequently used for CRISPR/Cas9-mediated knock out of TCR-PI3K-associated proteins.

### 5.2.3 CRISPR/Cas9-mediated knock out of TCR-PI3K signalling proteins in primary activated T cells

Proteins that had been identified by AP-MS as p110δ-interactors in primary activated T cells were the intended targets for CRISPR/Cas9-mediated knock out. To be able to examine the effect of their loss on TCR-induced PI3K signalling, p110δ-deficient T blasts were required as a positive control for disrupted PI3K signalling. Therefore, the first gene chosen for CRISPR/Cas9-mediated editing was *Pik3cd*, which encodes the PI3K catalytic isoform p110δ.

Two guide crRNA sequences were designed to uniquely target *Pik3cd* exon 2, with their Cas9 cleavage sites separated by 31 bp. To enable the selection and analysis of p110δ-deficient cells by flow cytometry, in the absence of a detectable marker for successful knock out, a multiplex gene editing strategy with simultaneous targeting of *Thy1* was used. To this end, recombinant Cas9 protein was complexed with equimolar amounts of *Pik3cd* gRNA 1 or 2 and *Thy1* gRNA 2, or equimolar amounts of both *Pik3cd* gRNAs without *Thy1* gRNA. Total T cells that had been activated for 48 hours were nucleofected with RNP complexes and then cultured for 5 days with IL-2. The efficiency of indel formation at the *Pik3cd* and *Thy1* target sites was assessed at 72 hours and 5 days post-nucleofection by Sanger sequencing and TIDE analysis (Figure 5.4).

Across two independent experiments, *Thy1* editing efficiency was consistently ~50 % at both 72 h and 5 days post-nucleofection. RNPs complexed with *Pik3cd* gRNA 1 or *Pik3cd* gRNA 2 generated low *Pik3cd* editing efficiencies of up to ~9 and 15 %, respectively, as estimated by TIDE analysis. In contrast, efficient *Pik3cd* editing was achieved with delivery of both *Pik3cd* RNP complexes combined, generating 57.6 % indel frequency within the population in one experiment. Notably, there was no clear depletion or enrichment of *Pik3cd*-edited cells from 72 h to 5 days post-nucleofection.

In parallel, TCR-PI3K signalling was investigated in *Pik3cd*-edited T blasts at day 5 post-nucleofection and compared with wild type cells that had been electroporated with gRNA alone. For this, total T cells were subjected to acute TCR stimulation for 2 minutes and cell lysates were analysed by immunoblotting for phosphorylated AKT (pAKT T308) (Figure 5.4). The pAKT signal detected was then quantified and normalised to AKT1 to allow comparison between samples (Figure 5.5). Across two independent experiments, there was a trend for reduced pAKT upon stimulation in *Pik3cd* RNP-nucleofected cells, compared with wild type, which correlated with increased frequency of *Pik3cd* disruption within the cell population (Figure 5.5A and 5.5B). Thus, the small reduction in induced pAKT in *Pik3cd*-edited cells could be explained by the low

frequency of *Pik3cd* disruption, and therefore the low proportion of heterozygous and homozygous p110δ knock out cells within the total cell population. Nevertheless, the cell population with 57.6 % *Pik3cd* indel frequency exhibited only 57 % of the pAKT signal induced in wild type cells, which indicates loss of p110δ within the population.

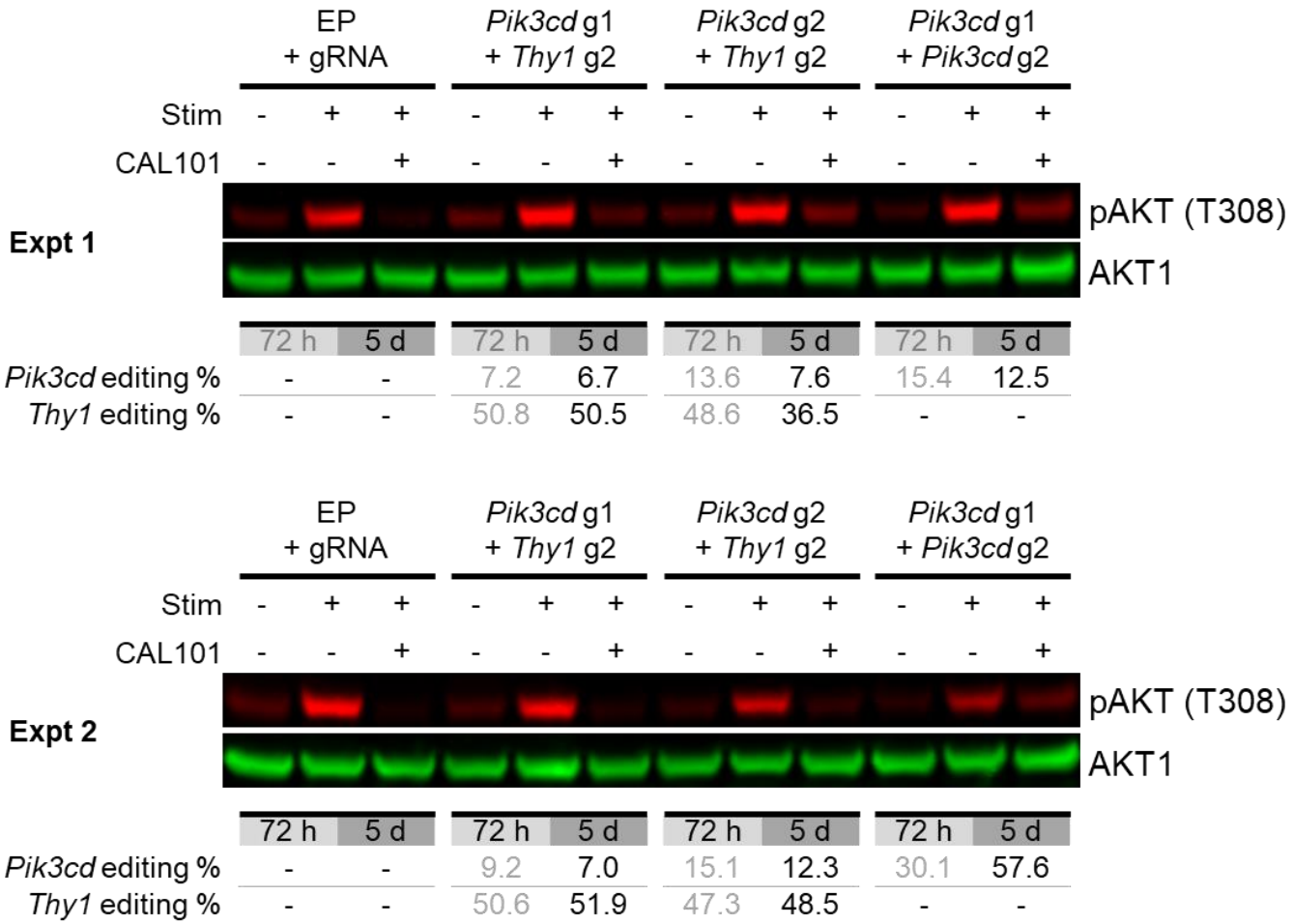


**Figure 5.4 PI3K-AKT signalling and gene editing efficiency in *Pik3cd* Cas9 RNP-nucleofected T blasts.**

Activated total T cells were nucleofected with Cas9 RNPs complexed with equimolar amounts of *Pik3cd* gRNA (g1 or g2) and *Thy1* gRNA (g2), or equimolar amounts of *Pik3cd* gRNA g1 and gRNA g2. Control (EP + gRNA) cells were electroporated with gRNA alone. At day 5 post-nucleofection, 4 million cells were stimulated with 4 µg/ml αCD3+αCD4+αCD8 plus 13 µg/ml crosslinking antibody for 2 minutes at 37°C, in the presence of 200 nM DMSO (-) or CAL101 (+), or left unstimulated in the presence of 200 nM DMSO. Cells were lysed and one-half of lysates were separated by SDS-PAGE and immunoblotted simultaneously for pAKT (T308) and total AKT1. Editing efficiency (indicated below immunoblots) was determined at 72 h and 5 days post-nucleofection. Editing % indicates the percentage of indels present within the total cell population at the Cas9 cleavage sites in *Pik3cd* and *Thy1*, as determined by TIDE analysis of Sanger sequencing traces of PCR amplicons spanning the targeted regions. Blots shown are from two independent experiments (Expt 1 and Expt 2).

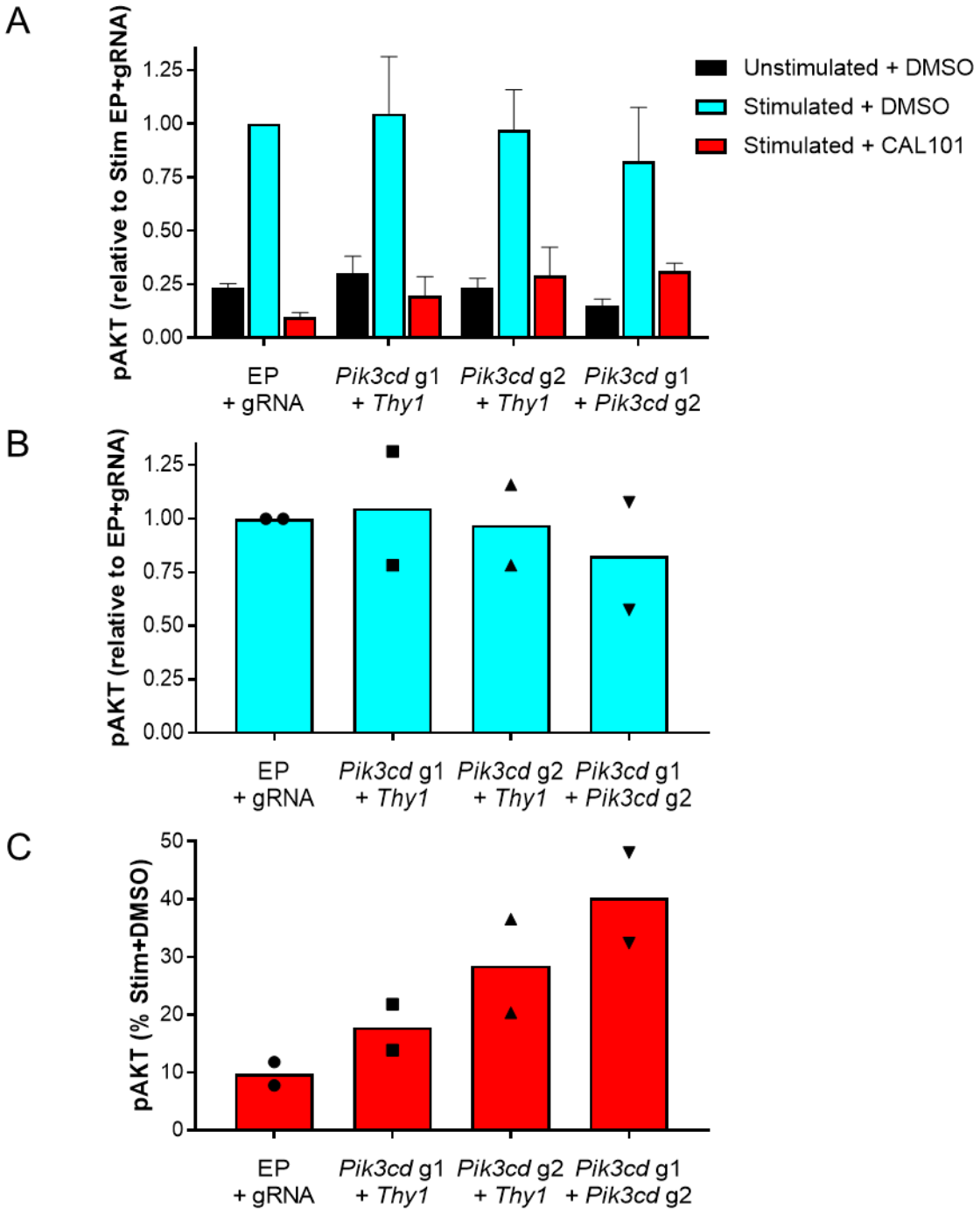


**Figure 5.5** ***Pik3cd*-edited T blasts exhibit reduced pAKT and p110δ-independent pAKT upon TCR stimulation.**

**A.** Quantification of pAKT signal intensity detected by immunoblotting in Figure 5.4, normalised to AKT1, expressed relative to that in stimulated EP+gRNA cells, set as 1. Data are from two independent experiments. Bars represent the mean, with error bars +SEM.

**B.** The same data as in A but from 'stimulated + DMSO' cells only, showing individual values from two independent experiments as scatter points, relative to that in stimulated EP+gRNA cells in each experiment. Bars represent the mean for each genotype.

**C.** Quantified pAKT, normalised to AKT1, in stimulated cells treated with 200 nM CAL101, relative to that in stimulated cells treated with 200 nM DMSO. Data are from two independent experiments. Bars represent the mean, with individual values shown as scatter points.

Interestingly, there was also a trend for increased residual pAKT in *Pik3cd*-edited cells upon stimulation in the presence of the p110δ-specific inhibitor CAL101 (Figure 5.5A). This was better examined by comparing the level of pAKT induced in the presence of CAL101 with that induced in DMSO-treated cells for each genotype (Figure 5.5C). In wild type cells treated with CAL101, the level of pAKT induced upon stimulation was only 10 % of that induced in DMSO-treated cells, demonstrating that the majority of AKT phosphorylation was p110δ-dependent. In contrast, 48 % of the pAKT level induced in DMSO-treated cells could be detected in CAL101-treated *Pik3cd*-edited cells that had 57.6 % indel frequency. Notably, the proportion of p110δ-independent pAKT upon stimulation positively correlated with the level of *Pik3cd* disruption within the cell population. This indicated that p110δ-independent phosphorylation of pAKT occurred in p110δ-deficient cells upon TCR stimulation.

Following successful CRISPR/Cas9-mediated knock out of *Pik3cd*, two guide crRNA sequences were designed to target exon 4 of *Pik3ap1*, which encodes BCAP. This exon is present in all *Pik3ap1* transcripts; thus, its disruption would enable knock out of all BCAP protein isoforms. The Cas9 cleavage sites of *Pik3ap1* gRNA 1 and gRNA 2 were separated by 47 bp to allow both guides to be combined for editing. As before, a multiplex strategy with simultaneous targeting of *Thy1* was also used. Activated total T cells were nucleofected with RNP complexes and indel frequency at both the *Pik3ap1* and *Thy1* target sites was assessed at 72 h and 5 days post-nucleofection (Figure 5.6).

RNP-nucleofection with either *Pik3ap1* guide RNA generated efficient indel formation at the *Pik3ap1* target site, with gRNA 1 achieving consistently higher editing frequencies of 37.7 - 54.1 %, compared with 9.3 - 21.8 % for gRNA 2. Interestingly, the combination of both guides targeting the same exon did not generate greater cutting efficiency than when gRNA 1 was used alone, indicating that cleavage at the gRNA 2 target site may have been a limiting factor. Notably, the frequency of *Pik3ap1* editing did not vary from 72 h to 5 days post-nucleofection in any case, indicating that there was no enrichment or depletion of BCAP-knock out cells. *Thy1* editing efficiency in multiplex nucleofections was also consistent at ~50 - 60 % at both 72 h and 5 days.

PI3K-AKT signalling was also examined in *Pik3ap1*-edited T blasts upon acute TCR stimulation at day 5 post-nucleofection (Figure 5.6). Phosphorylated AKT detected by immunoblotting was then quantified, normalised to AKT1 and compared with wild type (WT) non-electroporated cells (Figure 5.7A). This revealed a small but consistent trend for reduced pAKT upon TCR stimulation

in *Pik3ap1*-edited T blasts. By comparing the detected pAKT signal to the level of *Pik3ap1* disruption within each cell population, it was revealed that the greatest reduction in pAKT was associated with a higher frequency of *Pik3ap1* knockout (Figure 5.7B). In two independent experiments with 54.1 % and 44.2 % *Pik3ap1*-editing within the cell population, the pAKT signal upon stimulation was 30 % and 35 % lower than in WT cells, respectively. However, this association was not consistent at lower levels of editing; samples with 37.7 % and 17 % *Pik3ap1* disruption exhibited a 7 % and 35 % reduction in pAKT, respectively. This may reflect the fact that the measure of indel frequency does not distinguish between the proportion of heterozygous and homozygous knock out cells. In addition, a more appropriate control for multiplex edited *Pik3ap1* + *Thy1* knock out cells in this experiment would be *Thy1*-edited T blasts. Nevertheless, the observed defect in TCR-PI3K signalling in *Pik3ap1*-edited cells warranted further investigation.

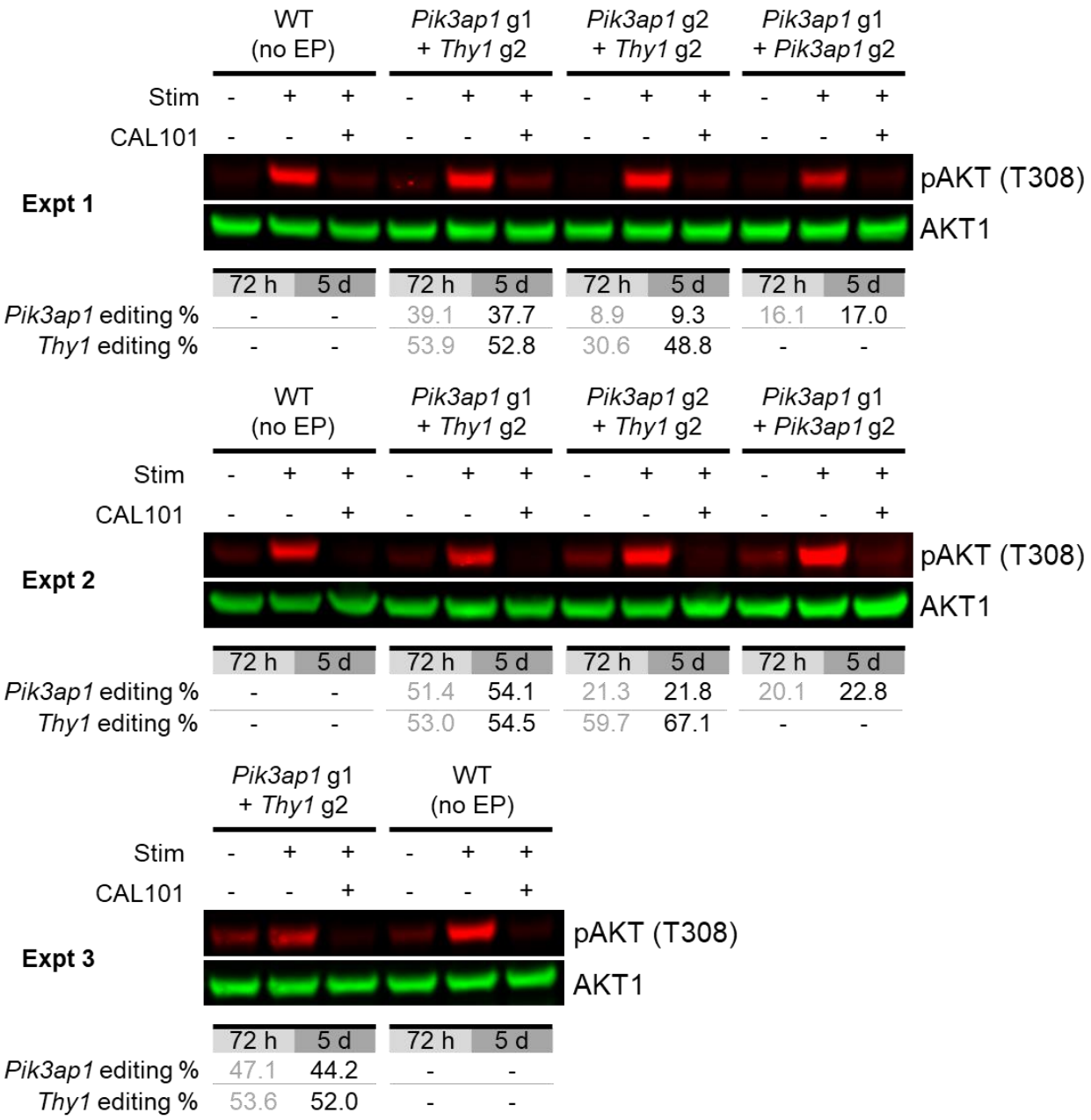


**Figure 5.6 PI3K-AKT signalling and gene editing efficiency in *Pik3ap1* Cas9 RNP-nucleofected T blasts.**

Activated total T cells were nucleofected with Cas9 RNPs complexed with equimolar amounts of *Pik3ap1* gRNA (g1 or g2) and *Thy1* gRNA (g2), or equimolar amounts of *Pik3ap1* gRNA g1 and gRNA g2. Control wild type (WT) cells were not electroporated. At day 5 post-nucleofection, 4 million cells were stimulated with 4 µg/ml αCD3+αCD4+αCD8 plus 13 µg/ml crosslinking antibody for 2 minutes at 37°C, in the presence of 200 nM DMSO (-) or CAL101 (+), or left unstimulated in the presence of 200 nM DMSO. Cells were lysed and one-half of lysates were separated by SDS-PAGE and immunoblotted simultaneously for pAKT (T308) and total AKT1. Editing efficiency (indicated below immunoblots) was determined at 72 h and 5 days post-nucleofection. Editing % indicates the percentage of indels present within the total cell population at the Cas9 cleavage sites in *Pik3ap1* and *Thy1*, as determined by TIDE analysis of Sanger sequencing traces of PCR amplicons spanning the targeted regions. Blots shown are from three independent experiments (Expt1, Expt2 and Expt3).

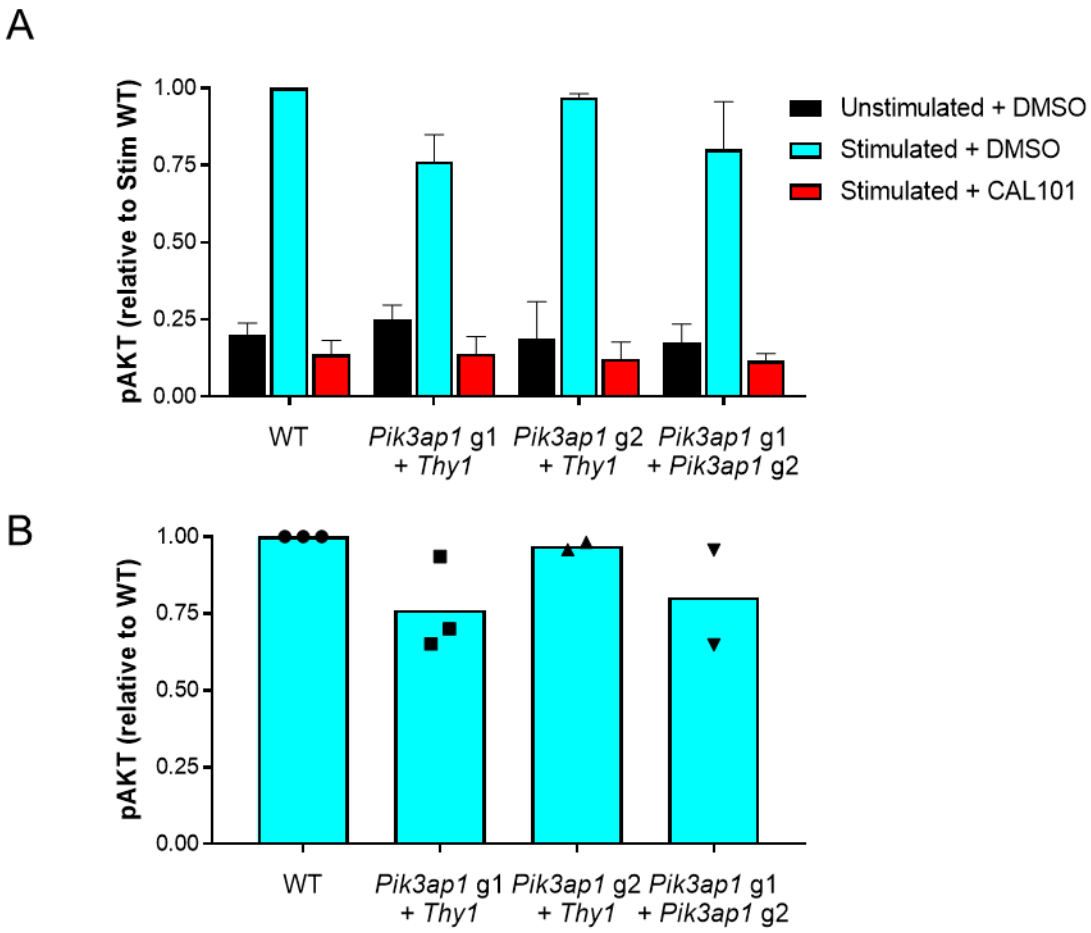


**Figure 5.7 Reduced pAKT upon TCR-stimulation in *Pik3ap1*-edited T blasts.**
**A.** Quantification of pAKT signal intensity as detected by immunoblotting in Figure 5.6, normalised to AKT1, expressed relative to that in stimulated WT cells, set as 1. Data are from three (for WT and *Pik3ap1* g1 + *Thy1*) or two (for *Pik3ap1* g2 + *Thy1* and *Pik3ap1* g1 + *Pik3ap1* g2) independent experiments. Bars represent the mean, with error bars +SEM.
**B.** The same data as in A but for 'stimulated + DMSO' cells only, indicating the individual pAKT values from two or three independent experiments as scatter points, relative to that in stimulated WT cells in each experiment. Bars represent the mean for each genotype.

ICOS was chosen as a third target for CRISPR/Cas9-mediated knock out from the proteins identified by AP-MS as TCR stimulation-dependent p110δ-interactors. Two guide crRNA sequences were designed to target *ICOS* exon 2, with Cas9 cleavage sites separated by 44 bp. RNP nucleofections of activated T cells were performed to test each guide in combination with *Thy1* gRNA, as well as both guides together without *Thy1* gRNA. The efficiency of indel formation at each target site was then assessed at 72 h and 5 days post-nucleofection (Figure 5.8A).

RNP complexes with either *ICOS* gRNA generated efficient editing of the *ICOS* target site, with gRNA 1 achieving marginally higher indel frequency than gRNA 2, of up to 54.4 % within the cell

population. In contrast, using a combination of both *ICOS* guides led to only ~20 % *ICOS*-editing. One explanation for this could be that Cas9 cleavage was sterically hindered by the presence of adjacent Cas9 molecules, potentially due to the organisation of this exon. However, this observation was based on one experiment only. The frequency of *ICOS* indels within the population did not vary from 72 h to 5 days post-nucleofection, indicating that there was no enrichment or depletion of ICOS-knock out cells. Interestingly, one population that was edited with both *ICOS* gRNA 1 and *Thy1* gRNA exhibited higher levels of *Thy1* editing (79.4 %) than that seen in all other experiments.

PI3K-AKT signalling upon acute TCR stimulation was also examined in *ICOS*-edited T blasts at day 5 post-nucleofection (Figure 5.8A). Phosphorylation of AKT was compared with that in *Thy1*-edited T blasts, for multiplex *Thy1 + ICOS*-edited cells, or wild type cells electroporated with gRNA alone, for *ICOS*-only edited cells (Figure 5.8B). Immunoblots from one experiment demonstrated that pAKT induction following TCR stimulation was slightly enhanced in *ICOS*-edited cells, both with and without simultaneous knock out of *Thy1*, compared with that induced in *Thy1*-only-edited cells or wild type cells. However, additional replicate experiments would be required to determine if this effect was reproducible.

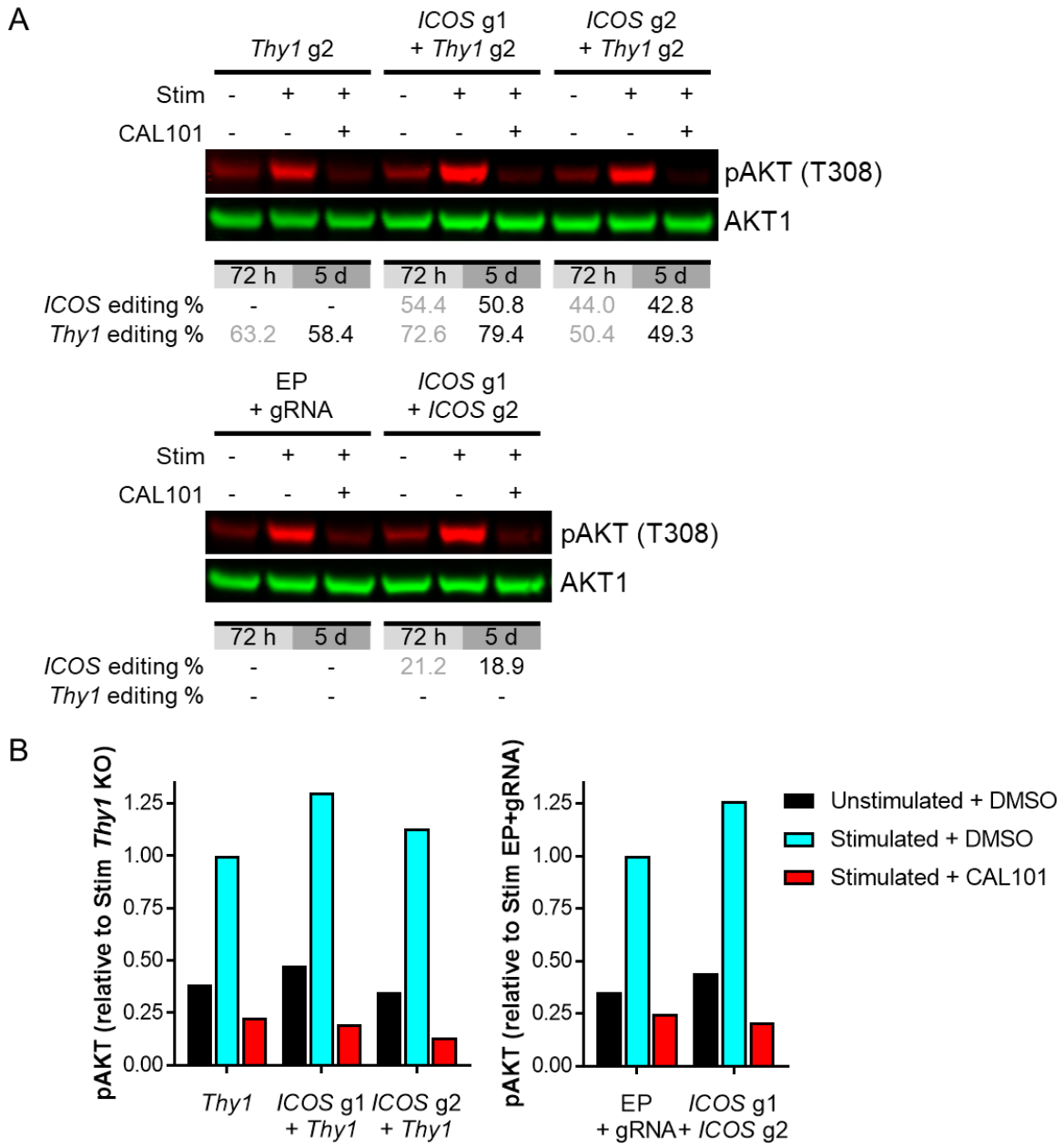


**Figure 5.8 PI3K-AKT signalling and gene editing efficiency in *ICOS* Cas9 RNP-nucleofected T blasts.**

Activated total T cells were nucleofected with Cas9 RNPs complexed with equimolar amounts of *ICOS* gRNA (g1 or g2) and *Thy1* gRNA (g2), or equimolar amounts of *ICOS* gRNA g1 and gRNA g2, or *Thy1* gRNA (g2) alone. Control (EP + gRNA) cells were electroporated with gRNA alone.

**A.** At day 5 post-nucleofection, 4 million cells were stimulated with 4 µg/ml αCD3+αCD4+αCD8 plus 13 µg/ml crosslinking antibody for 2 minutes at 37°C, in the presence of 200 nM DMSO (-) or CAL101 (+), or left unstimulated in the presence of 200 nM DMSO. Cells were lysed and one-half of lysates were separated by SDS-PAGE and immunoblotted simultaneously for pAKT (T308) and total AKT1. Editing efficiency (indicated below immunoblots) was determined at 72 h and 5 days post-nucleofection. Editing % indicates the percentage of indels present within the total cell population at the Cas9 cleavage sites in *ICOS* and *Thy1*, as determined by TIDE analysis.

**B.** Quantification of pAKT signal intensity as detected by immunoblotting in A, normalised to AKT1, presented relative to that in stimulated *Thy1*-edited cells, set as 1, (left), or relative to that in stimulated EP+gRNA cells, set as 1, (right). Data are from one experiment.

As a cell surface receptor, ICOS expression following gene disruption could, in theory, be analysed by flow cytometric analysis. However, specific antibody staining of cell surface ICOS in these experiments was not sufficiently higher than that of isotype control and did not allow separation of $ICOS^-$ and $ICOS^+$ populations. Therefore, the multiplex editing approach, with dual targeting of *Thy1* and *ICOS*, was used in subsequent experiments to be able to select *ICOS* knock out cells, in accord with the strategy used for p110δ and BCAP knock outs.

Overall, these experiments demonstrated successful knock out of *Pik3cd*, *Pik3ap1* and *ICOS* in primary mouse T blasts using CRISPR/Cas9 via RNP delivery. However, the efficiency of gene editing clearly varied depending on the gRNA used. Thus, the most efficient guides were chosen for subsequent experiments. *Thy1* editing efficiency within the cell population was generally consistent at 50 - 60 % across independent experiments. In contrast, *Pik3cd* and *Pik3ap1* editing sometimes varied between experiments, even when the same guide RNA sequences were used. Furthermore, based on the assumption that Cas9 editing generates a mixed population of heterozygous and homozygous knock out cells, the observed indel frequencies of ~50 % within the population suggests that not all cells in the population were edited. The presence of unedited, wild type cells could mask the detection of a knock out phenotype when using whole-population analyses such as immunoblotting. Therefore, a method for knock out-enrichment before acute TCR stimulation was required.

### 5.2.4 Altered PI3K-AKT signalling in BCAP, ICOS and p110δ knock out T blasts upon TCR stimulation

To improve the analysis of heterogenous knock out populations generated by the CRISPR/Cas9 RNP approach, edited T blasts were enriched before acute TCR stimulation at day 5 post-nucleofection. This was possible due to the multiplex editing strategy used, involving simultaneous targeting of *Thy1* with *Pik3cd*, *Pik3ap1* or *ICOS*. Based on the assumption that *Thy1*-knock out cells were also successfully edited at the second target locus, $CD90^-$ cells could be selected to analyse cells with knock out of *Pik3cd*, *Pik3ap1* or *ICOS*. To this end, T blasts edited with *Pik3cd-*, *Pik3ap1-* or *ICOS*-targeted RNPs were enriched by depletion of $CD90^+$ cells using anti-CD90-conjugated magnetic beads.

$CD90^-$-enriched and $CD90^+$-selected populations were then analysed for editing efficiency at both the *Thy1* target site and the second targeted locus. Indel frequency estimated by TIDE revealed that the second target gene, *Pik3cd*, *Pik3ap1* or *ICOS*, was edited at a much higher

frequency in CD90$^-$-enriched cells than in CD90$^+$ cells (Table 5.2). Very low editing of these genes was detected in CD90$^+$-selected cells. Moreover, across three independent experiments, the frequency of *Pik3cd*, *Pik3ap1* or *ICOS* editing was higher in CD90$^-$-enriched cells than in the total T cell population, by 1.9-fold on average, which was in agreement with the average 2.2-fold enrichment of edited *Thy1*. Overall, this indicated that the CD90$^+$-depletion strategy successfully enriched *Pik3cd*, *Pik3ap1* or *ICOS* knock out cells within the population.

Nevertheless, knock out efficiency varied depending on the target gene. *Pik3ap1* knock out was by far the most efficient, with up to 48 % editing of this gene within the CD90$^-$-enriched population. Surprisingly, *ICOS* and *Pik3cd* editing was lower than the levels seen in previous experiments, even though the more efficient guides were used. The concurrent high efficiency editing of *Thy1* within the same populations indicated that RNP-nucleofection had been successful, therefore suggesting that the low efficiency target gene editing was due to low frequency Cas9 cleavage or indel formation at the *ICOS* and *Pik3cd* target sites.

| Expt | Target KO | Total Cells | | CD90⁻-enriched | | CD90⁺-selected | | *Thy1* KO fold enrichment | Target KO fold enrichment |
|---|---|---|---|---|---|---|---|---|---|
| | | *Thy1* editing % | Target gene editing % | *Thy1* editing % | Target gene editing % | *Thy1* editing % | Target gene editing % | | |
| 1 | CD90 | 16.1 | - | 61.5 | - | 20.3 | - | 3.8 | - |
| | BCAP | 12.3 | 10.7 | 25.7 | 23.4 | 6.0 | 8.4 | 2.1 | 2.2 |
| | ICOS | 18.5 | 9.8 | 58.5 | 13.8 | 6.6 | 5.4 | 3.2 | 1.4 |
| | p110δ | 18.1 | 7.0 | 57.5 | 10.1 | 5.9 | * | 3.2 | 1.4 |
| 2 | CD90 | 38 | - | 70.8 | - | 12.8 | - | 1.9 | - |
| | BCAP | * | 18.4 | 70.4 | 48.2 | 9.5 | 7.2 | * | 2.6 |
| | ICOS | 53.7 | 16.5 | 75.0 | 23.0 | 14 | 10.2 | 1.4 | 1.4 |
| | p110δ | 31.9 | * | 61.5 | 8.7 | 9.6 | 5.4 | 1.9 | * |
| 3 | CD90 | 36.7 | - | 91.9 | - | 10.5 | - | 2.5 | - |
| | BCAP | 42.1 | 18.6 | 74.8 | 48.1 | 8.1 | 8.9 | 1.8 | 2.6 |
| | ICOS | 63.7 | 17.0 | 82.4 | * | 9.7 | 12.7 | 1.3 | * |
| | p110δ | 57.9 | * | 82.1 | 13.1 | 12.8 | 5.5 | 1.4 | * |

**Table 5.2 Gene editing efficiency in CD90⁻-enriched, CD90⁺-selected and total T blasts following RNP nucleofection.**

Activated total T cells were nucleofected with Cas9 RNPs complexed with *Thy1* gRNA 2 (CD90 KO), equimolar amounts of *Pik3ap1* gRNA 1 and *Thy1* gRNA g2 (BCAP KO), equimolar amounts of *ICOS* gRNA g1 and *Thy1* gRNA g2 (ICOS KO), or equimolar amounts of *Pik3cd* gRNA 1, *Pik3cd* gRNA 2 and *Thy1* gRNA g2 (p110δ KO). At day 5 post-nucleofection, CD90⁺ cells were depleted from the total populations using anti-CD90-conjugated magnetic beads. CD90⁺ cells were recovered for DNA purification and CD90⁻ cells were used for *in vitro* stimulation experiments.

Editing efficiency was determined at 5 days post-nucleofection in total cells before bead depletion, and CD90⁻-enriched and CD90⁺-selected cells after bead purification. Editing % indicates the percentage of indels present within the total cell population at the Cas9 cleavage sites in *Thy1*, *Pik3ap1, ICOS* or *Pik3cd*, as determined by TIDE analysis of Sanger sequencing traces of PCR amplicons spanning the targeted regions. KO fold enrichment values indicate the enrichment of *Thy1* or target gene editing in CD90⁻-enriched cells compared to Total Cells. Asterisks (*) indicate samples for which good quality Sanger sequencing traces could not be obtained, therefore TIDE analysis of indel frequency at the indicated target genes within these populations could not be performed. Data are from three independent experiments (Expt1, Expt2 and Expt3).

CD90⁻-enriched *Pik3cd-*, *Pik3ap1-*, and *ICOS*-edited cells were then subjected to acute TCR stimulation and cell lysates were analysed for pAKT by immunoblotting (Figure 5.9). The pAKT signals detected were quantified, normalised and compared to those in *Thy1* knock out cells (Figure 5.10).

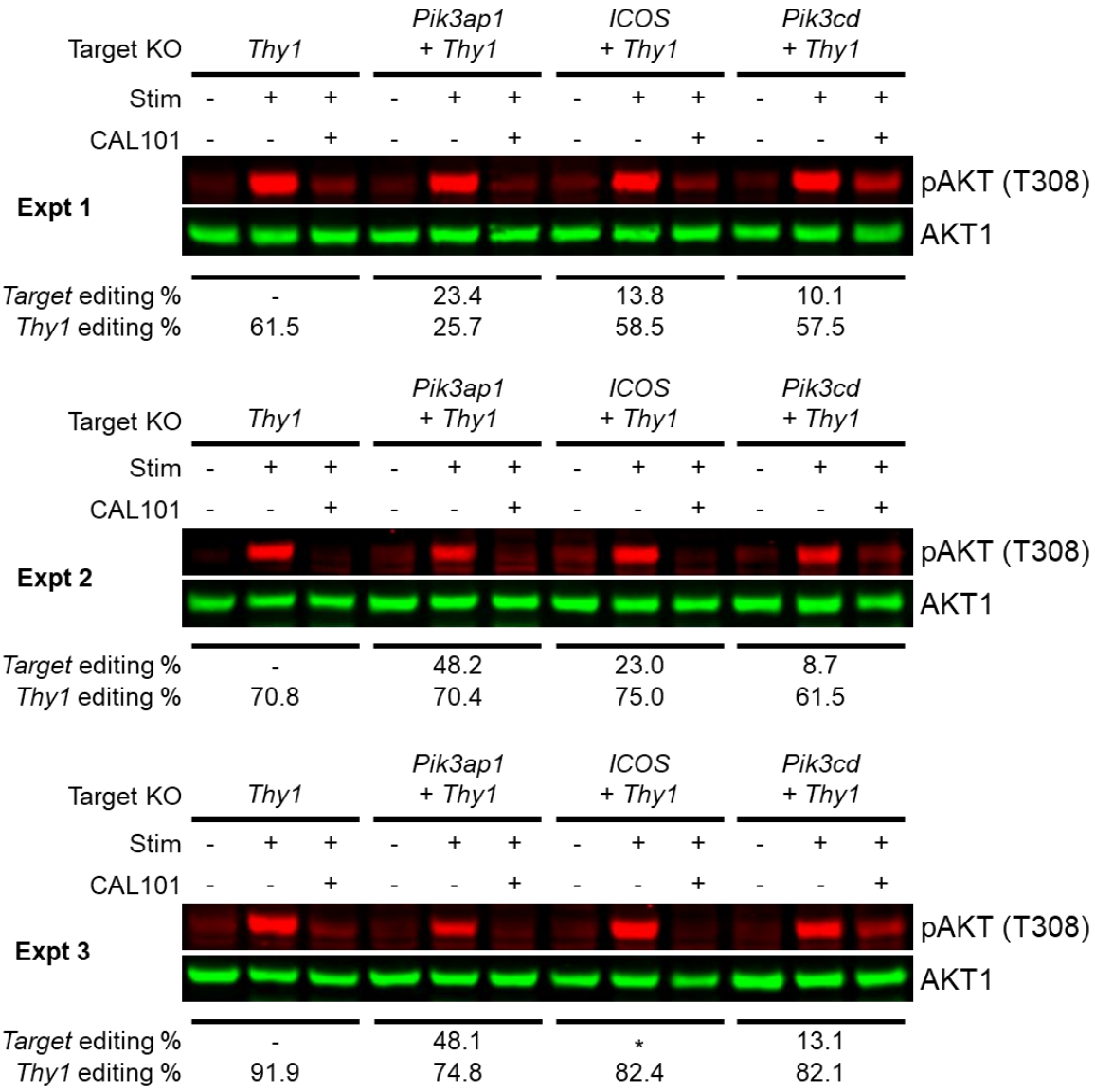


**Figure 5.9 PI3K-AKT signalling and gene editing efficiency in *Thy1*, *Pik3ap1*, *ICOS* and *Pik3cd* CRISPR/Cas9-edited T blasts.**

Activated total T cells were nucleofected with Cas9 RNPs complexed with either *Thy1* gRNA 2 (*Thy1*), equimolar amounts of *Pik3ap1* gRNA 1 and *Thy1* gRNA g2 (*Pik3ap1 + Thy1*), equimolar amounts of *ICOS* gRNA g1 and *Thy1* gRNA g2 (*ICOS + Thy1*), or equimolar amounts of *Pik3cd* gRNA 1, *Pik3cd* gRNA 2 and *Thy1* gRNA g2 (*Pik3cd + Thy1*). At day 5 post-nucleofection, $CD90^+$ cells were depleted from the total population using anti-CD90-conjugated magnetic beads. Two million $CD90^-$-enriched cells of each genotype were then stimulated with 4 µg/ml αCD3+αCD4+αCD8 plus 13 µg/ml crosslinking antibody for 2 minutes at 37°C, in the presence of 200 nM DMSO (-) or CAL101 (+), or left unstimulated in the presence of 200 nM DMSO. Cells were lysed and one-half of the lysates were separated by SDS-PAGE, followed by immunoblotting simultaneously for pAKT (T308) and total AKT1. Editing efficiency in $CD90^-$-enriched cells (indicated below immunoblots) was determined at 5 days post-nucleofection. Editing % indicates the percentage of indels present within the total cell population at the Cas9 cleavage sites in *Thy1*, *Pik3ap1, ICOS* or *Pik3cd*, as determined by TIDE analysis. High quality Sanger sequencing traces could not be obtained of the *ICOS* target site for the asterisked (*) sample, therefore TIDE analysis of *ICOS* indel frequency within this population could not be performed. Immunoblots are from three independent experiments (Expt 1, Expt 2 and Expt 3).

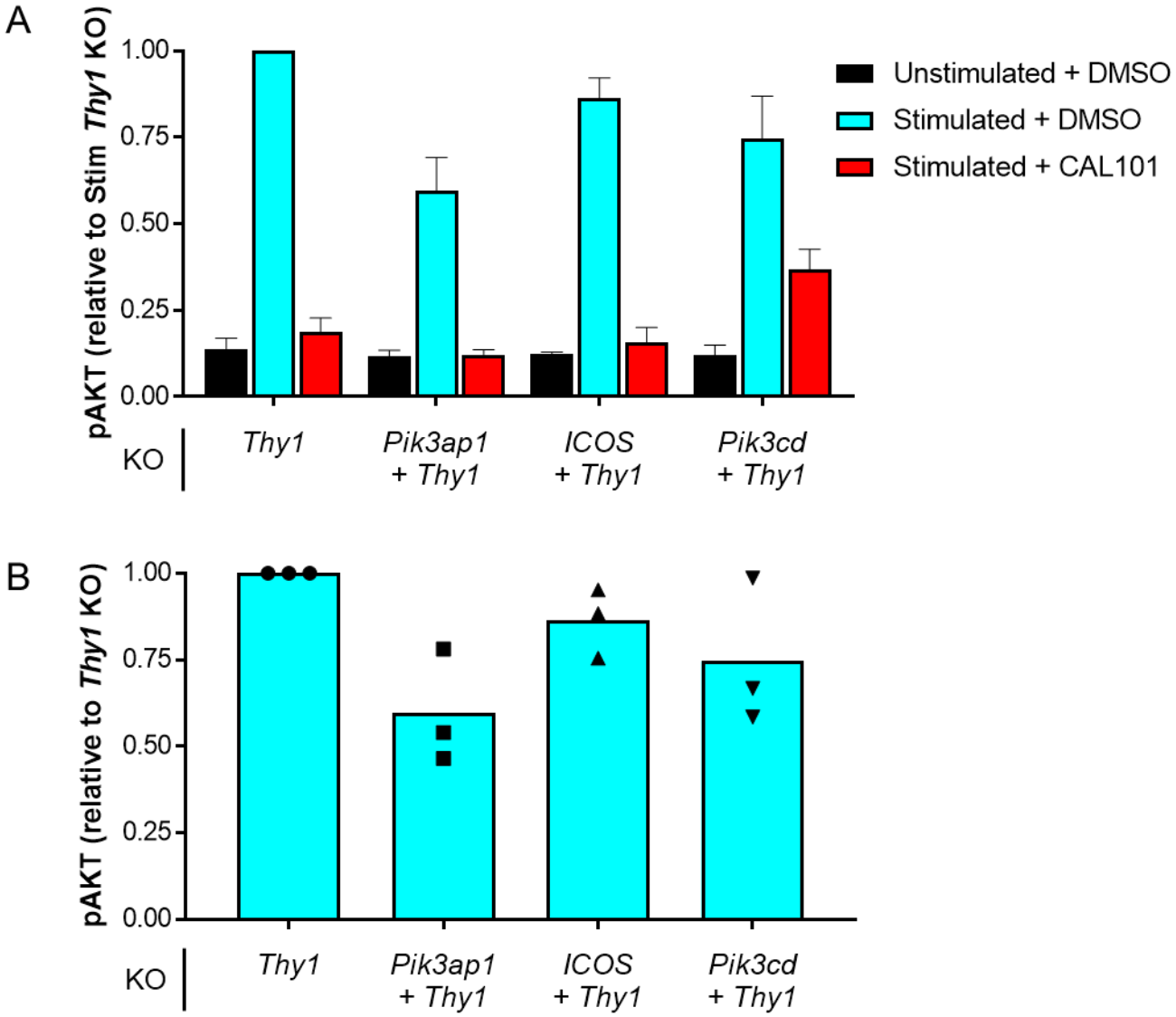


**Figure 5.10 Reduced pAKT upon TCR-stimulation in *Pik3ap1*-, *ICOS*- and *Pik3cd*-edited CD90$^-$ -enriched T blasts.**
**A.** Quantification of pAKT signal intensity as detected by immunoblotting in Figure 5.9, normalised to AKT1 and presented relative to pAKT in stimulated *Thy1*-edited cells, set as 1. Data are from three independent experiments. Bars represent the mean, with error bars +SEM.
**B.** The same data as in A but for 'Stimulated + DMSO' cells only, with the individual normalised pAKT values from three independent experiments represented as scatter points, relative to pAKT in stimulated *Thy1*-edited cells in each experiment. Bars represent the mean for each genotype.

In *Pik3ap1*-edited T blasts there was a clear trend of reduced pAKT upon TCR stimulation (Figure 5.10A and 5.10B). This stimulated pAKT signal was compared to that induced in control *Thy1*-edited cells across three independent experiments but was not found to be significantly different (adjusted p value 0.1638; repeated measures one-way ANOVA with Dunnett's multiple comparisons test). This was due to the variation in the observed pAKT signal across the three

experiments. Intriguingly, the level of reduction in pAKT correlated with the percentage of *Pik3ap1* editing within the cell population. A ~50 % reduction in pAKT was observed in two experiments where *Pik3ap1* indel frequency reached 48.2 and 48.1 %. In contrast, only a 22 % reduction in pAKT was seen in cells with 23.4 % *Pik3ap1* editing. These results strongly suggested that BCAP knock out impairs TCR-dependent PI3K-AKT signalling in activated T cells. Further experiments, using cells with a consistently high efficiency of BCAP knock out, would be required to test this hypothesis.

A trend of slightly reduced pAKT upon TCR stimulation was also observed in *ICOS*-edited T blasts (Figure 5.10). In cells with 13.8 and 23.0 % *ICOS* editing within the population, a 11.6 and 24.5 % reduction in pAKT signal was observed, respectively, compared with control *Thy1*-edited cells. Signalling in *ICOS*-edited cells was not found to be significantly different to that in control cells due to this variation (adjusted p value 0.2592; repeated measures one-way ANOVA with Dunnett's multiple comparisons test). Nevertheless, the observed trend indicates that ICOS may be important for TCR-induced activation of the PI3K-AKT pathway. Further experiments, using cells with a consistently high efficiency of ICOS knock out, would be required to test this hypothesis.

*Pik3cd*-edited T blasts also exhibited reduced pAKT upon TCR engagement, as expected, but this reduction was again variable (Figure 5.10). Consequently, pAKT in stimulated *Pik3cd*-edited cells was not found to be significantly different to that in *Thy1*-edited cells (adjusted p value 0.3616; repeated measures one-way ANOVA with Dunnett's multiple comparisons test). Nevertheless, in two independent experiments a 33.3 and 41.5 % reduction in the level of induced pAKT was observed, compared with control cells (Figure 5.10B). Interestingly, TIDE analysis of the sequenced *Pik3cd* target region estimated only low indel formation at this locus. While it cannot be excluded that these efficiencies were underestimated, this suggests that even partial loss of p110δ had a considerable impact on AKT activation. However, in one experiment, *Pik3cd*-edited cells exhibited pAKT levels equivalent to control, reflecting either low frequency knock out of p110δ within the population or that another PI3K subunit compensated for its loss.

Moreover, as seen in earlier experiments, *Pik3cd*-edited cells exhibited increased residual pAKT upon TCR stimulation in the presence of the p110δ-specific inhibitor CAL101 (Figure 5.11). In *Thy1*-, *Pik3ap1*- and *ICOS*-edited cells treated with CAL101, the level of pAKT induced upon TCR stimulation was only ~19 % of that induced in DMSO-treated cells, indicating that the majority of AKT phosphorylation was p110δ-dependent in these cells. In contrast, *Pik3cd*-edited CAL101-

treated cells exhibited, on average, 50 % of the pAKT level induced in DMSO-treated cells. This was significantly different to the residual pAKT signal in CAL101-treated *Thy1*-edited cells (adjusted p value of 0.0018; one-way ANOVA with Dunnett's multiple comparisons test). This strengthened the earlier conclusion that p110δ-deficient T blasts exhibit p110δ-independent activation of AKT upon TCR engagement.

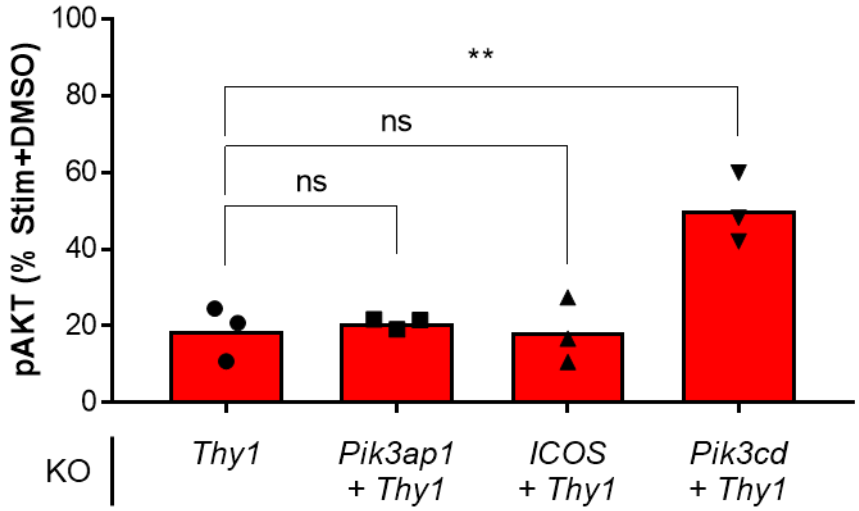


**Figure 5.11 p110δ-independent PI3K-AKT signalling in *Pik3cd*-edited CD90$^-$-enriched T blasts upon TCR-stimulation.**
Quantification of pAKT signal intensity in CAL101-treated TCR-stimulated cells, as detected by immunoblotting in Figure 5.9, normalised to AKT1 and expressed as a percentage of the pAKT in DMSO-treated TCR-stimulated cells. Bars represent the means of three independent experiments, with individual values shown as scatter points. The means for each genotype were compared to the mean of *Thy1*-edited cells by one-way ANOVA with Dunnett's multiple comparisons test. ** indicates statistically significant difference with a multiplicity adjusted p value of 0.0018. ns indicates no statistically significant difference.

Taken together, the study of PI3K-AKT signalling in CD90$^-$-enriched *Pik3ap1* and *ICOS* knock out cells provided evidence to support a positive regulatory role for BCAP and ICOS in the TCR-induced activation of PI3K in activated T cells. Nevertheless, further experiments, using cells with a consistently high efficiency of BCAP or ICOS knock out, would be required to robustly test this hypothesis.

### 5.2.5 Interrogating cytokine production in BCAP-, p110δ- and ICOS- deficient T blasts upon TCR stimulation

Biochemical analyses suggested that BCAP and ICOS positively regulate the PI3K-AKT pathway upon TCR engagement in activated T cells. This was reasoned to be mediated via the specific activation of p110δ, given that BCAP and ICOS were identified by MS as p110δ interactors and that phosphorylation of AKT upon TCR stimulation was p110δ-dependent in wild type T cells. Previous studies have shown that p110δ also regulates cytokine production in T cells (Okkenhaug *et al*, 2002; Liu *et al*, 2009; Gracias *et al*, 2016). TNFα and IFNγ production is reduced in mouse and human effector/memory T cells in the presence of a p110δ-specific inhibitor, indicating that p110δ activity is required for cytokine production in activated T cells (Soond *et al*, 2010). It was therefore hypothesised that, if BCAP and ICOS positively regulate p110δ activation, loss of BCAP or ICOS would impair cytokine production in T blasts upon TCR stimulation.

To evaluate whether knock out of BCAP or ICOS impaired cytokine production in T blasts, *Pik3ap1*, *ICOS* and *Pik3cd* CRISPR/Cas9-edited cells were stimulated for 8 hours with plate-bound anti-CD3, and intracellular TNFα production was then analysed by flow cytometry. These cells were generated from the same nucleofections as those studied in section 5.2.4.

Due to the multiplex CRISPR/Cas9 editing approach used thus far, cells that were edited at the *Pik3ap1*, *ICOS* or *Pik3cd* target locus could be selected based on CD90 cell surface expression. Earlier sequencing and TIDE analysis of $CD90^-$-enriched and $CD90^+$-selected cells confirmed that knock out of these target genes was enriched in $CD90^-$ cells. Therefore, $CD90^-$ cells could be selected following flow cytometry analysis to specifically study *Pik3ap1-*, *ICOS*- or *Pik3cd*-edited cells. However, it was unlikely that all $CD90^-$ cells would exhibit knock out of BCAP, ICOS or p110δ, based on the editing efficiencies within $CD90^-$-enriched populations that were estimated by TIDE analysis (Table 5.2). Nevertheless, by comparing $CD90^-$ and $CD90^+$ cells it would be possible to analyse the effect of *Pik3ap1*, *ICOS* or *Pik3cd* gene disruption. Conveniently, as *Thy1*-targeting did not result in a homogenous CD90-knock out population, $CD90^+$ cells from the same populations could be used as internal 'wild type' control cells, given that the earlier sequencing analysis also demonstrated that $CD90^+$ cells exhibited very low levels of target gene editing. Thus, this strategy was used to analyse intracellular TNFα production in BCAP, ICOS and p110δ knock out cells.

Production of TNFα upon TCR stimulation was first examined in $CD4^+$ T blasts (Figure 5.12). TNFα mean fluorescence intensity (MFI), detected by flow cytometry, was compared in $CD90^-TNF\alpha^+$ and $CD90^+TNF\alpha^+$ $CD4^+$ cells from each of the *Pik3ap1*, *ICOS* and *Pik3cd* multiplex-edited populations, as well as the control population that was only targeted for editing at the *Thy1* locus (Figure 5.12A). This analysis revealed that $CD90^-$ $CD4^+$ cells exhibited slightly higher TNFα MFI than $CD90^+$ $CD4^+$ cells. Interestingly, this difference was reduced in each of the multiplex-edited populations, such that *Pik3cd*-edited $CD90^-$ cells produced equivalent levels of TNFα as $CD90^+$ cells in the same sample. Due to this difference between $CD90^-$ and $CD90^+$ cells, it was also crucial to compare each of the multiplex-edited $CD90^-$ populations with *Thy1*-only edited $CD90^-$ cells, rather than $CD90^+$ cells from the same sample. To this end, TNFα production in *Pik3ap1*-, *ICOS*- and *Pik3cd*-edited $CD90^-$ cells was compared to that in *Thy1*-only edited $CD90^-$ cells (Figure 5.12B). There was no significant difference in TNFα MFI in each of the genotypes compared with *Thy1*-only edited $CD90^-$ cells (tested by one-way ANOVA with Dunnett's multiple comparisons test). This may have been due to variation across the three independent experiments owing to differences in gene editing efficiency. Nevertheless, *Pik3cd*-edited $CD90^-$ $CD4^+$ cells exhibited slightly reduced TNFα production compared to $CD90^-$ cells. Unexpectedly, there was a very small trend for increased TNFα production in *Pik3ap1*- and *ICOS*-edited $CD90^-$ cells, but this was not significant. Overall, it was interesting that the increased TNFα production observed in $CD90^-$ cells, relative to $CD90^+$ cells, was reduced upon simultaneous editing of *Pik3ap1*, *ICOS* or *Pik3cd* (Figure 5.12A). This suggests that loss of either BCAP, ICOS or p110δ causes a reduction in TCR-induced TNFα production in $CD90^-CD4^+$ T blasts. However, it could not be ruled out that low level *Pik3ap1*- and *ICOS*-editing in $CD90^+$ cells led to increased TNFα production in these cells.

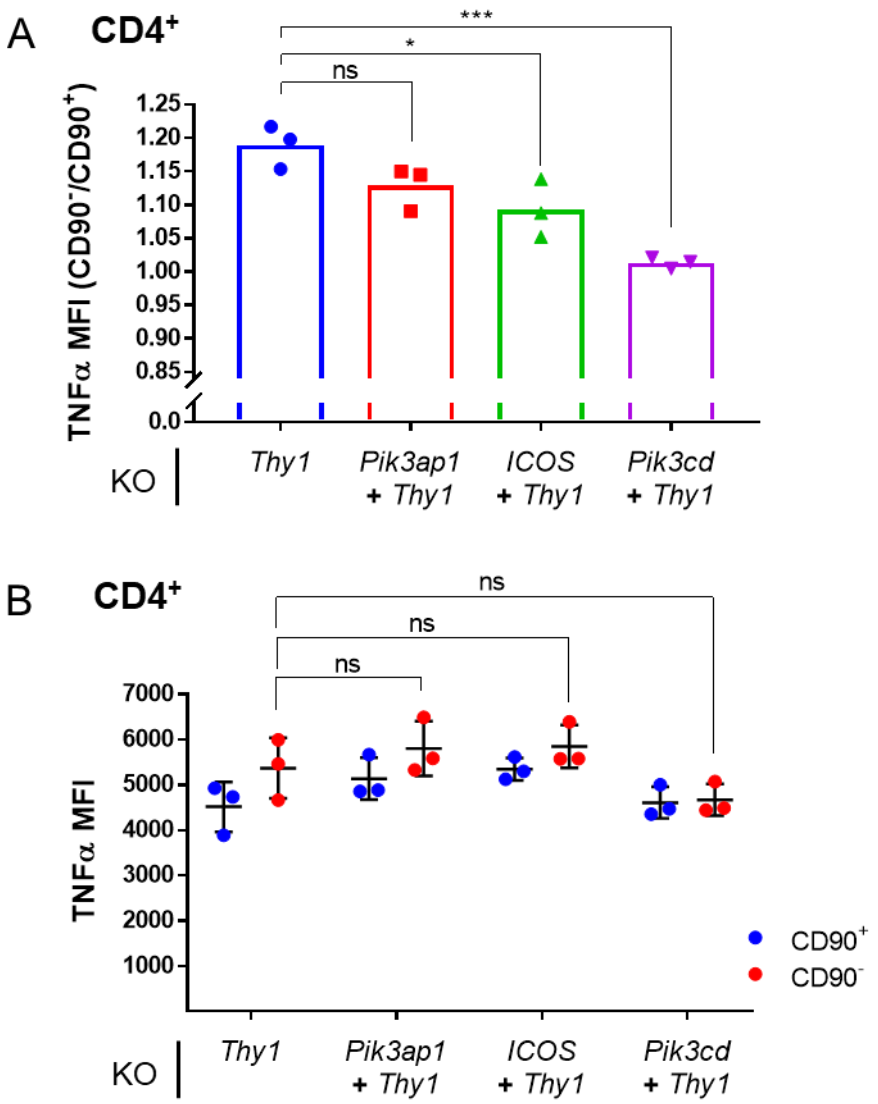


**Figure 5.12 TNFα production upon TCR stimulation in BCAP, ICOS and p110δ knock out CD4⁺ T blasts.**

Activated total T cells were nucleofected with Cas9 RNPs as detailed in Figure 5.9. At day 5 post-nucleofection, 200,000 cells of each genotype in duplicate were stimulated on 96-well plates coated with anti-CD3 (0.2 µg per well) in the presence of brefeldin A for 8 hours at 37°C. Cells were then analysed by flow cytometry for intracellular TNFα.

**A.** TNFα production in $CD4^+CD90^-$ cells relative to $CD4^+CD90^+$ cells. The mean fluorescence intensity (MFI) of TNFα antibody staining in $TNF\alpha^+CD90^-$ cells is expressed as a ratio of the TNFα MFI detected in $TNF\alpha^+CD90^+$ cells ($CD90^-/CD90^+$). Bars represent the means of three independent experiments, with individual values shown as scatter points. Each value represents the average of duplicate samples. The means for each genotype were compared to the mean for *Thy1*-edited cells by one-way ANOVA with Dunnett's multiple comparisons test. Asterisks indicate statistically significant differences with multiplicity adjusted p values of 0.0153 (*) and 0.0004 (***). ns indicates no statistically significant difference (adjusted p value 0.1126).

**B.** TNFα production in $CD4^+CD90^+$ and $CD4^+CD90^-$ T blasts. Individual values for TNFα MFI in $TNF\alpha^+$ cells from three independent experiments are shown as scatter points. Each value represents the average of duplicate samples. Black error bars show the mean ± SD. The means for $CD90^-$ cells of each genotype were compared to the mean for $CD90^-$ *Thy1*-edited cells by one-way ANOVA with Dunnett's multiple comparisons test. ns indicates no statistically significant difference.

TNFα production was also analysed in $CD8^+$ T blasts following TCR stimulation (Figure 5.13). $CD8^+TNF\alpha^+$ T blasts produced higher levels of TNFα than that seen in $CD4^+$ cells. In contrast to $CD4^+$ cells, $CD90^-$ $CD8^+$ cells exhibited slightly lower TNFα MFI than $CD90^+$ $CD8^+$ cells. This difference was greater in *Pik3ap1*- and *Pik3cd*-edited $CD90^-$ $CD8^+$ cells (Figure 5.13A). Therefore, it was again necessary to compare each of the multiplex-edited $CD90^-$ populations with *Thy1*-only edited $CD90^-$ cells, rather than $CD90^+$ cells. This revealed that there was no significant difference in TNFα MFI in each of the genotypes compared with *Thy1*-only edited $CD90^-$ cells (Figure 5.13B; tested by one-way ANOVA with Dunnett's multiple comparisons test). There was, however, a trend for decreased TNFα production in *Pik3cd*-edited $CD90^-$ $CD8^+$ cells, compared with *Thy1*-only edited $CD90^-$ $CD8^+$ cells. Overall, it was interesting that the reduced TNFα production in $CD90^-$ $CD8^+$ cells, relative to $CD90^+$ $CD8^+$ cells, was further decreased upon simultaneous editing of *Pik3ap1* or *Pik3cd* (Figure 5.13A). This suggests that loss of either BCAP or p110δ causes a reduction in TCR-induced TNFα production in $CD90^-CD8^+$ T blasts.

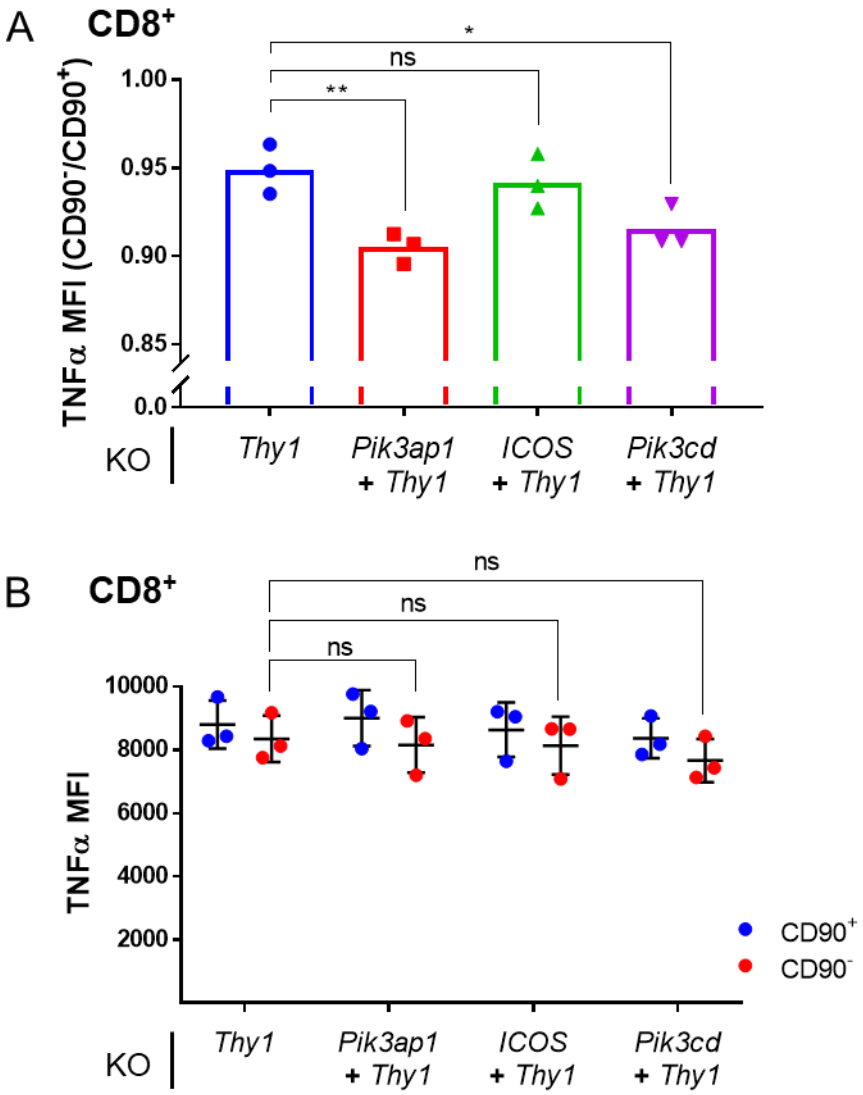


**Figure 5.13 TNFα production upon TCR stimulation in BCAP, ICOS and p110δ knock out CD8⁺ T blasts.**

Activated total T cells were nucleofected with Cas9 RNPs as detailed in Figure 5.9. At day 5 post-nucleofection, 200,000 cells of each genotype in duplicate were stimulated on 96-well plates coated with anti-CD3 (0.2 µg per well) in the presence of brefeldin A for 8 hours at 37°C. Cells were then analysed by flow cytometry for intracellular TNFα.

**A.** TNFα production in $CD8^+CD90^-$ cells relative to $CD8^+CD90^+$ cells. The mean fluorescence intensity (MFI) of TNFα antibody staining in $TNF\alpha^+CD90^-$ cells is expressed as a ratio of the TNFα MFI detected in $TNF\alpha^+CD90^+$ cells ($CD90^-/CD90^+$). Bars represent the means of three independent experiments, with individual values shown as scatter points. Each value represents the average of duplicate samples. The means for each genotype were compared to the mean for *Thy1*-edited cells by one-way ANOVA with Dunnett's multiple comparisons test. Asterisks indicate statistically significant differences with multiplicity adjusted p values of 0.0311 (*) and 0.0076 (**). ns indicates no statistically significant difference (adjusted p value 0.8237).

**B.** TNFα production in $CD8^+CD90^-$ and $CD8^+CD90^+$ T blasts. Individual values for TNFα MFI in $TNF\alpha^+$ cells from three independent experiments are shown as scatter points. Each value represents the average of duplicate samples. Black error bars show the mean ± SD. The means for $CD90^-$ cells of each genotype were compared to the mean for $CD90^-$ *Thy1*-edited cells by one-way ANOVA with Dunnett's multiple comparisons test. ns indicates no statistically significant difference.

The effect of p110δ-inhibition on TCR-induced TNFα production was also examined in $CD4^+$ and $CD8^+$ knock out T blasts. To this end, TNFα MFI was compared in CAL101- and DMSO-treated cells of each genotype (Figure 5.14). There was no difference in CAL101 sensitivity between *Thy1*-only edited $CD90^-$ and $CD90^+$ cells. This indicates that TNFα production is equally p110δ-dependent in $CD90^-$ and $CD90^+$ T blasts. It was also observed that TNFα production was reduced to a greater extent in CAL101-treated $CD4^+$ cells than $CD8^+$ cells. This suggests that TNFα production in $CD4^+$ T blasts is more p110δ-dependent than in $CD8^+$ T blasts. The effect of CAL101 on TNFα production in *Pik3ap1*-, *ICOS*- and *Pik3cd*-edited $CD90^-$ $CD4^+$ cells was then compared with the effect on *Thy1*-only edited $CD90^-$ cells (Figure 5.14A). There was no significant difference in CAL101 sensitivity in *Pik3ap1*- or *ICOS*-edited $CD90^-$ $CD4^+$ cells compared with *Thy1*-only edited $CD90^-$ $CD4^+$ cells. In contrast, TNFα production in *Pik3cd*-edited $CD90^-$ $CD4^+$ cells was significantly less sensitive to p110δ-inhibition than in *Thy1*-only edited $CD90^-$ $CD4^+$ cells (adjusted p value of 0.0102; one-way ANOVA with Dunnett's multiple comparisons test). This suggests that a higher proportion of TNFα production in the *Pik3cd*-edited $CD90^-$ population was p110δ-independent, possibly corresponding to p110δ-deficient $CD4^+$ cells. This phenotype was similar to that seen in earlier biochemical analyses of PI3K-AKT signalling in *Pik3cd*-edited $CD90^-$-enriched total T blasts.

The effect of CAL101 on TNFα production in *Pik3ap1*-, *ICOS*- and *Pik3cd*-edited $CD90^-$ $CD8^+$ cells was then analysed, with comparison to *Thy1*-only edited $CD90^-$ $CD8^+$ cells (Figure 5.14B). There was no significant difference in CAL101 sensitivity in any of the multiplex-edited $CD90^-$ $CD8^+$ cells compared with *Thy1*-only edited $CD90^-$ $CD8^+$ cells. However, *ICOS*- and *Pik3cd*-edited $CD90^-$ $CD8^+$ T blasts demonstrated slightly less CAL101 sensitivity with respect to TNFα production, suggesting that a higher proportion of TNFα production in these $CD90^-$ populations was p110δ-independent.

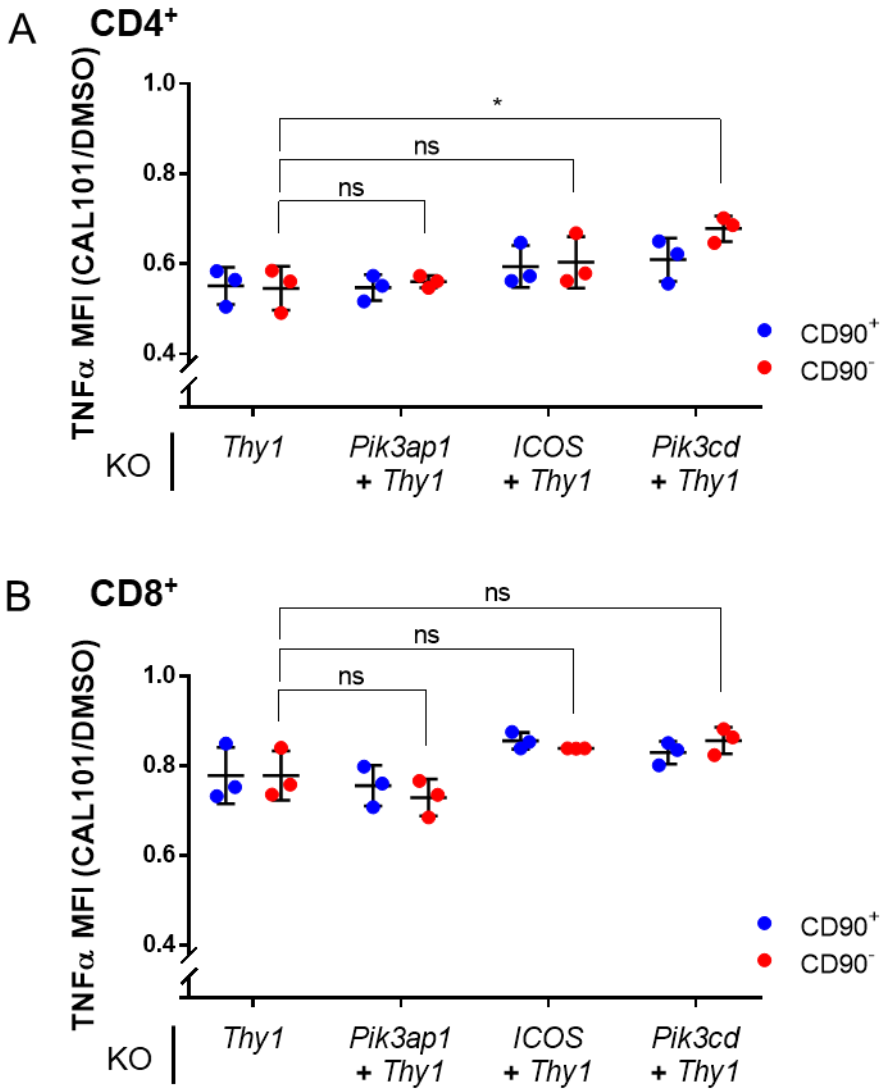


**Figure 5.14 The effect of p110δ-inhibition on TNFα production upon TCR stimulation in BCAP, ICOS and p110δ knock out T blasts**.

Activated total T cells were nucleofected with Cas9 RNPs as detailed in Figure 5.9. At day 5 post-nucleofection, 200,000 cells of each genotype in duplicate were stimulated on 96-well plates coated with anti-CD3 (0.2 µg per well) in the presence of brefeldin A and either 200 nM CAL101 or 200 nM DMSO for 8 hours at 37°C. Cells were then analysed by flow cytometry for intracellular TNFα. The mean fluorescence intensity (MFI) of TNFα antibody staining in CAL101-treated $TNF\alpha^{+}CD90^{-}$ (red) and $TNF\alpha^{+}CD90^{+}$ (blue) cells is expressed as a ratio of the TNFα MFI detected in the equivalent DMSO-treated cells (CAL101/DMSO). Individual values from three independent experiments are shown as scatter points. Each value represents the average of duplicate samples. Black error bars show the mean ± SD. The means for $CD90^{-}$ cells of each genotype were compared to the mean of $CD90^{-}$ *Thy1*-edited cells by one-way ANOVA with Dunnett's multiple comparisons test.

**A.** TNFα production in CAL101-treated $CD4^{+}$ T blasts, relative to DMSO treated cells. * indicates a statistically significant difference with a multiplicity adjusted p value of 0.0102. ns indicates no statistically significant difference.

**B.** TNFα production in CAL101-treated $CD8^{+}$ T blasts, relative to DMSO treated cells. ns indicates no statistically significant difference.

In addition to investigating TNFα production in knock out T blasts, the proportion of TNFα-IFNγ double cytokine producing cells upon TCR stimulation was considered. IFNγ production in effector/memory T cells is also regulated by p110δ (Soond *et al*, 2010), and TNFα-IFNγ double producing T cells represent those that have differentiated upon antigenic stimulation to a stage of enhanced effector function (Seder *et al*, 2008). Examination of $TNF\alpha^{+}IFN\gamma^{+}$ $CD90^{-}$ and $CD90^{+}$ cells within $CD4^{+}$ and $CD8^{+}$ populations from all knock out genotypes revealed that the percentage of these cells generated upon TCR stimulation followed the same trends observed for TNFα production in *Thy1-*, *Pik3ap1-*, *ICOS-* and *Pik3cd*-edited T blasts (Figure 5.15). In summary, a slightly higher proportion of $CD4^{+}$ $CD90^{-}$ cells were double producers than $CD4^{+}$ $CD90^{+}$ cells (Figure 5.15A). Interestingly, this difference was reduced slightly upon simultaneous editing of *Pik3ap1 or ICOS*, and significantly upon editing of *Pik3cd.* Each $CD4^{+}$ $CD90^{-}$ genotype was also compared with *Thy1*-only edited $CD90^{-}$ cells (Figure 5.15B). This revealed no significant difference in the proportion of double producers in *Pik3ap1-* or *Pik3cd*-edited $CD90^{-}$ T blasts compared to the control. There was, however, a small significant increase in double producers in *ICOS*-edited $CD90^{-}$ $CD4^{+}$cells. In the $CD8^{+}$ populations, a slightly lower proportion of $CD90^{-}$ cells were double producers than $CD90^{+}$ cells (Figure 5.15C). This difference was not significantly increased upon simultaneous editing of *Pik3ap1, ICOS* or *Pik3cd*, although there was some indication that *Pik3ap1*-editing had a small effect. Each $CD8^{+}$ $CD90^{-}$ genotype was then compared with *Thy1*-only edited $CD90^{-}$ cells (Figure 5.15D). This revealed no significant difference in the proportion of double producers in *Pik3ap1-, ICOS-* or *Pik3cd*-edited $CD90^{-}$ T blasts compared to the control.

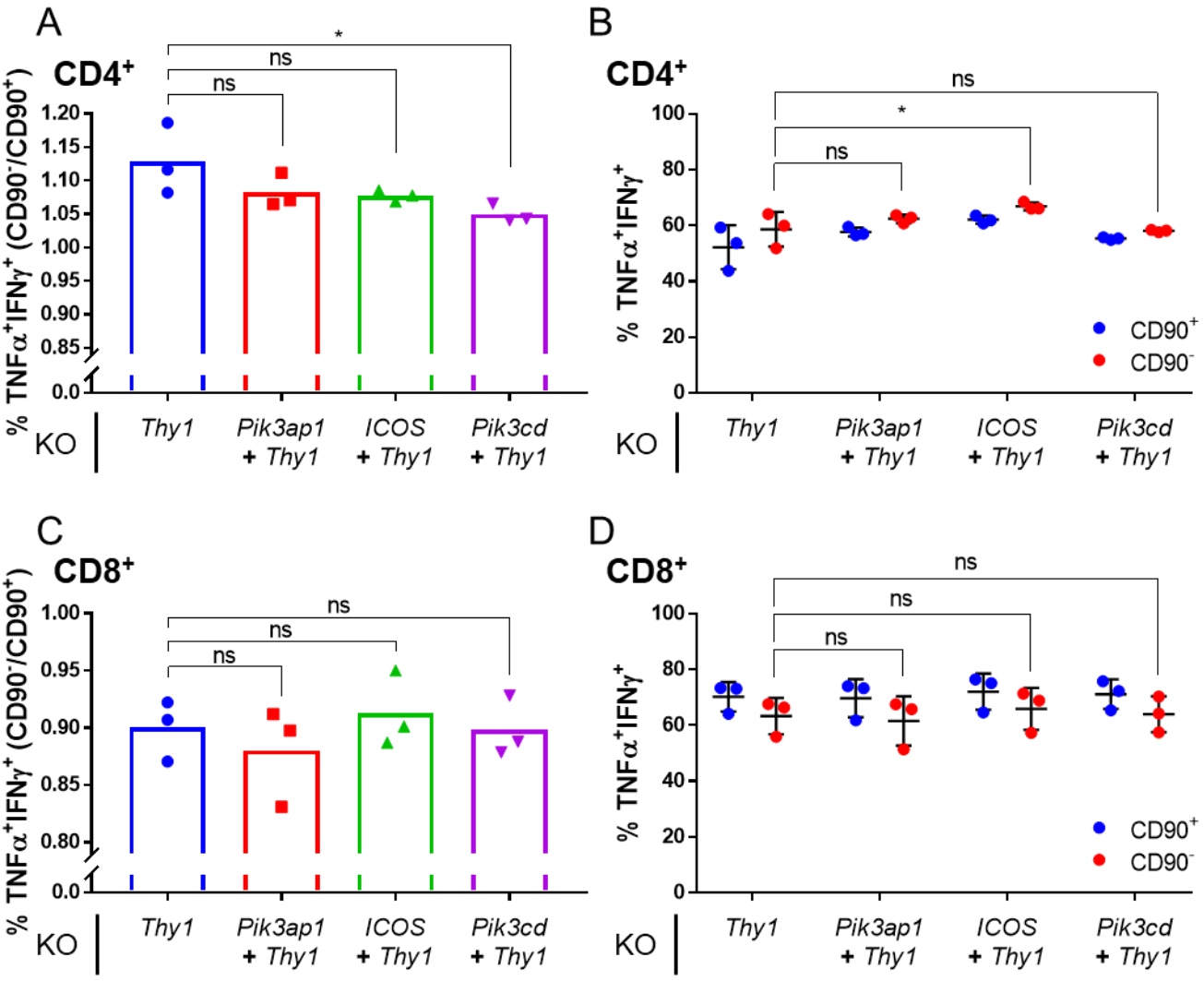


**Figure 5.15 The proportion of TNFα-IFNγ-producing cells upon TCR stimulation in BCAP, ICOS and p110δ knock out T blasts.**

Activated total T cells were nucleofected with Cas9 RNPs as detailed in Figure 5.9. At day 5 post-nucleofection, 200,000 cells of each genotype in duplicate were stimulated on 96-well plates coated with anti-CD3 (0.2 µg per well) in the presence of brefeldin A for 8 hours at 37°C. Cells were then analysed by flow cytometry for intracellular TNFα and IFNγ.

**A and C.** Percentage of $TNF\alpha^+IFN\gamma^+$ $CD90^-$ cells relative to $TNF\alpha^+IFN\gamma^+$ $CD90^+$ cells. The percentage of $TNF\alpha^+IFN\gamma^+CD90^-$ cells is expressed as a ratio of the percentage of $TNF\alpha^+IFN\gamma^+CD90^+$ cells ($CD90^-$/$CD90^+$). Bars represent the means of three independent experiments, with individual values shown as scatter points. Each value represents the average of duplicate samples. The means for each genotype were compared to the mean for *Thy1*-edited cells by one-way ANOVA with Dunnett's multiple comparisons test. In A, * indicates a statistically significant difference with a multiplicity adjusted p value of 0.0340. ns indicates no statistically significant difference.

**B and D.** Percentage of $TNF\alpha^+IFN\gamma^+$ $CD90^-$ cells and $TNF\alpha^+IFN\gamma^+$ $CD90^+$ cells. Individual percentages of $TNF\alpha^+IFN\gamma^+$ $CD90^-$ and $CD90^+$ cells from three independent experiments are shown as scatter points. Each value represents the average of duplicate samples. Black error bars show the mean ± SD. The means for $CD90^-$ cells of each genotype were compared to the mean for $CD90^-$ Thy1-edited cells by one-way ANOVA with Dunnett's multiple comparisons test. ns indicates no statistically significant difference. In B, * indicates a statistically significant difference with a multiplicity adjusted p value of 0.0372. ns indicates no statistically significant difference.

Taken together, the study of cytokine production upon TCR stimulation revealed only small differences in *Pik3ap1*-, *ICOS*- and *Pik3cd*-edited T blasts compared with *Thy1*-edited cells. In $CD8^+$ T blasts, there was a slight decrease in cytokine production upon *Pik3ap1* or *Pik3cd* knock out. In $CD4^+$ T blasts, there was a slight decrease in cytokine production upon *Pik3cd* knock out in $CD90^-$ cells. *Pik3ap1* or *ICOS* knock out reduced the phenotype of increased cytokine production in $CD90^-$ $CD4^+$ cells compared with $CD90^+$ $CD4^+$ cells. These experiments suggest that BCAP and ICOS play a role in regulating cytokine production in T blasts, but this may differ in $CD8^+$ and $CD4^+$ cells. However, the small differences observed, and the potential interplay with loss of CD90 expression, confounds the interpretation of these results. Furthermore, the differences in editing efficiency across the three independent experiments possibly contributed to the variability in cytokine production within each genotype, thus reducing the confidence in the observed differences. Further experiments, achieving a consistently high efficiency of target knock out, would be required to investigate these phenotypes. Nevertheless, one observed phenotype was in accord with earlier biochemical analyses of PI3K-AKT signalling in *Pik3cd*-edited $CD90^-$-enriched total T blasts. TNFα production in the *Pik3cd*-edited $CD4^+$ $CD90^-$ population was less p110δ-dependent than in *Thy1*-edited $CD4^+$ $CD90^-$ cells, and this trend was also noticeable in $CD8^+$ *Pik3cd*-edited cells and *ICOS*-edited $CD4^+$ and $CD8^+$ cells. This CAL101-resistant TNFα production may have originated from p110δ- and ICOS-deficient cells, thus suggesting that another PI3K isoform or pathway was compensating for their loss. However, further experiments would be required to investigate these small phenotypic differences.

## 5.3 Discussion

This body of work set out to develop a CRISPR/Cas9-mediated gene editing approach to knock out proteins of interest in primary mouse activated T cells. The results of this work have demonstrated that ribonucleoprotein (RNP) nucleofection is a viable and effective method for delivering Cas9 protein and guide RNA to primary mouse T cells. Using this approach, it was possible to successfully knock out genes encoding CD90, BCAP, ICOS and p110δ *in vitro* in both $CD4^+$ and $CD8^+$ T blasts. This enabled the subsequent study of the role of BCAP and ICOS in PI3K signalling in the same physiological setting in which they were identified by mass spectrometry as p110δ-interacting proteins.

As part of this study, the conditions for RNP nucleofection of primary activated mouse T cells were optimised, with respect to the amount of Cas9, gRNA and cells used. This process was

successful, achieving a substantial improvement in knock out efficiency from only 20 - 30 % to over 60 %. Despite this improvement, it was noted that the highest amount of Cas9 that was tested in optimisation experiments was also calculated as the optimal quantity for high efficiency knock out. This indicated that the experimental space tested did not cover the 'true' optimum. Hence, the maximum efficiency that could be achieved with the optimised protocol was predicted to equal the highest that was observed in the optimisation experiment, which was approximately 50 %. Indeed, in subsequent experiments, the frequency of indel formation at the *Thy1* locus was usually 50 - 60%. Therefore, it is possible that greater editing efficiency could be achieved using increased amounts of Cas9. Future work will include another set of optimisation experiments that test higher Cas9 protein amounts. The results from this should nevertheless take into account the resources available and the level of knock out efficiency required for downstream assays. Using flow cytometry-based single-cell analysis, ~50 % knock out within a population is generally acceptable if the edited cells can be selected using a cell surface or intracellular marker. In addition, the presence of unedited cells provides a useful internal control for phenotypic analysis. However, in the absence of a marker for successful knock out, or for whole-population analyses such as immunoblotting, high efficiency editing in the majority of the population would be required.

While the RNP nucleofection protocol is a focal point for improvement, the experiments in this study have shown that the guide crRNA sequence used has a significant impact on the editing efficiency achieved, as does the targeted locus itself. Consistently lower editing of *ICOS* and *Pik3cd* was observed compared to *Pik3ap1* and *Thy1*, as estimated by TIDE analysis. Thus, knock out efficiency for these targets may be improved in future experiments by designing new guide crRNAs. However, it is also likely that some genomic sequences are simply more resistant to editing than others (Wu *et al*, 2014; Liu *et al*, 2016). Alternatively, faithful repair of double strand breaks, without indel formation, may be more efficient at some genomic sites. Therefore, achieving equivalent knock out efficiency when targeting multiple genes may require gene-by-gene optimisation for future experiments.

Another interesting observation made in this study was the apparent higher efficiency of protein knock out in $CD8^+$ T blasts compared to $CD4^+$ cells. This did not appear to be due to slower protein turnover or a survival disadvantage in $CD4^+CD90^-$ T cells, thus suggesting that the extent of gene editing differed in these two subsets. This could be because $CD8^+$ cells are more proliferative than $CD4^+$ cells in response to IL-2 and enter the S phase of the cell cycle sooner

(Smith *et al*, 2017). By completing more rounds of cell division than $CD4^+$ cells in the presence of Cas9 RNPs, the $CD8^+$ population could accumulate a higher frequency of Cas9 cleavage-induced indels.

In the current study, knock out of the intracellular proteins p110δ and BCAP presented the challenge of how to select successfully edited cells in downstream analyses. This is a widely recognised difficulty in the implementation of CRISPR/Cas9-editing in primary human and mouse cells (Schumann *et al*, 2015). For cell surface targets, flow cytometry allows the separation of knock out cells upon analysis, and can also be used for flow cytometry-assisted cell sorting before biochemical analyses. In the current work, a multiplex editing strategy was used to solve the selection issue. This involved simultaneous Cas9-mediated disruption of *Thy1* with target genes, leading to the loss of CD90 surface expression on knock out cells. This study also confirmed by sequencing and TIDE analysis the assumption that CD90 knock out correlated with editing at the second target locus, thus demonstrating the validity of this selection method. Thus, this strategy allowed for the enrichment of $CD90^-$ knock out cells for biochemical analysis using anti-CD90-conjugated magnetic bead-mediated depletion of $CD90^+$ cells. It also enabled selection of $CD90^-$ cells, and comparison with $CD90^+$ cells, following flow cytometric analysis.

There were, however, two caveats associated with this approach. Firstly, sequencing and TIDE analysis of $CD90^-$-enriched cells revealed that the extent of target gene disruption within this population did not reach the same frequency as *Thy1* editing. The maximum observed editing of *Pik3ap1*, for example, was ~50 % within $CD90^-$-enriched cell populations. While this could, at most, reflect a ~100 % heterozygous BCAP knock out population, it is more likely that the population was heterogenous, with homozygous and heterozygous knock out cells. Thus, in the experiments presented in this study, selection or enrichment of $CD90^-$ cells did not necessarily equate to selection of BCAP, ICOS or p110δ knock out cells. Therefore, knockout phenotypes could have been masked by the presence of unedited or heterozygous cells within the $CD90^-$ population. In this respect, it is remarkable that functional impacts were observed in *ICOS*- and *Pik3cd*-edited $CD90^-$ cells in experiments where the editing efficiencies at the *ICOS* and *Pik3cd* loci, respectively, were estimated to be relatively low. There are two possible explanations for this: either, sequencing combined with TIDE analysis underestimated the extent of editing, or, even a partial deficiency in p110δ or ICOS has a detectable effect on T cell signalling. TIDE analysis has been shown to estimate indels similarly to next generation sequencing (Sentmanat *et al*, 2018) and is limited mainly by the quality of Sanger sequencing traces that can be

obtained for the target locus. Thus, the latter explanation may be likely. Further optimisation to the RNP nucleofection protocol in future experiments may lead to higher editing efficiency of *ICOS*, *Pik3ap1, Pik3cd* and *Thy1,* and this may bring the editing frequency of each target to equivalent levels. In this scenario, $CD90^-$ cells would represent a homogenous population of double knock outs and knock out phenotypes would not be diluted. Ideally, a highly efficient level of editing would remove the need for a method of selection.

The second caveat associated with the *Thy1* multiplex editing approach was only revealed upon the analysis of cytokine production in T blasts by flow cytometry. In these experiments, $CD90^-$ cells demonstrated slightly different levels of cytokine production than $CD90^+$ cells. Intriguingly, compared with $CD90^+$ cells, TNFα production and the proportion of TNFα-IFNγ double producers was higher in $CD90^-$ $CD4^+$ populations, but lower in $CD90^-$ $CD8^+$ populations. This suggests that loss of CD90 influences cytokine production in an inverse manner in $CD4^+$ and $CD8^+$ T cells. CD90 is a GPI-anchored protein highly expressed on the T cell surface, with a somewhat enigmatic role in cell adhesion and signalling. Its inherent lateral mobility between plasma membrane lipid domains has led to the hypothesis that it may influence the localisation of membrane-associated proteins (Barker & Hagood, 2009). In this respect, loss of CD90 could impair or augment TCR signalling by altering the trafficking or partitioning of molecules such as the TCR itself, or SFKs via their palmitoylated residues (Shenoy-Scaria *et al*, 1993). In any case, the observed effect of CD90 knock out in the experiments presented herein necessitated that multiplex-edited $CD90^-$ cells be compared with *Thy1*-only knock out $CD90^-$ cells as a control.

Biochemical analysis of PI3K-AKT signalling upon TCR stimulation in the knock out T blasts generated in this work revealed trends for reduced AKT phosphorylation upon loss of BCAP, ICOS or p110δ. Phosphorylation of AKT was reduced by up to 50 % in total T blast populations exhibiting 50 % knock out of *Pik3ap1*, encoding BCAP. Phosphorylation of AKT was reduced by up to 25 % in total T blast populations exhibiting lower editing frequency of *ICOS*. In populations with seemingly low editing of *Pik3cd*, encoding p110δ, up to a 40 % reduction in AKT phosphorylation was observed. Due to variable CRISPR/Cas9 editing efficiency, it was necessary to correlate observed phenotypes with the extent of target gene disruption in the population of cells analysed. It was generally consistent that higher gene disruption led to greater reduction in PI3K-AKT signalling, which adds confidence to the interpretation of the phenotypes as being resultant of loss-of-function editing of the specific target. It also supports the conclusion that BCAP and ICOS are positive regulators of PI3K signalling. Thus, BCAP may play an analogous role

to that in B cells, serving as a PI3K adaptor recruiting p110δ to the TCR in activated T cells. ICOS may also act as a PI3K adaptor in the absence of ICOS ligation, upon TCR and CD4/CD8 crosslinking.

Analysis of PI3K-AKT signalling in the presence of p110δ-specific pharmacological inhibition revealed an interesting adaptation in *Pik3cd* knock out T blasts. TCR stimulation induced p110δ-independent phosphorylation of AKT in these cells, which accounted for 50 % of the pAKT induced. This suggests that another PI3K isoform, possibly p110α, substituted for p110δ in *Pik3cd*-edited T blasts. Interestingly, a similar phenotype was observed when investigating cytokine production upon TCR stimulation. *Pik3cd* knock out $CD4^+$ cells, and to an extent $CD8^+$ cells, exhibited a higher proportion of p110δ-independent TNFα production, suggesting that another isoform may have compensated for its loss. It was also clear from these experiments that TNFα production in T blasts is not completely sensitive to p110δ inhibition. The p110δ-specific inhibitor CAL101 reduced TNFα production by approximately 20 % and 40 % in $CD8^+$ and $CD4^+$ cells, respectively. This suggests that measuring cytokine production is perhaps not a robust assay to study the effect of protein knock out on p110δ-mediated signalling in activated T cells. Indeed, the effects of *Pik3ap1*, *ICOS* or *Pik3cd* knock out on cytokine production that were observed in this study were very small. This would have been exacerbated by the extent of gene editing, and consequently the proportion of knock out cells, within the populations studied. Thus, robust conclusions could not be drawn from the results. Nevertheless, there was evidence to suggest that BCAP and ICOS play a role in regulating cytokine production in T blasts, but this may differ in $CD8^+$ and $CD4^+$ cells. This would correspond with their proposed function as adaptor proteins for PI3K at the TCR signalosome. Further experiments are required to test this hypothesis.

To conclude, this body of work has developed a CRISPR/Cas9-mediated gene editing approach using RNP nucleofection to disrupt proteins of interest in primary mouse activated T cells. Knock out of genes encoding BCAP, ICOS and p110δ allowed interrogation of their functions by biochemical and flow cytometry analyses. The results of these assays, in combination with analyses of CRISPR/Cas9 editing efficiency, strongly suggest that improvements to knock out efficiency will reveal robust knock out phenotypes in future experiments. Optimising gene editing efficiency would also likely remove the need for a selection marker for knock out cells, and thus abrogate the associated caveats. Nevertheless, this study has demonstrated that multiplex CRISPR-editing can be used to remove a surface marker on edited cells, which can

subsequently enable enrichment or selection for whole-population or single-cell analysis methods, respectively. This CRISPR/Cas9 approach has been used thus far to study the function of BCAP and ICOS in TCR-PI3K signalling in primary T blasts. Following further optimisation, it can be used to target other p110δ-associated proteins that were identified by mass spectrometry.

# Chapter 6

# Discussion

A key aim of this study was to identify proteins involved in the recruitment and activation of p110δ upon engagement of the TCR. Using a combination of proteomic, biochemical and gene editing approaches, this work has identified proteins that associate with p110δ in activated $CD4^+$ T cells before and after TCR stimulation and interrogated the roles of two proposed regulators of PI3K activity, BCAP and ICOS.

The physiological relevance of this work is evidenced by its investigation of endogenous proteins in primary murine T lymphocytes throughout. Previous studies of TCR and PI3K signalling using immortalised T cell lines have yielded conflicting results with respect to T cell activation and co-stimulation, in part because they exhibit constitutive PI3K activation (Astoul *et al*, 2001). This can be attributed to the fact that Jurkat T cell lines lack expression of a number of key proteins, including PTEN and SHIP-1 (Gioia *et al*, 2018). Thus, the results of the proteomic analysis herein provide a valuable insight into the molecular events of T cell activation proximal to the TCR. They also shed light on the mechanisms of PI3K activation via the TCR and identify new players in this pathway.

An important aspect of this study was the optimisation of the AviTag affinity purification approach, specifically for the isolation of p110 isoforms from primary lymphocytes following TCR stimulation. This was with the aim to improve the recovery of transient stimulation-dependent PI3K complexes. The technique was subsequently coupled with a quantitative proteomic analysis for the unbiased identification of proteins associated with p110δ in primary $CD4^+$ T cells. Analyses of the proteins identified by mass spectrometry led to the selection of 24 proteins of interest that specifically associated with p110δ. Strikingly, 11 of these proteins were distinctly associated with p110δ in a TCR stimulation-dependent manner, indicating that they may be involved in the regulation of PI3K activity upon TCR engagement. Notably, the successful isolation and identification of such interactors highlights the efficacy of the optimised purification protocol and quantitative proteomic analysis.

## 6.1 The p110δ interactome in activated CD4$^+$ T cells

The majority of the 24 p110δ-associated proteins identified in this study are known to play a role in TCR signal transduction. Moreover, the molecular mechanisms of their recruitment to the TCR signalosome are well studied, albeit not necessarily resolved. Remarkably, many have been found to interact directly with p85 in previous studies, either in primary lymphocytes, Jurkat T cells or *in vitro*, as reviewed in Chapter 3. Thus, it is possible to speculate on the molecular organisation and regulation of the p110δ interactome that was identified herein. The constitutive or TCR stimulation-dependent nature of each association provides invaluable context to the models proposed.

Collectively, the proteomic analysis suggests that p110δ associates with several interconnected protein complexes at the TCR signalosome. One such complex may involve the Gab-family adaptors, GAB2 and GAB3, which are recruited to tyrosine phosphorylated LAT via GRB2 and associate with $PIP_3$ in the plasma membrane (Yamasaki *et al*, 2003). Binding to the GAB YxxM motifs is one plausible mechanism by which PI3K may be simultaneously recruited to the TCR signalosome and activated. The inclusion of the tyrosine phosphatase SHP-2 in this complex, through binding to GAB2, could provide a means to downregulate PI3K activity by disrupting these phosphotyrosine-dependent interactions; this is speculative based on a similar mechanism observed for GAB1:SHP-2 in other cell types (Koncz *et al*, 2001; Zhang *et al*, 2002), but warrants further investigation. Interestingly, GAB2-deficient naïve T cells exhibit increased proliferation in response to anti-CD3 or anti-CD3+anti-CD28 co-stimulation, indicating that GAB2 plays an inhibitory role in TCR stimulation in naïve cells. Further interrogation of the PI3K-AKT pathway in GAB2-deficient activated T cells is required to investigate its role in PI3K regulation.

The p110δ interactome comprised several proteins that interact with CBL, including CBL itself, and thus it is possible that PI3K also forms a complex with CBL upon TCR stimulation. Indeed, CBL is tyrosine phosphorylated at a YxxM motif upon TCR stimulation (Hunter *et al*, 1999). Aside from its E3 ubiquitin ligase activity, the multidomain architecture of CBL suggests that it could act as a scaffolding protein. In this respect, it is intriguing that p110δ was found to be constitutively associated with the CBL interactors CRK, CRKL, CD2AP and SH3KBP1. These proteins could therefore facilitate the association of PI3K with CBL upon TCR stimulation. A further addition to this model is based on the identification of the co-receptor CD5 as a stimulation-dependent p110δ interactor. It has been demonstrated that CBL associates with CD5 upon CD3+CD4 crosslinking in primary murine activated CD4$^+$ T cells (Voisinne *et al*, 2016).

Thus, the proposed CBL:PI3K complex could be localised to the plasma membrane via CD5. Alternatively, CBL:PI3K may be localised to the TCR via the TCR stimulation-dependent CD3ζ:ZAP-70:CBL complex that has been observed in Jurkat T cells (Wang *et al*, 2001). An obvious question is whether the proposed association of p85 with CBL leads to the ubiquitination of PI3K, as observed in other cell types (Dufour *et al*, 2008; Bulut *et al*, 2013). This would indicate another level of regulation of PI3K activity in T cells. Experiments examining the ubiquitination status of p85 and p110δ upon TCR stimulation would be required to investigate this further. Nevertheless, it is interesting that CBL-deficient mature $CD4^+$ T cells exhibit reduced proliferation and ERK activation in response to anti-CD3 stimulation (Naramura *et al*, 2002). It could be that the adaptor function of CBL mediates a positive regulatory role upon TCR stimulation in mature T cells, involving the recruitment and activation of p110δ.

An interesting link between the proposed GAB:PI3K and CBL:PI3K complexes are the proteins CRK and CRKL; the Crk-family SH2 domain can bind to phosphorylated YxxP motifs present in both CBL and GAB2, as well as the tyrosine phosphorylated CD3ζ chain (Reedquist *et al*, 1996; Sármay *et al*, 2006; Dong *et al*, 2017). Moreover, the Crk-family proteins are thought to stabilise the binding of p85 to CBL (Gelkop *et al,* 2001). CRK and CRKL were both constitutively associated with p110δ in the present study, and thus could represent key adaptors that allow recruitment of PI3K to the TCR signalosome upon tyrosine phosphorylation of CBL, GAB2 and CD3ζ.

Proteomic analysis also revealed that p110δ associated with the co-stimulatory receptors ICOS and CD28 upon TCR stimulation, both of which contain YxxM motifs in their cytoplasmic tails. It is intriguing that this association with ICOS and CD28 occurred upon CD3+CD4 crosslinking alone, in the absence of professional antigen-presenting cells that express their natural ligands ICOS-L and B7-1/B7.2, respectively. This suggests that ICOS and CD28 may act as adaptors for PI3K recruitment to the plasma membrane independently of ligation. In support of this, a recent report indicated that p85α associates with ICOS in primary mouse $CD4^+$ T cells upon CD3 crosslinking alone (Pedros *et al*, 2016). One explanation for the apparent 'in trans' TCR-induced recruitment of PI3K to ICOS and CD28 is that, following the clustering of CD3 and CD4 at the cell surface, ICOS and CD28 co-receptors are also co-localised with the TCR and are tyrosine phosphorylated at their YxxM motifs, allowing p85 to bind. This may serve to amplify or sustain PI3K activity at the plasma membrane. It would therefore be interesting to examine the

production of $PIP_3$ and phosphorylation of AKT over time following CD3+CD4 crosslinking in ICOS-deficient and CD28-deficient $CD4^+$ T blasts.

One limitation of the proteomic analysis performed herein is that it only provides a snapshot of the p110δ interactome at the 1 minute timepoint following TCR stimulation. An indication of how these proteins regulate PI3K recruitment and activation following TCR stimulation could be obtained via a time-resolved AP-MS analysis. This would uncover the sequence of protein interactions with p110δ and transient patterns of binding, thus revealing the temporal organisation of the p110δ protein network. It would be interesting to see whether tyrosine phosphorylated components of the proposed PI3K:CBL and PI3K:GAB complexes show similar kinetics of assembly with, and disassembly from, p110δ. Furthermore, it was noteworthy that several negative regulatory proteins were found to be associated with p110δ, including CBL and the phosphatases STS-2 and SHP-2. Uncovering the dynamics of their interaction with p110δ could provide an interesting perspective to the membrane proximal events leading to TCR downregulation. Therefore, as part of the present study, p110δ affinity purifications have been performed at several timepoints following TCR stimulation of $CD4^+$ T blasts and, at the time of writing, await analysis by mass spectrometry.

## 6.2 BCAP as an adaptor for PI3K in activated T cells

Perhaps the most surprising adaptor identified as a p110δ-specific interactor in this study was BCAP, due to the fact that it was not previously known to be expressed in T lymphocytes. Further work has demonstrated that BCAP is upregulated in activated $CD4^+$ T cells and is rapidly tyrosine phosphorylated upon TCR stimulation, and this appears to correlate with its association with p85. Thus, BCAP appears to be a key component of the TCR signalling pathway in activated T cells. Based on these results, and the proposed role for BCAP as a PI3K adaptor in B cells (Okada *et al*, 2000; Castello *et al*, 2013), it is likely that BCAP acts as an adaptor for PI3K in activated T cells.

To investigate this hypothesis, this study used a CRISPR/Cas9 gene editing approach to knock out BCAP (*Pik3ap1*) in primary activated murine T cells. Interrogation of PI3K-AKT signalling in *Pik3ap1*-edited cells provided evidence to support the hypothesis that BCAP plays a positive regulatory role in the TCR-induced activation of PI3K in activated T cells. Notably, T blasts with a high level of *Pik3ap1*-gene disruption demonstrated a concomitant reduction in phosphorylated

AKT upon TCR stimulation. However, as discussed previously, further experiments studying T blasts with a consistently high efficiency of BCAP knock out are required to robustly test this hypothesis. Interestingly, at the time of writing, a report was published demonstrating a role for BCAP in the clonal expansion and differentiation of effector and memory $CD8^+$ T cells (Singh *et al*, 2018). Furthermore, *Pik3ap1*$^{-/-}$ activated $CD8^+$ T cells demonstrated reduced phosphorylation of AKT upon stimulation with anti-CD3. This supports the observations and conclusions from the present study that BCAP acts as an adaptor for the recruitment and activation of PI3K in activated T cells upon TCR stimulation.

Nevertheless, the mechanism by which BCAP may recruit p110δ to the TCR signalosome is unclear. Intriguingly, the adaptor NCK1 was identified in the present study as a constitutively-associated p110δ interactor. In B cells, NCK proteins bind to a proline-rich region in BCAP via their SH3 domains and are thought to recruit BCAP to the phosphorylated Igα chain of the BCR upon stimulation (Castello *et al*, 2013). In T cells, NCK is recruited to both the CD3ε chain and SLP-76 upon TCR stimulation (Gil *et al*, 2002; Koretzky *et al*, 2006). Furthermore, NCK-deficient T cells exhibit greatly reduced TCR-induced proliferation (Roy *et al*, 2010). Therefore, this study proposes that NCK1, constitutively associated with PI3K, may facilitate the interaction between p85 and BCAP and subsequently recruit this complex to the CD3ε chain or SLP-76 upon TCR stimulation. Further experiments are required to test this hypothesis. In the first instance, co-immunoprecipitation studies in primary $CD4^+$ T cells could investigate whether these proteins form a complex upon TCR stimulation. Notably, BCAP also contains consensus binding motifs for the SH2 domains of GRB2 (YxNx) and SHP-2 (YxxV) (Songyang *et al*, 1993, 1994). As GRB2 and SHP-2 were also identified in the present p110δ AP-MS study, it would be interesting to examine whether BCAP forms a complex with these proteins upon TCR stimulation.

BCAP is thought to interact with p85 via three phosphorylated YxxM motifs (Okada *et al*, 2000; Inabe & Kurosaki, 2002). BCAP also contains three proline-rich regions, and it is not known if these interact with the SH3 domain of p85. It would be interesting to examine if the BCAP YxxM motifs are tyrosine phosphorylated upon TCR stimulation in activated T cells. Thus, a phosphoproteomic analysis is planned in subsequent work to identify the phosphorylation sites within endogenous BCAP isolated from primary $CD4^+$ T blasts following TCR stimulation. To further elucidate the regulation of BCAP in T cells, it would be necessary to investigate the tyrosine kinases responsible for the rapid tyrosine phosphorylation of BCAP downstream of the TCR; LCK, FYN and ZAP-70 are potential candidates. Experiments examining BCAP tyrosine

phosphorylation in the presence Src-family- and ZAP-70-selective kinase inhibitors could be performed for this purpose.

## 6.3 TCR-PI3K signalling in activated T cells

It is noteworthy that two of the TCR stimulation-induced p110δ interactors identified in this study, BCAP and ICOS, are only expressed in activated T cells. ICOS is not expressed on resting T cells but is rapidly induced in activated T cells following TCR crosslinking (Hutloff *et al*, 1999). Similarly, the present study revealed that BCAP is not expressed in naïve $CD4^+$ T cells but is upregulated in activated $CD4^+$ and $CD8^+$ T cells. This intriguing observation suggests that there may be a rewiring of TCR-induced signalling upon differentiation of effector T cells, which specifically alters the regulation of PI3K activity. Interestingly, ICOS appears to be responsible for the recruitment of the p50α PI3K regulatory subunit to the immune synapse in activated cells; the p50α isoform does not appear to be recruited to the immune synapse in resting cells (Fos *et al*, 2008). p50α has been associated with higher p110 lipid kinase activity than other p85 isoforms (Inukai *et al*, 2001). Nevertheless, ICOS also recruits p85α (Gigoux *et al*, 2009; Pedros *et al*, 2016). Thus, ICOS expression in activated T cells may serve to induce a higher level of PI3K activity upon TCR stimulation. In light of the results of the present proteomic study, this could occur independently of ICOS ligation. The consequence of BCAP upregulation in activated T cells is unclear. It may simply serve to provide an additional means of PI3K recruitment to the TCR. Collectively, this rewiring of the TCR-PI3K pathway may be responsible for the lower threshold of activation exhibited by activated T cells, by reducing the number of TCRs required to be engaged by peptide-MHC for PI3K-AKT pathway activation (Chandok & Farber, 2004).

The pertinent question, therefore, is whether p110δ is recruited to the TCR in naïve T cells via the same complexes and mechanisms proposed here in activated T cells. To answer this, it would be necessary to investigate the p110δ interactome downstream of the TCR in naïve T cells. To this end, the AviTag AP-MS approach used in this work to study p110δ in $CD4^+$ T blasts has been applied to the isolation and identification of p110δ complexes from naïve $CD4^+$ T cells. At the time of writing, this experiment requires further analysis. The results of this investigation will provide further invaluable insight into the p110δ interactome, as well as the regulation of PI3K activity upon TCR stimulation in naïve T cells. Moreover, comparison with the p110δ interactome in $CD4^+$ T blasts may uncover changes in the mechanisms of TCR-PI3K signalling upon $CD4^+$ T cell differentiation.

Taken as a whole, the proteomic analysis performed herein suggests that, in activated T cells, no single adaptor is essential for PI3K recruitment and activation. Instead, it is possible that the adaptors identified perform redundant roles. Physiologically, this would provide a means for both the amplification and maintenance of TCR-induced PI3K signalling; several YxxM motif-containing proteins could recruit multiple p110δ heterodimers to its substrate $PIP_2$ and collectively sustain PI3K localisation and activation at the membrane. This would allow previously activated effector T cells to initiate a rapid and robust response to antigen recognition via the TCR.

Intrinsic to this model is that loss of only one adaptor at the TCR signalosome may not affect the recruitment or activation of PI3K. This presents a difficulty for the investigation of the functional importance the p110δ-associated proteins identified in this study. Nevertheless, it is important to systematically assess the contribution of each protein to PI3K signalling in primary $CD4^+$ T cells. In addition, since several of their reported interactions with p85 have only been demonstrated *in vitro* or in Jurkat T cells, it would be important to validate these in primary cells, in the context of CD3+CD4 crosslinking. To this end, this study used a CRISPR/Cas9-mediated gene editing approach to knock out the p110δ-asscociated proteins BCAP and ICOS in primary T blasts and interrogate their role in PI3K-AKT signalling. A CRISPR/Cas9 approach was chosen for several reasons, including the number of target proteins to be investigated and the availability of relevant knock out mouse models. In relation to the latter, studying the consequences of constitutive gene deletion in mice also has clear limitations, as cellular mechanisms are likely to adapt and compensate for the absence of the gene product. Furthermore, the loss of a protein that is important for TCR-PI3K signalling could block the development of mature lymphocytes or alter the expression of proteins during development that subsequently impacts the signalling pathways in mature cells (Saveliev & Tybulewicz, 2009). Conditional deletion of the genes in mature T cells would alleviate some of these limitations. CRISPR/Cas9 editing via RNP nucleofection goes a step further as it allows for the study of protein loss at a specific stage of T cell activation or differentiation. In the present study, wild type cells were activated for two days prior to gene knock out, thus allowing the interrogation of TCR-induced PI3K signalling in the absence of BCAP or ICOS specifically in activated T cells. This was a highly appropriate model, as these proteins are expressed only in activated T cells.

Nevertheless, as previously discussed, it would be desirable to study the interactome of PI3K in naïve T cells in future experiments. To interrogate the roles of identified interaction partners in

naïve cells would require either conditional deletion in mature T cells or application of CRISPR/Cas9 gene editing to non-activated naïve T cells. However, primary murine naïve T cells die within 48 hours in the absence of TCR stimulation *in vitro*, within the time that would be required for Cas9 editing (Vella *et al*, 1997). Interestingly, CRISPR/Cas9-mediated gene knock out has recently been achieved in non-activated naïve murine T cells that were maintained in the presence of the cytokine IL-7 (Seki & Rutz, 2018). This approach could be applied in future studies interrogating the recruitment and activation of p110δ downstream of the TCR in naïve T cells.

This study has shown that CRISPR/Cas9 can be used successfully for multiplex gene editing in primary T cells. In this case, it was used to incorporate a selection marker via simultaneous knock out of CD90. The real power of multiplex editing, however, lies in the capability to knock out multiple genes of interest. Proteomic analysis of the p110δ interactome suggests that several adaptor proteins may perform redundant roles in the recruitment and activation of p110δ upon TCR stimulation. Thus, it would be interesting to knock out several p110δ-associated adaptors and examine the effect on the PI3K-AKT pathway. For example, combined loss of NCK1 and BCAP, or CRK and GAB2, may reveal the key complexes that are required for p110δ regulation.

## 6.4 The role of p110α in mature T cells

The work presented herein has led to the identification of proteins that may regulate p110δ recruitment and activation upon TCR engagement. However, it remains poorly understood why p110δ is the dominant class IA isoform activated downstream of the TCR. Phosphorylation of AKT and production of $PIP_3$ following TCR stimulation are dependent on the kinase activity of p110δ (Okkenhaug *et al*, 2002; Stark *et al*, 2018). This is despite the fact that p110α heterodimers are also present in T cells, as shown in this study. Furthermore, p110α possesses a higher intrinsic specific activity than p110δ (Meier *et al*, 2004). One hypothesis that could explain the dominance of p110δ in mature T cells is that p110δ is preferentially recruited or activated by the TCR signalosome. To test this, it would be necessary to identify the proteins associated with p110α in T cells upon TCR stimulation. This could reveal whether p110α is also recruited to the TCR or if it is sequestered elsewhere in the cell. In support of the latter, p110α was not identified with p110δ complexes in the proteomic analysis carried out in this study. Earlier experiments demonstrated that p110α can be efficiently purified from primary T

lymphocytes using the AviTag AP approach. Thus, it would be possible to perform a quantitative proteomic analysis of the p110α interactome in primary T cells. Furthermore, the 10-plex nature of the TMT-labelling approach would allow for a high-throughput quantitative comparison of p110δ and p110α affinity purifications, thus enabling the identification of isoform-specific interaction partners.

An interesting observation was made during this study following the CRISPR/Cas9-mediated disruption of *Pik3cd*, encoding p110δ, in activated T cells. *Pik3cd*-edited cell populations exhibited p110δ-independent phosphorylation of AKT upon TCR stimulation, whereas phosphorylation of AKT was almost completely p110δ-dependent in *Pik3cd*-unedited cells. Given that the efficiency of *Pik3cd* knock out was low, it was assumed that a heterogenous population of wild type and p110δ-deficient cells were present within the cell populations stimulated. Therefore, in the presence of a p110δ-selective inhibitor, it was likely that the p110δ-deficient cells were the source of the phosphorylated AKT detected. These experiments suggest that another PI3K p110 isoform is able to compensate for the loss of p110δ in activated T cells. To test this hypothesis, isoform-selective inhibitors targeting p110α, p110β and p110γ could be used to examine the isoform-dependency of PI3K-AKT signalling in *Pik3cd*-edited cells. Importantly, these experiments should be performed on homogenous *Pik3cd* knock out cell populations.

## 6.5 CRISPR/Cas9 gene editing in primary murine T lymphocytes

To interrogate the TCR-PI3K signalling pathway in primary T cells, this study developed a CRISPR/Cas9-mediated gene editing approach to knock out proteins of interest in primary mouse activated T cells. This work demonstrated that RNP nucleofection is a viable delivery method to introduce Cas9 protein and gRNA into activated T cells and allows for efficient target gene disruption. Of note, this is the first demonstration of successful RNP nucleofection and editing of total non-purified activated murine T cells. The application of this approach to the targeted knock out of BCAP, ICOS and p110δ revealed both the power of the technique and the associated caveats, as discussed in Chapter 5. Overall, there are three main aspects of the strategy that require further optimisation: efficiency, selection, and the phenotypic assay.

The efficiency of CRISPR/Cas9 gene editing will likely be improved via further optimisation of the RNP nucleofection protocol. The aim of this would be to achieve near complete gene knock out

within a cell population, such that the requirement for a method of selection is eliminated. However, if high efficiency editing cannot be reached for a particular intracellular target it would be necessary to select for knock out cells. This study has demonstrated that simultaneous knock out of a cell surface marker enables the enrichment or selection of edited cells for whole-population or single-cell analysis, respectively. Although, as observed following knock out of CD90, loss of the marker can generate a phenotypic effect. Alternative strategies for knock out selection include the use of fluorescently-labelled tracrRNA that can be detected by flow cytometry (Kornete *et al*, 2018). However, there are two main disadvantages to this method. First, cells may incorporate tracrRNA independently of Cas9. Second, selection of tracrRNA-positive cells would be required within the half-life of the RNA. This would involve cell sorting shortly after electroporation, which may reduce cell viability by subjecting cells to additional stress before expansion.

An alternative selection approach makes use of Cas9-transgenic mice, which also overcomes the requirement of Cas9 protein delivery by electroporation (Platt *et al*, 2014; Chu *et al*, 2016). Inducible Cas9-transgenic mice are a valuable development as they reduce the risk of off-target gene editing that is associated with constitutive Cas9 expression (Katigbak *et al*, 2018). In this system, expression of Cas9 and GFP from the same genetic locus can be temporally controlled in primary cells *in vitro* by administration of doxycycline. Primary T cells expressing Cas9 and GFP would likely exhibit a higher efficiency of gene editing, due to consistent levels of Cas9 protein in all cells, and also provide a means of knock out selection, contingent upon efficient gRNA delivery (Harrison *et al*, 2014; Chu *et al*, 2016). The disadvantage is the exposure of primary T cells to the cytotoxicity of doxycycline, and the requirement for transgenic animals (Ermak *et al*, 2003). Nevertheless, primary T cells from inducible Cas9-mice could be considered for future CRISPR/Cas9 knock out experiments.

Due to variable CRISPR/Cas9 editing efficiency achieved in this study, it was necessary to correlate observed knock out phenotypes with the extent of target gene disruption in the population of cells analysed. While this provided meaningful insight, it illustrated the fact that heterogenous knock out populations are not compatible with whole-population analyses such as immunoblotting. It would be more appropriate to measure phosphorylated AKT (pAKT) in a heterogenous population using a quantitative single-cell approach, such as intracellular flow cytometry. Indeed, this was tested as part of this study. However, only weak fluorescence intensity for pAKT was observed in the experiments conducted, which limited the ability to

detect differences between genotypes. This could be due to a combination of factors, including loss of phosphorylation or fluorescence during processing, non-specific binding of the fluorescently-conjugated pAKT antibody, and the higher autofluorescence of blasted T cells. Thus, this technique requires further optimisation to enable the analysis of edited T blasts. Nevertheless, the detection of pAKT by immunoblotting is a sensitive, specific and reliable assay, and a robust approach to indirectly measure p110δ activity. Thus, it could be used in future experiments to interrogate TCR-PI3K signalling in homogenous knock out populations.

## 6.6 Conclusion

This work has optimised the AviTag AP system for the isolation of endogenous p110 isoforms from primary murine lymphocytes and subsequently employed a quantitative mass spectrometry-based proteomics approach to identify endogenous proteins that interact with p110δ in primary activated $CD4^+$ T cells. This analysis has identified multiple adaptor proteins and co-stimulatory receptors that may regulate p110δ activity at the TCR signalosome, including the adaptor BCAP. Biochemical analyses revealed that BCAP is upregulated in activated T cells and rapidly tyrosine phosphorylated upon TCR stimulation. Collectively, this work suggests that BCAP is a key adaptor for PI3K downstream of the TCR, specifically in activated T cells.

This study has also developed a CRISPR/Cas9-mediated gene editing approach to disrupt targets of interest in primary murine activated T cells via ribonucleoprotein (RNP) nucleofection. This system was used to investigate the roles of BCAP and ICOS in TCR-induced PI3K signalling and cytokine production in activated T cells. Collectively, this work has demonstrated that AP-MS coupled with CRISPR/Cas9 is a powerful system for the identification and interrogation of signalling pathway components in primary T lymphocytes.

Using this approach, this work has shed light on the previously ambiguous mechanisms of p110δ recruitment and activation downstream of the TCR. The p110δ-associated proteins that have been identified require further biochemical and genetic analysis to uncover the molecular mechanisms of TCR-PI3K signalling.

# Chapter 7

# Materials and methods

## 7.1 Mice

p110δ$^{Avi/Avi}$, BirA$^{+/+}$ and p110α$^{Avi/WT}$BirA$^{+/-}$ C57BL/6J mice were a generous gift from T Chessa, L Stephens and P Hawkins (Inositol Laboratory, Babraham Institute). These mice were housed under specific pathogen-free conditions within the Babraham Institute Biological Services Unit and genotyping was performed by Transnetyx (Cordova, TN). Wild type C57BL/6J mice used for experiments in Chapter 5 were purchased from The Jackson Laboratory and housed at the Cancer Research UK Cambridge Institute Biological Resources Unit. All transgenic mice and wild type mice were culled when aged 8 - 12 weeks according to Schedule 1 procedures.

## 7.2 Purification of naïve T cells

Axillary, brachial, mesenteric and inguinal lymph nodes were isolated from mice and homogenised in ice-cold MACS buffer (MB; calcium and magnesium free 1X PBS (in-house), 0.5 % BSA (Sigma #A7906), 2 mM EDTA (Invitrogen #AM9261) by passing through 40 µm cell strainers (BD Biosciences) using a syringe plunge. Cells were washed once by centrifugation at 400 × g for 5 minutes at 4°C and counted using the CASY cell counter (Scharfe Systems). Cells were resuspended in 1 ml of a FITC-conjugated antibody cocktail (anti-MHCII I-A$^b$, anti-CD25, anti-CD19, anti-CD49b, anti-CD69, anti-B220 and anti-CD11b, with addition of anti-CD8a for the purification of CD4$^+$ cells; all at 1:500 dilution in MB; see Table 7.1 for antibody details) per $10^8$ cells and incubated on ice for 30 minutes in the dark. Cells were washed in ice-cold MB and resuspended in 90 µl MB and 10 µl anti-FITC microbeads (Miltenyi Biotec #130-048-701) per $10^7$ cells followed by incubation at 4°C for 15 minutes. Cells were washed in ice-cold MB and naïve T cells were isolated by negative selection using LS magnetic columns (Miltenyi Biotec #130-042-401) according to the manufacturer's instructions and collected in ice-cold MB. Purity of the cells was confirmed by flow cytometry as greater than 85 %.

| Specificity | Clone | Supplier | Catalogue Number |
|---|---|---|---|
| MHCII I-$A^b$ | AF6-120.1 | BD Biosciences | 553551 |
| CD25 | PC61 | BioLegend | 102006 |
| CD19 | 6D5 | BioLegend | 115506 |
| CD49b | DX5 | BioLegend | 108906 |
| CD69 | H1.2F3 | BioLegend | 104506 |
| B220 | RA3-6B2 | BioLegend | 103206 |
| CD11b | M1/70 | BioLegend | 101205 |
| CD8a | 53-6.7 | BioLegend | 100706 |

**Table 7.1 Antibodies used for T cell purification**

## 7.3 Activation and expansion of primary T cells *in vitro*

Axillary, brachial, mesenteric and inguinal lymph nodes were isolated from mice and homogenised in ice-cold MB by passing through 40 µm cell strainers (BD Biosciences) using a syringe plunge. Cells were washed once by centrifugation at 400 × g for 5 minutes at 4°C and counted using the CASY cell counter (Scharfe Systems). Cells were resuspended at $5 \times 10^6$ cells/ml in 5 % RPMI media (RMPI 1640 + L-glutamine (Life Technologies #21875-034), 5 % heat inactivated FBS (Labtech #FBS-SA-10454/500), 100 U/ml penicillin-streptomycin (Life Technologies #15140-122), 50 µM β-mercaptoethanol (Life Technologies #31350-010)) containing 1 ug/ml anti-CD3 (145-2C11; in-house) and incubated in 6-well plates (Thermo Scientific #140685) at 37°C and 5 % $CO_2$ for 48 hours. Cells were then pooled, collected by centrifugation at 400 × g for 5 minutes at 37°C and resuspended at $0.5 \times 10^6$ cells/ml in 5 % RPMI media containing 20 ng/ml recombinant human IL-2 (rhIL-2; PeproTech #200-02). Cells were incubated in upright 75 or 175 $cm^2$ flasks (Thermo Scientific #156499, #159910) at 37°C and 5 % $CO_2$ for 5 days, with supplementation of rhIL-2 and media every 2 days to maintain a cell concentration of $1 \times 10^6$ cells/ml.

## 7.4 Purification of activated T cells (T blasts)

T blasts from *in vitro* culture were pooled in 50 ml falcons by centrifugation at 400 × g for 5 minutes, resuspended in 5 % RPMI and counted using the CASY cell counter (Scharfe Systems). Cells were pelleted once more and resuspended in 1 ml of a FITC-conjugated antibody cocktail (anti-I-$A^b$ (MHCII), anti-CD19 and anti-CD49b, with addition of anti-CD8a for the purification of $CD4^+$ cells; all at 1:500 dilution in MB; see Table 7.1) per $10^8$ cells and incubated on ice for 30 minutes in the dark. Cells were washed in ice-cold MB and then resuspended in 90 µl MB and 10 µl anti-FITC microbeads (Miltenyi Biotec #130-048-701) per $10^7$ cells followed by incubation at

4°C for 15 minutes. Cells were washed in ice-cold MB and T blasts were isolated by negative selection using LS magnetic columns (Miltenyi Biotec #130-042-401) according to the manufacturer's instructions and collected in ice-cold MB.

To enrich for $CD90^-$ cells following CRISPR/Cas9 gene editing, T blasts at day 5 post-nucleofection were pooled in 15 ml falcons and counted. Cells were pelleted by centrifugation at 400 × g for 5 minutes and resuspended in 90 µl MB and 10 µl anti-CD90.2 microbeads (Miltenyi Biotec #130-049-101) per $10^7$ cells followed by incubation at 4°C for 15 minutes. Cells were washed in ice-cold MB and then passed through MS magnetic columns (Miltenyi Biotec #130-042-201) according to the manufacturer's instructions, and $CD90^-$-enriched cells were collected in ice-cold MB. The $CD90^+$ fraction was collected by plunging the magnetic columns with 1 ml ice-cold MB.

## 7.5 TCR stimulation *in vitro*

Following purification of naïve T cells or T blasts, cells were resuspended at 4 x $10^6$ cells/ml in 0.5 % RPMI (RMPI 1640 + L-glutamine, 0.5 % heat inactivated FBS, 100 U/ml penicillin-streptomycin, 50 µM β-mercaptoethanol) and rested for 75 minutes at 37°C. For experiments involving pharmacological inhibition of p110δ, the media was supplemented with 200 nM DMSO (Sigma #D8418) or CAL101 (AstraZeneca, in-house). Cells were collected by centrifugation at 400 × g for 5 minutes and then incubated at 2 × $10^7$ cells/ml in 0.5 % RPMI containing 4 µg/ml anti-CD3 (145-2C11; BioLegend #100314) and 4 µg/ml anti-CD4 (RM4.5; BioLegend #100520) for 30 minutes on ice. For some experiments, anti-CD28 (37.51; BioLegend #102112) or anti-CD8a (53-6.7; BioLegend #100716), and DMSO or CAL101, were also included, as indicated in accompanying figure legends. Cells were then washed by centrifugation at 400 × g and resuspended in ice-cold 0.5 % RPMI at 2 × $10^7$ cells/ml. T cells were incubated at 37°C for 2 minutes before addition of 13 µg/ml goat anti-Armenian Hamster IgG (Jackson ImmunoResearch #127-005-099) and further incubation at 37°C for 1 minute, or the times indicated in accompanying figure legends. Cells were immediately centrifuged at 800 × g for 2 minutes at 4°C and then resuspended in ice-cold lysis buffer.

## 7.6 Purification of naïve splenic B cells

Mouse spleens were homogenised in ice-cold MB by passing through 40 µm cell strainers (BD Biosciences) using a syringe plunge. Cells were washed once by centrifugation at 400 × g for 5 minutes at 4°C and red blood cells (RBC) were lysed by incubation with 1 ml RBC lysis buffer

(Sigma-Aldrich #R77570) per spleen for 5 minutes at room temperature. Lysis was quenched with ice-cold MB and cells were collected by centrifugation and counted using the CASY cell counter (Scharfe Systems). Naïve B cells were isolated using a mouse B cell Isolation Kit (Miltenyi Biotec #130-090-862). Briefly, cells were resuspended in 40 µl MB and 10 µl biotin-conjugated antibody cocktail per $10^7$ cells and incubated at 4°C for 5 minutes, followed by addition of 30 µl MB and 20 µl anti-biotin microbeads per $10^7$ cells and further incubation at 4°C for 10 minutes. Naïve B cells were isolated by negative selection using LS magnetic columns (Miltenyi Biotec #130-042-401) according to the manufacturer's instructions and collected in ice-cold MB.

## 7.7 BCR stimulation *in vitro*

Following purification of naïve B cells, cells were resuspended at 4 x $10^6$ cells/ml in 0.5 % RPMI (RMPI 1640 + L-glutamine, 0.5 % heat inactivated FBS, 100 U/ml penicillin-streptomycin, 50 µM β-mercaptoethanol) and rested for 75 minutes at 37°C. Cells were collected by centrifugation at 400 × g for 5 minutes and then incubated at 2 × $10^7$ cells/ml in 0.5 % RPMI containing 50 µg/mL goat anti-mouse IgM $(F(ab')_2$ fragment; Jackson ImmunoResearch #115-036-075) for 30 minutes on ice. B cells were stimulated by incubation at 37°C for 2.5 minutes, or the times indicated in accompanying figure legends. Cells were immediately centrifuged at 800 × g for 2 minutes at 4°C and then resuspended in ice-cold lysis buffer.

## 7.8 Lysis buffers and cell lysis

For experiments shown in Figures 2.2 – 2.6, lymphocytes were lysed in 'standard' recipe lysis buffer, comprising 1 % IGEPAL CA-630 (Sigma #I8896), 50 mM HEPES, 150 mM NaCl, 5 mM EDTA, 10 mM NaF, 10 mM Iodoacetamide and 5 mM Proteoloc Protease Inhibitor Cocktail (Expedeon Ltd). Protease inhibitor cocktail was added to the lysis buffer immediately before use. Cells were resuspended in 50 µl (Figure 2.2) or 500 µl (Figures 2.3 – 2.6) ice-cold lysis buffer and lysed on ice for 10 minutes. Insoluble material was cleared by centrifugation at 17,000 × g for 10 minutes at 4°C.

For all other experiments, lymphocytes were lysed in a 'modified' lysis buffer, comprising 1 % IGEPAL CA-630, 50 mM HEPES, 150 mM NaCl, 1 mM EDTA, 1 mM EGTA, 25 mM NaF, 10 mM Iodoacetamide, 2.5 mM sodium pyrophosphate, 5 mM β-glycerophosphate, 5 mM sodium orthovandate and 5 mM Proteoloc Protease Inhibitor Cocktail (Expedeon Ltd). To prepare activated sodium orthovanadate, a 200 mM solution was adjusted to pH 10 and boiled 3 - 5 times until the solution remained colourless and stabilised at pH 10. Aliquots were then frozen

at -20°C until use. Protease inhibitor and sodium orthovanadate was added to the lysis buffer immediately before use.

For affinity purification experiments, cells were resuspended in 600 µl ice-cold lysis buffer per $10^8$ cells, lysed on ice for 10 minutes and insoluble material was cleared by ultracentrifugation at 96,416 × g for 5 minutes at 4°C. For immunoprecipitation or immunoblotting experiments, cells were resuspended in 100 µl ice-cold lysis buffer per $10^7$ cells, lysed on ice for 10 minutes and cleared by centrifugation at 20,000 × g for 10 minutes at 4°C.

The protein concentration of cell lysates was determined using the Pierce 660 nm Protein Assay Kit (Thermo Scientific #22662) according to the manufacturer's Microplate Procedure instructions. Briefly, 10 µl of lysate and pre-diluted BSA Protein Assay Standards were incubated with 150 µl of Protein Assay reagent for 5 minutes at room temperature and the absorbance was measured at 660 nm using a FLUOstar Omega plate reader (BMG Labtech). Protein concentration was determined using a standard curve of the blank-corrected absorbances for each BSA standard.

## 7.9 Affinity purification

Streptavidin-conjugated paramagnetic beads (Dynabeads M-280 Streptavidin; Invitrogen #11205D) were prepared by washing three times in ice-cold lysis buffer using the DynaMag-2 magnetic rack (Invitrogen) and then resuspended in an equal volume of lysis buffer on ice.

Fresh lysates from 1 × $10^8$ cells were immediately incubated with 60 µl streptavidin-conjugated beads for 30 minutes on a rotating wheel at 4°C. Beads were then separated using the magnetic rack and 'post' lysates were retrieved. Beads were washed three times with 1 ml ice-cold lysis buffer, each time with five rotations at 4°C and separation using the magnetic rack on ice. Washed beads were then resuspended in 60 µl 1X NuPAGE LDS Sample Buffer (Invitrogen #NP0007) and boiled at 95°C for 5 minutes. Beads were allowed to return to room temperature and were then separated by using the magnetic rack. Eluates were retrieved to low-protein binding Eppendorf microcentrifuge tubes (Sigma #Z666505) and snap frozen in liquid nitrogen.

## 7.10 Immunoprecipitation

To prepare 50 % protein-A-sepharose bead slurry for immunoprecipitation, 0.2 g lyophilised beads (Sigma #P3391) were hydrated in 10 ml 1X PBS for 1.5 hours at room temperature with agitation. Beads were washed once in 10 ml PBS and resuspended in an equal volume of PBS with 0.1 % sodium azide (Sigma #S2002) and stored at 4°C for up to 1 week. Immediately before

use, beads were washed three times in lysis buffer and resuspended in an equal volume of lysis buffer.

Lysates from $1 \times 10^7$ cells were incubated with 2 µl rabbit polyclonal anti-mouse-BCAP (a kind gift from T. Kurosaki) or 10 µl normal rabbit IgG (Cell Signaling Technology #2729) for 45 minutes at 4°C with rotation, followed by addition of 50 µl of 50 % protein-A-sepharose bead slurry and further incubation for 30 minutes at 4°C with rotation. Beads were then washed three times with 450 µl lysis buffer by centrifugation at 12,000 × g for 30 seconds at 4°C. Beads were resuspended in 25 µl 2X NuPage LDS sample buffer (Invitrogen) with 20 mM DTT and proteins were eluted from the beads by boiling at 95 °C for 5 minutes, followed by centrifugation at 13,000 × g for 2 minutes at room temperature. This protocol was scaled appropriately for immunoprecipitation from $2 \times 10^7$ cells.

## 7.11 Immunoblotting via enhanced chemiluminescence (ECL) detection

Immunoblots presented in Figures 2.2 and 2.3 were produced via the ECL method, as follows. Cell lysates were boiled at 70°C for 10 minutes in 1X NuPAGE LDS Sample Buffer (Invitrogen #NP0007) supplemented with 20 mM DTT. NuPAGE 4-12% Bis-Tris Gels (Invitrogen #NP0322BOX) were loaded with 25 µl of each sample and 15 µl of Novex Sharp Pre-stained Protein Standard (Invitrogen #LC5800) and run for 1 hour at 200 V in NuPAGE SDS MOPS Running Buffer (Invitrogen #NP0001) using the XCell SureLock Mini-Cell Electrophoresis System (Invitrogen). Proteins were transferred onto PVDF membranes (Millipore #IPVH00010) in 1X NuPAGE Transfer Buffer (Invitrogen #NP0006-1) containing 20 % methanol and 0.1 % NuPAGE Antioxidant (Invitrogen #NP0005) using the XCell II Blot Module (Invitrogen) for 1 hour at 30 V.

Membranes were blocked for 1 hour with shaking at room temperature in 5 % (w/v) milk in TBST (0.1 % Tween-20, 150 mM NaCl, 50 mM Tris-HCl, pH 7.6). Membranes were rinsed in TBST and incubated with primary antibody according to Table 7.2. Membranes were washed three times with TBST for 10 minutes each and then incubated for 1 hour at room temperature with shaking with either 1:25,000 HRP-conjugated polyclonal goat anti-rabbit IgG (Dako #P0448) or 1:10,000 HRP-conjugated polyclonal goat anti-mouse IgG (Dako #P0448) in 5 % milk in TBST. Membranes were washed three times for 10 minutes each then incubated for 5 minutes in the dark with Immobilon Western Chemiluminescent HRP substrate (Millipore #WBKLS0500) according to the manufacturer's instructions. Membranes were exposed to Amersham

Hyperfilm ECL (GE Healthcare #28-9068-40) and films were developed using a Compact X4 developer (Xograph).

## 7.12 Immunoblotting via near-infrared (NIR) fluorescence detection

Immunoblots, except those in Chapter 2 Figure 2.2 and 2.3, were produced via NIR fluorescence detection, as follows. Cell lysate samples were denatured and reduced in 1X NuPAGE LDS Sample Buffer (Invitrogen #NP0007) with 20 mM DTT at 70°C for 10 minutes. Lysate, AP and IP Samples were subjected to SDS-PAGE, alongside 3 µl Chameleon Duo pre-stained protein ladder (LI-COR #928-60000), on NuPAGE 4-12% Bis-Tris Gels (Invitrogen) at 200 V for 45 – 75 minutes using the XCell SureLock Mini-Cell Electrophoresis System (Invitrogen) with NuPAGE SDS MOPS Running Buffer (Invitrogen #NP0001). Proteins were transferred onto Immobilon-FL PVDF membrane (Millipore #IPFL00010) at 30 V for 65 minutes in 1X NuPAGE Transfer Buffer (Invitrogen #NP0006-1) containing 20 % methanol and 0.1 % NuPAGE Antioxidant (Invitrogen #NP0005) using the XCell II Blot Module (Invitrogen).

Membranes were blocked in 5% BSA (w/v) TBST for 1 hour at room temperature with shaking and then incubated with primary antibody (Table 7.2) in 5% BSA TBST with 0.05 % $NaN_3$ overnight at 4°C. For detection of pAKT and AKT1, membranes were incubated with both primary antibodies simultaneously. Membranes were washed four times over 30 mins in TBST and then incubated with secondary antibody goat anti-rabbit IRDye® 680RD (1:10,000; LI-COR #926-68071) or goat anti-mouse IRDye® 800CW (1:10,000; LI-COR #926-68070) in 5% BSA TBST for 1 hour in the dark at room temperature. For detection of pAKT and AKT1, membranes were incubated with both secondary antibodies simultaneously. Membranes were then washed as before and allowed to dry in the dark at room temperature for 1 hour between Whatman paper. Dry membranes were imaged using an Odyssey® CLx Imaging System (LI-COR) in the 700 nm and 800 nm channels. Membranes were reactivated in 100 % methanol for 10 seconds before further antibody probing.

| Specificity | Raised in | Supplier | Catalogue no. | Diluent | Dilution | Incubation |
|---|---|---|---|---|---|---|
| AviTag | Rabbit pAb | GenScript | A00674 | 5% BSA- PBST | 1:1000 | RT 1.5 h |
| β-actin | Mouse mAb | Santa Cruz | sc-47778 | 5% milk-TBST | 1:400 | RT 1 h |
| GRB2 | Mouse mAb | BD Biosciences | 610112 | 5% BSA-TBST | 1:1000 | 4°C O/N |
| NCK1 | Rabbit mAb | Cell Signaling Technology | 2319S | 5% milk-TBST | 1:1000 | 4°C O/N |
| p110α | Rabbit mAb | Cell Signaling Technology | 4249 | 5% milk-TBST | 1:2000 | 4°C O/N |
| p110δ | Rabbit pAb | Santa Cruz | sc-7176 | 5% BSA-TBST | 1:200 | 4°C O/N |
| Pan-p85 | Rabbit pAb | Millipore | 06-195 | 5% BSA-TBST | 1:2000 | 4°C O/N |
| pAKT (T308) | Rabbit mAb | Cell Signaling Technology | 4056 | 5% BSA-TBST | 1:1000 | 4°C O/N |
| AKT1 | Mouse mAb | Cell Signaling Technology | 2967 | 5% BSA-TBST | 1:1000 | 4°C O/N |
| pTyr | Mouse mAb | Millipore | 05-321 | 5% BSA-TBST | 1:1000 | 4°C O/N |
| BCAP | Rabbit pAb | Gift from T. Kurosaki | | 5% BSA-TBST | 1:2000 | 4°C O/N |

**Table 7.2 Antibodies used for immunoblotting.**
mAb, monoclonal; pAb, polyclonal; RT, room temperature; O/N, overnight; h, hour.

## 7.13 Immunoblot quantification

The signal intensity for pAKT, AKT, p85 and p110δ detected by NIR fluorescence immunoblotting was quantified using Image Studio Lite Version 5.2 software (LI-COR). Rectangles were positioned to encompass each band and the signal was calculated as the total signal less the product of the background and area. The background was computed as the median intensity of pixels above and below the rectangles with a border size of 1 pixel. The pAKT signal was normalised by dividing by the signal for AKT, or β-actin for p85 and p110δ signals, in the same lane. Graphical and statistical analyses were performed in GraphPad Prism version 7 (GraphPad Software, Inc), as detailed in figure legends and the text.

## 7.14 Preparation of peptide samples for mass spectrometry analyses

For the targeted mass spectrometry (MS) analysis of a ~115 kDa protein, 35 µl (one-half) of each denatured affinity purification sample was subjected to SDS-PAGE on a 10-well NuPAGE 4-12% Bis-Tris Gel (Invitrogen #NP0335BOX) alongside 5 µl Chameleon Duo pre-stained protein ladder (LI-COR #928-60000). The gel was run at 200 V for 1 hour in NuPAGE SDS MOPS Running Buffer (Invitrogen #NP0001) and then proteins were visualised with InstantBlue Coomassie Protein Stain (Expedeon #ISB1L). The region encompassing 110 – 120 kDa was excised from the gel using the 100 kDa marker and p110δ protein band as reference.

*The following steps were performed by Katarzyna Wojdyla at the Babraham Institute MS facility.*

For quantitative TMT-based MS analysis, denatured affinity purification samples were subjected to SDS-PAGE on Bolt 10% Bis-Tris Plus Gels (Invitrogen) and run at 160 V in NuPAGE MES SDS running buffer (Invitrogen # NP0002) until samples fully entered the gel. Gels were washed briefly with miliQ water and proteins were visualised with Coomassie dye (Imperial Protein Stain, ThermoFisher Scientific) and excised.

Gel slices for all MS experiments were cut into 1 x 1 mm cubes and transferred to Eppendorf LoBind Protein tubes (Sigma-Aldrich/Merck). Coomassie dye was removed by sequential washes in 150 µl 12.5 mM ammonium bicarbonate (AMBI) and 50 % acetonitrile (ACN) with 20 minutes sonication, repeated until gel pieces turned transparent. Samples were then dehydrated with 150 µl 100 % ACN for 10 minutes with sonication. After removing ACN, gel pieces were rehydrated in reduction buffer (10 mM DTT in 25 mM AMBI) and incubated for 60 minutes at 50°C. Reduction buffer was removed and gel pieces were incubated with an equal volume of alkylation buffer (50 mM iodoacetamide in 25 mM AMBI) for 60 min at room temperature with shaking in the dark. Reduced and alkylated samples were washed with 150 µl 25 mM AMBI followed by dehydration with 150 µl 100 % ACN and 10 minutes sonication, repeated twice. ACN was then removed and samples dried in a vacuum centrifuge. Finally, gel pieces were rehydrated for 15 - 20 min at room temperature with trypsin solution (10 ng/µl trypsin in 50 mM triethylammonium bicarbonate (TEAB) with 0.1% octylglucoside) before addition of further TEAB to a total volume of 50 µl for overnight digestion at 30°C.

For in-gel tandem mass tag (TMT) labelling, TMT-10 plex tags (ThermoFisher Scientific #90110) were brought to room temperature and each 0.2 mg TMT aliquot was resuspended in 20 µl 100 % ACN and added to individual digested samples. Peptides were labelled for 1 hour at room temperature with sonication and vortexing every 15 minutes. Labelling was quenched with 0.3 % hydroxylamine for 30 minutes at room temperature with sonication. TMT-labelled peptides were extracted from gel pieces with 100 % ACN in a series of 3 washes consisting of 25 µl 100 % ACN and 10 minutes sonication per wash. Final extracts from all samples were combined in 1:1 ratio and dried in a vacuum centrifuge. The dried sample (containing 10 TMT-labelled samples) was resuspended in 16 µl 0.2 % $NH_3$ for high pH reverse phase fractionation on the UltiMate 3000 system (ThermoFisher Scientific). An in-house made microcolumn (0.53 x 200 mm packed with ReproSil-Pur C18-AQ resin, 3 µm particle size (Dr. Maisch, Germany) was used for peptide separation at 20 µl/min using linear gradient 0 - 40% ACN over 30 minutes. Eluted peptides were manually collected into 1-minute fractions and stored at -80°C until further use.

## 7.15 nLC-MS/MS analysis of TMT-labelled samples

*The following analyses were performed by Katarzyna Wojdyla and David Oxley at the Babraham Institute MS facility.*

Peptide-enriched fractions were analysed by nano-liquid chromatography-tandem mass spectrometry (nLC-MS/MS) using an EASY-nLC System (ThermoFisher Scientific) interfaced via a nano-electrospray ion source onto a Q Exactive Plus hybrid Quadrupole-Orbitrap mass spectrometer (ThermoFisher Scientific). An in-house made pre-column (100 µm ID fritted fused silica packed with POROS 20 R2 reversed-phase resin) and analytical column (75 µm ID x 15 cm fused silica capillary with integrated emitter (New Objective) packed with ReproSil-Pur C18-AQ resin (2.1 µm; Dr. Maisch, Germany)) were used for peptide separation. Half of each fraction was used. Samples were loaded onto the pre-column in solvent A (0.1 % formic acid) at a flow rate corresponding to 60 bar. Peptides were then separated over the analytical column at a flow rate of 300 nl/min using a linear gradient from 5 – 35 % solvent B (100 % ACN) over 60 - 90 minutes. Eluted peptides were ionised by applying a 1.6 - 1.7 kV voltage and introduced to the mass spectrometer as gas-phase ions. MS1 scans were only triggered when a threshold of 3e6 ions or 50 ms was reached and were acquired in the Orbitrap mass analyser with a mass resolution of 70,000 and a scan range of m/z 350-1800. The 12 most intense ions from each MS1 spectrum were isolated in the quadrupole mass analyser using a 1.2 m/z window and fragmented using higher-energy collisional dissociation (HCD) with normalised collision energy (NCE) of 30 and 35. MS2 scans of fragment ions were only triggered when a threshold of 5e4 ions or 500 ms was reached and were acquired in the Orbitrap mass analyser with a mass resolution of 35,000 and mass range starting at 100 m/z. Fragmented ions were excluded from repeated analysis for 30 seconds. MS and MS2 spectra were recorded in Xcalibur 3.0 (ThermoFisher Scientific).

Raw MS data were processed in Proteome Discoverer 2.1 (ThermoFisher Scientific). First, raw data from all the fractions were combined and searched against the mouse UniProt database (52026 entries) and Global Proteome Machine database of common contaminants (57 entries) using Mascot search engine. Trypsin was set as the specific protease with a maximum of two missed cleavage sites allowed. Peptide mass tolerance was set to 10 ppm and fragment mass tolerance was set to 20 mmu. Carbamidomethylation of cysteine and TMT modification of the peptide N-terminus and lysine side chains were set as fixed modifications. Oxidation of methionine was set as a variable modification. Only high confidence peptides were used, with a 0.01 target peptide

FDR, and a minimum of 1 unique peptide was required for successful protein identification. Reporter ion intensities were extracted from MS2 spectra that exceeded an average reporter signal-to-noise threshold of 10 with a co-isolation interference lower than 50%. Reporter ion intensities were normalised to the total peptide amount per channel within Proteome Discoverer 2.1.

## 7.16 nLC-MS/MS analysis of gel slice samples

*The following analyses were performed by Katarzyna Wojdyla and David Oxley at the Babraham Institute MS facility.*

Peptides extracted from the 110 – 120 kDa gel slice were analysed by nano-liquid chromatography-tandem mass spectrometry (nLC-MS/MS) using the UltiMate 3000 liquid chromatography system system (ThermoFisher Scientific) interfaced via a nano-electrospray ion source onto a Q Exactive Plus hybrid Quadrupole-Orbitrap mass spectrometer (ThermoFisher Scientific). An in-house made pre-column (100 µm ID fritted fused silica packed with POROS 20 R2 reversed-phase resin) and analytical column (75 µm ID x 15 cm fused silica capillary with integrated emitter (New Objective) packed with ReproSil-Pur C18-AQ resin (2.1 µm; Dr. Maisch, Germany)) were used for peptide separation. Samples were loaded onto the pre-column in solvent A (0.1 % formic acid) at a flow rate of 6 µl/min and then separated over the analytical column at a flow rate of 250 nl/min using a linear gradient from 0 – 40 % solvent B (100 % ACN) over 30 minutes. Eluted peptides were ionised by applying a 1.8 kV voltage and introduced to the mass spectrometer as gas-phase ions. MS1 scans were only triggered when a threshold of 3e6 ions or 100 ms was reached and were acquired in the Orbitrap mass analyser with a mass resolution of 70,000 and a scan range of m/z 350-1800. The 10 most intense ions from each MS1 spectrum were isolated in the quadrupole mass analyser using a 1.2 m/z window and fragmented using higher-energy collisional dissociation (HCD) with normalised collision energy (NCE) of 27. MS2 scans of fragment ions were only triggered when a threshold of 1e5 ions or 300 ms was reached and were acquired in the Orbitrap mass analyser with a mass resolution of 17,500 and mass range starting at 100 m/z. Fragmented ions were excluded from repeated analysis for 10 seconds. MS and MS2 spectra were recorded in Xcalibur 3.0 (ThermoFisher Scientific).

Raw MS data were processed in Proteome Discoverer 1.4 (ThermoFisher Scientific). Spectra were searched against the mouse UniProt database (74290 entries) and Global Proteome Machine database of common contaminants (247 entries) using Mascot. Trypsin was set as the specific

protease with a maximum of three missed cleavage sites allowed. Peptide mass tolerance was set to 10 ppm and fragment mass tolerance was set to 20 mmu. Carbamidomethylation of cysteine was set as a fixed modification. Oxidation of methionine and phosphorylation of serine, threonine and tyrosine were set as variable modifications. Only high confidence peptides were used, with a 0.01 target peptide FDR, and a minimum of 1 unique peptide was required for successful protein identification. Precursor ions area detector node was used for label-free protein quantitation within Proteome Discoverer 1.4

## 7.17 Proteomics data analysis in Perseus

Quantified proteomics data was analysed in Perseus Version 1.6.2.2. Abundance values for 3473 proteins quantified in all stimulated control purifications and all stimulated p110δ purifications were loaded into Perseus and log2 transformed. Biological triplicates were grouped by categorical annotation of rows. A 'Two sample T-test' was performed on the two groups and corrected for multiple hypothesis testing using a permutation-based false discovery rate (FDR) with a threshold of either 0.05 or 0.20 and an S0 of 0. The values for -Log(P-value) and Student's T-test Difference were exported to GraphPad Prism version 7 (GraphPad Software, Inc) to create a volcano scatter plot.

To generate a heatmap visualising the relative abundance of selected proteins of interest across all nine samples using Perseus, protein abundance values were first normalised using Z-score transformation. Unsupervised hierarchical clustering was then performed on rows using Euclidean distance and average linkage.

## 7.18 Preparation of samples for RNA sequencing

*The following experiments were performed by Hicham Bouabe.*

Naïve ($CD44^{-}CD62L^{hi}$) $CD8^{+}$ T cells were purified by flow cytometry-assisted cell sorting from splenic cells isolated from wild type mice. Wild type mice were infected intravenously with $2 \times 10^{6}$ colony forming units of ΔActA-Lm-Ova and spleens were isolated on day 7 post-infection. Effector ($CD44^{+}CD62L^{lo}$H-$2K^{b}$-SIINFEKL$^{+}$ antigen-specific) $CD8^{+}$ T cells were purified by flow cytometry-assisted cell sorting from splenic cells. Cells were then frozen at -80°C. RNA was isolated from cell samples using a modified protocol based on reagents from RNAqueous-Micro Total RNA Isolation Kit (ThermoFisher Scientific) and Pellet Paint Co-Precipitant (Novagen) RNA precipitation procedure. DNA was removed by treatment with DNaseI from the RNAqueous-

Micro Kit. cDNA libraries for sequencing were prepared from 150 ng total RNA using TruSeq Stranded Total RNA Library Prep Kit with Ribo-Zero Gold (Illumina #RS-122-2301).

## 7.19 CRISPR oligonucleotides and Cas9 protein

Two CRISPR RNA (crRNA) guide sequences were designed per target gene using the CRISPR3 web-based tool (AstraZeneca, proprietary software). Pairs of guides were only chosen if their base pair separation was a non-multiple of 3 and if they targeted all transcripts of a gene. Preference was given to guides targeting early exons. Guides with a predicted efficacy score greater than 0.500 and a low probability of off-targets in a coding region (pCoding < 0.500) were selected. Guides predicted to have off-targets with only one mismatch were not acceptable.

crRNA sequences, as shown in Table 7.3, were purchased from Integrated DNA Technologies (IDT) in the Alt-R® CRISPR-Cas9 format. Universal trans-activating crRNA (tracrRNA) was also purchased from IDT in the Alt-R® CRISPR-Cas9 tracrRNA format. Carrier DNA was purchased from IDT as a PAGE Ultramer® DNA Oligo with the following sequence: CCAGCAGAACACCCCCATCGGCGACGGCCCCGTGCTGCTGCCCGACAACCACTACCTGAGCACCCAGTCC GCCCTGAGCAAAGACCCCAACGAGA.

Oligonucleotides were resuspended in Nuclease-Free IDTE Buffer (IDT) to a concentration of 100 µM and stored at -80°C. Recombinant *S. pyogenes* Cas9 (AstraZeneca, in-house) was stored at -80°C in 20 mM HEPES pH 7.4, 150 mM KCl, 1 mM TCEP and 10 % (v/v) glycerol.

| crRNA | Targeted exon | Sequence (5’ – 3’) |
|---|---|---|
| *Thy1* gRNA 1 | Exon 2 | GCGGGAGCGGTACGTGTGCT |
| *Thy1* gRNA 2 | Exon 2 | TCAGCCTGACCCGAGAGAAG |
| *Pik3cd* gRNA 1 | Exon 2 | AGTTAATGAGCTTCTTCACG |
| *Pik3cd* gRNA 2 | Exon 2 | TCGGGCCACGAGGCGCAGCA |
| *Pik3ap1* gRNA 1 | Exon 4 | CAGTGTGCCTTCCACCCGGA |
| *Pik3ap1* gRNA 2 | Exon 4 | ACGGTCTCTGTGAAAGCACC |
| *ICOS* gRNA 1 | Exon 2 | GCAGAAGTAATAGCTTCCCT |
| *ICOS* gRNA 2 | Exon 2 | AGGTTCCTTTCTTGAAAAGG |

**Table 7.3 CRISPR RNA (crRNA) sequences used for CRISPR/Cas9 gene editing**

## 7.20 RNP nucleofection of primary mouse T blasts

crRNA:tracrRNA duplexes (gRNA) and Cas9 ribonucleoproteins (RNPs) were prepared fresh for each RNP experiment. tracrRNA and crRNA were mixed in equimolar amounts and annealed at 95°C for 5 min, then cooled to room temperature to a final duplex concentration of 50 uM.

Recombinant Cas9 protein was mixed with gRNA in the amounts and combinations indicated in the figure legends, or in the optimised ratio 10 µg:94 pmol (Cas9:gRNA), to a total volume of 7 µl per nucleofection in Neon Buffer R (Invitrogen #MPK1096T). Cas9:gRNA complexes were then incubated at room temperature for 30 minutes to generate Cas9 RNPs.

Activated T cells were pooled following 48-hour stimulation with 1 µg/ml anti-CD3 (as detailed in section 7.3) and centrifuged at 350 × g for 5 minutes at 22°C. Cells were resuspended in warm 5 % RPMI and counted using the EVE™ Automated Cell Counter (NanoEntek). Cells were washed once in sterile 1X PBS (Life Technologies #10010-015) and resuspended in Neon Buffer R at a concentration of $2.16 \times 10^6$ cells per 5 µl. Cells were immediately added to RNP complexes along with 0.2 µg carrier DNA to a final volume of 12 µl per nucleofection, which was then electroporated in 10 µl Neon tips (Invitrogen #MPK1096T) using the Neon transfection system programme #24 (voltage: 1600 V, width: 10 ms, pulses: 3; Invitrogen). Each nucleofection mixture was then dispensed into 940 µl pre-warmed 5 % RPMI containing 20 ng/ml rhIL-2 in 12-well plates and incubated at 37°C. After 2 hours, cells were split across three wells and then expanded for 5 days, with supplementation of rhIL-2 and media at 48 and 72 hours post-nucleofection to maintain a cell concentration of $1 – 2 \times 10^6$ cells/ml. Cell aliquots of 100 µl were taken at 48 and 72 hours and cell pellets were stored at -20°C for later DNA extraction and sequencing analysis.

## 7.21 DNA extraction, PCR and Sanger sequencing

To extract genomic DNA for sequencing analysis, cell pellets were resuspended in 50 µl DirectPCR Cell Lysis Reagent (Viagen Biotech #301-C) with 0.8 µg/µl proteinase K (Invitrogen #100005393) and incubated at 85°C for 45 minutes. Lysates were then used directly for PCR amplification of a ~1000 bp region spanning each Cas9 cleavage site, using the Phusion Flash High-Fidelity PCR Master Mix (Thermo Scientific #F-548L), as follows:

| | |
|---|---|
| Cell lysate | 1 µl |
| 2X Phusion Flash PCR Master Mix | 25 µl |
| Forward primer | 0.25 µl |
| Reverse primer | 0.25 µl |
| $H_2O$ | 23.5 µl |

Primers as detailed in Table 7.4 were purchased from Eurogentec (Seraing, Belgium) as lyophilised oligonucleotides, resuspended in TE buffer (pH 8; in-house), and used at a final concentration of 0.5 µM. The PCR cycling conditions used are listed in Table 7.5. PCR products were purified for sequencing using the illustra GFX PCR DNA and Gel Band Purification Kit (GE

Healthcare #28903470) according to the manufacturer's instructions, with elution of the DNA in 20 µl $H_2O$. Sanger sequencing of purified PCR amplicons was carried out by GATC (Eurofins Genomics, Germany) using the Supremerun Tube service and the relevant forward primer, as listed in Table 7.4.

| Gene target | Primer | Primer sequence (5' – 3') | Product length (bp) |
|---|---|---|---|
| *Thy1* | Forward | GGATCTAGGAACTCCTCTTGCTG | 1056 |
| | Reverse | GGCGCTTTCTCATCTTAGCGG | |
| *Pik3cd* | Forward | CCAGATTTGCCCGATGAGACAATTA | 993 |
| | Reverse | AGGGGCAGAACAAAGATGGGTC | |
| *Pik3ap1* | Forward | GAAGGCCAATAGTCACCAAGGG | 1020 |
| | Reverse | AGCATATGGTATCTACATGGGCATT | |
| *ICOS* | Forward | ATTCTGTCTATCACATGAAAAGCCC | 1000 |
| | Reverse | TACAAATGTGACTAATAGGTGGTGC | |

**Table 7.4 Primer sequences for PCR**

| Cycle step | Temperature (°C) | Time | Cycles |
|---|---|---|---|
| Initial denaturation | 98 | 10 s | 1 |
| Denaturation<br>Annealing<br>Extension | 98<br>60.3<br>72 | 1 s<br>5 s<br>20 s | 33 |
| Final extension | 72<br>4 | 1 min<br>Hold | 1 |

**Table 7.5 PCR thermocycling conditions**

## 7.22 Tracking of Indels by Decomposition (TIDE) analysis

To estimate insertion-deletion (indel) frequencies, Sanger sequencing chromatograms of PCR amplicons were analysed using TIDE version 1.1.2, AZ version v03 (AstraZeneca, proprietary software based on https://tide.deskgen.com/). Chromatograms were input as .ab1 files along with the sequences of the gRNAs used for editing. Analyses were performed using a reference sequence from unedited wild type cells. The aberrant sequence signal across the sequenced length was examined to exclude regions of poor sequence quality from the alignment window (the sequence used to align the control and test sample) and decomposition window (the sequence segment used for decomposition). The maximum size of insertions and deletions modelled in decomposition was adjusted to achieve $R^2$ values close to or greater than 0.9 to indicate good algorithm performance.

## 7.23 Cell surface staining and flow cytometry

For the analysis of extracellular surface markers at 48 and 72 hours post-nucleofection, T blasts from culture were pelleted by centrifugation at 400 × g for 5 minutes, resuspended in 1X PBS (Life Technologies #10270-106) and transferred to V-bottom 96-well plates (Greiner #651201). Cells were centrifuged at 400 × g for 5 minutes at 4°C and resuspended in 50 µl/well 1X PBS containing Live/Dead Fixable Blue Stain (1:400 dilution; Invitrogen #L23105) followed by incubation for 30 minutes at 4°C in the dark. Cells were then washed once in FACS buffer (FB; 1% BSA (Sigma #A7906), 1X PBS (Life Technologies #10270-106), 2 mM EDTA) and resuspended in 50 µl/well of 1:1 FB:Brilliant violet staining buffer (FB:BV; BD Biosciences #563794) containing antibodies for extracellular markers or isotype controls (Table 7.6). Cells were incubated for 30 minutes at 4°C in the dark, washed once in FB and then fixed for 15 minutes at room temperature in the dark with 100 µl Fixation Buffer (BioLegend #420801). Cells were washed twice in FB and finally resuspended in 100 µl FB before analysis using a BD LSRFortessa flow cytometer (BD Biosciences). Data obtained by flow cytometry was analysed using FlowJo version 10.4.1 (FlowJo, LLC). Graphical and statistical analyses were performed in GraphPad Prism version 7 (GraphPad Software, Inc), as detailed in figure legends and the text.

## 7.24 Antibody stimulation of T blasts in culture

Flat-bottom 96-well plates (Sigma #CLS3595-50EA) were coated overnight at 37°C with 100 µl PBS per well containing 2 µg/ml anti-CD3 (145-2C11; BioLegend #100314). T blasts at day 5 post-nucleofection were pooled by centrifugation at 300 × g for 5 minutes and resuspended in fresh 5% RPMI (RMPI 1640 + L-glutamine, 5 % heat inactivated FBS, 100 U/ml penicillin-streptomycin, 50 µM β-mercaptoethanol). Cells were then plated at 200,000 per well and supplemented with 200 nM CAL101 or 200 nM DMSO. After 1 hour incubation at 37 °C, cells were incubated for a further 7 hours in the presence of brefeldin A (BD GolgiPlug™ Protein Transport Inhibitor, 1:1000 dilution; BD Biosciences #555029).

## 7.25 Intracellular flow cytometry

For the analysis of intracellular cytokines following 8-hour antibody stimulation, cells were transferred from flat-bottom 96-well plates to V-bottom 96-well plates (Greiner #651201) on ice and pelleted by centrifugation at 400 × g for 5 minutes at 4°C. Cells were washed once in FACS buffer (FB) and then resuspended in 50 µl/well FB:BV buffer containing antibodies for extracellular markers or isotype controls (Table 7.6) and Fixable Viability Dye eFluor 780 (1:5,000

dilution; Invitrogen #65-0865-14). Cells were incubated for 30 minutes at 4°C in the dark, washed once in FB and then fixed for 15 minutes on ice in the dark with 100 µl fixation/permeabilization solution (BD Cytofix/Cytoperm kit; BD Biosciences #554714). Cells were washed twice in FB and stored overnight at 4°C in the dark. Cells were then centrifuged at 720 × g for 3 minutes at 4°C, resuspended in 1X BD Perm/Wash Buffer (BD Biosciences #554714) and again centrifuged at 720 × g, before resuspension in 50 µl/well Perm/Wash Buffer containing antibodies for intracellular cytokines or isotype controls (Table 7.6). Cells were incubated for 30 minutes at 4°C in the dark and then washed twice, first in Perm/Wash Buffer and then FB. Cells were finally resuspended in 100 µl FB before analysis using a BD LSRFortessa flow cytometer (BD Biosciences).

| Specificity | Clone | Conjugation | Dilution | Supplier | Catalogue No. |
|---|---|---|---|---|---|
| TCRb | H57-597 | PerCP/Cy5.5 | 1:400 | BioLegend | 109228 |
| CD4 | RM4-5 | BV711 | 1:800 | BioLegend | 100557 |
| CD8a | 53-6.7 | FITC | 1:600 | BioLegend | 100706 |
| CD44 | 1M7 | BUV737 | 1:200 | BD Biosciences | 564392 |
| CD62L | MEL14 | PE-CF594 | 1:200 | BD Biosciences | 562404 |
| CD90.2 | 53-2.1 | BV605 | 1:200 | BioLegend | 140317 |
| ICOS | 7E.17G9 | APC | 1:200 | eBioscience | 17-9942-82 |
| IFNγ | XMG1.2 | PE/Cy7 | 1:200 | BioLegend | 505826 |
| TNFα | MD6-XT 22 | Pacific Blue | 1:200 | BioLegend | 506318 |
| CD16/32 (Fc block) | 93 | Unconjugated | 1:100 | eBioscience | 14-0161-86 |
| Rat IgG1 κ | RTK2071 | PE/Cy7 | 1:200 | BioLegend | 400416 |
| Rat IgG1 κ | RTK2071 | Pacific Blue | 1:200 | BioLegend | 400419 |
| Rat IgG2b κ | RTK4530 | APC | 1:200 | BioLegend | 400611 |
| Rat IgG2a κ | RTK2758 | BV605 | 1:200 | BioLegend | 400540 |
| Armenian hamster IgG | HTK888 | PerCP/Cy5.5 | 1:400 | BioLegend | 400931 |

**Table 7.6 Antibodies used for flow cytometry**

## 7.26 Optimisation of experimental parameters

To optimise the RNP nucleofection protocol by response surface methodology, Design-Expert Version 6.0.9 (Stat-Ease, Inc.) software was used to design experimental runs using Box-Behnken design with the following parameters: $0.5 \times 10^6 \leq$ cell number $\leq 2.5 \times 10^6$; 1 µg ≤ Cas9 amount ≤ 10 µg; 25 pmol ≤ gRNA amount ≤ 125 pmol. Responses for cutting efficiency %, protein KO % and cell viability % from 17 experimental runs were input and Design-Expert developed quadratic models for each response that were found to be significant by analysis of variance (ANOVA). Optimisation parameters were set to maximise cutting efficiency and protein KO,

within the limits 30 – 100 %, and to target cell viability of 43.5 % (the maximum observed) and response surface analysis calculated the optimum values for each factor.

# Chapter 8

# References


Adams SJ, Aydin IT & Celebi JT (2012) GAB2--a Scaffolding Protein in Cancer. *Mol. Cancer Res.* **10:** 1265–1270

Aebersold R & Mann M (2003) Mass spectrometry-based proteomics. *Nature* **422:** 198–207

Alcázar I, Cortés I, Zaballos A, Hernandez C, Fruman DA, Barber DF & Carrera AC (2009) p85beta phosphoinositide 3-kinase regulates CD28 coreceptor function. *Blood* **113:** 3198–208

Alessi DR, James SR, Downes CP, Holmes AB, Gaffney PR, Reese CB & Cohen P (1997) Characterization of a 3-phosphoinositide-dependent protein kinase which phosphorylates and activates protein kinase Balpha. *Curr. Biol.* **7:** 261–9

Amzel LM, Huang C-H, Mandelker D, Lengauer C, Gabelli SB & Vogelstein B (2008) Structural comparisons of class I phosphoinositide 3-kinases. *Nat. Rev. Cancer* **8:** 665–9

Andersson EC, Christensen JP, Marker O & Thomsen AR (1994) Changes in cell adhesion molecule expression on T cells associated with systemic virus infection. *J. Immunol.* **152:** 1237–45

Arimura Y, Kato H, Dianzani U, Okamoto T, Kamekura S, Buonfiglio D, Miyoshi-Akiyama T, Uchiyama T & Yagi J (2002) A co-stimulatory molecule on activated T cells, H4/ICOS, delivers specific signals in Th cells and regulates their responses. *Int. Immunol.* **14:** 555–566

Astoul E, Edmunds C, Cantrell DA & Ward SG (2001) PI 3-K and T-cell activation: limitations of T-leukemic cell lines as signaling models. *Trends Immunol.* **22:** 490–6

Au-Yeung BB, Shah NH, Shen L & Weiss A (2018) ZAP-70 in Signaling, Biology, and Disease. *Annu. Rev. Immunol.* **36:** 127–156

Backer JM (2010) The regulation of class IA PI 3-kinases by inter-subunit interactions. *Curr. Top. Microbiol. Immunol.* **346:** 87–114

Backer JM (2008) The regulation and function of Class III PI3Ks: novel roles for Vps34. *Biochem. J.* **410:** 1–17

Balagopalan L, Coussens NP, Sherman E, Samelson LE & Sommers CL (2010) The LAT Story: A Tale of Cooperativity, Coordination, and Choreography. *Cold Spring Harb. Perspect. Biol.* **2:** a005512–a005512

Balbis A, Baquiran G, Bergeron JJM & Posner BI (2000) Compartmentalization and Insulin-Induced Translocations of Insulin Receptor Substrates, Phosphatidylinositol 3-Kinase, and Protein Kinase B in Rat Liver [1]. *Endocrinology* **141:** 4041–4049

Bamberger M, Santos AM, Gonçalves CM, Oliveira MI, James JR, Moreira A, Lozano F, Davis SJ & Carmo AM (2011) A new pathway of CD5 glycoprotein-mediated T cell inhibition dependent on inhibitory phosphorylation of Fyn kinase. *J. Biol. Chem.* **286:** 30324–36

Ban YH, Oh S-C, Seo S-H, Kim S-M, Choi I-P, Greenberg PD, Chang J, Kim T-D & Ha S-J (2017) miR-150-Mediated Foxo1 Regulation Programs CD8 + T Cell Differentiation. *Cell Rep.* **20:** 2598–2611

Barber EK, Dasgupta JD, Schlossman SF, Trevillyan JM & Rudd CE (1989) The CD4 and CD8 antigens are coupled to a protein-tyrosine kinase (p56lck) that phosphorylates the CD3 complex. *Proc. Natl. Acad. Sci. U. S. A.* **86:** 3277–81

Barford D & Neel BG (1998) Revealing mechanisms for SH2 domain mediated regulation of the protein tyrosine phosphatase SHP-2. *Structure* **6:** 249–54

Barker TH & Hagood JS (2009) Getting a grip on Thy-1 signaling. *Biochim. Biophys. Acta - Mol. Cell Res.* **1793:** 921–923

Beavitt S-JE, Harder KW, Kemp JM, Jones J, Quilici C, Casagranda F, Lam E, Turner D, Brennan S, Sly PD, Tarlinton DM, Anderson GP & Hibbs ML (2005) Lyn-deficient mice develop severe, persistent asthma: Lyn is a critical negative regulator of Th2 immunity. *J. Immunol.* **175:** 1867–75

Beitner-Johnson D, Blakesley VA, Shen-Orr Z, Jimenez M, Stannard B, Wang LM, Pierce J & LeRoith D (1996) The proto-oncogene product c-Crk associates with insulin receptor substrate-1 and 4PS. Modulation by insulin growth factor-I (IGF) and enhanced IGF-I signaling. *J. Biol. Chem.* **271:** 9287–90

Bergman M, Mustelin T, Oetken C, Partanen J, Flint NA, Amrein KE, Autero M, Burn P & Alitalo K (1992) The human p50csk tyrosine kinase phosphorylates p56lck at Tyr-505 and down regulates its catalytic activity. *EMBO J.* **11:** 2919–24

Bilal MY & Houtman JCD (2015) GRB2 Nucleates T Cell Receptor-Mediated LAT Clusters That Control PLC-γ1 Activation and Cytokine Production. *Front. Immunol.* **6:** 141

Blagoev B, Kratchmarova I, Ong S-E, Nielsen M, Foster LJ & Mann M (2003) A proteomics strategy to elucidate functional protein-protein interactions applied to EGF signaling. *Nat. Biotechnol.* **21:** 315–318

Bothur E, Raifer H, Haftmann C, Stittrich A-B, Brüstle A, Brenner D, Bollig N, Bieringer M, Kang C-H, Reinhard K, Camara B, Huber M, Visekruna A, Steinhoff U, Repenning A, Bauer U-M, Sexl V, Radbruch A, Sparwasser T, Mashreghi M-F, et al (2015) Antigen receptor-mediated depletion of FOXP3 in induced regulatory T-lymphocytes via PTPN2 and FOXO1. *Nat. Commun.* **6:** 8576

Brinkman EK, Chen T, Amendola M & van Steensel B (2014) Easy quantitative assessment of genome editing by sequence trace decomposition. *Nucleic Acids Res.* **42:** e168

Brownlie RJ & Zamoyska R (2013) T cell receptor signalling networks: branched, diversified and bounded. *Nat. Rev. Immunol.* **13:** 257–269

Bruyns E, Marie-Cardine A, Kirchgessner H, Sagolla K, Shevchenko A, Mann M, Autschbach F, Bensussan A, Meuer S & Schraven B (1998) T cell receptor (TCR) interacting molecule (TRIM), a novel disulfide-linked dimer associated with the TCR-CD3-zeta complex, recruits intracellular signaling proteins to the plasma membrane. *J. Exp. Med.* **188:** 561–75

Bubeck Wardenburg J, Fu C, Jackman JK, Flotow H, Wilkinson SE, Williams DH, Johnson R, Kong G, Chan AC & Findell PR (1996) Phosphorylation of SLP-76 by the ZAP-70 protein-tyrosine kinase is required for T-cell receptor function. *J. Biol. Chem.* **271:** 19641–4

Bulut GB, Sulahian R, Yao H & Huang LJ (2013) Cbl ubiquitination of p85 is essential for Epo-induced EpoR endocytosis. *Blood* **122:** 3964–72

Burger T (2018) Gentle Introduction to the Statistical Foundations of False Discovery Rate in Quantitative Proteomics. *J. Proteome Res.* **17:** 12–22

Burke JE, Perisic O, Masson GR, Vadas O & Williams RL (2012) Oncogenic mutations mimic and enhance dynamic events in the natural activation of phosphoinositide 3-kinase p110α (PIK3CA). *Proc. Natl. Acad. Sci.* **109:** 15259–15264

Burke JE & Williams RL (2013) Dynamic steps in receptor tyrosine kinase mediated activation of class IA phosphoinositide 3-kinases (PI3K) captured by H/D exchange (HDX-MS). *Adv. Biol. Regul.* **53:** 97–110

Burke JE, Vadas O, Berndt A, Finegan T, Perisic O & Williams RL (2011) Dynamics of the phosphoinositide 3-kinase p110δ interaction with p85α and membranes reveals aspects of regulation distinct from p110α. *Structure* **19:** 1127–37

Burke JE & Williams RL (2015) Synergy in activating class I PI3Ks. *Trends Biochem. Sci.* **40:** 88–100

Cao L, Ding Y, Hung N, Yu K, Ritz A, Raphael BJ & Salomon AR (2012) Quantitative Phosphoproteomics Reveals SLP-76 Dependent Regulation of PAG and Src Family Kinases in T Cells. *PLoS One* **7:** e46725

Carbone CB, Kern N, Fernandes RA, Hui E, Su X, Garcia KC & Vale RD (2017) In vitro reconstitution of T cell receptor-mediated segregation of the CD45 phosphatase. *Proc. Natl. Acad. Sci. U. S. A.* **114:** E9338–E9345

Carpino N, Turner S, Mekala D, Takahashi Y, Zang H, Geiger TL, Doherty P & Ihle JN (2004) Regulation of ZAP-70 Activation and TCR Signaling by Two Related Proteins, Sts-1 and Sts-2. *Immunity* **20:** 37–46

Castello A, Gaya M, Tucholski J, Oellerich T, Lu K, Tafuri A, Pawson T, Wienands J, Engelke M & Batista F (2013) Nck-mediated recruitment of BCAP to the BCR regulates the PI(3)K-Akt pathway in B cells. *Nat. Immunol.* **14:** 966-975

Chandok MR & Farber DL (2004) Signaling control of memory T cell generation and function. *Semin. Immunol.* **16:** 285–293

Chen GI & Gingras A-C (2007) Affinity-purification mass spectrometry (AP-MS) of serine/threonine phosphatases. *Methods* **42:** 298–305

Chen L & Flies DB (2013) Molecular mechanisms of T cell co-stimulation and co-inhibition. *Nat. Rev. Immunol.* **13:** 227–42

Chu VT, Graf R, Wirtz T, Weber T, Favret J, Li X, Petsch K, Tran NT, Sieweke MH, Berek C, Kühn R & Rajewsky K (2016) Efficient CRISPR-mediated mutagenesis in primary immune cells using

CrispRGold and a C57BL/6 Cas9 transgenic mouse line. *Proc. Natl. Acad. Sci. U. S. A.* **113:** 12514–12519

Coornaert B, Baens M, Heyninck K, Bekaert T, Haegman M, Staal J, Sun L, Chen ZJ, Marynen P & Beyaert R (2008) T cell antigen receptor stimulation induces MALT1 paracaspase–mediated cleavage of the NF-κB inhibitor A20. *Nat. Immunol.* **9:** 263–271

Costello PS, Gallagher M & Cantrell DA (2002) Sustained and dynamic inositol lipid metabolism inside and outside the immunological synapse. *Nat. Immunol.* **3:** 1082–1089

Coudronniere N, Villalba M, Englund N & Altman A (2000) NF-kappa B activation induced by T cell receptor/CD28 costimulation is mediated by protein kinase C-theta. *Proc. Natl. Acad. Sci. U. S. A.* **97:** 3394–9

Dbouk HA, Vadas O, Shymanets A, Burke JE, Salamon RS, Khalil BD, Barrett MO, Waldo GL, Surve C, Hsueh C, Perisic O, Harteneck C, Shepherd PR, Harden TK, Smrcka A V., Taussig R, Bresnick AR, Nurnberg B, Williams RL & Backer JM (2012) G Protein-Coupled Receptor-Mediated Activation of p110β by Gβγ Is Required for Cellular Transformation and Invasiveness. *Sci. Signal.* **5:** ra89-ra89

Dbouk HA, Pang H, Fiser A & Backer JM (2010) A biochemical mechanism for the oncogenic potential of the p110beta catalytic subunit of phosphoinositide 3-kinase. *Proc. Natl. Acad. Sci. U. S. A.* **107:** 19897–902

de Boer E, Rodriguez P, Bonte E, Krijgsveld J, Katsantoni E, Heck A, Grosveld F & Strouboulis J (2003) Efficient biotinylation and single-step purification of tagged transcription factors in mammalian cells and transgenic mice. *Proc. Natl. Acad. Sci. U. S. A.* **100:** 7480–5

Deane JA, Trifilo MJ, Yballe CM, Choi S, Lane TE & Fruman DA (2004) Enhanced T cell proliferation in mice lacking the p85beta subunit of phosphoinositide 3-kinase. *J. Immunol.* **172:** 6615–25

DebBurman SK, Ptasienski J, Benovic JL & Hosey MM (1996) G protein-coupled receptor kinase GRK2 is a phospholipid-dependent enzyme that can be conditionally activated by G protein betagamma subunits. *J. Biol. Chem.* **271:** 22552–22562

DeGrendele HC, Kosfiszer M, Estess P & Siegelman MH (1997) CD44 activation and associated primary adhesion is inducible via T cell receptor stimulation. *J. Immunol.* **159:** 2549–53

Delgado P, Cubelos B, Calleja E, Martínez-Martín N, Ciprés A, Mérida I, Bellas C, Bustelo XR & Alarcón B (2009) Essential function for the GTPase TC21 in homeostatic antigen receptor signaling. *Nat. Immunol.* **10:** 880–888

Demydenko D (2010) c-Cbl mediated ubiquitylation and regulation of cell surface exposure of CD5. *Biochem. Biophys. Res. Commun.* **392:** 500–504

Denley A, Kang S, Karst U & Vogt PK (2008) Oncogenic signaling of class I PI3K isoforms. *Oncogene* **27:** 2561–2574

Dennehy KM, Broszeit R, Ferris WF & Beyers AD (1998) Thymocyte activation induces the association of the proto-oncoprotein c-cbl and ras GTPase- activating protein with CD5. *Eur. J. Immunol.* **28:** 1617–1625

Dennehy KM, Broszeit R, Garnett D, Durrheim GA, Spruyt LL & Beyers AD (1997) Thymocyte activation induces the association of phosphatidylinositol 3-kinase and pp120 with CD5. *Eur. J. Immunol.* **27:** 679–686

Dikic I (2002) CIN85/CMS family of adaptor molecules. *FEBS Lett.* **529:** 110–115

Dinkel BA, Kremer KN, Rollins MR, Medlyn MJ & Hedin KE (2018) GRK2 mediates TCR-induced transactivation of CXCR4 and TCR-CXCR4 complex formation that drives PI3Kγ/PREX1 signaling and T cell cytokine secretion. *J. Biol. Chem.* **293:** 14022–14039

Dobbins J, Gagnon E, Godec J, Pyrdol J, Vignali DAA, Sharpe AH & Wucherpfennig KW (2016) Binding of the cytoplasmic domain of CD28 to the plasma membrane inhibits Lck recruitment and signaling. *Sci. Signal.* **9:** ra75

Dong G, Kalifa R, Nath PR, Gelkop S & Isakov N (2017) TCR crosslinking promotes Crk adaptor protein binding to tyrosine-phosphorylated CD3ζ chain. *Biochem. Biophys. Res. Commun.* **488:** 541–546

Dornan GL, Siempelkamp BD, Jenkins ML, Vadas O, Lucas CL & Burke JE (2017) Conformational disruption of PI3Kδ regulation by immunodeficiency mutations in PIK3CD and PIK3R1. *Proc. Natl. Acad. Sci. U. S. A.* **114:** 1982–1987

D'Oro U, Sakaguchi K, Appella E & Ashwell JD (1996) Mutational analysis of Lck in CD45-negative T cells: dominant role of tyrosine 394 phosphorylation in kinase activity. *Mol. Cell. Biol.* **16:** 4996–5003

Doudna JA & Charpentier E (2014) The new frontier of genome engineering with CRISPR-Cas9. *Science (80-. ).* **346:** 1258096–1258096

Dufour C, Guenou H, Kaabeche K, Bouvard D, Sanjay A & Marie PJ (2008) FGFR2-Cbl interaction in lipid rafts triggers attenuation of PI3K/Akt signaling and osteoblast survival. *Bone* **42:** 1032–1039

Dunham WH, Mullin M & Gingras A-C (2012) Affinity-purification coupled to mass spectrometry: Basic principles and strategies. *Proteomics* **12:** 1576–1590

Ermak G, Cancasci VJ & Davies KJ. (2003) Cytotoxic effect of doxycycline and its implications for tet-on gene expression systems. *Anal. Biochem.* **318:** 152–154

Esensten JH, Helou YA, Chopra G, Weiss A & Bluestone JA (2016) CD28 Costimulation: From Mechanism to Therapy. *Immunity* **44:** 973-988

Fabre S, Lang V, Harriague J, Jobart A, Unterman TG, Trautmann A & Bismuth G (2005) Stable activation of phosphatidylinositol 3-kinase in the T cell immunological synapse stimulates Akt signaling to FoxO1 nuclear exclusion and cell growth control. *J. Immunol.* **174:** 4161–71

Falasca M & Maffucci T (2012) Regulation and cellular functions of class II phosphoinositide 3-kinases. *Biochem. J.* **443:** 587–601

Feshchenko EA, Smirnova E V, Swaminathan G, Teckchandani AM, Agrawal R, Band H, Zhang X, Annan RS, Carr SA & Tsygankov AY (2004) TULA: an SH3- and UBA-containing protein that binds to c-Cbl and ubiquitin. *Oncogene* **23:** 4690–4706

Foletta VC, Segal DH & Cohen DR (1998) Transcriptional regulation in the immune system: all roads lead to AP-1. *J. Leukoc. Biol.* **63:** 139–52

Fos C, Salles A, Lang V, Carrette F, Audebert S, Pastor S, Ghiotto M, Olive D, Bismuth G & Nunès JA (2008) ICOS ligation recruits the p50alpha PI3K regulatory subunit to the immunological synapse. *J. Immunol.* **181:** 1969–77

Freeley M & Long A (2013) Advances in siRNA delivery to T-cells: potential clinical applications for inflammatory disease, cancer and infection. *Biochem. J* **455:** 133–147

Friend SF, Deason-Towne F, Peterson LK, Berger AJ & Dragone LL (2014) Regulation of T cell receptor complex-mediated signaling by ubiquitin and ubiquitin-like modifications. *Am. J. Clin. Exp. Immunol.* **3:** 107–23

Fritsch R, de Krijger I, Fritsch K, George R, Reason B, Kumar MS, Diefenbacher M, Stamp G & Downward J (2013) RAS and RHO families of GTPases directly regulate distinct phosphoinositide 3-kinase isoforms. *Cell* **153:** 1050–63

Fruman DA, Rameh LE & Cantley LC (1999) Phosphoinositide binding domains: embracing 3-phosphate. *Cell* **97:** 817–20

Garçon F, Patton DT, Emery JL, Hirsch E, Rottapel R, Sasaki T & Okkenhaug K (2008) CD28 provides T-cell costimulation and enhances PI3K activity at the immune synapse independently of its capacity to interact with the p85/p110 heterodimer. *Blood* **111:** 1464–71

Gaud G, Lesourne R & Love PE (2018) Regulatory mechanisms in T cell receptor signalling. *Nat. Rev. Immunol.* **18:** 485–497

Gelkop S, Babichev Y & Isakov N (2001) T cell activation induces direct binding of the Crk adapter protein to the regulatory subunit of phosphatidylinositol 3-kinase (p85) via a complex mechanism involving the Cbl protein. *J. Biol. Chem.* **276:** 36174–82

Gerondakis S & Siebenlist U (2010) Roles of the NF-kappaB pathway in lymphocyte development and function. *Cold Spring Harb. Perspect. Biol.* **2:** a000182

Giai Gianetto Q, Couté Y, Bruley C & Burger T (2016) Uses and misuses of the fudge factor in quantitative discovery proteomics. *Proteomics* **16:** 1955–1960

Gigoux M, Shang J, Pak Y, Xu M, Choe J, Mak TW & Suh W-K (2009) Inducible costimulator promotes helper T-cell differentiation through phosphoinositide 3-kinase. *Proc. Natl. Acad. Sci. U. S. A.* **106:** 20371–6

Gil D, Schamel WWA, Montoya M, Sá Nchez-Madrid F & Alarcó B (2002) Recruitment of Nck by CD3 Reveals a Ligand-Induced Conformational Change Essential for T Cell Receptor Signaling and Synapse Formation. *Cell* **109**: 901-912

Gingras A-C, Gstaiger M, Raught B & Aebersold R (2007) Analysis of protein complexes using mass spectrometry. *Nat. Rev. Mol. Cell Biol.* **8:** 645–654

Gioia L, Siddique A, Head SR, Salomon DR & Su AI (2018) A genome-wide survey of mutations in the Jurkat cell line. *BMC Genomics* **19:** 334

Gomes-Silva D, Srinivasan M, Sharma S, Lee CM, Wagner DL, Davis TH, Rouce RH, Bao G, Brenner MK & Mamonkin M (2017) CD7-edited T cells expressing a CD7-specific CAR for the therapy of T-cell malignancies. *Blood* **130:** 285–296

Gorman JA, Babich A, Dick CJ, Schoon RA, Koenig A, Gomez TS, Burkhardt JK & Billadeau DD (2012) The cytoskeletal adaptor protein IQGAP1 regulates TCR-mediated signaling and filamentous actin dynamics. *J. Immunol.* **188:** 6135–44

Gout I, Middleton G, Adu J, Ninkina NN, Drobot LB, Filonenko V, Matsuka G, Davies AM, Waterfield M & Buchman VL (2000) Negative regulation of PI 3-kinase by Ruk, a novel adaptor protein. *EMBO J.* **19:** 4015–4025

Gracias DT, Boesteanu AC, Fraietta JA, Hope JL, Carey AJ, Mueller YM, Kawalekar OU, Fike AJ, June CH & Katsikis PD (2016) Phosphatidylinositol 3-Kinase p110δ Isoform Regulates CD8+ T Cell Responses during Acute Viral and Intracellular Bacterial Infections. *J. Immunol.* **196:** 1186–98

Griffin GE, Liu Y, Li C, Jin W, Shattock RJ, Wang P, Wu B, Guan X, Hu B, Du T & Hu Q (2015) Inhibition of HIV-1 infection of primary CD4+ T-cells by gene editing of CCR5 using adenovirus-delivered CRISPR/Cas9. *J. Gen. Virol.* **96:** 2381–2393

Gu H, Pratt JC, Burakoff SJ & Neel BG (1998) Cloning of p97/Gab2, the major SHP2-binding protein in hematopoietic cells, reveals a novel pathway for cytokine-induced gene activation. *Mol. Cell* **2:** 729–40

Guillermet-Guibert J, Bjorklof K, Salpekar A, Gonella C, Ramadani F, Bilancio A, Meek S, Smith AJH, Okkenhaug K & Vanhaesebroeck B (2008) The p110β isoform of phosphoinositide 3-kinase signals downstream of G protein-coupled receptors and is functionally redundant with p110γ. *Proc. Natl. Acad. Sci.* **105:** 8292–8297

Guo X, Yan C, Li H, Huang W, Shi X, Huang M, Wang Y, Pan W, Cai M, Li L, Wu W, Bai Y, Zhang C, Liu Z, Wang X, Zhang XF, Tang C, Wang H, Liu W, Ouyang B, et al (2017) Lipid-dependent conformational dynamics underlie the functional versatility of T-cell receptor. *Cell Res.* **27:** 505–525

Guy CS & Vignali DAA (2009) Organization of proximal signal initiation at the TCR:CD3 complex. *Immunol. Rev.* **232:** 7–21

Halabi S, Sekine E, Verstak B, Gay NJ & Moncrieffe MC (2017) Structure of the Toll/Interleukin-1 Receptor (TIR) Domain of the B-cell Adaptor That Links Phosphoinositide Metabolism with the Negative Regulation of the Toll-like Receptor (TLR) Signalosome. *J. Biol. Chem.* **292:** 652–660

Hamilton KS, Phong B, Corey C, Cheng J, Gorentla B, Zhong X, Shiva S & Kane LP (2014) T Cell Receptor-Dependent Activation of mTOR Signaling in T Cells Is Mediated by Carma1 and MALT1, But Not Bcl10. *Sci. Signal.* **7:** ra55-ra55

Hardwick JS & Sefton BM Activation of the Lck Tyrosine Protein Kinase by Hydrogen Peroxide Requires the Phosphorylation of Tyr-394. *Proc. Natl. Acad. Sci. U. S. A.* **92:** 4527–4531

Harriague J & Bismuth G (2002) Imaging antigen-induced PI3K activation in T cells. *Nat. Immunol.* **3:** 1090–1096

Harrison MM, Jenkins B V, O'Connor-Giles KM & Wildonger J (2014) A CRISPR view of development. *Genes Dev.* **28:** 1859–72

Hedman AC, Smith JM & Sacks DB (2015) The biology of IQGAP proteins: beyond the cytoskeleton. *EMBO Rep.* **16:** 427–46

Hedrick SM, Hess Michelini R, Doedens AL, Goldrath AW & Stone EL (2012) FOXO transcription factors throughout T cell biology. *Nat. Rev. Immunol.* **12:** 649–61

Helou YA & Salomon AR (2015) Protein networks and activation of lymphocytes. *Curr. Opin. Immunol.* **33:** 78–85

Hendel A, Bak RO, Clark JT, Kennedy AB, Ryan DE, Roy S, Steinfeld I, Lunstad BD, Kaiser RJ, Wilkens AB, Bacchetta R, Tsalenko A, Dellinger D, Bruhn L & Porteus MH (2015) Chemically modified guide RNAs enhance CRISPR-Cas genome editing in human primary cells. *Nat. Biotechnol.* **33:** 985–989

Hermann-Kleiter N & Baier G (2010) NFAT pulls the strings during CD4 T helper cell effector functions. *Blood* **115:** 2989–2997

Hers I, Vincent EE & Tavaré JM (2011) Akt signalling in health and disease. *Cell. Signal.* **23:** 1515–1527

Hogquist KA & Jameson SC (2014) The self-obsession of T cells: how TCR signaling thresholds affect fate 'decisions' and effector function. *Nat. Immunol.* **15:** 815–23

Holdorf AD, Lee K-H, Burack WR, Allen PM & Shaw AS (2002) Regulation of Lck activity by CD4 and CD28 in the immunological synapse. *Nat. Immunol.* **3:** 259–264

Houslay DM, Anderson KE, Chessa T, Kulkarni S, Fritsch R, Downward J, Backer JM, Stephens LR & Hawkins PT (2016) Coincident signals from GPCRs and receptor tyrosine kinases are uniquely transduced by PI3Kβ in myeloid cells. *Sci. Signal.* **9:** ra82-ra82

Houtman JCD, Yamaguchi H, Barda-Saad M, Braiman A, Bowden B, Appella E, Schuck P & Samelson LE (2006) Oligomerization of signaling complexes by the multipoint binding of GRB2 to both LAT and SOS1. *Nat. Struct. Mol. Biol.* **13:** 798–805

Huang H, Li L, Wu C, Schibli D, Colwill K, Ma S, Li C, Roy P, Ho K, Songyang Z, Pawson T, Gao Y & Li SS-C (2008) Defining the specificity space of the human SRC homology 2 domain. *Mol. Cell. Proteomics* **7:** 768–84

Huang Y, Clarke F, Karimi M, Roy NH, Williamson EK, Okumura M, Mochizuki K, Chen EJH, Park T-J, Debes GF, Zhang Y, Curran T, Kambayashi T & Burkhardt JK (2015) CRK proteins selectively regulate T cell migration into inflamed tissues. *J. Clin. Invest.* **125:** 1019–32

Huber TB, Hartleben B, Kim J, Schmidts M, Schermer B, Keil A, Egger L, Lecha RL, Borner C, Pavenstädt H, Shaw AS, Walz G & Benzing T (2003) Nephrin and CD2AP associate with phosphoinositide 3-OH kinase and stimulate AKT-dependent signaling. *Mol. Cell. Biol.* **23:** 4917–28

Hui E & Vale RD (2014) In vitro membrane reconstitution of the T-cell receptor proximal signaling network. *Nat. Struct. Mol. Biol.* **21:** 133–42

Hunter S, Burton EA, Wu SC & Anderson SM (1999) Fyn associates with Cbl and phosphorylates tyrosine 731 in Cbl, a binding site for phosphatidylinositol 3-kinase. *J. Biol. Chem.* **274:** 2097–106

Hutloff A, Dittrich AM, Beier KC, Eljaschewitsch B, Kraft R, Anagnostopoulos I & Kroczek RA (1999) ICOS is an inducible T-cell co-stimulator structurally and functionally related to CD28. *Nature* **397:** 263–266

Inabe K & Kurosaki T (2002) Tyrosine phosphorylation of B-cell adaptor for phosphoinositide 3-kinase is required for Akt activation in response to CD19 engagement. *Blood* **99:** 584–9

Inukai K, Funaki M, Anai M, Ogihara T, Katagiri H, Fukushima Y, Sakoda H, Onishi Y, Ono H, Fujishiro M, Abe M, Oka Y, Kikuchi M & Asano T (2001) Five isoforms of the phosphatidylinositol 3-kinase regulatory subunit exhibit different associations with receptor tyrosine kinases and their tyrosine phosphorylations. *FEBS Lett.* **490:** 32–8

Itakura E, Kishi C, Inoue K & Mizushima N (2008) Beclin 1 forms two distinct phosphatidylinositol 3-kinase complexes with mammalian Atg14 and UVRAG. *Mol. Biol. Cell* **19:** 5360–72

Jaber N & Zong W-X (2013) Class III PI3K Vps34: essential roles in autophagy, endocytosis, and heart and liver function. *Ann. N. Y. Acad. Sci.* **1280:** 48–51

James JR & Vale RD (2012) Biophysical mechanism of T-cell receptor triggering in a reconstituted system. *Nature* **487:** 64–9

Janas ML, Varano G, Gudmundsson K, Noda M, Nagasawa T & Turner M (2010) Thymic development beyond β-selection requires phosphatidylinositol 3-kinase activation by CXCR4. *J. Exp. Med.* **207:** 247–261

Jenkins MK, Ashwell JD & Schwartz RH (1988) Allogeneic non-T spleen cells restore the responsiveness of normal T cell clones stimulated with antigen and chemically modified antigen-presenting cells. *J. Immunol.* **140:** 3324–30

June CH, Ledbetter JA, Gillespie MM, Lindsten T & Thompson CB (1987) T-cell proliferation involving the CD28 pathway is associated with cyclosporine-resistant interleukin 2 gene expression. *Mol. Cell. Biol.* **7:** 4472–81

Juntilla MM, Wofford JA, Birnbaum MJ, Rathmell JC & Koretzky GA (2007) Akt1 and Akt2 are required for alphabeta thymocyte survival and differentiation. *Proc. Natl. Acad. Sci. U. S. A.* **104:** 12105–10

Katigbak A, Robert F, Paquet M & Pelletier J (2018) Inducible Genome Editing with Conditional CRISPR/Cas9 Mice. *G3 (Bethesda).* **8:** 1627–1635

Kean MJ, Couzens AL & Gingras A-C (2012) Mass spectrometry approaches to study mammalian kinase and phosphatase associated proteins. *Methods* **57:** 400–408

Kihara A, Noda T, Ishihara N & Ohsumi Y (2001) Two distinct Vps34 phosphatidylinositol 3-kinase complexes function in autophagy and carboxypeptidase Y sorting in Saccharomyces cerevisiae. *J. Cell Biol.* **152:** 519–30

Kim S, Kim D, Cho SW, Kim J & Kim J-S (2014) Highly efficient RNA-guided genome editing in human cells via delivery of purified Cas9 ribonucleoproteins. *Genome Res.* **24:** 1012–9

Kim S, Koo T, Jee H-G, Cho H-Y, Lee G, Lim D-G, Shin HS & Kim J-S (2018) CRISPR RNAs trigger innate immune responses in human cells. *Genome Res.* **28:** 367–373

Kok K, Nock GE, Verrall EAG, Mitchell MP, Hommes DW, Peppelenbosch MP & Vanhaesebroeck B (2009) Regulation of p110δ PI 3-Kinase Gene Expression. *PLoS One* **4:** e5145

Kölsch U, Arndt B, Reinhold D, Lindquist JA, Jüling N, Kliche S, Pfeffer K, Bruyns E, Schraven B & Simeoni L (2006) Normal T-cell development and immune functions in TRIM-deficient mice. *Mol. Cell. Biol.* **26:** 3639–48

Koncz G, Tóth GK, Bökönyi G, Kéri G, Pecht I, Medgyesi D, Gergely J & Sármay G (2001) Co-clustering of Fcγ and B cell receptors induces dephosphorylation of the Grb2-associated binder 1 docking protein. *Eur. J. Biochem.* **268:** 3898–3906

König R, Huang L-Y & Germain RN (1992) MHC class II interaction with CD4 mediated by a region analogous to the MHC class I binding site for CD8. *Nature* **356:** 796–798

Koretzky GA, Abtahian F & Silverman MA (2006) SLP76 and SLP65: complex regulation of signalling in lymphocytes and beyond. *Nat. Rev. Immunol.* **6:** 67–78

Kornete M, Marone R & Jeker LT (2018) Highly Efficient and Versatile Plasmid-Based Gene Editing in Primary T Cells. *J. Immunol.* **200:** 2489–2501

Kulkarni S, Sitaru C, Jakus Z, Anderson KE, Damoulakis G, Davidson K, Hirose M, Juss J, Oxley D, Chessa TAM, Ramadani F, Guillou H, Segonds-Pichon A, Fritsch A, Jarvis GE, Okkenhaug K, Ludwig R, Zillikens D, Mocsai A, Vanhaesebroeck B, et al (2011) PI3K  Plays a Critical Role in Neutrophil Activation by Immune Complexes. *Sci. Signal.* **4:** ra23-ra23

Laplante M & Sabatini DM (2012) mTOR Signaling in Growth Control and Disease. *Cell* **149:** 274–293

Lee CH, Li W, Nishimura R, Zhou M, Batzer AG, Myers MG, White MF, Schlessinger J, Skolnik EY & Skolnik EY (1993) Nck associates with the SH2 domain-docking protein IRS-1 in insulin-stimulated cells. *Proc. Natl. Acad. Sci. U. S. A.* **90:** 11713–7

Lee H & Tsygankov AY (2013) Cbl-family proteins as regulators of cytoskeleton-dependent phenomena. *J. Cell. Physiol.* **228:** 2285–2293

Lee K-H, Dinner AR, Tu C, Campi G, Raychaudhuri S, Varma R, Sims TN, Burack WR, Wu H, Wang J, Kanagawa O, Markiewicz M, Allen PM, Dustin ML, Arup †, Chakraborty K & Shaw AS The Immunological Synapse Balances T Cell Receptor Signaling and Degradation. Science **302:** 1218-1222

Lemmon MA (2008) Membrane recognition by phospholipid-binding domains. *Nat. Rev. Mol. Cell Biol.* **9:** 99–111

Lettau M, Pieper J & Janssen O (2009) Nck adapter proteins: functional versatility in T cells. *Cell Commun. Signal.* **7:** 1

Li L, Guo X, Shi X, Li C, Wu W, Yan C, Wang H, Li H & Xu C (2017) Ionic CD3-Lck interaction regulates the initiation of T-cell receptor signaling. *Proc. Natl. Acad. Sci. U. S. A.* **114:** E5891–E5899

Li Z, Adams RM, Chourey K, Hurst GB, Hettich RL & Pan C (2012) Systematic Comparison of Label-Free, Metabolic Labeling, and Isobaric Chemical Labeling for Quantitative Proteomics on LTQ Orbitrap Velos. *J. Proteome Res.* **11:** 1582–1590

Liang Y, Cucchetti M, Roncagalli R, Yokosuka T, Malzac A, Bertosio E, Imbert J, Nijman IJ, Suchanek M, Saito T, Wülfing C, Malissen B & Malissen M (2013) The lymphoid lineage–specific actin-uncapping protein Rltpr is essential for costimulation via CD28 and the development of regulatory T cells. *Nat. Immunol.* **14:** 858–866

Liu D, Zhang T, Marshall AJ, Okkenhaug K, Vanhaesebroeck B & Uzonna JE (2009) The p110δ isoform of phosphatidylinositol 3-kinase controls susceptibility to Leishmania major by regulating expansion and tissue homing of regulatory T cells. *J. Immunol.* **183:** 1921–1933

Liu S-L, Wang Z-G, Hu Y, Xin Y, Singaram I, Gorai S, Zhou X, Shim Y, Min J-H, Gong L-W, Hay N, Zhang J & Cho W (2018) Quantitative Lipid Imaging Reveals a New Signaling Function of Phosphatidylinositol-3,4-Bisphophate: Isoform- and Site-Specific Activation of Akt. *Mol. Cell* **71:** 1092–1104.e5

Liu X, Yue P, Khuri FR & Sun S-Y (2005) Decoy receptor 2 (DcR2) is a p53 target gene and regulates chemosensitivity. *Cancer Res.* **65:** 9169–75

Liu X, Homma A, Sayadi J, Yang S, Ohashi J & Takumi T (2016) Sequence features associated with the cleavage efficiency of CRISPR/Cas9 system. *Sci. Rep.* **6:** 19675

Love PE & Hayes SM (2010) ITAM-mediated signaling by the T-cell antigen receptor. *Cold Spring Harb. Perspect. Biol.* **2:** a002485

Lozano F, Simarro M, Calvo J, Vilà JM, Padilla O, Bowen MA & Campbell KS (2000) CD5 signal transduction: positive or negative modulation of antigen receptor signaling. *Crit. Rev. Immunol.* **20:** 347–58

Lučić I, Rathinaswamy MK, Truebestein L, Hamelin DJ, Burke JE & Leonard TA (2018) Conformational sampling of membranes by Akt controls its activation and inactivation. *Proc. Natl. Acad. Sci. U. S. A.* **115:** E3940–E3949

Luissint A-C, Lutz PG, Calderwood DA, Couraud P-O & Bourdoulous S (2008) JAM-L-mediated leukocyte adhesion to endothelial cells is regulated in cis by alpha4beta1 integrin activation. *J. Cell Biol.* **183:** 1159–73

Maffucci T & Falasca M (2014) New insight into the intracellular roles of class II phosphoinositide 3-kinases. *Biochem. Soc. Trans.* **42:** 1378–82

Mandal PK, Ferreira LMR, Collins R, Meissner TB, Boutwell CL, Friesen M, Vrbanac V, Garrison BS, Stortchevoi A, Bryder D, Musunuru K, Brand H, Tager AM, Allen TM, Talkowski ME, Rossi DJ & Cowan CA (2014) Efficient Ablation of Genes in Human Hematopoietic Stem and Effector Cells using CRISPR/Cas9. *Cell Stem Cell* **15:** 643–652

Mandelker D, Gabelli SB, Schmidt-Kittler O, Zhu J, Cheong I, Huang C-H, Kinzler KW, Vogelstein B & Amzel LM (2009) A frequent kinase domain mutation that changes the interaction between PI3Kalpha and the membrane. *Proc. Natl. Acad. Sci. U. S. A.* **106:** 16996–7001

Manning BD & Toker A (2017) Leading Edge Review AKT/PKB Signaling: Navigating the Network. *Cell* **169:** 381–405

Mavrommati I, Cisse O, Falasca M & Maffucci T (2016) Novel roles for class II Phosphoinositide 3-Kinase C2β in signalling pathways involved in prostate cancer cell invasion. *Sci. Rep.* **6:** 23277

Meier TI, Cook JA, Thomas JE, Radding JA, Horn C, Lingaraj T & Smith MC (2004) Cloning, expression, purification, and characterization of the human Class Ia phosphoinositide 3-kinase isoforms. *Protein Expr. Purif.* **35:** 218–224

Meisner H, Conway BR, Hartley D & Czech MP (1995) Interactions of Cbl with Grb2 and phosphatidylinositol 3'-kinase in activated Jurkat cells. *Mol. Cell. Biol.* **15:** 3571–8

Miled N, Yan Y, Hon W-C, Perisic O, Zvelebil M, Inbar Y, Schneidman-Duhovny D, Wolfson HJ, Backer JM & Williams RL (2007) Mechanism of Two Classes of Cancer Mutations in the Phosphoinositide 3-Kinase Catalytic Subunit. *Science (80-. ).* **317:** 239–242

Moon KD, Post CB, Durden DL, Zhou Q, De P, Harrison ML & Geahlen RL (2005) Molecular basis for a direct interaction between the Syk protein-tyrosine kinase and phosphoinositide 3-kinase. *J. Biol. Chem.* **280:** 1543–51

Morris JH, Knudsen GM, Verschueren E, Johnson JR, Cimermancic P, Greninger AL & Pico AR (2014) Affinity purification-mass spectrometry and network analysis to understand protein-protein interactions. *Nat. Protoc.* **9:** 2539–54

Mueller DL, Jenkins MK & Schwartz RH (1989) An accessory cell-derived costimulatory signal acts independently of protein kinase C activation to allow T cell proliferation and prevent the induction of unresponsiveness. *J. Immunol.* **142:** 2617–28

Myers MG, Mendez R, Shi P, Pierce JH, Rhoads R & White MF (1998) The COOH-terminal tyrosine phosphorylation sites on IRS-1 bind SHP-2 and negatively regulate insulin signaling. *J. Biol. Chem.* **273:** 26908–14

Naramura M, Kole HK, Hu RJ & Gu H (1998) Altered thymic positive selection and intracellular signals in Cbl-deficient mice. *Proc. Natl. Acad. Sci. U. S. A.* **95:** 15547–52

Naramura M, Jang I-K, Kole H, Huang F, Haines D & Gu H (2002) c-Cbl and Cbl-b regulate T cell responsiveness by promoting ligand-induced TCR down-modulation. *Nat. Immunol.* **3:** 1192–1199

Nguyen V, Cao L, Lin JT, Hung N, Ritz A, Yu K, Jianu R, Ulin SP, Raphael BJ, Laidlaw DH, Brossay L & Salomon AR (2009) A new approach for quantitative phosphoproteomic dissection of signaling pathways applied to T cell receptor activation. *Mol. Cell. Proteomics* **8:** 2418–31

Nika K, Soldani C, Salek M, Paster W, Gray A, Etzensperger R, Fugger L, Polzella P, Cerundolo V, Dushek O, Höfer T, Viola A & Acuto O (2010) Constitutively active Lck kinase in T cells drives antigen receptor signal transduction. *Immunity* **32:** 766–77

Nishida K, Yoshida Y, Itoh M, Fukada T, Ohtani T, Shirogane T, Atsumi T, Takahashi-Tezuka M, Ishihara K, Hibi M & Hirano T (1999) Gab-family adapter proteins act downstream of cytokine and growth factor receptors and T- and B-cell antigen receptors. *Blood* **93:** 1809-1816

Nojima H, Adachi M, Matsui T, Okawa K, Tsukita S & Tsukita S (2008) IQGAP3 regulates cell proliferation through the Ras/ERK signalling cascade. *Nat. Cell Biol.* **10:** 971–978

Okada T, Maeda A, Iwamatsu A, Gotoh K & Kurosaki T (2000) BCAP: the tyrosine kinase substrate that connects B cell receptor to phosphoinositide 3-kinase activation. *Immunity* **13:** 817–27

Okkenhaug K, Bilancio A, Farjot G, Priddle H, Sancho S, Peskett E, Pearce W, Meek SE, Salpekar A, Waterfield MD, Smith AJH & Vanhaesebroeck B (2002) Impaired B and T cell antigen receptor signaling in p110delta PI 3-kinase mutant mice. *Science* **297:** 1031–4

Okkenhaug K & Fruman DA (2010) PI3Ks in lymphocyte signaling and development. *Curr. Top. Microbiol. Immunol.* **346:** 57–85

Okkenhaug K, Patton DT, Bilancio A, Garçon F, Rowan WC & Vanhaesebroeck B (2006) The p110delta isoform of phosphoinositide 3-kinase controls clonal expansion and differentiation of Th cells. *J. Immunol.* **177:** 5122–8

Okkenhaug K & Vanhaesebroeck B (2003) PI3K in lymphocyte development, differentiation and activation. *Nat. Rev. Immunol.* **3:** 317–330

Ong S-E & Mann M (2005) Mass spectrometry–based proteomics turns quantitative. *Nat. Chem. Biol.* **1:** 252–262

Osakabe Y, Watanabe T, Sugano SS, Ueta R, Ishihara R, Shinozaki K & Osakabe K (2016) Optimization of CRISPR/Cas9 genome editing to modify abiotic stress responses in plants. *Sci. Rep.* **6:** 26685

Pacold ME, Suire S, Perisic O, Lara-Gonzalez S, Davis CT, Walker EH, Hawkins PT, Stephens L, Eccleston JF & Williams RL (2000) Crystal structure and functional analysis of Ras binding to its effector phosphoinositide 3-kinase gamma. *Cell* **103:** 931–43

Palacios EH & Weiss A (2004) Function of the Src-family kinases, Lck and Fyn, in T-cell development and activation. *Oncogene* **23:** 7990–8000

Park WS, Heo W Do, Whalen JH, O'Rourke NA, Bryan HM, Meyer T & Teruel MN (2008) Comprehensive identification of PIP3-regulated PH domains from C. elegans to H. sapiens by model prediction and live imaging. *Mol. Cell* **30:** 381–92

Paz PE, Wang S, Clarke H, Lu X, Stokoe D & Abo A (2001) Mapping the Zap-70 phosphorylation sites on LAT (linker for activation of T cells) required for recruitment and activation of signalling proteins in T cells. *Biochem. J.* **356:** 461-471

Pedros C, Zhang Y, Hu JK, Choi YS, Canonigo-Balancio AJ, Yates JR, Altman A, Crotty S & Kong K-F (2016) A TRAF-like motif of the inducible costimulator ICOS controls development of germinal center TFH cells via the kinase TBK1. *Nat. Immunol.* **17:** 825–833

Penela P, Murga C, Ribas C, Lafarga V, Mayor F & Jr (2010) The complex G protein-coupled receptor kinase 2 (GRK2) interactome unveils new physiopathological targets. *Br. J. Pharmacol.* **160:** 821–32

Plas DR, Johnson R, Pingel JT, Matthews RJ, Dalton M, Roy G, Chan AC & Thomas ML (1996) Direct regulation of ZAP-70 by SHP-1 in T cell antigen receptor signaling. *Science* **272:** 1173–6

Platt RJ, Chen S, Zhou Y, Yim MJ, Swiech L, Kempton HR, Dahlman JE, Parnas O, Eisenhaure TM, Jovanovic M, Graham DB, Jhunjhunwala S, Heidenreich M, Xavier RJ, Langer R, Anderson DG, Hacohen N, Regev A, Feng G, Sharp PA, et al (2014) CRISPR-Cas9 Knockin Mice for Genome Editing and Cancer Modeling. *Cell* **159:** 440–455

Pleiman CM, Hertz WM & Cambier JC (1994) Activation of phosphatidylinositol-3' kinase by Src-family kinase SH3 binding to the p85 subunit. *Science* **263:** 1609–12

Prasad K V, Cai YC, Raab M, Duckworth B, Cantley L, Shoelson SE & Rudd CE (1994) T-cell antigen CD28 interacts with the lipid kinase phosphatidylinositol 3-kinase by a cytoplasmic Tyr(P)-Met-Xaa-Met motif. *Proc. Natl. Acad. Sci. U. S. A.* **91:** 2834–8

Prasad K V, Janssen O, Kapeller R, Raab M, Cantley LC & Rudd CE (1993) Src-homology 3 domain of protein kinase p59fyn mediates binding to phosphatidylinositol 3-kinase in T cells. *Proc. Natl. Acad. Sci. U. S. A.* **90:** 7366–70

Raab M, da Silva AJ, Findell PR & Rudd CE (1997) Regulation of Vav-SLP-76 binding by ZAP-70 and its relevance to TCR zeta/CD3 induction of interleukin-2. *Immunity* **6:** 155–64

Ramadani F, Bolland DJ, Garcon F, Emery JL, Vanhaesebroeck B, Corcoran AE & Okkenhaug K (2010) The PI3K isoforms p110alpha and p110delta are essential for pre-B cell receptor signaling and B cell development. *Sci. Signal.* **3:** ra60

Rameh LE & Cantley LC (1999) The role of phosphoinositide 3-kinase lipid products in cell function. *J. Biol. Chem.* **274:** 8347–50

Rao N, Miyake S, Reddi AL, Douillard P, Ghosh AK, Dodge IL, Zhou P, Fernandes ND & Band H (2002) Negative regulation of Lck by Cbl ubiquitin ligase. *Proc. Natl. Acad. Sci. U. S. A.* **99:** 3794–9

Rauniyar N, Yates JR & III (2014) Isobaric labeling-based relative quantification in shotgun proteomics. *J. Proteome Res.* **13:** 5293–309

Rebeaud F, Hailfinger S, Posevitz-Fejfar A, Tapernoux M, Moser R, Rueda D, Gaide O, Guzzardi M, Iancu EM, Rufer N, Fasel N & Thome M (2008) The proteolytic activity of the paracaspase MALT1 is key in T cell activation. *Nat. Immunol.* **9:** 272–281

Reedquist KA, Fukazawa T, Panchamoorthy G, Langdon WY, Shoelson SE, Druker BJ & Band H (1996) Stimulation through the T cell receptor induces Cbl association with Crk proteins and the guanine nucleotide exchange protein C3G. *J. Biol. Chem.* **271:** 8435–42

Ren J, Zhang X, Liu X, Fang C, Jiang S, June CH & Zhao Y (2017) A versatile system for rapid multiplex genome-edited CAR T cell generation. *Oncotarget* **8:** 17002–17011

Rodriguez-Viciana P, Warne PH, Vanhaesebroeck B, Waterfield MD & Downward J (1996) Activation of phosphoinositide 3-kinase by interaction with Ras and by point mutation. *EMBO J.* **15:** 2442–51

Rodriguez-Viciana P, Sabatier C & McCormick F (2004) Signaling specificity by Ras family GTPases is determined by the full spectrum of effectors they regulate. *Mol. Cell. Biol.* **24:** 4943–54

Rodriguez-Viciana P, Warne PH, Dhand R, Vanhaesebroeck B, Gout I, Fry MJ, Waterfield MD & Downward J (1994) Phosphatidylinositol-3-OH kinase as a direct target of Ras. *Nature* **370:** 527–532

Roncagalli R, Cucchetti M, Jarmuzynski N, Grégoire C, Bergot E, Audebert S, Baudelet E, Menoita MG, Joachim A, Durand S, Suchanek M, Fiore F, Zhang L, Liang Y, Camoin L, Malissen M & Malissen B (2016) The scaffolding function of the RLTPR protein explains its essential role for CD28 co-stimulation in mouse and human T cells. *J. Exp. Med.* **213:** 2437–2457

Roncagalli R, Hauri S, Fiore F, Liang Y, Chen Z, Sansoni A, Kanduri K, Joly R, Malzac A, Lähdesmäki H, Lahesmaa R, Yamasaki S, Saito T, Malissen M, Aebersold R, Gstaiger M & Malissen B (2014) Quantitative proteomics analysis of signalosome dynamics in primary T cells identifies the surface receptor CD6 as a Lat adaptor-independent TCR signaling hub. *Nat. Immunol.* **15:** 384–92

Rostislavleva K, Soler N, Ohashi Y, Zhang L, Pardon E, Burke JE, Masson GR, Johnson C, Steyaert J, Ktistakis NT & Williams RL (2015) Structure and flexibility of the endosomal Vps34 complex reveals the basis of its function on membranes. *Science (80-. ).* **350:** aac7365-aac7365

Roy E, Togbe D, Holdorf AD, Trubetskoy D, Nabti S, Küblbeck G, Klevenz A, Kopp-Schneider A, Leithäuser F, Möller P, Bladt F, Hämmerling G, Arnold B, Pawson T & Tafuri A (2010) Nck adaptors are positive regulators of the size and sensitivity of the T-cell repertoire. *Proc. Natl. Acad. Sci. U. S. A.* **107:** 15529–34

Rudd CE & Schneider H (2003) Unifying concepts in CD28, ICOS and CTLA4 co-receptor signalling. *Nat. Rev. Immunol.* **3:** 544–556

Rupp LJ, Schumann K, Roybal KT, Gate RE, Ye CJ, Lim WA & Marson A (2017) CRISPR/Cas9-mediated PD-1 disruption enhances anti-tumor efficacy of human chimeric antigen receptor T cells. *Sci. Rep.* **7:** 737

Salek M, McGowan S, Trudgian DC, Dushek O, de Wet B, Efstathiou G & Acuto O (2013) Quantitative phosphoproteome analysis unveils LAT as a modulator of CD3ζ and ZAP-70 tyrosine phosphorylation. *PLoS One* **8:** e77423

Samelson LE (2002) Signal transduction mediated by the T cell antigen receptor: the role of adapter proteins. *Annu. Rev. Immunol.* **20:** 371–394

San Luis B, Sondgeroth B, Nassar N & Carpino N (2011) Sts-2 is a phosphatase that negatively regulates zeta-associated protein (ZAP)-70 and T cell receptor signaling pathways. *J. Biol. Chem.* **286:** 15943–54

Sarbassov DD, Guertin DA, Ali SM & Sabatini DM (2005) Phosphorylation and Regulation of Akt/PKB by the Rictor-mTOR Complex. *Science* **307:** 1098–1101

Sármay G, Angyal A, Kertész Á, Maus M & Medgyesi D (2006) The multiple function of Grb2 associated binder (Gab) adaptor/scaffolding protein in immune cell signaling. *Immunol. Lett.* **104:** 76–82

Saudemont A, Garçon F, Yadi H, Roche-Molina M, Kim N, Segonds-Pichon A, Martín-Fontecha A, Okkenhaug K & Colucci F (2009) p110gamma and p110delta isoforms of phosphoinositide 3-

kinase differentially regulate natural killer cell migration in health and disease. *Proc. Natl. Acad. Sci. U. S. A.* **106:** 5795–800

Saveliev A & Tybulewicz VLJ (2009) Lymphocyte signaling: beyond knockouts. *Nat. Immunol.* **10:** 361–4

Schmid MC, Avraamides CJ, Dippold HC, Franco I, Foubert P, Ellies LG, Acevedo LM, Manglicmot JRE, Song X, Wrasidlo W, Blair SL, Ginsberg MH, Cheresh DA, Hirsch E, Field SJ & Varner JA (2011) Receptor tyrosine kinases and TLR/IL1Rs unexpectedly activate myeloid cell PI3kγ, a single convergent point promoting tumor inflammation and progression. *Cancer Cell* **19:** 715–27

Schulze-Luehrmann J & Ghosh S (2006) Antigen-Receptor Signaling to Nuclear Factor κB. *Immunity* **25:** 701–715

Schumann K, Lin S, Boyer E, Simeonov DR, Subramaniam M, Gate RE, Haliburton GE, Ye CJ, Bluestone JA, Doudna JA & Marson A (2015) Generation of knock-in primary human T cells using Cas9 ribonucleoproteins. *Proc. Natl. Acad. Sci. U. S. A.* **112:** 10437–42

Seder RA, Darrah PA & Roederer M (2008) T-cell quality in memory and protection: implications for vaccine design. *Nat. Rev. Immunol.* **8:** 247–258

Seki A & Rutz S (2018) Optimized RNP transfection for highly efficient CRISPR/Cas9-mediated gene knockout in primary T cells. *J. Exp. Med.* **215:** 985–997

Sentmanat MF, Peters ST, Florian CP, Connelly JP & Pruett-Miller SM (2018) A Survey of Validation Strategies for CRISPR-Cas9 Editing. *Sci. Rep.* **8:** 888

Shenoy-Scaria AM, Timson Gauen LK, Kwong J, Shaw AS & Lublin DM (1993) Palmitoylation of an Amino-Terminal Cysteine Motif of Protein Tyrosine Kinases p56lck and p59fyn Mediates Interaction with Glycosyl-Phosphatidylinositol-Anchored Proteins. *Mol. Cell. Biol*. **13:** 6385-92

Shim EK, Jung SH & Lee JR (2011) Role of two adaptor molecules SLP-76 and LAT in the PI3K signaling pathway in activated T cells. *J. Immunol.* **186:** 2926–35

Shim EK, Moon CS, Lee GY, Ha YJ, Chae S-K & Lee JR (2004) Association of the Src homology 2 domain-containing leukocyte phosphoprotein of 76 kD (SLP-76) with the p85 subunit of phosphoinositide 3-kinase. *FEBS Lett.* **575:** 35–40

Siempelkamp BD, Rathinaswamy MK, Jenkins ML & Burke JE (2017) Molecular mechanism of activation of class IA phosphoinositide 3-kinases (PI3Ks) by membrane-localized HRas. *J. Biol. Chem.* **292:** 12256–12266

Singh MD, Ni M, Sullivan JM, Hamerman JA & Campbell DJ (2018) B cell adaptor for PI3-kinase (BCAP) modulates CD8+ effector and memory T cell differentiation. *J. Exp. Med.* **215:** 2429–2443

Skolnik EY, Lee CH, Batzer A, Vicentini LM, Zhou M, Daly R, Myers MJ, Backer JM, Ullrich A & White MF (1993) The SH2/SH3 domain-containing protein GRB2 interacts with tyrosine-phosphorylated IRS1 and Shc: implications for insulin control of ras signalling. *EMBO J.* **12:** 1929–36

Smith GA, Taunton J & Weiss A (2017) IL-2Rβ abundance differentially tunes IL-2 signaling dynamics in CD4+ and CD8+ T cells. *Sci. Signal.* **10:** eaan4931

So L & Fruman DA (2012) PI3K signalling in B- and T-lymphocytes: new developments and therapeutic advances. *Biochem. J.* **442:** 465–81

Songyang Z, Shoelson SE, Chaudhuri M, Gish G, Pawson T, Haser WG, King F, Roberts T, Ratnofsky S & Lechleider RJ (1993) SH2 domains recognize specific phosphopeptide sequences. *Cell* **72:** 767–78

Songyang Z, Shoelson SE, McGlade J, Olivier P, Pawson T, Bustelo XR, Barbacid M, Sabe H, Hanafusa H, Yi T & al. et (1994) Specific motifs recognized by the SH2 domains of Csk, 3BP2, fps/fes, GRB-2, HCP, SHC, Syk, and Vav. *Mol. Cell. Biol.* **14:** 2777–85

Soond DR, Bjørgo E, Moltu K, Dale VQ, Patton DT, Torgersen KM, Galleway F, Twomey B, Clark J, Gaston JSH, Taskén K, Bunyard P & Okkenhaug K (2010) PI3K p110delta regulates T-cell cytokine production during primary and secondary immune responses in mice and humans. *Blood* **115:** 2203–13

Spitaler M & Cantrell DA (2004) Protein kinase C and beyond. *Nat. Immunol.* **5:** 785–790

Stark A-K, Chandra A, Chakraborty K, Alam R, Carbonaro V, Clark J, Sriskantharajah S, Bradley G, Richter AG, Banham-Hall E, Clatworthy MR, Nejentsev S, Hamblin JN, Hessel EM, Condliffe AM & Okkenhaug K (2018) PI3Kδ hyper-activation promotes development of B cells that exacerbate Streptococcus pneumoniae infection in an antibody-independent manner. *Nat. Commun.* **9:** 3174

Starr TK, Jameson SC & Hogquist KA (2003) Positive and negative selection of T cells. *Annu. Rev. Immunol.* **21:** 139–176

Stephens LR, Eguinoa A, Erdjument-Bromage H, Lui M, Cooke F, Coadwell J, Smrcka AS, Thelen M, Cadwallader K, Tempst P & Hawkins PT (1997) The G beta gamma sensitivity of a PI3K is dependent upon a tightly associated adaptor, p101. *Cell* **89:** 105–14

Stirnweiss A, Hartig R, Gieseler S, Lindquist JA, Reichardt P, Philipsen L, Simeoni L, Poltorak M, Merten C, Zuschratter W, Prokazov Y, Paster W, Stockinger H, Harder T, Gunzer M & Schraven B (2013) T cell activation results in conformational changes in the Src family kinase Lck to induce its activation. *Sci. Signal.* **6:** ra13

Stittrich A-B, Haftmann C, Sgouroudis E, Kühl AA, Hegazy AN, Panse I, Riedel R, Flossdorf M, Dong J, Fuhrmann F, Heinz GA, Fang Z, Li N, Bissels U, Hatam F, Jahn A, Hammoud B, Matz M, Schulze F-M, Baumgrass R, et al (2010) The microRNA miR-182 is induced by IL-2 and promotes clonal expansion of activated helper T lymphocytes. *Nat. Immunol.* **11:** 1057–1062

Stokoe D, Stephens LR, Copeland T, Gaffney PR, Reese CB, Painter GF, Holmes AB, McCormick F & Hawkins PT (1997) Dual role of phosphatidylinositol-3,4,5-trisphosphate in the activation of protein kinase B. *Science* **277:** 567–70

Su S, Hu B, Shao J, Shen B, Du J, Du Y, Zhou J, Yu L, Zhang L, Chen F, Sha H, Cheng L, Meng F, Zou Z, Huang X & Liu B (2016) CRISPR-Cas9 mediated efficient PD-1 disruption on human primary T cells from cancer patients. *Sci. Rep.* **6:** 20070

Suire S, Coadwell J, Ferguson GJ, Davidson K, Hawkins P & Stephens L (2005) p84, a New Gβγ-Activated Regulatory Subunit of the Type IB Phosphoinositide 3-Kinase p110γ. *Curr. Biol.* **15:** 566–570

Sun XJ, Wang L-M, Zhang Y, Yenush L, Myers Jr MG, Glasheen E, Lane WS, Pierce JH & White MF (1995) Role of IRS-2 in insulin and cytokine signalling. *Nature* **377:** 173–177

Swat W, Montgrain V, Doggett TA, Douangpanya J, Puri K, Vermi W & Diacovo TG (2006) Essential role of PI3K  and PI3K  in thymocyte survival. *Blood* **107:** 2415–2422

Thompson A, Schäfer J, Kuhn K, Kienle S, Schwarz J, Schmidt G, Neumann T, Johnstone R, Mohammed AKA & Hamon C (2003) Tandem mass tags: a novel quantification strategy for comparative analysis of complex protein mixtures by MS/MS. *Anal. Chem.* **75:** 1895–904

Timson Gauen LK, Kong AN, Samelson LE & Shaw AS (1992) p59fyn tyrosine kinase associates with multiple T-cell receptor subunits through its unique amino-terminal domain. *Mol. Cell. Biol.* **12:** 5438–46

Tong L (2013) Structure and function of biotin-dependent carboxylases. *Cell. Mol. Life Sci.* **70:** 863–91

Tsantikos E, Quilici C, Harder KW, Wang B, Zhu H-J, Anderson GP, Tarlinton DM & Hibbs ML (2009) Perturbation of the CD4 T Cell Compartment and Expansion of Regulatory T Cells in Autoimmune-Prone Lyn-Deficient Mice. *J. Immunol.* **183:** 2484–2494

Tsukumo S, Unno M, Muto A, Takeuchi A, Kometani K, Kurosaki T, Igarashi K & Saito T (2013) Bach2 maintains T cells in a naive state by suppressing effector memory-related genes. *Proc. Natl. Acad. Sci. U. S. A.* **110:** 10735–40

Turner JM, Brodsky MH, Irving BA, Levin SD, Perlmutter RM & Littman DR (1990) Interaction of the unique N-terminal region of tyrosine kinase p56lck with cytoplasmic domains of CD4 and CD8 is mediated by cysteine motifs. *Cell* **60:** 755–65

Tyanova S & Cox J (2018) Perseus: A Bioinformatics Platform for Integrative Analysis of Proteomics Data in Cancer Research. In *Cancer Systems Biology: Methods and Protocols. Methods in Molecular Biology, vol 1711* pp 133–148. Humana Press, New York, NY

Tyanova S, Temu T, Sinitcyn P, Carlson A, Hein MY, Geiger T, Mann M & Cox J (2016) The Perseus computational platform for comprehensive analysis of (prote)omics data. *Nat. Methods* **13:** 731–740

Vadas O, Burke JE, Zhang X, Berndt A & Williams RL (2011) Structural basis for activation and inhibition of class I phosphoinositide 3-kinases. *Sci. Signal.* **4:** re2

Vanhaesebroeck B & Alessi DR (2000) The PI3K-PDK1 connection: more than just a road to PKB. *Biochem. J.* **346 Pt 3:** 561–76

Vanhaesebroeck B, Guillermet-Guibert J, Graupera M & Bilanges B (2010) The emerging mechanisms of isoform-specific PI3K signalling. *Nat. Rev. Mol. Cell Biol.* **11:** 329–341

Varma R, Campi G, Yokosuka T, Saito T & Dustin ML (2006) T Cell Receptor-Proximal Signals Are Sustained in Peripheral Microclusters and Terminated in the Central Supramolecular Activation Cluster. *Immunity* **25:** 117–127

Vella A, Teague TK, Ihle J, Kappler J & Marrack P (1997) Interleukin 4 (IL-4) or IL-7 prevents the death of resting T cells: stat6 is probably not required for the effect of IL-4. *J. Exp. Med.* **186:** 325–30

Verdino P, Witherden DA, Havran WL & Wilson IA (2010) The molecular interaction of CAR and JAML recruits the central cell signal transducer PI3K. *Science* **329:** 1210–4

Villarroya-Beltri C, Baixauli F, Mittelbrunn M, Fernández-Delgado I, Torralba D, Moreno-Gonzalo O, Baldanta S, Enrich C, Guerra S & Sánchez-Madrid F (2016) ISGylation controls exosome secretion by promoting lysosomal degradation of MVB proteins. *Nat. Commun.* **7:** 13588

Voisinne G, García-Blesa A, Chaoui K, Fiore F, Bergot E, Girard L, Malissen M, Burlet-Schiltz O, Gonzalez de Peredo A, Malissen B & Roncagalli R (2016) Co-recruitment analysis of the CBL and CBLB signalosomes in primary T cells identifies CD5 as a key regulator of TCR-induced ubiquitylation. *Mol. Syst. Biol.* **12:** 876

Wang HY, Altman Y, Fang D, Elly C, Dai Y, Shao Y & Liu YC (2001) Cbl promotes ubiquitination of the T cell receptor zeta through an adaptor function of Zap-70. *J. Biol. Chem.* **276:** 26004–11

Wang H, Kadlecek TA, Au-Yeung BB, Goodfellow HES, Hsu L-Y, Freedman TS & Weiss A (2010) ZAP-70: an essential kinase in T-cell signaling. *Cold Spring Harb. Perspect. Biol.* **2:** a002279

Wang J, Auger KR, Jarvis L, Shi Y & Roberts TM (1995) Direct association of Grb2 with the p85 subunit of phosphatidylinositol 3-kinase. *J. Biol. Chem.* **270:** 12774–80

Wang J & Reinherz EL (2012) The structural basis of αβ T-lineage immune recognition: TCR docking topologies, mechanotransduction, and co-receptor function. *Immunol. Rev.* **250:** 102–119

Wang W, Ye C, Liu J, Zhang D, Kimata JT & Zhou P (2014) CCR5 Gene Disruption via Lentiviral Vectors Expressing Cas9 and Single Guided RNA Renders Cells Resistant to HIV-1 Infection. *PLoS One* **9:** e115987

Watanabe S, Take H, Takeda K, Yu Z-X, Iwata N & Kajigaya S (2000) Characterization of the CIN85 Adaptor Protein and Identification of Components Involved in CIN85 Complexes. *Biochem. Biophys. Res. Commun.* **278:** 167–174

Waters SB & Pessin JE (1996) Insulin receptor substrate 1 and 2 (IRS1 and IRS2): what a tangled web we weave. *Trends Cell Biol.* **6:** 1–4

Webb LMC, Vigorito E, Wymann MP, Hirsch E & Turner M (2005) Cutting edge: T cell development requires the combined activities of the p110gamma and p110delta catalytic isoforms of phosphatidylinositol 3-kinase. *J. Immunol.* **175:** 2783–7

Weinger JG, Gohari P, Yan Y, Backer JM, Varnum B & Shafit-Zagardo B (2008) In brain, Axl recruits Grb2 and the p85 regulatory subunit of PI3 kinase; in vitro mutagenesis defines the requisite binding sites for downstream Akt activation. *J. Neurochem.* **106:** 134–46

Wikenheiser DJ & Stumhofer JS (2016) ICOS Co-Stimulation: Friend or Foe? *Front. Immunol.* **7:** 304

Witherden DA, Verdino P, Rieder SE, Garijo O, Mills RE, Teyton L, Fischer WH, Wilson IA & Havran WL (2010) The junctional adhesion molecule JAML is a costimulatory receptor for epithelial gammadelta T cell activation. *Science* **329:** 1205–10

Wittlich M, Koenig BW, Hoffmann S & Willbold D (2007) Structural characterization of the transmembrane and cytoplasmic domains of human CD4. *Biochim. Biophys. Acta - Biomembr.* **1768:** 2949–2960

Wu H, Shekar SC, Flinn RJ, El-Sibai M, Jaiswal BS, Sen KI, Janakiraman V, Seshagiri S, Gerfen GJ, Girvin ME & Backer JM (2009) Regulation of Class IA PI 3-kinases: C2 domain-iSH2 domain contacts inhibit p85/p110alpha and are disrupted in oncogenic p85 mutants. *Proc. Natl. Acad. Sci. U. S. A.* **106:** 20258–63

Wu X, Scott DA, Kriz AJ, Chiu AC, Hsu PD, Dadon DB, Cheng AW, Trevino AE, Konermann S, Chen S, Jaenisch R, Zhang F & Sharp PA (2014) Genome-wide binding of the CRISPR endonuclease Cas9 in mammalian cells. *Nat. Biotechnol.* **32:** 670–676

Wunderlich L, Faragó A, Downward J & Buday L (1999) Association of Nck with tyrosine-phosphorylated SLP-76 in activated T lymphocytes. *Eur. J. Immunol.* **29:** 1068–1075

Wurster AL, Withers DJ, Uchida T, White MF & Grusby MJ (2002) Stat6 and IRS-2 cooperate in interleukin 4 (IL-4)-induced proliferation and differentiation but are dispensable for IL-4-dependent rescue from apoptosis. *Mol. Cell. Biol.* **22:** 117–26

Xu C, Gagnon E, Call ME, Schnell JR, Schwieters CD, Carman C V., Chou JJ & Wucherpfennig KW (2008) Regulation of T Cell Receptor Activation by Dynamic Membrane Binding of the CD3ε Cytoplasmic Tyrosine-Based Motif. *Cell* **135:** 702–713

Xu W, Harrison SC & Eck MJ (1997) Three-dimensional structure of the tyrosine kinase c-Src. *Nature* **385:** 595–602

Yamanashi Y, Mori S, Yoshida M, Kishimoto T, Inoue K, Yamamoto T & Toyoshima K (1989) Selective expression of a protein-tyrosine kinase, p56lyn, in hematopoietic cells and association with production of human T-cell lymphotropic virus type I. *Proc. Natl. Acad. Sci. U. S. A.* **86:** 6538–42

Yamasaki S, Nishida K, Sakuma M, Berry D, McGlade CJ, Hirano T & Saito T (2003) Gads/Grb2-mediated association with LAT is critical for the inhibitory function of Gab2 in T cells. *Mol. Cell. Biol.* **23:** 2515–29

Yamazaki T, Takeda K, Gotoh K, Takeshima H, Akira S & Kurosaki T (2002) Essential immunoregulatory role for BCAP in B cell development and function. *J. Exp. Med.* **195:** 535–45

Yan Q, Barros T, Visperas PR, Deindl S, Kadlecek TA, Weiss A & Kuriyan J (2013) Structural basis for activation of ZAP-70 by phosphorylation of the SH2-kinase linker. *Mol. Cell. Biol.* **33:** 2188–201

Yang M, Chen T, Li X, Yu Z, Tang S, Wang C, Gu Y, Liu Y, Xu S, Li W, Zhang X, Wang J & Cao X (2015) K33-linked polyubiquitination of Zap70 by Nrdp1 controls CD8+ T cell activation. *Nat. Immunol.* **16:** 1253–1262

Yang W, Steen H & Freeman MR (2008) Proteomic approaches to the analysis of multiprotein signaling complexes. *Proteomics* **8:** 832–851

Yokosuka T, Kobayashi W, Sakata-Sogawa K, Takamatsu M, Hashimoto-Tane A, Dustin ML, Tokunaga M & Saito T (2008) Spatiotemporal regulation of T cell costimulation by TCR-CD28 microclusters and protein kinase C theta translocation. *Immunity* **29:** 589–601

Yu J, Zhang Y, McIlroy J, Rordorf-Nikolic T, Orr GA & Backer JM (1998) Regulation of the p85/p110 phosphatidylinositol 3'-kinase: stabilization and inhibition of the p110alpha catalytic subunit by the p85 regulatory subunit. *Mol. Cell. Biol.* **18:** 1379–87

Zeng R, Cannon JL, Abraham RT, Way M, Billadeau DD, Bubeck-Wardenberg J & Burkhardt JK (2003) SLP-76 coordinates Nck-dependent Wiskott-Aldrich syndrome protein recruitment with Vav-1/Cdc42-dependent Wiskott-Aldrich syndrome protein activation at the T cell-APC contact site. *J. Immunol.* **171:** 1360–8

Zhang SQ, Tsiaras WG, Araki T, Wen G, Minichiello L, Klein R & Neel BG (2002) Receptor-specific regulation of phosphatidylinositol 3'-kinase activation by the protein tyrosine phosphatase Shp2. *Mol. Cell. Biol.* **22:** 4062–72

Zhang W, Trible RP, Zhu M, Liu SK, McGlade CJ & Samelson LE (2000) Association of Grb2, Gads, and phospholipase C-gamma 1 with phosphorylated LAT tyrosine residues. Effect of LAT tyrosine mutations on T cell angigen receptor-mediated signaling. *J. Biol. Chem.* **275:** 23355–61

Zhang W, Sloan-Lancaster J, Kitchen J, Trible RP & Samelson LE (1998) LAT: The ZAP-70 Tyrosine Kinase Substrate that Links T Cell Receptor to Cellular Activation. *Cell* **92:** 83–92

Zhang X, Vadas O, Perisic O, Anderson KE, Clark J, Hawkins PT, Stephens LR & Williams RL (2011) Structure of lipid kinase p110β/p85β elucidates an unusual SH2-domain-mediated inhibitory mechanism. *Mol. Cell* **41:** 567–78

Zhao L & Vogt PK (2008) Helical domain and kinase domain mutations in p110α of phosphatidylinositol 3-kinase induce gain of function by different mechanisms. *Proc. Natl. Acad. Sci.* **105:** 2652–2657